SIMULTANEOUS HYPOCENTER AND VELOCITY MODEL ESTIMATION USING DIRECT AND REFLECTED PHASES FROM MICROEARTHQUAKES RECORDED WITHIN THE CENTRAL RIO GRANDE RIFT, NEW MEXICO

by

Hans E. Hartse

Submitted in Partial Fulfillment of
the Requirements for the Degree of
Doctor of Philosophy

New Mexico Institute of Mining and Technology
Socorro, New Mexico, 87801

October, 1991

Abstract

Constraining focal depths using direct P and S arrivals recorded with the Socorro seismic network is often difficult because station spacing is large relative to earthquake depths. To improve hypocenter estimates, and especially the depth of focus estimate, I have incorporated the clear, strong S_zS, P_zP, and S_zP reflected phases from the Socorro mid-crustal magma body into the earthquake location process. The project required three major steps: (1) writing an inversion program (based on generalized least squares) which uses both direct and reflected phases to simultaneously solve for hypocenters and a velocity model, (2) assembling a large arrival time data set, and (3) inverting the data to obtain a flat-layered velocity model most appropriate for locating Socorro-area earthquakes using direct and reflected phases.

The data assembled are from 75 local earthquakes with an epicentral distribution of 2400 km^2 surrounding Socorro. Between 6 and 11 stations recorded each event, and an average of 20 arrival times were read per event. The complete data set consists of 564 P, 485 S, 169 S_zS, 77 P_zP, and 160 S_zP arrival times. Before inverting, timing errors of between 0.075 and 0.450 s were assigned each arrival, depending on pick quality. Each inversion converged while retaining all eigenvalues. Using extreme high-velocity (6.5 km s^{-1}) and low-velocity (5.3 km s^{-1}) starting models parameter estimates were unchanged, indicating results are not initial-model dependent. The errors reported below are for one standard deviation.

I found a compressional velocity (V_p) for the upper 10 km of crust of 5.95 $\pm$ 0.05 km s^{-1}, a V_p for mid-crust (between 10 km and the magma body) of 5.80 $\pm$ 0.08 km s^{-1}, an average depth to the magma body reflector of 18.75 $\pm$ 0.28 km, Poisson's ratio of 0.256 $\pm$ 0.002 for the upper layer, Poisson's ratio of 0.228 $\pm$ 0.007 for the lower layer, and station corrections ranging from -0.204 to 0.672 s. These findings suggest that V_p probably decreases slightly in the ductile crust (lower layer) while V_s increases slightly (3.41 to 3.44 km s^{-1}) with depth. A close fit between observed reflected phase arrival times and model arrival times, and an

even distribution of positive and negative reflected-phase residuals across the study area indicates that the magma body's upper surface is essentially flat.

Focal depth estimates were improved by more than a factor of 3 when locations were found by including reflections. For the 75 events, depth error averaged 0.59 ± 0.12 km while depth error averaged 1.90 ± 0.95 km when only direct arrivals were used. Average origin time error was reduced by a factor of 2 when reflections were included.

Acknowledgments

I would like to acknowledge the individuals who have contributed to this project. First, I thank my advisor, Al Sanford. His extensive knowledge of the Socorro magma body and microearthquake seismogram interpretation was essential for the success of this study. I thank John Knapp, my "second" advisor for his suggestions, insights, and encouragement. His recommendations and advice have led to a stronger, more complete dissertation. I also thank my other committee members, Allan Gutjahr, Larry Jaksha, and Marshall Reiter. They all offered suggestions which improved this dissertation. Most importantly, I thank my wife, Peggy Barroll, for her continual support and encouragement. Without her I would have never continued my graduate studies and surely would never have started this project.

The Society of Exploration Geophysicists partially funded this research through a scholarship provided by their Education Foundation.

Table of Contents

List of Figures

List of Tables

1. Introduction

Background and Primary Objectives

The Socorro area of central New Mexico (Figure 1.1) is one of the most geophysically interesting segments of the Rio Grande rift. Seismically it is the most active area in New Mexico [*Sanford et al.*, 1979]. Many felt events have been reported from this area, and activity often occurs in swarms. One notable swarm in 1906 and 1907 lasted several months, at times produced shocks felt as frequently as one each hour [*Reid*, 1910], and included three large shocks, each estimated as maximum intensity VIII on the Rossi-Forel scale [*Sanford and Einarson*, 1982]. Instruments deployed since 1960 have recorded numerous microearthquakes in this area. These seismograms are well known for reflections off a mid-crustal (approximately 19 km deep) magma body. The recordings show strong, distinct S_zS, S_zP, and P_zP reflected phases [*Sanford and Long*, 1965; *Sanford et al.*, 1973; *Sanford et al.*, 1977; *Ake and Sanford*, 1988]. In addition to these anomalous microearthquake phases, strong P reflections from the same discontinuity have been recorded using Vibroseis techniques [*Brown et al.*, 1979]. The seismically mapped magma body outline [*Rinehart et al.*, 1979; *Gridley*, 1989] (Figure 1.2) closely matches an area of surface uplift [*Larsen et al.*, 1986], suggesting the magma body is still active. *Ouchi* [1983] sites geomorphic evidence indicating uplift over the magma body has been occurring for at least the past 20,000 years.

Since 1981 a permanent, telemetered seismic network (Figure 1.2) has recorded many high quality seismograms which often show both direct and reflected phases. The direct phases have been used routinely to locate events with the program HYPO71 (Revised) [*Lee and Lahr*, 1975]. A potential shortcoming of using only direct arrivals is that to obtain well-constrained focal depth estimates at least one recording station used in the location procedure should have an epicentral distance of less than or equal to the focal depth [*Lee and Stewart*, 1981]. In other words, the ratio of horizontal to vertical distance between an event and the nearest station should, ideally, be less than one. This requires station spacing to be

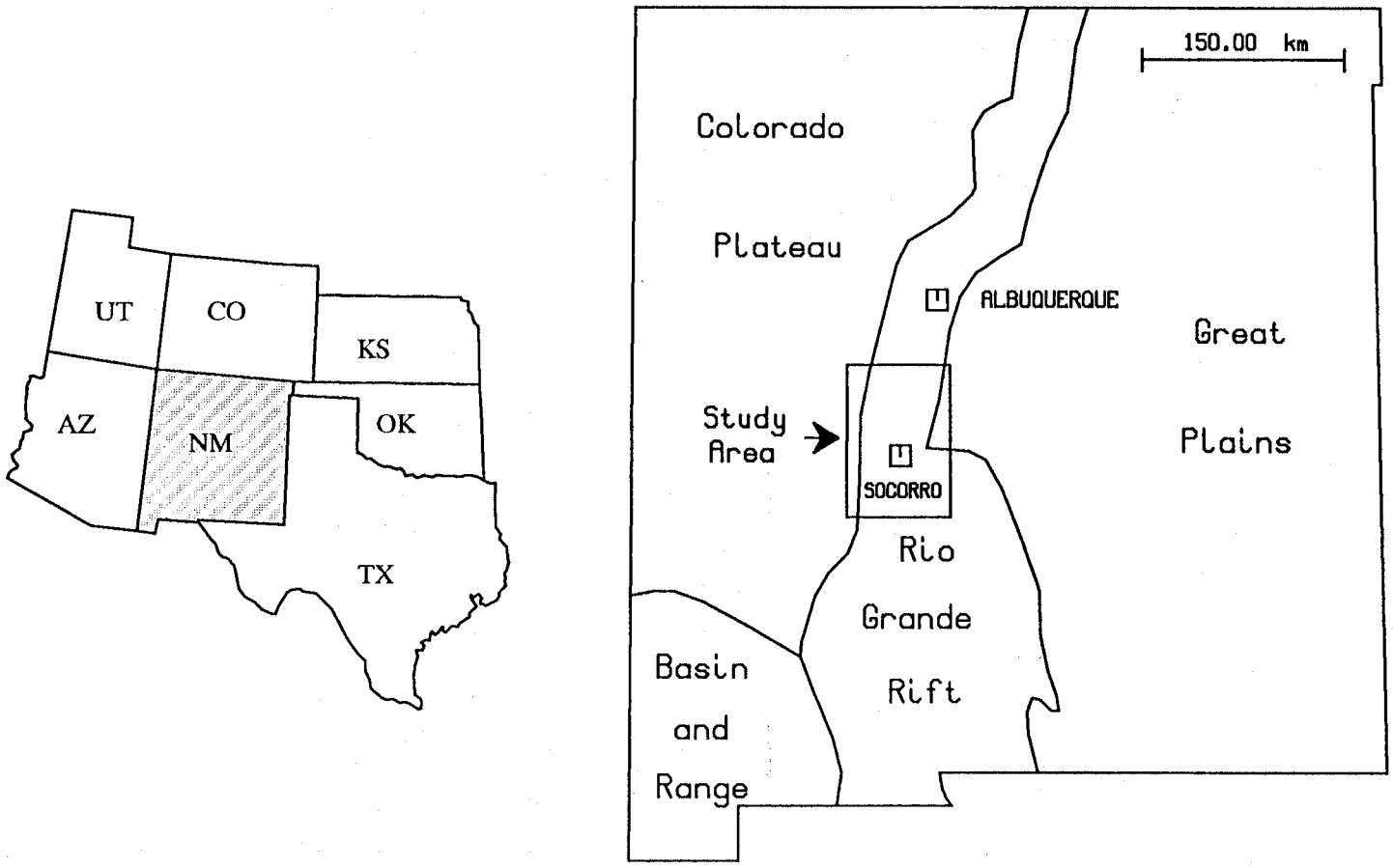

Fig. 1.1. Study area outline in relation to New Mexico, the Rio Grande rift, and adjacent physiographic provinces.

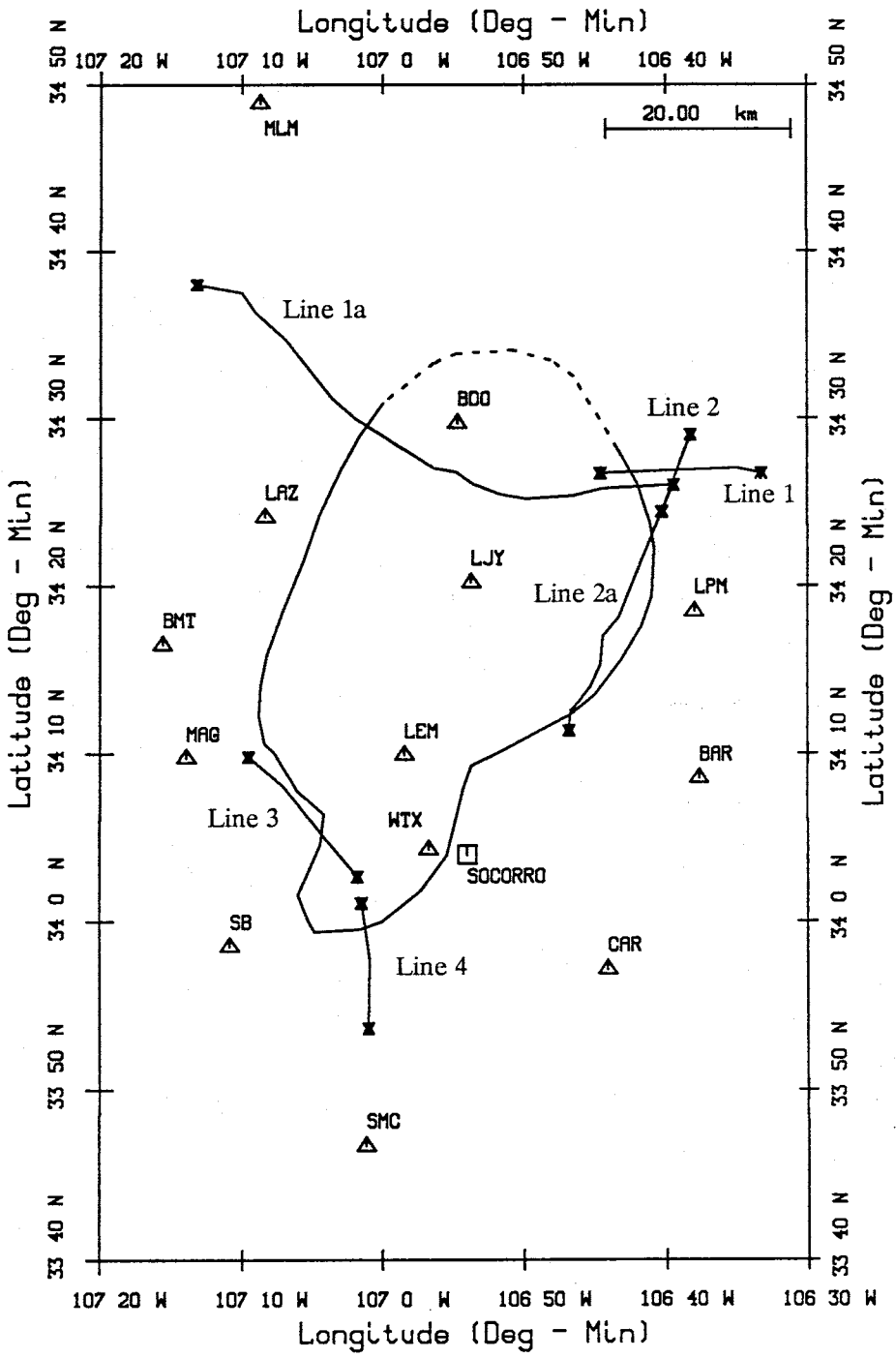

Fig. 1.2. Detailed map of study area showing seismic stations (triangles), COCORP lines, and the magma body outline as mapped by *Rinehart et al.* [1979].

approximately equal to the shallowest events expected within a network if all events are to be accurately located.

Because events in the Socorro area are believed to occur between depths of 4 and 12 km [*King*, 1986], the station spacing of the Socorro network is too coarse to constrain focal depth estimates of many events. One solution to this problem is to obtain supplemental data during swarms or aftershock sequences by deploying temporary stations close to areas of activity. Another solution is to incorporate additional phases into the location problem. Because reflected phases have been reliably identified and are quite common on Socorro-area seismograms, I have expanded the routine earthquake location procedure to include these additional phases and better constrain hypocenter estimates.

In this dissertation I show how reflections can be incorporated into the location process, and then locate local earthquakes by combining direct and reflected phases. I found that the inclusion of the reflected phases significantly reduces focal depth error and origin time error. Depending on station distribution and available phases, the error on focal depth is reduced by a factor of three (on average) compared to when only direct arrivals are used.

To incorporate reflected phases into the location problem, velocity between the recording stations and the reflector must be known. Also, an accurate depth to the reflector is necessary. Knowing the velocity model is as important to the location problem as is the ability to combine phases. Therefore, while simultaneously finding locations of a carefully selected set of earthquakes, I jointly determined a velocity model in the Rio Grande rift of central New Mexico down to the depth of the magma body.

In summary the major objectives of this research were twofold:

1. Develop an inversion technique which uses all commonly identified phases seen on Socorro-area seismograms while jointly solving for hypocenters and a velocity model.

2. Apply the method to a suite of earthquake arrival times to estimate a velocity model most appropriate for locating earthquakes in central New Mexico.

Secondary goals were to:

1. Investigate possible dip or unevenness on the upper surface of the magma body. This is an important consideration because I made the assumption for both locating events and estimating a velocity model that the magma body is flat or close to flat. If I found significant dip, then reflections may degrade rather than improve locations.

2. Compare locations when reflections have been used with locations obtained when only direct arrivals are used. This comparison emphasizes the improvement when reflections are included.

3. Interpret the new findings for V_p, Poisson's ratio (ν), and, hence, V_s as they relate to crustal composition, temperature, and possibly crustal fluid content and fluid pressure.

4. Use well-constrained focal depths to better define the limits of the seismogenic zone.

Overview of Method

I solve the joint hypocenter-velocity problem using generalized least squares inversion. The general assumption behind joint inversion is that earthquake arrival times contain information about both the event locations and the velocity model through which the seismic waves propagate. Hence, from a suite of earthquake arrival times it is possible to extract a velocity model and the hypocenter parameters of each event.

Solving the joint problem as a least squares inversion is a fairly common occurrence in network seismology. For instance *Crosson* [1976], *Aki and Lee* [1976], *Ward* [1980], and *Hawley et al.*, [1981] have all reported on the procedure. An important feature of my approach is that I use all available primary and secondary arrivals. Many previous researchers limit their data to only first arrivals and

allow the event locations to determine the phase type as either direct or critically refracted. Using my approach, phases are identified by the seismologist before data inversion. It is this prior, fixed identification which provides additional constraint to both locations and velocity model estimation.

For this project I assume a flat-layered model with constant velocities. Hence, the unknowns are V_p in all layers, Poisson's ratio (ν) in all layers, and depth to the upper surface of the magma body. To correct for near-surface velocity variations, I also solve for station corrections. Thus, I assume significant velocity variations occur only near the surface below the recording stations. The arrival time data I use in this project come from a suite of 75 earthquakes. Because I solve the joint hypocenter-velocity problem, the hypocenter parameters (latitude, longitude, focal depth, and origin time) for each event are also found. The data are both direct and reflected arrival times from the the phases P, S, S_zS, S_zP, and P_zP. Considering all parameters and data, this project involves finding nearly 320 unknowns from nearly 1500 data.

Figure 1.3, the recording geometry of a station 25 km from an event which is only 6 km deep, helps show why I chose reflected phases to improve hypocenter estimates. The direct P and S phases provide little constraint on focal depth because of the large source-to-receiver distance. However, the downgoing leg of the S_zS phase has a horizontal-to-vertical distance ratio slightly less than one, provided the reflector is 19 km deep, and the downgoing leg of the S_zP phase has a horizontal-to-vertical distance ratio much less than one. Thus, for shallow events the reflected phases can provide a constraint on focal depth estimates even though event-to-station epicentral distances are large. Figure 1.3 also shows that to successfully use reflections in location procedures the velocity model through which these phases propagate must be known. This is especially true for the reflector depth. If reflector depth is wrong, then focal depth will also be wrong.

One way to simultaneously resolve focal depth and reflector depth is illustrated in Figure 1.4, a plot of possible reflector depth-focal depth pairs for the S_zP and

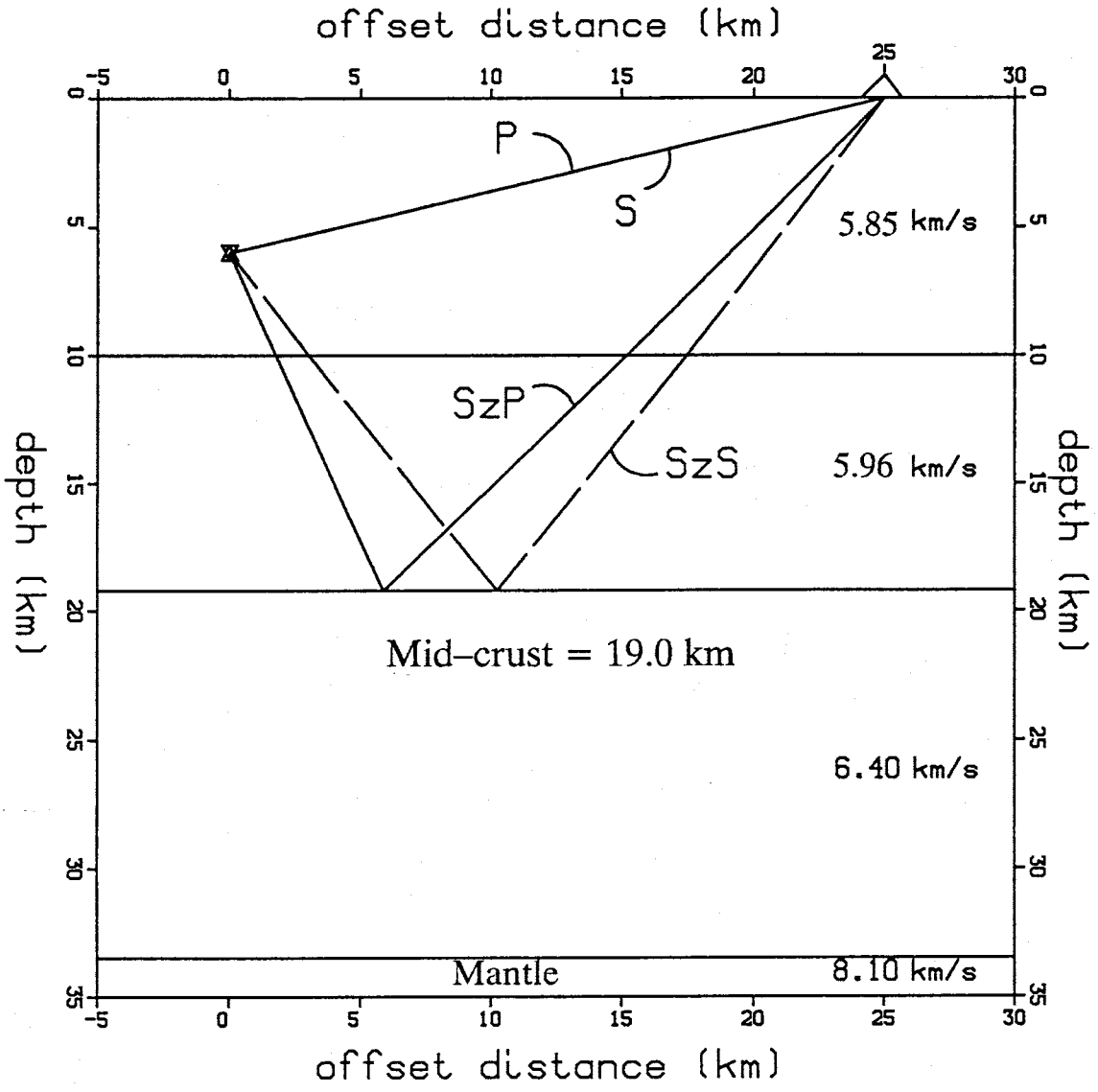

Fig. 1.3. Ray paths of direct and reflected phases emanating from a shallow earthquake (6 km focal depth) and arriving at a station 25 km from the event epicenter. Velocity model is from *Ward et al.* [1981], *Rinehart and Sanford* [1981], and *Singer* [1989].

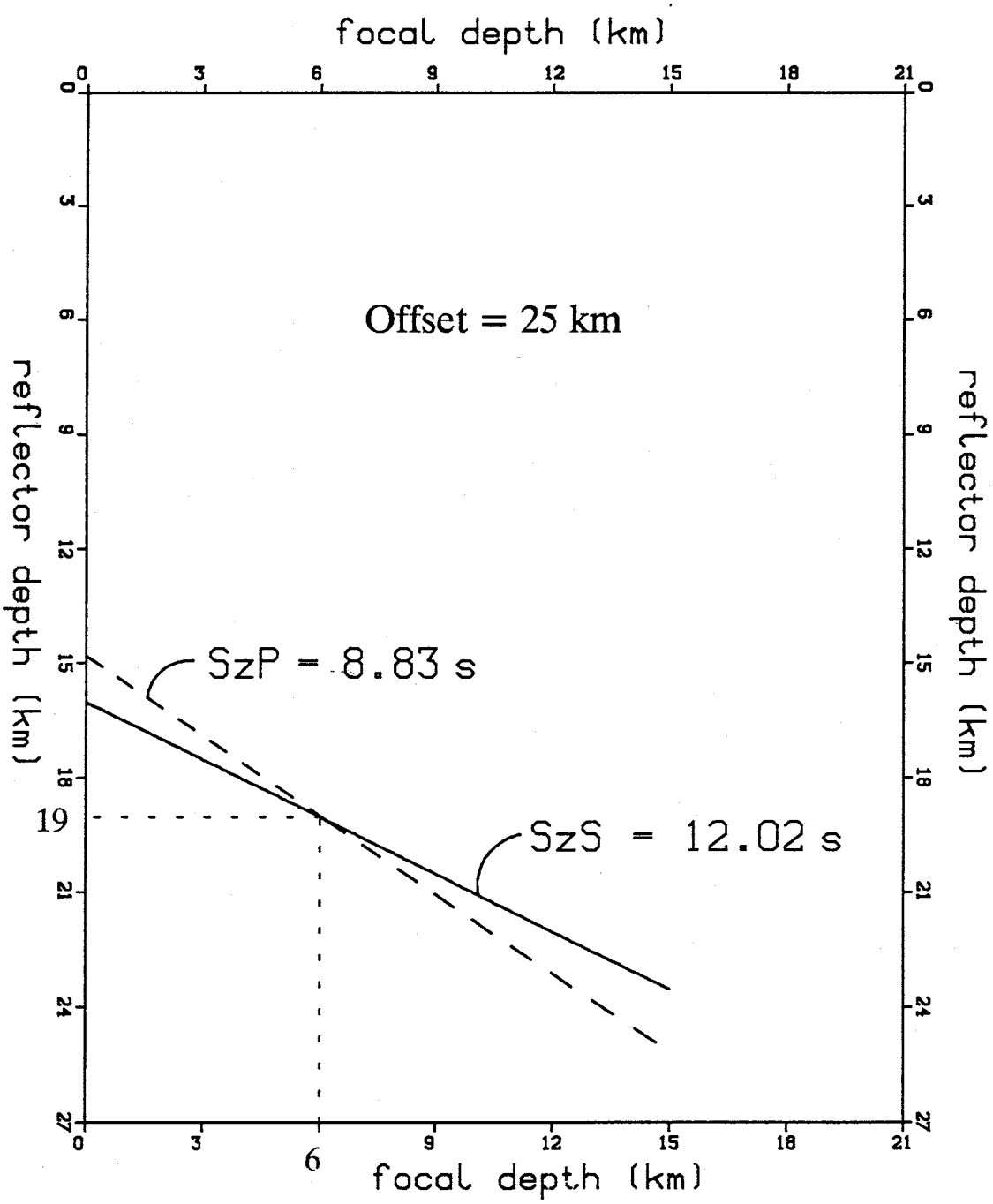

Fig. 1.4. Reflector depth versus focal depth for S_zP (dashed line) and S_zS (solid line) phases recorded at a station 25 km from the event's epicenter. Each point on the S_zP line corresponds to a recording geometry which produces a traveltime of 8.83 s, and each point on the S_zS line corresponds to a recording geometry which produces a traveltime of 12.02 s. Thus, a single phase can not resolve the trade-off between reflector depth and focal depth. But when combined, the two phases define a unique reflector depth (at 19 km) and focal depth (at 6 km) which satisfy the traveltime requirements for both arrivals.

S_zS phases shown in Figure 3. For these matched S_zP-S_zS pairs (reflections from a single event recorded at the same station), focal depth and reflector depth can be uniquely determined. That is, for any reflected phase there are many different combinations of focal depth and reflector depth which will all produce the same traveltime between source and receiver. But, if matched reflection pairs are recorded, only one unique focal depth and reflector depth combination exists which satisfies the traveltime requirements for both phases. My data set contains over 100 pairs of these matched S_zP-S_zS or S_zP-P_zP phases.

Organization and Contents of the Paper

This sub-section describes the remaining subjects covered in this paper. First, in **Geological and Geophysical Setting**, I review the general geology and geophysical signature of the Rio Grande rift, emphasizing the Socorro area. Next, in **Previous Studies** I describe in more detail previous pertinent geophysical studies. This section covers seismic investigations of the rift and surrounding provinces, including velocity, Poisson's ratio, and seismogenic zone studies. This background information is important because many of my results will be compared directly to the findings of these previous investigations. Next, in **Method** I review generalized least squares inverse theory, including eigenvalue-eigenvector decomposition, and explain the specifics of how I solve the joint hypocenter-velocity model problem. In **Synthetic Data Tests** I explain how I generated synthetic data and then used that data to test for programming errors. The tests were also necessary to determine how many events and various phases would be necessary to solve the proposed problem. Next, in **Data** I explain the nature of the final data assembled, make some general observations, and compare my data to previous researchers' data. In **Results** I present my findings, emphasizing (1) improvement in earthquake location estimates and (2) the flatness on the upper surface of the magma body. Next, in **Case Study** I apply the new location tool to the Arroyo del Coyote microearthquake swarm of 1985. This section demonstrates the usefulness of reflected phases to specific earthquake studies within the Socorro area. In **Discussion** I consider

how my findings may relate to crustal composition, heat flow, and the accumulation of magma at mid-crustal levels. I also present some guidelines for using reflections in the location process. I finish with **Summary and Conclusions** and **Suggestions for Further Studies.**

2. Geological and Geophysical Setting

Rio Grande Rift

The Rio Grande rift, recognized as a major continental rift system in the 1970's [*Chapin*, 1979], extends south from central Colorado into Chihuahua, Mexico as a series of en echelon grabens (Figure 2.1). At least 1000 km long, the rift can be divided into three major segments The northern segment extends from near Leadville to Alamosa and is characterized by a north-northwest trend paralleling the late Paleozoic and Laramide structural grain. Some researchers extend the rift north from Leadville, across northern Colorado, and into Wyoming [*Eaton* 1986], but most definitions place the northern limit of the rift in central Colorado. The central segment, from Alamosa to Socorro, is characterized by a series of en echelon basins trending north-northeast and separated by northeast-trending basement lineaments. Extending south from Socorro, the southern segment is a series of north-trending parallel basins and ranges with a width approximately two and a half times the width of the central and northern segments.

Rifting began in the southern segment around 32 Ma, closely following the large ash flow eruptions associated with the Datil-Mogollon volcanic field of southwest New Mexico. Early rift volcanism was a mixture of basaltic-andesites interbedded with silica-rich ash flows. Rifting progressed to the north by around 27 Ma [*Chapin,* 1979]. Synrift sediments and volcanics are preserved from 26 Ma to the present, indicating rifting started as a depression and not doming followed later by a depression. Rift volcanism was widespread until a lull in activity occurred between 20 Ma and 13 Ma. Volcanic activity increased following the lull, but volcanism changed from dominantly basaltic-andesites to a mixture of basalts and rhyolites. By examining the orientations of dikes and radiometric age-dating, *Aldrich et al.* [1986] found that the stress orientation of the rift has remained east-west throughout the rift process, while stress orientations outside the rift, but within New Mexico, have changed. They attribute the constant stress orientation of the rift to control by earlier Laramide structural grain.

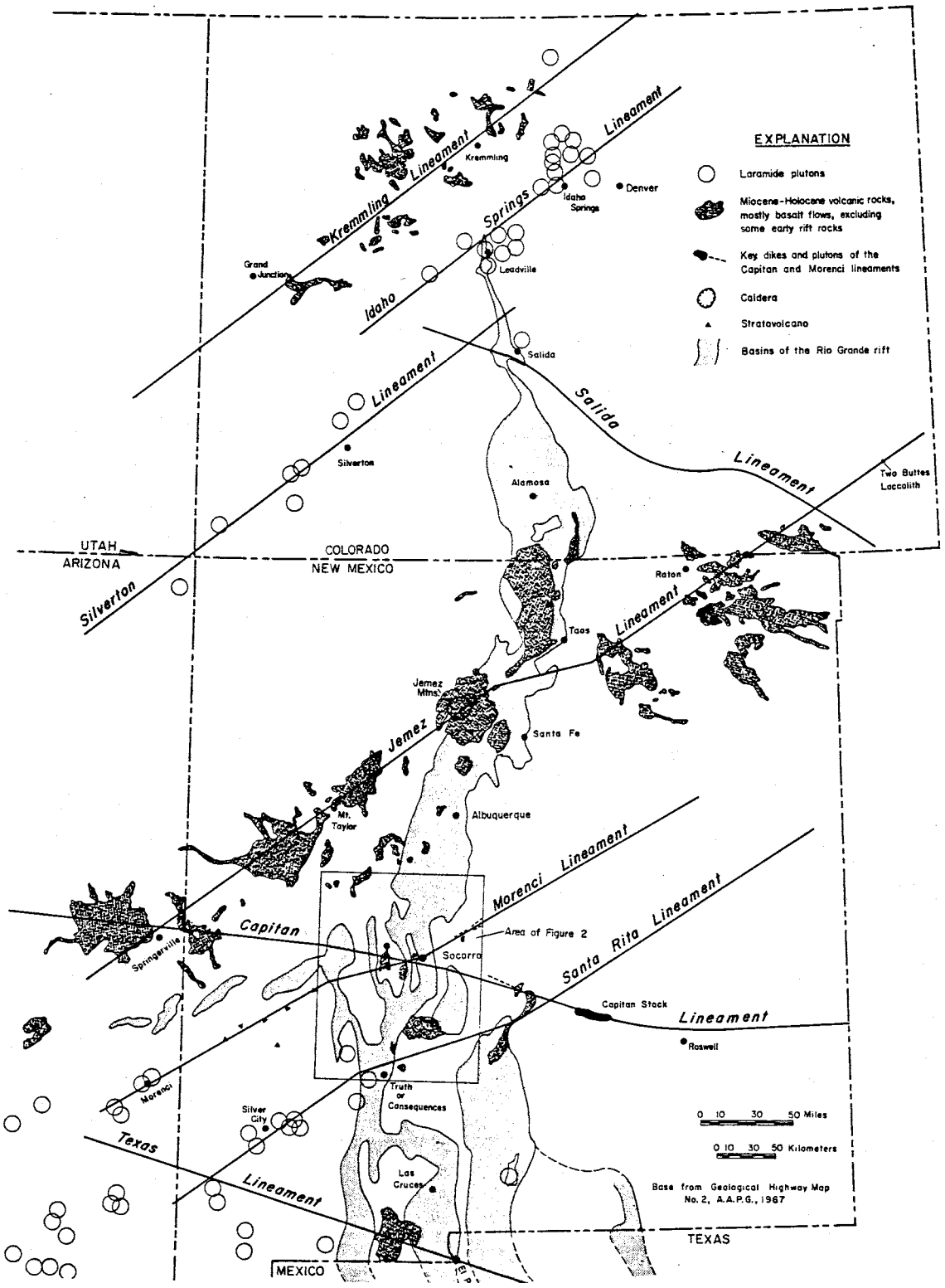

Fig. 2.1. The Rio Grande rift from central Colorado to Mexico. Note the Morenci lineament crossing the Socorro area (boxed region). From *Chapin et al.* [1978].

Socorro Area

The study area, the central rift around Socorro, is bounded on the west by the Colorado Plateau province, on the southwest by the southern Basin and Range province, and on the east by the Great Plains and southern Rocky Mountains provinces (Figure 1.1). Rifting began in the Socorro area 29 Ma [*Chapin*, 1978]. Near Socorro, the Morenci lineament (Figure 2.1), a basement feature trending southwest-northeast from Arizona into central New Mexico, cuts the rift [*Chapin*, 1978]. The lineament may also have influenced the development of the Socorro accommodation zone; an approximately 2 km wide boundary between two domains of domino style fault blocks with opposite tilts on opposite sides of the zone [*Chapin*, 1989]. The Socorro accommodation zone appears to be related to at least six caldera centers ranging in age from approximately 24 to 32 Ma [*Chapin*, 1989]. Between pyroclastic eruptions associated with the caldera centers, significant volumes of mafic lavas were erupted. Bimodal volcanism has continued in the Socorro area, the most recent eruption occurring 3.6 Ma.

Seismically the Socorro area is the most active in New Mexico [*Sanford et al.*, 1979]. Many of the earthquakes occur in swarms which may be associated with small volumes of magma in the upper crust [*Sanford and Einarson*, 1982]. One swarm area which may indicate upper-crustal magma injection is about 15 km southwest of Socorro. *Ward* [1980] found a low upper-crustal P velocity in this area. In approximately the same area, *Carpenter and Sanford* [1985] found three regions of low Q. *Chapin* [1989] points out that the Socorro accommodation zone crosses through this swarm area (Figure 2.2).

The Socorro area has had large earthquakes occurring with swarms. Two notable swarms, each with many felt events and each lasting several months, occurred during the years 1904 and 1906-1907 [*Sanford et al.*, 1977]. The 1906-1907 swarm produced almost daily felt events and at times shocks were felt as frequently as one each hour. This swarm contained three large shocks which are estimated to have reached a maximum intensity VIII on the Rossi-Forel scale [*Sanford and*

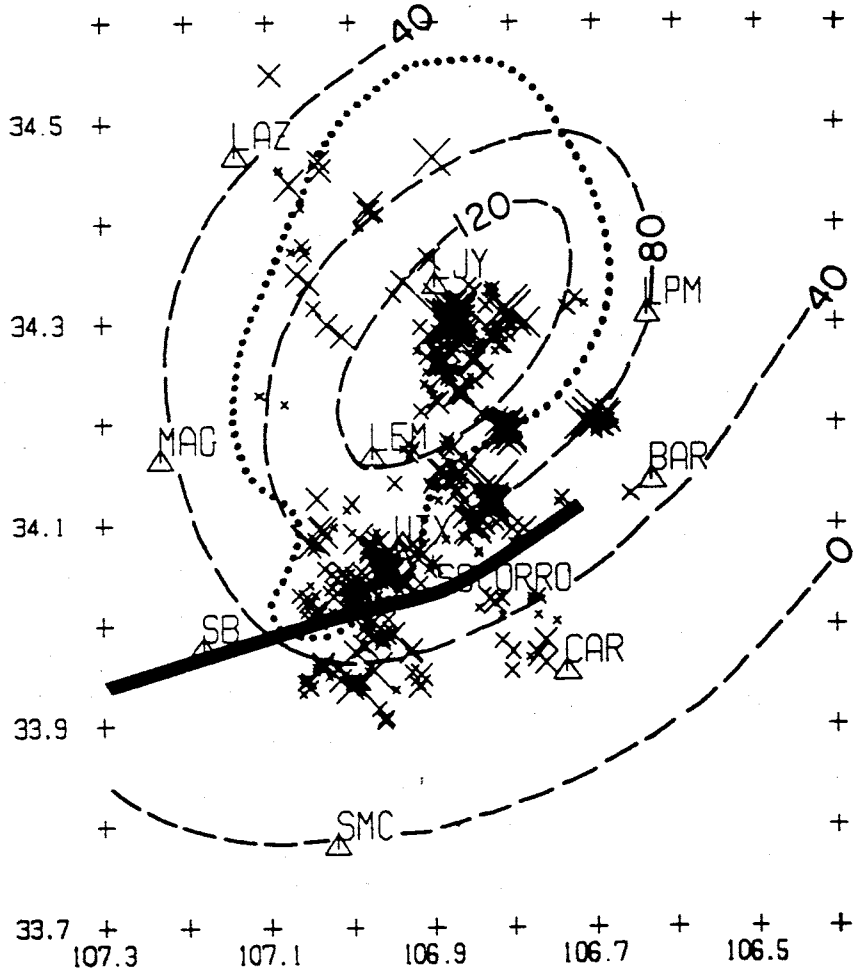

Fig. 2.2. The Socorro accommodation zone (bold line) in relation to the swarm area between stations SB and WTX. Earthqaukes from between September, 1982 and December, 1985 are shown with X's (from *Sanford et al.*, 1990), outline of the magma body is the dotted line (from *Rinehart et al.* 1979), and labeled contours are surface uplift in millimeters (from *Larson and Reilinger* 1986).

Einarson, 1982]. *Sanford et al.* [1977] compared this swarm to the Matsushiro swarm of 1965-1967. The cause of the Matsushiro swarm has been attributed to magma movement in the crust by *Stuart and Johnson* [1975].

Despite the possible presence of upper crustal magma near Socorro, *Barroll and Reiter* [1990] demonstrated that heat flow extremes between the Socorro Mountain block and La Jencia basin (490 mW m^{-2} in Socorro Mountain and less than 50 mW m^{-2} only 10 km away in La Jencia basin) can be explained by ground water flow. They do not rule out the possible presence of magma, but show that ground water flow is necessary to produce such extremes. They estimate average heat flow for the Socorro area at 90 mW m^{-2}.

3. Previous Studies

Overview

This section reviews previous crustal and upper mantle studies from central New Mexico and surrounding areas. These areas include the Great Plains province, the Colorado Plateau, the southeastern Basin and Range, and the Rio Grande rift (Figure 1.1). Researchers have used surface wave, critically refracted head wave, reflected, and direct arrival data in prior investigations. The surface wave and head wave data have been used to study velocity distribution within the crust and upper mantle. The reflection studies, utilizing arrivals off the magma body, can be divided into two categories: (1) investigations using microearthquake data and (2) investigations using surface-source Vibroseis data. In addition to providing velocity information, reflections have been used to map the upper surface of the magma body and investigate the internal structure of the magma body. The direct arrivals have been used to estimate upper crustal velocity structure in the Socorro area and are used routinely to locate earthquakes in central New Mexico. The depths of located events provide some constraint on the dimensions of the seismogenic zone. Direct arrivals have also been used to estimate Poisson's ratio within the Rio Grande rift.

The investigations discussed below are identified on maps and results are compiled in tables. Since the present study concerns the upper and middle crust, I present more detail on the upper 20 km of crust than on the lower crust and upper mantle.

Surface Wave Studies

Surface wave investigations have been conducted within the Rio Grande rift both parallel and transverse to the rift axis. In addition, surface waves have been used to investigate provinces adjacent to the rift (Figure 3.1). Table 3.1 summarizes these investigations. The studies rely on long period Rayleigh wave data from earthquakes or explosions. The data are commonly processed to identify phase and

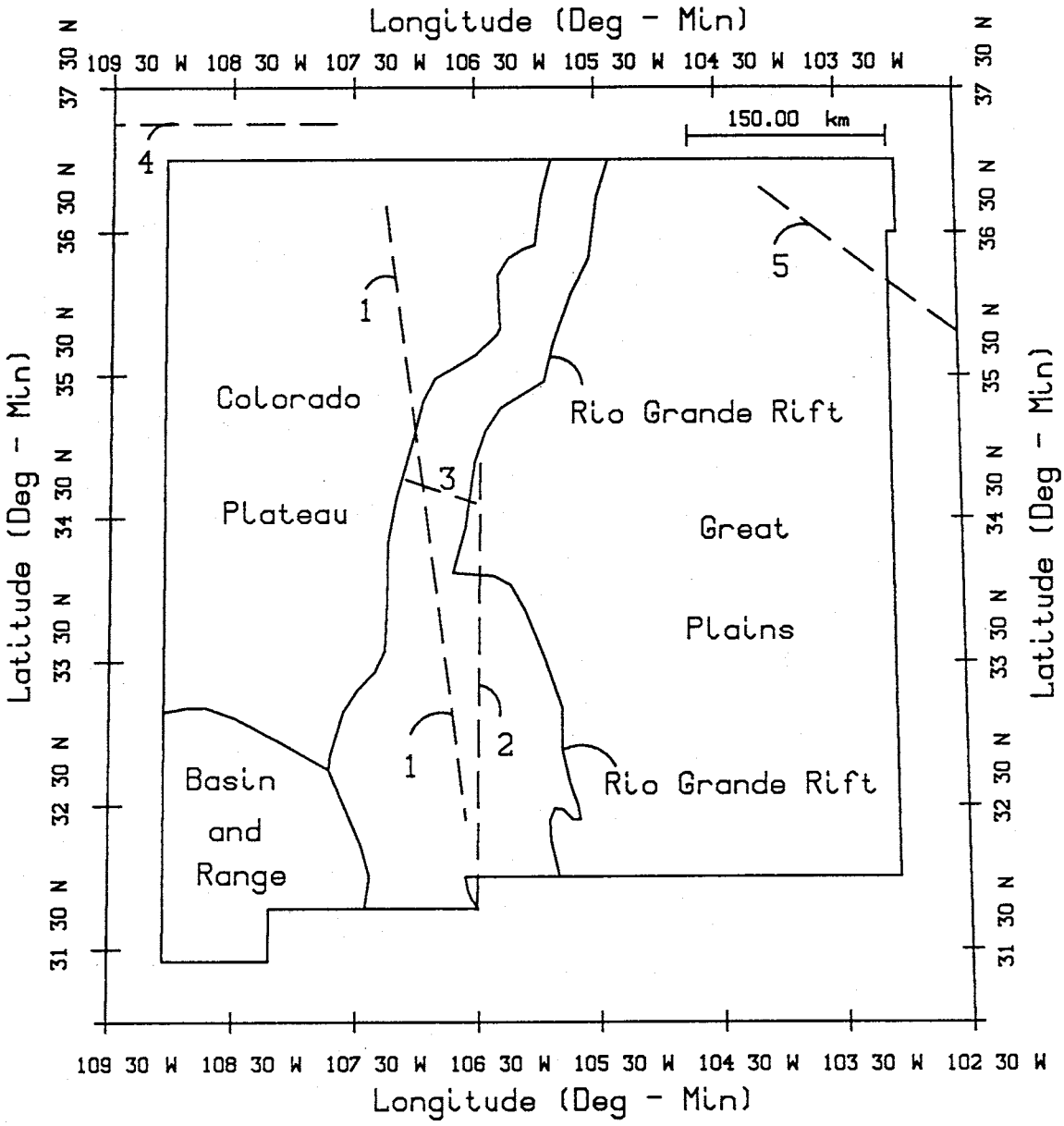

Fig. 3.1. Location of surface wave studies within the Rio Grande rift and adjacent provinces. See Table 3.1 for details.

TABLE 3.1. Surface Wave Investigations
Rio Grande Rift and Adjacent Provinces

Investigators and Year	Province	Method	V_s (km s^{-1})	Depth Range (km)
1. Keller et al., 1979	Rio Grande rift, GASBUGGY to Las Cruces	Phase and group velocity inversion	3.4 3.6 3.7 4.4	2 - 20 20-25 25-35 mantle
2. Sinno and Keller, 1986	Rio Grande rift, El Paso to Albuquerque	Phase and group velocity inversion	3.49 3.64 4.25	1.4 - 19.7 19.7-31.8 mantle
3. Schule et al., 1986	Rio Grande rift, Albuquerque-Belen Basin	Phase velocity inversion	3.31 3.10 3.39 3.70 3.34 3.02	2.65 - 3.65 3.65 - 6.65 6.65 - 8.65 8.65 - 13.65 13.65 - 16.65 16.65 - 19.65
4. Keller et al., 1979	Colorado Plateau	Phase and group velocity inversion	3.6 3.7 4.5	1.3 - 16.2 16.2 - 45.6 mantle
5. Keller et al., 1979	Great Plains	Phase and group velocity inversion	3.5 3.8 3.9 4.6	3.0 - 15.0 15.0 - 39.0 39.0 - 48.0 mantle

group velocities that are inverted for crustal and upper mantle shear wave velocity structure. Using surface wave data, generally, only shear velocity is treated as an unknown; flat layer boundaries and values for Poisson's ratio and density are assumed and held constant during the inversion.

Surface wave studies tend to be low in velocity and depth resolution. For example, *Sinno et al.* [1986] present resolving kernals that show mid-crustal velocities tend to be averaged values over 5 to 8 km of crust. *Schlue et al.* [1986] present resolving kernals showing their velocity estimates below 20 km depth are almost entirely initial-model dependent. Despite this lack of resolution, the surface wave studies shown in Table 3.1 provide the majority of crustal and upper mantle shear velocity information within New Mexico.

Within the Rio Grande rift shear velocities derived from surface wave studies tend to be slightly lower than velocities from the Colorado Plateau and Great Plains. Beneath basin fill and down to mid-crustal depths rift velocities have generally been reported as between 3.4 and 3.5 km s^{-1} (Table 3.1). *Schlue et al.* [1986] report low velocity layers from the Albuquerque-Belen basin. These layers occur between 3.65 and 6.65 km (3.10 km s^{-1}) and between 16.65 and 19.65 km (3.02 km s^{-1}). *Schlue et al.* also report a high velocity layer between 8.65 and 13.65 km (3.70 km s^{-1}). They hypothesize that the deeper low velocity layer may be associated with the northern end of the Socorro magma body.

Refraction Studies

Refraction studies in New Mexico (Figure 3.2) can be placed into three general categories. First are studies involving ray paths that do not cross or travel within the Rio Grande rift. Second, are studies involving ray paths that have crossed the rift and have also traveled through other tectonic provinces. The third category are studies involving ray paths that have traveled and been recorded entirely within the rift. Because the rift boundaries are poorly defined, this last category of study is difficult to identify. Table 3.2 summarizes refraction studies.

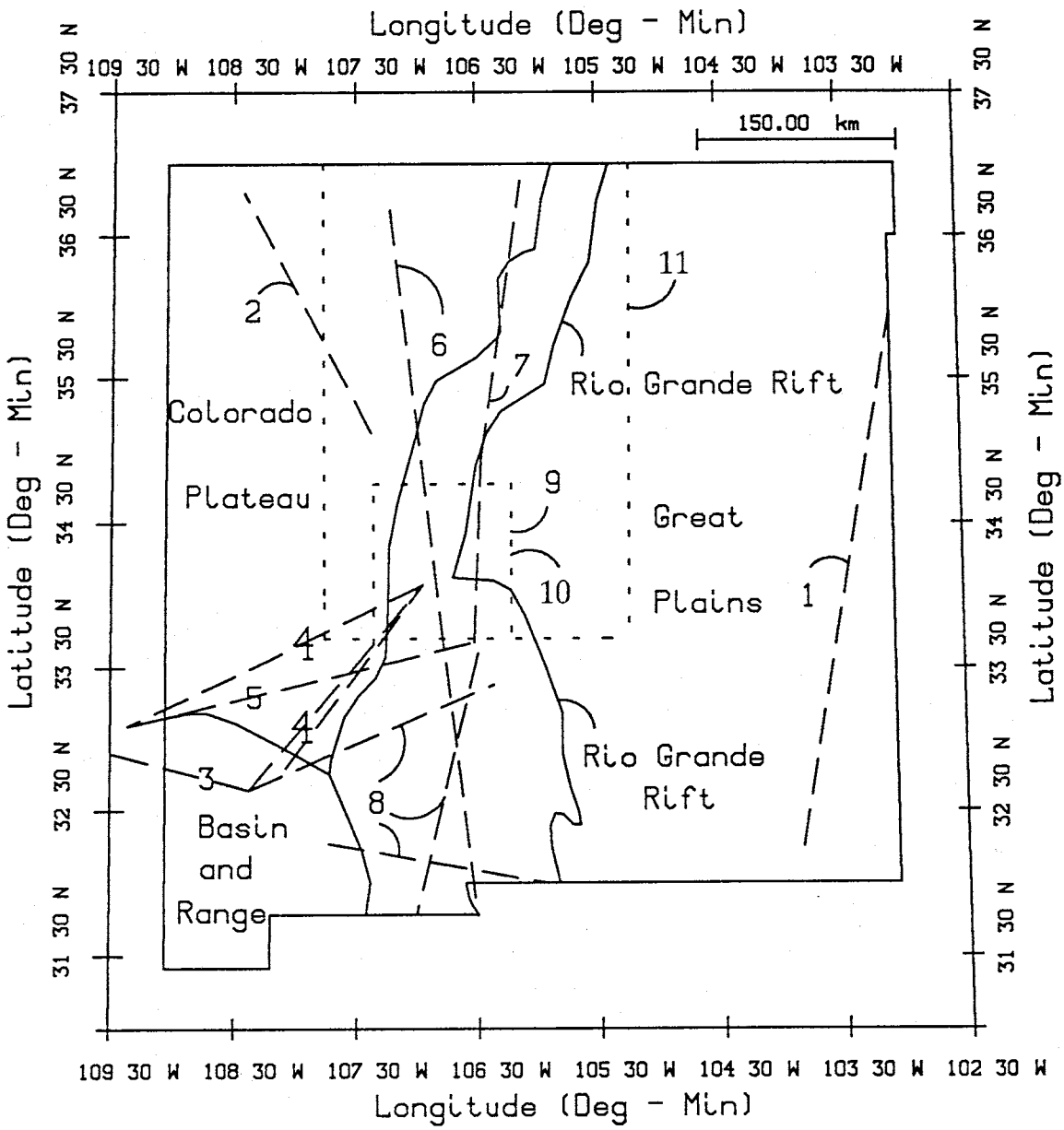

Fig. 3.2. Location of refraction studies within the Rio Grande rift and adjacent provinces. See Table 3.2 for details.

TABLE 3.2. Refraction Investigations
Rio Grande Rift and Adjacent Provinces

Investigators and Year	Province	Method	V_p (km s^{-1})	Depth Range (km)
1. Stewart and Pakiser, 1962	Great Plains	Conventional refraction interpretation - unreversed	4.93 6.14 6.72 7.10 8.23	0.0 - 4.2 4.2 - 19.2 19.2 - 31.1 31.1-50.8 mantle
2. Jaksha and Evans, 1984	Colorado Plateau	Conventional refraction interpretation - reversed, time term analysis	3.6 6.1 7.00 8.0	0.0 - 3.0 3.0 - 31.0 31.0 - 48.0 mantle
3. Gish et al., 1981	Southeastern Basin and Range	Synthetic seismograms, inversion of head waves and reflections - reversed	6.10 6.65 7.80	0.0 - 15.0 15.0 - 28.0 mantle
4. Dee, 1973	Rio Grande rift and southwest New Mexico	Conventional refraction interpretation - unreversed	6.2 8.1	0.0 - 34.2 mantle
5. Jaksha, 1982	Rio Grande rift and southwest New Mexico	Conventional refraction interpretation and $t^2 - x^2$ analysis - reversed	4.0 6.0 6.5 8.0	0.0 - 3.0 3.0 - 25.0 25.0 - 34.0 mantle
6. Toppozada and Sanford, 1976	Rio Grande rift - GASBUGGY to Las Cruces	Conventional refraction interpretation - reversed	5.80 6.15 7.9	0.0 - 18.6 18.6 - 39.9 mantle
7. Olsen et al., 1979	Rio Grande rift - central and northern New Mexico -	Inversion of head wave and reflected arrivals - unreversed	4.3 6.0 6.4 7.6	0.0 - 3.2 3.2 - 21.4 21.4 - 33.7 mantle
8. Sinno et al., 1986	Southern Rio Grande rift - 3 lines	Synthetic seismograms, 1 line reversed, 2 lines unreversed	5.93 6.12 6.67 7.70	5.0 - 12.0 12.0 - 21.0 21.0 - 30.0 mantle

TABLE 3.2. Refraction Investigations
Rio Grande Rift and Adjacent Provinces - Continued

Investigators and Year	Province	Method	V_p (km s^{-1})	Depth Range (km)
9. Carlson, 1983	Rio Grande rift in Socorro area	Time term analysis of P_g, P^*, and P_n	5.76 6.25 6.48 8.08	2.5 - 6.0 6.0 - 19.0 19.0 - 32.5 mantle
10. Singer, 1989	Rio Grande rift in Socorro area	Time term analysis of P_g, P^*, and P_n	5.95 6.40 8.14	2.5-10.0 19.4 - 33.5 mantle
11. Murdock and Jaksha, 1981	Rio Grande rift - central and northern New Mexico	Time term analysis of P_n	8.0	41.6 (mantle) beneath Albuquerque

Most investigators have used conventional refraction lines with large explosions (often from open pit mines) as energy sources. These surveys commonly record P_g (the Phanerozoic-Precambrian head wave), P_n (the crust-mantle head wave), and occasionally P^* (a mid-crustal head wave). Some investigators have incorporated wide-angle reflections from the mid-crust and the crust-mantle boundary into refraction interpretations. Other investigators have utilized time-term techniques applied to seismic network data. While reading about these studies, it should be remembered that head wave investigations provide velocity information from below interfaces with significant velocity increases. They do not detect low velocity zones. All head wave velocities reported below are for compressional waves.

East of the Rio Grande rift *Stewart and Pakiser* [1962] investigated crustal velocity structure of the Great Plains province using the GNOME underground nuclear explosion. The north-trending line used in the study was unreversed. They interpreted the data to infer a four-layer crust with velocities increasing from 4.9 to 7.1 km s^{-1}. They found a P_g velocity of 6.14 km s^{-1}, and below 19.2 km depth velocity increased to 6.72 km s^{-1}. The total crustal thickness found was approximately 51 km, and P_n velocity was estimated as 8.2 km s^{-1}.

Within the Colorado Plateau province *Jaksha and Evans* [1984] calculated a 48 km thick crust with velocities increasing from 3.6 to 7.0 km s^{-1}. Both upper and mid-crust velocity was estimated at 6.1 km s^{-1}. They found velocity in the lower crust to be 7.00 km s^{-1}, and P_n velocity was estimated at 8.0 km s^{-1}. Their velocities were based on a reversed refraction line 220 km long and time-term analysis of P_n arrivals recorded on a seismograph network in northwest New Mexico. Their results agree well with the findings of *Roller* [1965].

In the southern Basin and Range province of southeast Arizona and southwest New Mexico *Gish et al.* [1981] report a crustal thickness of 28 km with velocities increasing from 6.10 to 6.65 km s^{-1}. They calculated a P_n velocity of 7.8 km s^{-1}. For the region they classified as the Transition Zone, between the southern Basin

and Range and the Colorado Plateau, *Gish et al.* estimated a 32 km thick crust with velocities increasing from 5.8 to 6.5 km s^{-1}. For this area they found a P_n velocity of only 7.6 km s^{-1}. All findings were based on a 260 km long, reversed line between open pit copper mines.

There have been several studies involving wave paths partially within the rift. Three of these studies are mentioned here. *Dee* [1973] recorded open pit copper mine blasts from southwestern New Mexico and southeastern Arizona using stations within the Socorro area. Picking only first breaks, he identified critically refracted phases P_g and P_n. *Dee's* single layer crustal interpretation found an average crustal thickness of 34.2 km and velocity of 6.2 km s^{-1} overlying mantle with a velocity of 8.1 km s^{-1}. Station spacing used in this study did not allow for the detection of mid-crustal, P^*, first arrivals.

Covering a geographical area similar to *Dee, Jaksha* [1982] interpreted a reversed refraction profile between Morenci, Arizona and the White Sands Missile Range in central New Mexico. *Jaksha* found a 6.0 km s^{-1} P_g velocity in the upper crust. The line was reversed and some reflections were included in the interpretation.

Toppozada and Sanford [1976] interpreted refraction data from the 1967 GASBUGGY underground nuclear explosion in northern New Mexico. This 548 km long line began on the Colorado Plateau before entering the rift near Albuquerque. They interpreted a two-layer crust with velocities increasing from 6.15 to 6.75 km s^{-1} and a mantle velocity of 8.1 km s^{-1}. The upper-crustal velocity dropped to 5.8 km s^{-1} within the rift, and, after correcting for dip using independent earthquake data, mantle velocity was revised to 7.9 km s^{-1}. Average depth to the mid-crust was 19 km and average depth to the mantle was 40 km.

The final category of refraction studies are those using data exclusively from within the rift. *Olsen et al.* [1979] used a large chemical blast to record a 350 km long line northward from central New Mexico. They found a crustal thickness of 33 km and velocity in the mantle of only 7.6 km s^{-1} along the unreversed line. Upper

crustal velocity was reported as 6.0 km s^{-1}

Sinno et al. [1986] have interpreted refraction data from three lines in south-central New Mexico. They identified several critically refracted phases and several far-offset reflections. They concluded that the southern rift has only a 27 to 28 km thick crust and a P_n velocity of 7.7 km s^{-1}. They reported a velocity of 6.12 km s^{-1} between 12.0 and 21.0 km depth and a velocity of 5.93 km s^{-1} between 5.0 and 12.0 km depth. Although these values are similar to those reported by *Gish et al.* [1981] for the southeastern Basin and Range, *Sinno et al.* believe their results show the southern rift is a distinctly separate province from the adjacent southern Basin and Range.

Refraction studies concerning the area directly beneath the Socorro network have been completed by *Carlson* [1983] and *Singer* [1989]. Both researchers interpreted first arriving phases using time-term analysis of earthquake and explosion data recorded on the Socorro network. *Singer* used modified time-term analyses to obtain a general crustal model from P_g, P^*, and P_n arrivals and investigated the possibility of a dipping crust-mantle interface and velocity anisotropy. *Singer* found an average velocity of 5.95 km s^{-1} between 2.5 and 10.0 km and a velocity of 6.4 km s^{-1} beneath a velocity interface at approximately 19.4 km. However, because of poor resolving power of the P^* arrivals, the mid-crustal interface could not be well defined. He found an average depth to the mantle of 33.5 km and a P_n velocity of 8.14 km s^{-1}.

Reflected Phase Studies

Several investigators have used reflected phases recorded by seismic networks in the Socorro area. *Sanford and Holmes* [1961] noted the existence of anomalous phases, suggested they could be reflections, but did not attempt to identify them. Efforts in the 1960's and 1970's were concentrated on phase identification, recognition of the strong mid-crustal reflector as magma, and mapping the lateral extent of the magma body. Table 3.3 summarizes these early studies along with more recent

TABLE 3.3. Microearthquake Reflected Phase Investigations
Socorro Area of Rio Grande Rift

Investigators and Year	Method	Data Types	Primary Results
1. Sanford and Long, 1965	Amplitude versus offset and travel time modeling	S_zS and S_zP reflections	Identified S_zS and S_zP as reflections
2. Sanford et al., 1973	Arrival time modeling	S_zS and S_zP reflections	Reflector near 18 km depth
3. Sanford et al., 1977	Reflection point mapping	S_zS and S_zP reflections	Reflector is magma and first map constructed
4. Rinehart et al., 1979	Refection point mapping	S_zS reflections	Areal extent of magma body 1700 km^2
5. Rinehart and Sanford, 1981	Travel time inversion	S_zS reflections	V_s of 3.41 ± 0.03 km s^{-1} to the magma body at 19.2 ± 0.6 km, also a V_s of 3.44 ± 0.03 km s^{-1} between 10 and 19.2 km
6. Ake and Sanford, 1988	Digital signal processing and forward modeling	S_zS and P_zP reflections	Internal structure of magma body examined
7. Gridley, 1989	Reflection point mapping	S_zS reflections	Magma body areal extent revised

investigations. All studies mentioned in this sub-section have been undertaken within the Socorro area (Figure 1.1). *Sanford and Long* [1965] first identified two strong phases arriving after direct S as the reflections S-to-P (S_zP) and S-to-S (S_zS). *Sanford et al.* [1973] attributed these phases to an interface between rigid and non-rigid crust. *Sanford et al.* [1977] concluded this interface was the top of a sill-like magma body at near 19 km depth and mapped it using reflection points. *Rinehart et al.* [1979] remapped the magma body and estimated its areal extent at a minimum of 1700 km^2. *Gridley* [1989] updated the mapped outline of the Socorro magma body by carefully searching microearthquake seismograms recorded on the Socorro network between 1982 and 1988. Using this new data set and hypocenter coordinates from the earthquake location program HYPO71, the southwest and southeast sides of the magma body were extended relative to the mapping of *Rinehart et al.* [1979]. *Ake and Sanford* [1988] provide a detailed model of the internal structure of the Socorro magma body and, through signal processing of digital data, present strong evidence for the presence of magma.

Rinehart and Sanford [1981] have been the only previous researchers to use the magma body microearthquake reflection times in an inversion. Using hypocenter parameters obtained with the earthquake location scheme of *Ward* [1980], they used the S_zS phase to invert for S velocity structure and a depth to the magma body. Several models were fit to the observations by dividing the crust into different layers and areas. They found that using only S_zS data, V_s and depth to the magma body could not be simultaneously resolved. However, using a best-fitting reflector depth of 19.2 $\pm$0.6 km they found a V_s of 3.41 km s^{-1} from the surface to the reflector. They also found a V_s of 3.44 km s^{-1} between 10 and 19.2 km.

In 1975 and 1976 COCORP acquired 155 kilometers of Vibroseis data in the Socorro area (Figure 1.2). Interpretation of these lines also revealed an unusually strong reflector near 19 km depth and attributed it to mid-crustal accumulations of magma. For details of the initial interpretations of these lines see *Brown et al.* [1979] and *Brown et al.* [1980]. *Brocher* [1981] used the COCORP data to model

the internal structure of the magma body and *de Voogd et al.* [1988] have interpreted the lines following data reprocessing, inferring that rift-bounding faults penetrate no deeper than 13 km.

Direct Arrival Studies

Direct arrival data have been, and are presently being used by New Mexico Tech investigators to study the many microearthquakes recorded with the Socorro network. Figure 3.3 identifies and Table 3.4 summarizes these studies. *Ward* [1980] used direct P arrivals in an inversion to study upper-crustal velocity structure near Socorro. He found a half-space, upper-crustal velocity of 5.85 km s^{-1} and calculated a set of station corrections for earthquake location purposes. Dividing the crust into volumes, he found an anomalously low-velocity block southwest of Socorro, which he attributed to magma in the upper crust. *Ward's* half-space model has been used to locate Socorro-area earthquakes since 1980.

King [1986] used earthquake locations estimated with direct arrivals to study hypocenter distributions in the Socorro area. He found the seismogenic zone was between 4 and 12 km beneath the surface. However, he also concluded that if only direct arrivals were used, focal depth estimates were poorly constrained, and hence the dimensions of the seismogenic zone could not be well constrained. *King* suggested incorporating reflections into the location process to better constrain focal depth estimates.

Within the rift, Poisson's ratio (ν) has been studied between Socorro and Albuquerque, in the Socorro area, and in north-central New Mexico. All studies relied on direct P and S phases emanating from local microearthquakes. Thus, these studies examined ν only within the seismogenic zone (the upper 10 to 12 km of crust). *Sakdejayont* [1974] found an average ν of 0.217 between Socorro and Albuquerque using events between stations SNM and ALQ. Both *Caravella* [1976] and *Fender* [1978] obtained values for ν from the immediate Socorro area. *Caravella* found ν of 0.262 and *Fender* found a value of 0.251. In the Valles Caldera

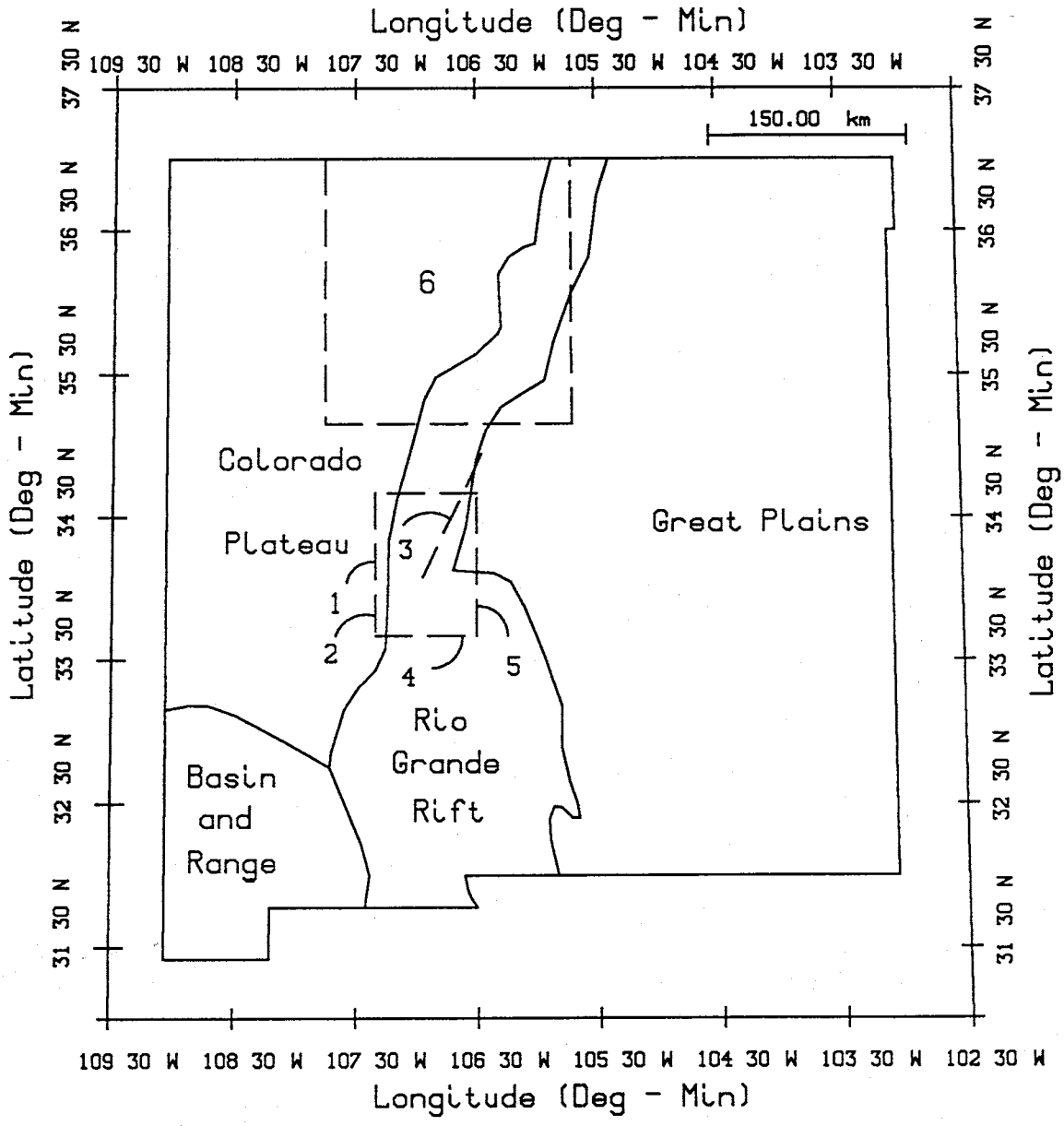

Fig. 3.3. Location of direct arrival studies within the Rio Grande rift. See Table 3.4 for details.

TABLE 3.4. Direct Arrival Investigations Including Poison's Ratio (ν) Studies Within The Rio Grande Rift

Investigators and Year	Method	Data Types	Primary Results
1. Ward *et al.* 1981,	Arrival time inversion	Direct P arrivals from local micro-earthquakes	Halfspace V_p of 5.85 $\pm$0.02 km s^{-1}, plus a 3-d velocity model of crustal blocks
2. King, 1986	Hypocenter cross sections and histograms	Direct P and S arrivals from local micro-earthquakes	Seismogenic zone between 4 and 12 km
3. Sakdejayont, 1974	$S-P$ times from 32 earthquakes occuring between Socorro and Albuquerque	Direct P and S arrivals recorded at stations SNM and ALQ	$\nu = 0.217 \pm 0.012$
4. Caravella, 1976	Wadati diagrams from 50 microearthquakes recorded in the Socorro area	Direct P and S arrivals	$\nu = 0.262 \pm 0.034$
5. Fender, 1978	Wadati diagrams from 294 microearthquakes recorded in the Socorro area	Direct P and S arrivals	$\nu = 0.251 \pm 0.052$
6. Carpenter and Cash, 1988	Wadati diagrams from 26 microearthquakes recorded in the Valles Caldera area	Direct P and S arrivals	$\nu = 0.25$

area of north-central New Mexico *Carpenter and Cash* [1988] found an average ν of 0.25.

Previous Work Summary

Figure 3.4 indicates the locations of the generalized crustal cross sections shown in Figures 3.5 and 3.6. These cross sections help summarize many of the investigations discussed above. Within the rift both P and S velocities in the upper crust are slightly lower than the adjacent Great Plains, southeastern Basin and Range, and Colorado Plateau provinces. The rift upper crustal P velocities have been reported between 5.80 and 5.95 km s^{-1} and S velocities have been estimated between 3.40 and 3.50 km s^{-1}. These values contrast with P velocities of 6.00 to 6.15 km s^{-1} and S velocities of 3.50 to 3.60 km s^{-1} outside the rift. The low rift velocities from the upper crust are probably caused by increased faulting and fracturing associated with rifting.

Crustal thicknesses of the central Colorado Plateau and the Great Plains are around 50 km, while the crustal thickness of the rift varies from near 30 km in the southern rift to over 40 km in north-central New Mexico (Figure 3.5). The depth to the mantle for the southeastern Basin and Range and what is probably the southernmost Colorado Plateau is similar to the depth beneath the Socorro area of the rift, about 30 to 34 km (Figure 3.6). P_n velocities within the rift from northern and central New Mexico are similar to P_n velocities of the Great Plains and Colorado Plateau, between 8.00 and 8.14 km s^{-1}. P_n velocities for the southern rift and southeastern Basin and Range are lower, ranging between 7.70 and 7.80 km s^{-1}. The thinned crust and lower velocities in the southern rift and southeastern Basin and Range indicate that rifting has probably been more extensive in southern New Mexico than northern and central New Mexico.

It is important to note here that I am studying the Socorro-area velocity model down to mid-crustal depths (19 to 20 km). The model parameters I am estimating are V_p, Poisson's ratio, and the depth to the magma body's upper surface. Beneath

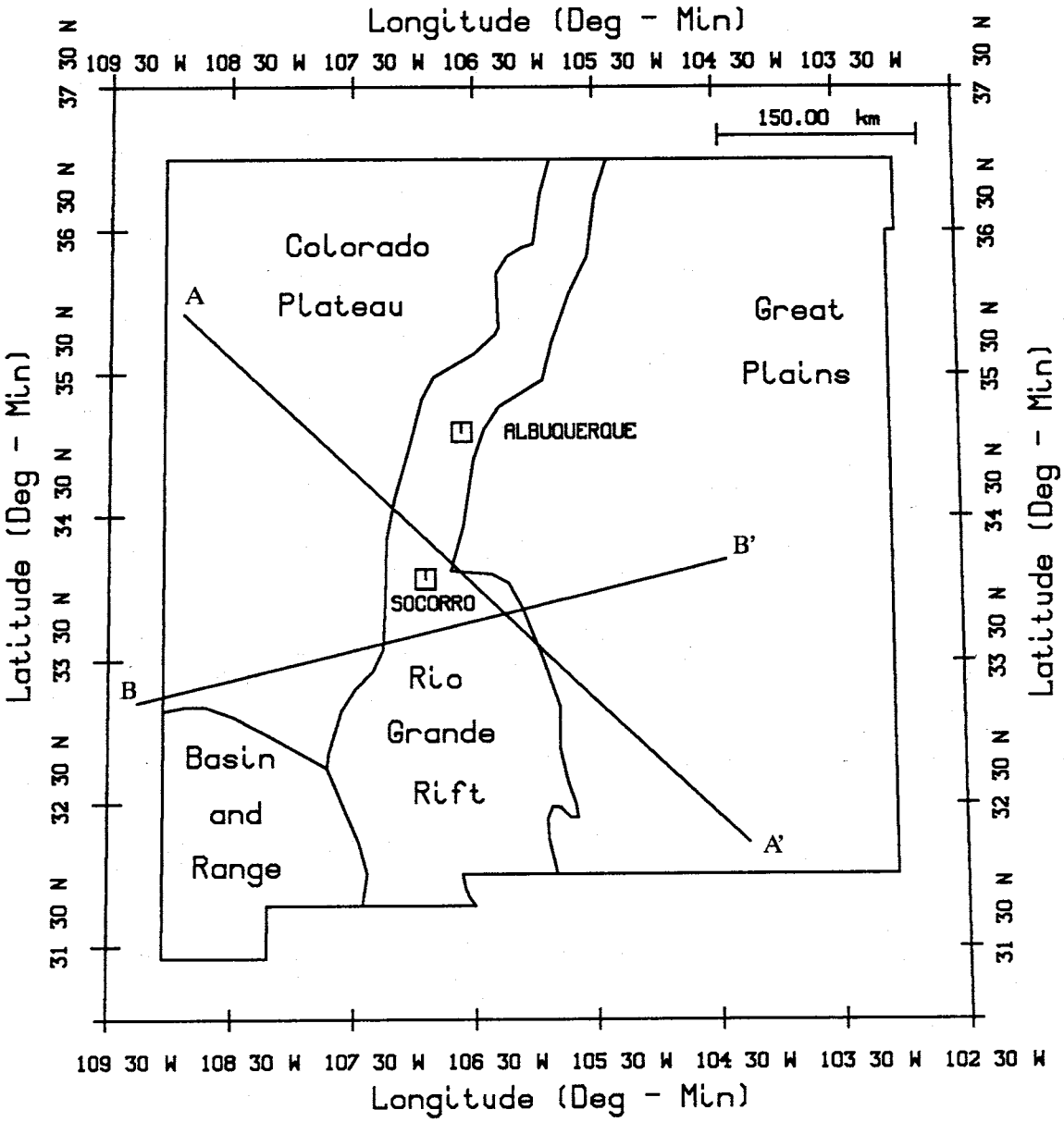

Fig. 3.4. Locations of generalized crustal cross sections AA' and BB'.

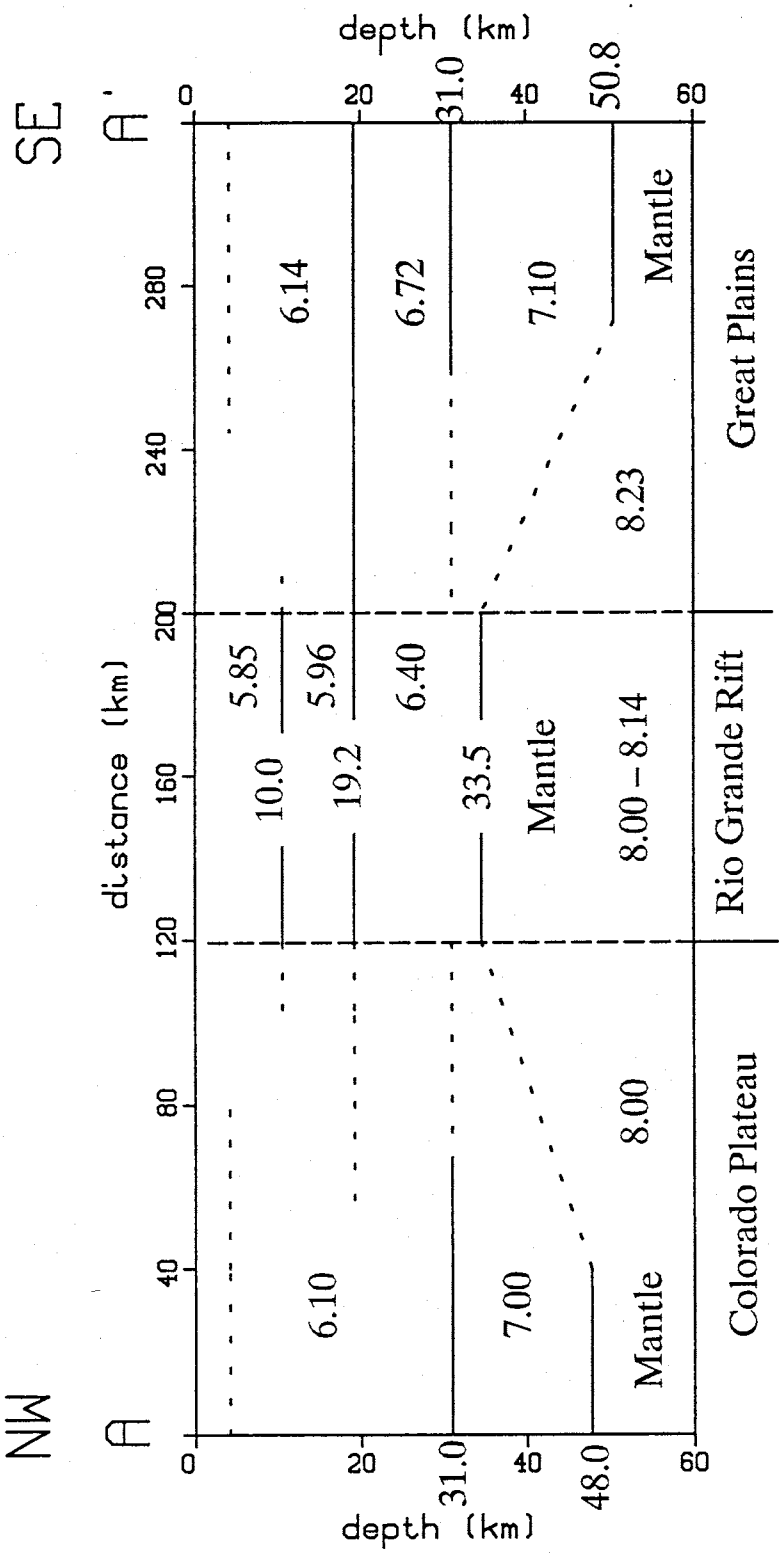

Fig. 3.5. Generalized crustal cross section AA', Colorado Plateau to Great Plains. P velocities are in km s^{-1} and depths are in km. Vertical exaggeration is 2:1. From *Jaksha and Evans* [1984], *Ward* [1980], *Rinehart and Sanford* [1981], *Singer* [1989], Stewart and Pakiser [1962].

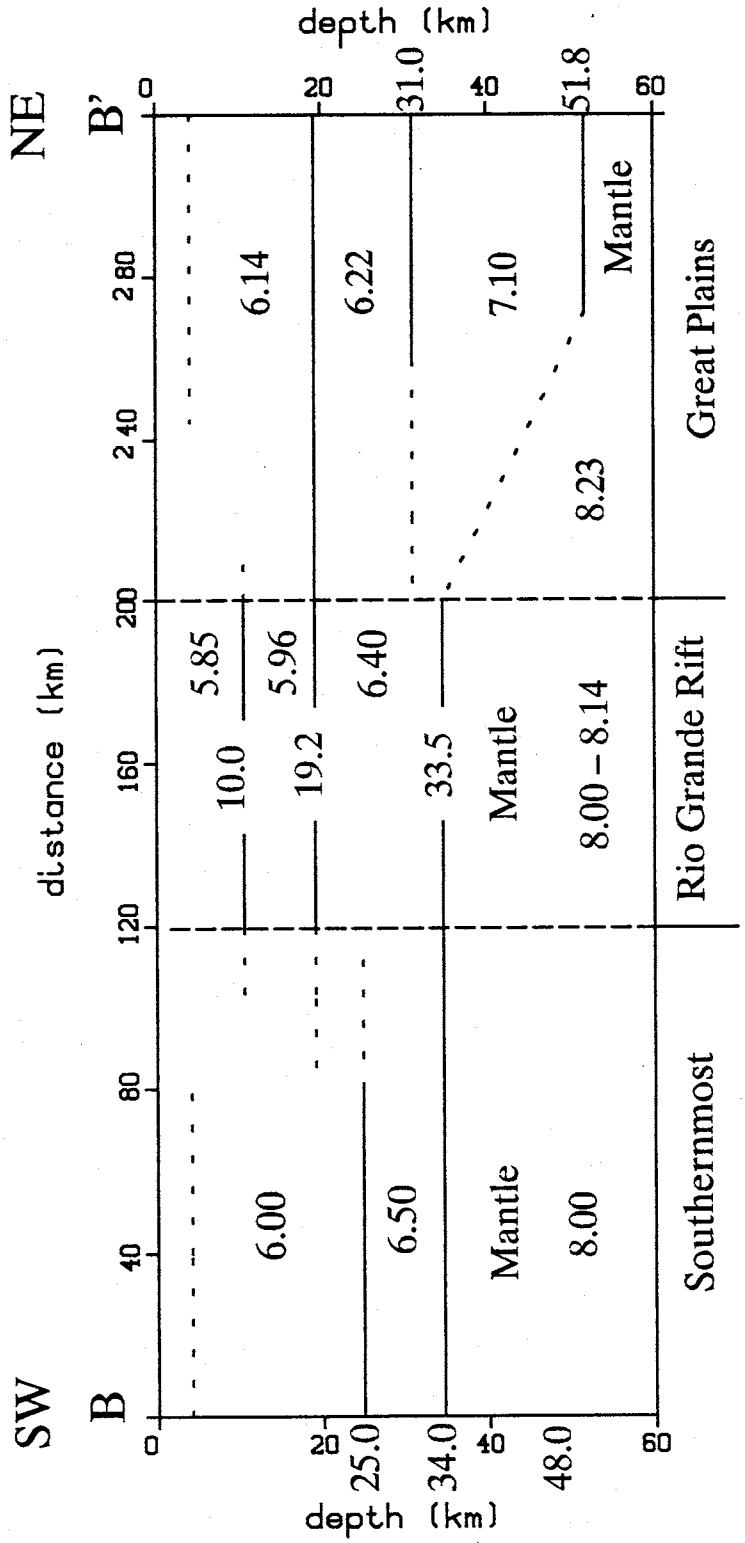

Fig. 3.6. Generalized crustal cross section BB', Southernmost Colorado Plateau to Great Plains. P velocities are in km s^{-1} and depths are in km. Vertical exaggeration is 2:1. From *Jaksha* [1982], *Ward* [1980], *Rinehart and Sanford* [1981], *Singer* [1989], Stewart and Pakiser [1962].

the seismogenic zone, but above the magma body, V_p and Poisson's ratio have never been estimated by previous investigators. The 5.96 km s^{-1} velocity shown in Figure 3.5 is derived from a V_s of 3.41 km s^{-1} [*Rinehart and Sanford*, 1981] and an assumed Poisson's ratio of 0.25. It is also important to note that my investigation is the first in New Mexico to combine direct and reflected arrivals from earthquakes and is also the first inversion to combine compressional and shear data. This has allowed me to simultaneously resolve both depth to the magma body and velocity above the magma body. Previously, *Rinehart and Sanford* [1981], using S_zS reflections, could not resolve both depth and velocity, and estimated a magma body depth by holding constant an average V_s.

4. Method

Inverse Theory

Inverse methods have been successfully applied to the joint hypocenter-velocity problem for many years. Here, I review the key points of inverse theory and explain how inverse methods will be specifically applied to this project. The primary sources for much of this discussion are *Jackson* [1972] and *Braille* [1973]. Table 4.1 explains most of the notation used below.

If y_i^{ob}, $i=1, n$ are n discrete observations and x_j^e, $j=1, m$ are m parameters describing an earth model, then assuming the observations are a function of the earth parameters, for each y_i^{ob},

$$y_i^{ob} = f_i\left(x_1^e, \cdots x_m^e\right) \tag{1}$$

For the problem I am solving here, the observations (y_i^{ob} 's) are arrival times read from microearthquake seismograms and the parameters describing the earth model (x_j^e 's) are earthquake locations (latitudes, longitudes, focal depths, and origin times) and a velocity model (P velocities, magma body depth, Poisson's ratios, and station corrections).

Assuming an initial earth model with parameters x_j^0, theoretical data y_i^{th} can be calculated (a forward problem) and compared to the observations. There will be a difference between the observations and the theoretical data because of an overly simplified model choice, poor initial model selection, and noise (measurement error) in the observed data. Inverse methods are used to improve the choice of model parameters so $y_i^{ob} - y_i^{th}$ are reduced.

Expanding each $f_i\left(x_1^e, \cdots x_m^e\right)$ in a Taylor series about the initial model yields

$$y_i^{ob} = \epsilon_i + f_i\left(x_1^0, \cdots x_m^0\right) + \sum_{j=1}^{m} \frac{\partial f_i\left(x_1^0, \cdots x_m^0\right)}{\partial x_j}\left(x_j^e - x_j^0\right) + \cdots \tag{2}$$

where ϵ_i is the error associated with each datum. The higher order terms of the

TABLE 4.1. Notation Used in **Method** Section

Variable	Meaning
y_i^{ob}	observed data, $i = 1, n$ observations
y_i^{th}	theoretical or model data, $i = 1, n$ observations
ϕ_i	assumed measurement error of the ith observation
ϵ_i	actual measurement error of the ith observation
Δy_i	difference between observed and theoretical data
$\mathbf{\Delta y}$	vector of all Δy_i
x_j^e	real model parameter, $j = 1, m$ parameters
x_j^0	initial model parameter, $j = 1, m$ parameters
γ_j	anticipated difference between x_j^e and x_j^0
Δx_j	actual difference between a real and initial parameter
$\mathbf{\Delta x}$	vector of all Δx_j
$\mathbf{\Delta \hat{x}}$	estimate of $\mathbf{\Delta x}$
σ_j	standard deviation of the jth parameter estimate
$\mathbf{A}$	n x m matrix of partial derivatives
$\mathbf{H}$	m x n inverse matrix of $\mathbf{A}$
$\mathbf{R}$	m x m parameter resolution matrix
$\mathbf{S}$	n x n data resolution matrix
R	measure of how well assumed data errors match residuals
r_j	measure of resolution of the jth parameter
$\mathbf{V}$	m x m matrix of eigenvectors of parameter space
$\mathbf{U}$	n x n matrix eigenvectors of data space
$\mathbf{\Lambda}$	n x m diagonal matrix eigenvalues
τ_{ijk}	arrival time of kth phase at jth station for ith event
T_{ijk}	travel time of kth phase at jth station for ith event
o_i	origin time of ith event
σ_j	station correction of jth station
$\mathbf{A}_i$	single-event location sub-matrix
$\mathbf{\Omega}_i$	velocity-depth sub-matrix
$\mathbf{\Theta}_i$	station correction sub-matrix
ν_i	Poisson's ratio sub-matrix

series have been dropped, implying $f_i\left(x_1^e, \cdots x_m^e\right)$ is linear or, if $f_i\left(x_1^e, \cdots x_m^e\right)$ is nonlinear, the initial model is sufficiently close to the actual earth model so the higher order terms are small and can be ignored. In practice, because the joint problem is nonlinear, it must be solved iteratively. The number of iterations depends on the assumed starting model and the type of problem being solved. Linear problems can be solved with one iteration, regardless of the assumed starting model.

Noting that

$$y_i^{th} = f_i\left(x_1^0, \cdots x_m^0\right), \; j=1, \; m, \tag{3}$$

then (2) can be rewritten as

$$\left(y_i^{ob} - y_i^{th}\right) = \epsilon_i + \sum_{j=1}^{m} \frac{\partial f_i\left(x_1^0, \cdots x_m^0\right)}{\partial x_j} \left(x_j^e - x_j^0\right). \tag{4}$$

In matrix form this is

$$\Delta \mathbf{y} = \mathbf{A}\Delta \mathbf{x} + \epsilon, \tag{5}$$

where $\Delta \mathbf{y}$ is a column vector of length n, representing differences between observed and theoretical data, $\mathbf{A}$ is a matrix with dimensions of n rows by m columns of the partial derivatives, $\Delta \mathbf{x}$ is a column vector of length m representing the differences between actual model parameters and the initial model parameters, and ϵ is a column vector of length n representing noise in the data.

If the number of observations exceeds the number of model parameters ($n > m$), as is the case for this project, and assuming the errors (ϵ) are normally distributed, then by minimizing the square of the errors with respect to the unknown parameters, a solution for $\Delta \mathbf{x}$ is

$$\mathbf{H}\Delta \mathbf{y} = \mathbf{H}\mathbf{A}\Delta \mathbf{x} = \Delta \hat{\mathbf{x}}, \tag{6}$$

where

$$\mathbf{H} = \left(\mathbf{A}^T\mathbf{A}\right)^{-1}\mathbf{A}^T, \tag{7}$$

and $\Delta\hat{\mathbf{x}}$ is a vector of parameter difference estimates.

Jackson [1972] defined two matrices which provide information about the inversion. The first is

$$\mathbf{R} = \mathbf{HA}, \tag{8}$$

which is known as the model resolution matrix. If $\left(\mathbf{A}^T\mathbf{A}\right)^{-1}$ exists, then $\mathbf{R}$ will be the identity matrix, $\mathbf{I}$, and the solution is unique. The second information matrix is

$$\mathbf{S} = \mathbf{AH}, \tag{9}$$

which is a measure of data independence. $\mathbf{S}$ is sometimes referred to as the information density matrix. If $\left(\mathbf{A}^T\mathbf{A}\right)^{-1}$ exists and $\mathbf{S} = \mathbf{I}$, then all residuals are 0 (the model data match the observed data exactly). For the case where $\mathbf{S} = \mathbf{I}$ and residuals are not 0, the closer each diagonal of $\mathbf{S}$ is to 1, the more independent information a datum is providing to the solution.

$\mathbf{H}$ can also be used to calculate the standard deviations on each new parameter estimate by

$$\sigma_j^2 = H_{ji} H_{ij}, \tag{10}$$

where σ_j is the standard deviation on parameter j.

In practice, because all data collected in a field situation contain errors, each Δy_i must be weighted by its expected measurement error, ϕ_i. Each element of Δy_i and each row of $\mathbf{A}$ can be weighted as

$$\Delta y_i = \Delta y_i' / \phi_i, \tag{11}$$

and

$$A_{ij} = A_{ij}' / \phi_i, \; j = 1, m, \tag{12}$$

where the primes represent the unweighted cases. The appropriateness of data weights can be checked by

$$R = \left[\frac{1}{n} \sum_{i=1}^{n} \left(\frac{\Delta y_i}{\phi_i} \right)^2 \right]^{\frac{1}{2}}. \tag{13}$$

If R is much greater than 1, then the ϕ_i's are too small or the initial model is a poor approximation of the actual model. If R is much less than 1, then the ϕ_i's are too large or the initial model closely fits the actual model. Equal weights need not be applied to all data. Assigning appropriate data weights is important because parameter uncertainties are highly sensitive to assumed data errors.

When solving least squares problems for different types of parameters, often the parameter differences contained in $\Delta\mathbf{x}$ will vary widely in numerical amplitude. For example, when solving for a velocity the appropriate Δx_j may be only 0.05 or 0.1 km s^{-1} while the Δx_j for an epicenter coordinate may be 10 to 25 km. *Hawley et al.* [1981] point out that parameter differences can be approximately normalized before inverting by weighting $\mathbf{A}$ with the expected values of each Δx_j (anticipated differences between the earth and initial parameters). Thus,

$$A_{ij} = \gamma_j A_{ij}', \; i = 1, \; n, \tag{14}$$

and each

$$\Delta x_j = \Delta x'_j \; / \gamma_j, \tag{15}$$

where γ_j is the anticipated parameter difference. Since parameter weighting has been applied to $\mathbf{A}$, then the weighting on each σ_j (from (10)) and each $\Delta\hat{x}_j$ (from (6) must be removed in order to restore units. This is accomplished by multiplying each σ_j and $\Delta\hat{x}_j$ by the appropriate γ_j.

Despite parameter weighting, for some problems, $\mathbf{A}^T\mathbf{A}$ will still often be singular or close to singular, making it difficult to invert. For hypocenter estimation, *Lee and Stewart* [1981] point out that this is often the case, requiring that some other method of solving (7) be used. For this study I chose eigenvalue-eigenvector analysis (generalized least squares) because *Ward* [1980] found that it produced more realistic error estimates than damped least squares for the joint problem.

Eigenvalue Decomposition

If **B** is a square matrix, then

$$\mathbf{Bc} = \lambda \mathbf{c}, \tag{16}$$

is an eigenvalue equation of **B** [*Kreyszig*, 1979, pp 349-350]. The λ is a number and is an eigenvalue or characteristic value of the matrix **B**. The **c** is the corresponding eigenvector, provided **c** is not 0.

For the problem being solved, there are more data than parameters. Hence, **B** in (16) will not be square. *Lanczos* [1961] presents the fundamental decomposition theorem for such a case which states

$$\mathbf{A} = \mathbf{U}\Lambda\mathbf{V}^T. \tag{17}$$

Assuming **A** has dimensions nxm, **V** is an mxm matrix whose columns are eigenvectors of the parameter space, **U** is an nxn matrix whose columns contain eigenvectors of the data space, and Λ is an nxm diagonal matrix of eigenvalues.

In practice, the matrix $\mathbf{A}^T\mathbf{A}$ is formed and

$$\mathbf{A}^T\mathbf{AV} = \Lambda^2\mathbf{V}, \tag{18}$$

an eigenvalue problem similar to (16), is solved for **V** and Λ^2. Next **U** is found with

$$\mathbf{U} = \mathbf{AV}\Lambda^{-1}. \tag{19}$$

Finally **H** is found by

$$\mathbf{H} = \mathbf{V}_p \Lambda_p^{-1} \mathbf{U}_p^T. \tag{20}$$

The subscript p is included to indicate that only the p positive eigenvalues and their associated eigenvectors found in (18) are used to solve (20) if the rank of **A** is less than m. When **H** is found using (20) it is known as the natural inverse of **A** [*Lancos*, 1961] and will always exist. Hence, when $\mathbf{A}^T\mathbf{A}$ is singular or close to singular, **H** can still be found and used to solve (6). This method of finding the natural inverse, **H**, is often known as generalized least squares (GLS).

If eigenvalues are greater than zero, but small, they can be removed from the **H** calculation. This will cause the solution to (6) to become more model dependent. This dependence can be quantified [*Jackson,* 1972] for each parameter being estimated by

$$r_j = \sum_{i=1}^{m} \left[\left(\sum_{k=1}^{q} V_{jk} V_{ik} \right) - \delta_{ji} \right]^2 . \tag{21}$$

where $q \leq p$ is the number of eigenvalues kept in the calculation of **H**, m is the number of columns in the **V** matrix, δ_{ji} is the Kronecker delta, and j corresponds to the parameter in question. Thus, for every parameter being estimated, the solutions to (10) and (21) can be plotted against q. This produces a set of trade-off curves between data dependence and model dependence. When all possible eigenvalues can be kept in a solution, the least squares solution is found and each r_j will be 0. The solution is completely data dependent, but standard deviations on each parameter will be a maximum. As eigenvalues are removed from a solution, r_j will approach 1 and standard deviation will be reduced, but the parameter estimates will become totally dependent on the initial model.

Specific Application

A given arrival time, τ_{ijk}, can be expressed as a function of travel time, T_{ijk} (based on hypocenter coordinates, station coordinates, and velocity model), an event origin time o_i, and a station correction θ_j. The subscript i corresponds to an event, j corresponds to a station, and k corresponds to a phase. Thus, arrival time can be expressed as

$$\tau_{ijk} = o_i + T_{ijk} + \theta_j . \tag{22}$$

Each T_{ijk} is a function of the unknown parameters velocity, reflector depth, the earthquake location, and, if the travel time is a shear phase, Poisson's ratio.

For the joint hypocenter-velocity inversion, the **A** matrix of partial derivatives will be diagonal on the left and rectangular on the right. If f is the total number of

events in the inversion, then $\mathbf{A}$ will have the form

$$\mathbf{A} = \begin{bmatrix} \mathbf{A}_1 & 0 & \cdot & \cdot & \cdot & \cdot & 0 & \Omega_1 & \Theta_1 & \nu_1 \\ 0 & \cdot & 0 & \cdot & \cdot & \cdot & \cdot & \cdot & \cdot & \cdot \\ \cdot & 0 & \cdot & 0 & \cdot & \cdot & \cdot & \cdot & \cdot & \cdot \\ \cdot & \cdot & 0 & \mathbf{A}_i & 0 & \cdot & \cdot & \Omega_i & \Theta_i & \nu_i \\ \cdot & \cdot & \cdot & 0 & \cdot & 0 & \cdot & \cdot & \cdot & \cdot \\ \cdot & \cdot & \cdot & \cdot & 0 & \cdot & 0 & \cdot & \cdot & \cdot \\ 0 & \cdot & \cdot & \cdot & \cdot & 0 & \mathbf{A}_f & \Omega_f & \Theta_f & \nu_f \end{bmatrix}, \tag{23}$$

where $\mathbf{A}_i$ is a sub-matrix representing the four hypocenter parameters of event i, Ω_i is a sub-matrix representing velocity parameters and reflector depth, Θ_i is a sub-matrix representing station corrections, and ν_i is a sub-matrix associated with Poisson's ratio in each layer.

Each sub-matrix $\mathbf{A}_i$ will be of the form

$$\mathbf{A}_i = \begin{bmatrix} \frac{\partial \tau_{i11}}{\partial x_i} & \frac{\partial \tau_{i11}}{\partial y_i} & \frac{\partial \tau_{i11}}{\partial z_i} & 1 \\ \cdot & \cdot & \cdot & \cdot \\ \frac{\partial \tau_{i1p}}{\partial x_i} & \frac{\partial \tau_{i1p}}{\partial y_i} & \frac{\partial \tau_{i1p}}{\partial z_i} & 1 \\ \cdot & \cdot & \cdot & \cdot \\ \cdot & \cdot & \cdot & \cdot \\ \frac{\partial \tau_{ijk}}{\partial x_i} & \frac{\partial \tau_{ijk}}{\partial y_i} & \frac{\partial \tau_{ijk}}{\partial z_i} & 1 \\ \cdot & \cdot & \cdot & \cdot \\ \cdot & \cdot & \cdot & \cdot \\ \cdot & \cdot & \cdot & \cdot \\ \frac{\partial \tau_{isp}}{\partial x_i} & \frac{\partial \tau_{isp}}{\partial y_i} & \frac{\partial \tau_{isp}}{\partial z_i} & 1 \end{bmatrix} \tag{24}$$

The x, y, and z denote the hypocenter coordinates; longitude, latitude, and focal depth. A total of s stations recorded the event and a total of p phases were picked at a particular station. Note that p may vary from station to station. That is, some stations may record only direct phases for a particular event while other stations may record both direct and reflected phases. Thus, the total number of rows in $\mathbf{A}_i$

depends on how many stations recorded the event and how many phases from each seismogram can be reliably identified. The total number of rows in $\mathbf{A}_i$ will always equal the total number of arrival times picked for a particular event. The fourth column of $\mathbf{A}_i$ represents origin time, but the partial derivative of arrival time with respect to origin time will always be 1 (equation (22)). If a single-event location is being estimated, then the problem is reduced to solving a single $\mathbf{A}_i$ matrix for the four hypocenter parameters latitude, longitude, depth, and origin time.

The generalized velocity-depth sub-matrix $\mathbf{\Omega}_i$ will be of the form

$$\mathbf{\Omega}_i = \begin{bmatrix} \frac{\partial \tau_{i11}}{\partial v_1} & \cdots & \frac{\partial \tau_{i11}}{\partial v_g} & \frac{\partial \tau_{i11}}{\partial h_1} & \cdots & \frac{\partial \tau_{i11}}{\partial h_{g-1}} \\ \vdots & & \vdots & \vdots & & \vdots \\ \frac{\partial \tau_{i1p}}{\partial v_1} & \cdots & \frac{\partial \tau_{i1p}}{\partial v_g} & \frac{\partial \tau_{i1p}}{\partial h_1} & \cdots & \frac{\partial \tau_{i1p}}{\partial h_{g-1}} \\ \vdots & & \vdots & \vdots & & \vdots \\ \frac{\partial \tau_{ijk}}{\partial v_1} & \cdots & \frac{\partial \tau_{ijk}}{\partial v_g} & \frac{\partial \tau_{ijk}}{\partial h_1} & \cdots & \frac{\partial \tau_{ijk}}{\partial h_{g-1}} \\ \vdots & & \vdots & \vdots & & \vdots \\ \vdots & & \vdots & \vdots & & \vdots \\ \frac{\partial \tau_{isp}}{\partial v_1} & \cdots & \frac{\partial \tau_{isp}}{\partial v_g} & \frac{\partial \tau_{isp}}{\partial h_1} & \cdots & \frac{\partial \tau_{isp}}{\partial h_{g-1}} \end{bmatrix} \tag{25}$$

The v represents compressional velocity in each layer and h stands for layer depth. Each $\mathbf{\Omega}_i$ will have a maximum of $2g-1$ columns, where g represents the total number of velocities being solved. For the most general case there will be one less layer depth than the number of layer velocities, assuming the final layer is treated as a half space. For the specific problem I am solving there will be three columns in this matrix. They represent compressional velocity in the layers of (1) the brittle upper crust and (2) the ductile crust beneath the seismogenic zone but above the top of the magma body. The third column represents the depth to the top of the magma body. Because I have no data which directly samples the base of the

seismogenic zone, the trade-off between velocity and depth to the bottom of the first layer can not be resolved, and, hence, this depth is held fixed. The number of rows in each $\mathbf{\Omega}_i$ will be the same as the number of rows in the corresponding $\mathbf{A}_i$ matrix.

Some of the partial derivatives in each $\mathbf{\Omega}_i$ matrix are 0 because some of the arrival times included for the inversion contain no information about certain layers. For instance, a direct P arrival will contain no information about magma body depth because no part of direct P ever travels to magma body depths.

Each $\mathbf{\Theta}_i$, a station correction sub-matrix, will have the form

$$\mathbf{\Theta}_i = \begin{bmatrix} 1 & 0 & \cdot & \cdot & 0 \\ \cdot & \cdot & \cdot & \cdot & \cdot \\ 1 & \cdot & \cdot & \cdot & \cdot \\ 0 & \cdot & 0 & \cdot & \cdot \\ \cdot & \cdot & 1 & \cdot & \cdot \\ \cdot & \cdot & \cdot & \cdot & \cdot \\ \cdot & \cdot & 1 & \cdot & 0 \\ \cdot & \cdot & 0 & \cdot & 1 \\ \cdot & \cdot & \cdot & \cdot & \cdot \\ 0 & \cdot & \cdot & 0 & 1 \end{bmatrix} \tag{26}$$

Because each column vector consists of partial derivatives of arrival times with respect to a particular station correction, only those times recorded at the station in question produce non-zero derivatives. Referring to (22) all non-zero derivatives are 1. The joint determination of station corrections and origin times is non-unique because of the trade-off between station corrections and origin times *Pujol*, [1988]. To overcome this trade-off, the correction at one station is held constant while all other corrections are allowed to vary. This results in a total of $s-1$ columns in the station correction matrix, where s is the total number of stations which have recorded data.

Finally, the Poisson's ratio sub-matrix, ν_i, will be of the form

$$\nu_i = \begin{bmatrix} \frac{\partial \tau_{i11}}{\partial \nu_1} & \cdot & \frac{\partial \tau_{i11}}{\partial \nu_g} \\ \cdot & \cdot & \cdot \\ \frac{\partial \tau_{i1p}}{\partial \nu_1} & \cdot & \frac{\partial \tau_{i1p}}{\partial \nu_g} \\ \cdot & \cdot & \cdot \\ \cdot & \cdot & \cdot \\ \frac{\partial \tau_{ijk}}{\partial \nu_1} & \cdot & \frac{\partial \tau_{ijk}}{\partial \nu_g} \\ \cdot & \cdot & \cdot \\ \cdot & \cdot & \cdot \\ \cdot & \cdot & \cdot \\ \frac{\partial \tau_{isp}}{\partial \nu_1} & \cdot & \frac{\partial \tau_{isp}}{\partial \nu_g} \end{bmatrix} . \qquad (27)$$

Only those arrival times involving S produce non-zero derivatives. Thus, direct S, S_zS, and S_zP contribute to the estimation of the Poisson's ratio. There are g possible parameters to solve for in this sub-matrix; the same as the number of velocities in the velocity-depth sub-matrix.

Theoretical arrival times are found by ray tracing. The theoretical times are necessary to compare with the observed arrival times (find the $\Delta\mathbf{y}$ vector). When a phase is timed, the seismologist identifies the phase type by assigning a code to the specific arrival time. (See **Appendix A** for details.) Depending on the phase code, P or S velocities are assigned to the model, and then rays are found between the source and receiver along a path controlled by the phase code. The ray paths are found by shooting a fan of rays with varying take-off angles until a ray is found which encounters the receiver. Snell's law is obeyed at all velocity interfaces. By summing the times along the different ray segments the traveltime for an entire ray path is found.

Poisson's ratio and V_p are used to describe the velocity model used in this problem. When necessary, V_s is found from the relationship between the ratio of P

and S velocity to Poisson's ratio:

$$\frac{V_p}{V_s} = \left[\frac{2-2\nu}{1-2\nu}\right]^{\frac{1}{2}}. \tag{28}$$

Partial derivatives are necessary to construct the **A** matrix. I estimate derivatives using central differences. That is,

$$\frac{\partial f(x)}{\partial x} = \frac{f(x+h)-f(x-h)}{2h}, \tag{29}$$

where h is a small fraction of x. Hence, to find a single partial derivative two slightly different ray paths and corresponding travel times must be found which are based on slightly different parameters. The same ray tracing subroutines which are used to calculate theoretical arrival time data are used to find partial derivatives. *Hawley et al.* [1981] report solving a joint hypocenter-velocity problem where some approximated derivatives were in error by up to 10%. They found that the errors only affected the rate of convergence, not the final solution. From synthetic and real data tests my approximations also worked well. No problems with convergence or numerical stability were encountered.

5. Synthetic Data Tests

Overview

I ran several tests with synthetic data before attempting to invert real data. The synthetic data were generated both with and without random noise added. The noise-free data were used to check for programming errors in the inversion algorithm. The noise-added data were used to approximate how many and what kinds of real data would be necessary to solve the proposed problem. It is important to note that the synthetic data used in these tests were generated with the same ray-tracing programs used in the forward modeling section of the inversion program. That is, these data are not derived from three-dimensional models with lateral and vertical velocity variations which simulate the real earth. Because of these limitations, the test results should be thought of as indicators of probable results rather than absolute predictors of results for cases when real data are used.

Below are details on model selection, data generation, noise-free tests, and noise-added tests. Descriptions of the synthetic data generating program and the joint inversion program are in **Appendix A.**

Selecting a Model

The purpose of this research was to find a velocity model appropriate for locating earthquakes using direct and reflected phases. That is, I was seeking a general model with flat layers, P velocities, Poisson's ratios, and station corrections as unknowns. *Ward* [1980], using direct P arrivals, found that a half-space velocity with station corrections worked well for locating Socorro-area earthquakes. Following *Ward*, I chose to parameterize my model from the surface to the deepest events of my data set (the approximate base of the seismogenic zone) as a single constant-velocity layer. *Ward* found the low-velocity, variable-thickness Phanerozoic layer near the surface could be compensated for by station corrections. I also chose to compensate near-surface model variations with station corrections. Because no previous researchers have ever estimated V_p or Poisson's ratio between the

approximate base of the seismogenic zone and the upper surface of the magma body, I assumed velocity in this interval could be different than in the upper layer and selected this interval as the second layer of the model.

This parameterization does not imply velocities in the upper and lower layers are internally constant, nor does it mean there is a sharp velocity contrast at the approximate base of the seismogenic zone. Rather, I assumed that velocity within each of the layers does not vary significantly, but there could be differences in average velocities and Poisson's ratios between the two layers.

Data Generation

The velocity model selected to generate synthetic data was derived from previous investigator's findings (Figure 5.1). I used a two layer model with P velocities in the upper layer of 5.85 km s^{-1} [*Ward et al.*, 1981] and 5.96 km s^{-1} in the lower layer. The lower layer velocity was calculated using V_s of 3.44 km s^{-1} [*Rinehart and Sanford*, 1981] and an assumed Poisson's ratio of 0.25. The interface between the two layers was 12 km deep, approximating the base of the seismogenic zone [*King*, 1986]. The mid-crustal magma body was 19.2 km deep [*Rinehart and Sanford*, 1981]. Poisson's ratio in the upper layer was 0.260 [*Caravella*, 1976 and *Fender*, 1978].

The synthetic data were generated so they would closely match the real data I was likely to use in the inversion. The same names and coordinates for stations which recorded the real data were used to generate the synthetic data. Epicenters, focal depths, origin times, phase types, and phase weights were all selected randomly. The synthetic event locations were constrained so they would fall within the network by limiting maximum gaps between stations to less than 135°. All synthetic events occurred within ± 25 km in the east-west direction from station SNM, and within ± 30 km in the north-south direction from SNM. Focal depths were allowed to vary randomly between 4.0 and 12.0 km depth.

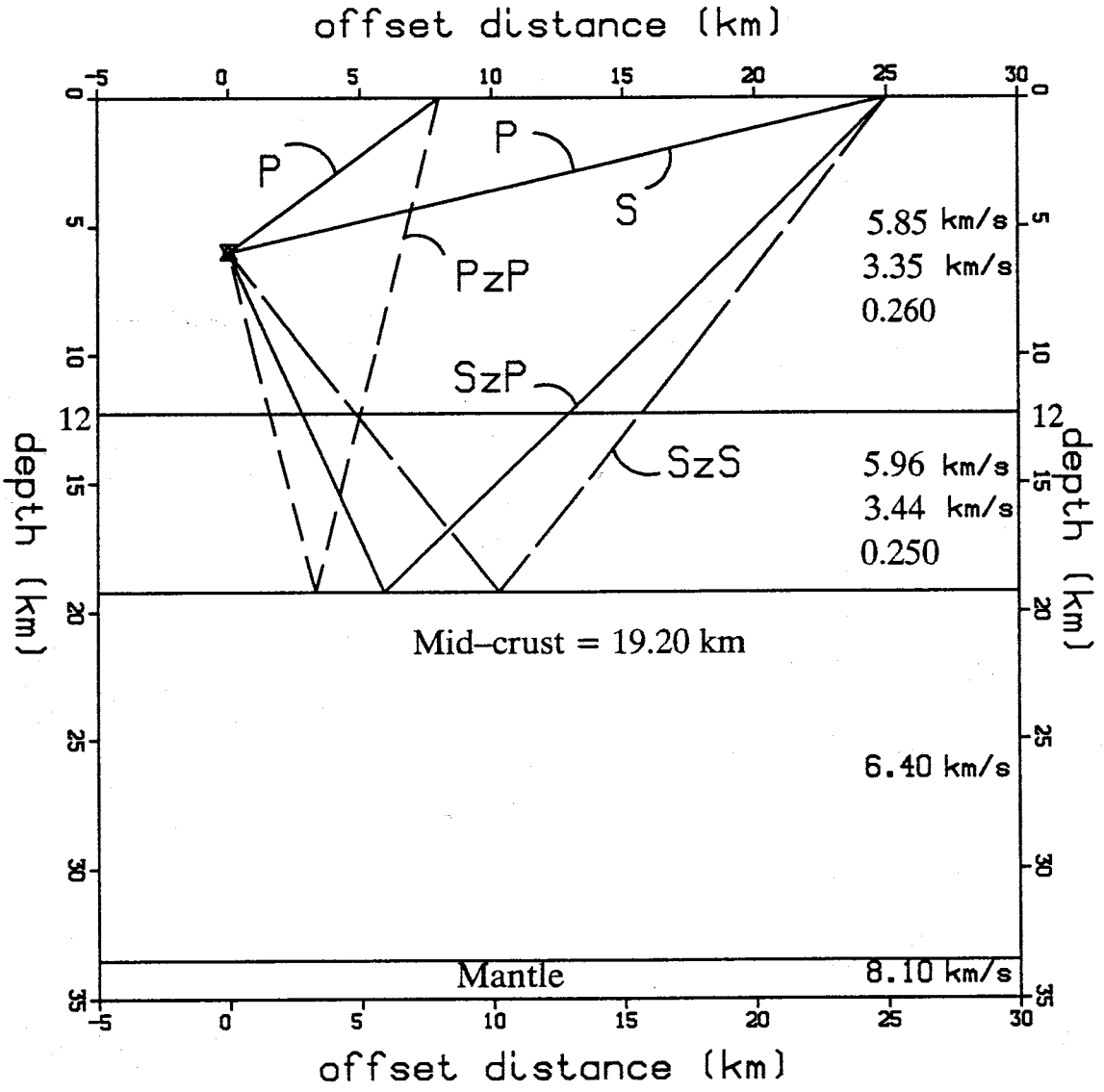

Fig. 5.1. Velocity model used to generate synthetic data. From *Ward* [1980], *Rinehart and Sanford* [1981], *Singer* [1989], *Caravella* [1976].

I also attempted to make the numbers of the different phases match the real data. For each synthetic event, stations at which direct P arrivals occurred were randomly selected from a list of nine possible stations. On average, for any single event, direct P arrivals were allowed at 90 percent of the network stations. If a P arrival was not present at a station, then no other phases were allowed at that station. This was intended to simulate the case of a disabled station or excessive noise at a station. Other than being required to have an accompanying direct P arrival, the stations at which the secondary arrivals occurred were also chosen randomly. Seventy percent of the stations were allowed direct S arrivals. For each event, from one to three stations were allowed to have an S_zP - S_zS pair, and from zero to two stations were allowed to have a P_zP arrival. A total of three to eight reflections were required for each event.

I assigned timing errors to all synthetic data. These errors varied from 0.075 s to 0.375 s. From experience with real data, I required 80 percent of all synthetic P arrivals to be assigned a timing error of 0.075 s and the remainder of P arrivals to be assigned an error of 0.15 s. One half of the S arrivals were assigned errors 0f 0.225 s and the other half were assigned errors of 0.300 s. One half of all reflected phases were assigned errors of 0.300 s and the other half were assigned errors of 0.375 s.

When necessary, normally distributed noise was generated by summing 12 uniform random numbers. The maximum size of the random noise was controlled by the assigned weight (timing error) of each phase. The random noise added to a synthetic arrival time was not allowed to exceed the assumed timing error. For instance, if a P arrival was assigned a weight of 0, then the maximum size of the random noise added to that arrival time would be 0.075 s. The sign of the noise was randomly selected as either positive or negative.

Noise-Free Tests

Figures 5.2, 5.3, and 5.4 demonstrate that my hypocenter estimation algorithm is free of programming errors. Figure 5.2 shows 50 synthetic epicenters (hexagons) and the epicenter estimates (crosses) of those synthetic events based on noise-free data. Figure 5.3 is a plot of synthetic event depths and the depth estimates found with the hypocenter algorithm. Figure 5.4 is a plot of synthetic origin times and the origin time estimates found with the hypocenter algorithm. The same velocity model used to generate the synthetic event data was used to invert the data. Clearly the hypocenter estimation algorithm works correctly as the known parameters and the parameter estimates match.

The hypocenter estimates were all found after three to five iterations, depending on the particular event. Initial epicenter parameters had the same coordinates as the nearest station to the event, all initial focal depths were set at 7.0 km, and initial origin times were estimated from $S-P$ intervals. I defined convergence when no parameter varied by more than 0.005 times its unit value when compared to the previous iteration. Thus, depths, longitudes, and latitudes are defined as converged when there values no longer vary between iterations by more than 0.005 km. Origin time is defined as converged when it no longer varies between iterations by more than 0.005 s.

The second noise-free data test involved solving the joint hypocenter-velocity model problem. This included solving for station corrections, velocities in the upper and lower layers, Poisson's ratio in the upper and lower layers, and magma body depth while also solving for the epicenters, focal depths, and origin times of all 50 events. I used the same synthetic data set which had been generated for the first noise-free test. Table 5.1 lists the model parameter results for this test. All eigenvalues were retained during this test. This means the diagonals of the resolution matrix (**R**, Equation 8) are all 1. All velocity model parameters, including station corrections, were accurately obtained in five iterations. The plots of the 50 hypocenter parameters are identical to those shown in Figures 5.2, 5.3, and 5.4 and,

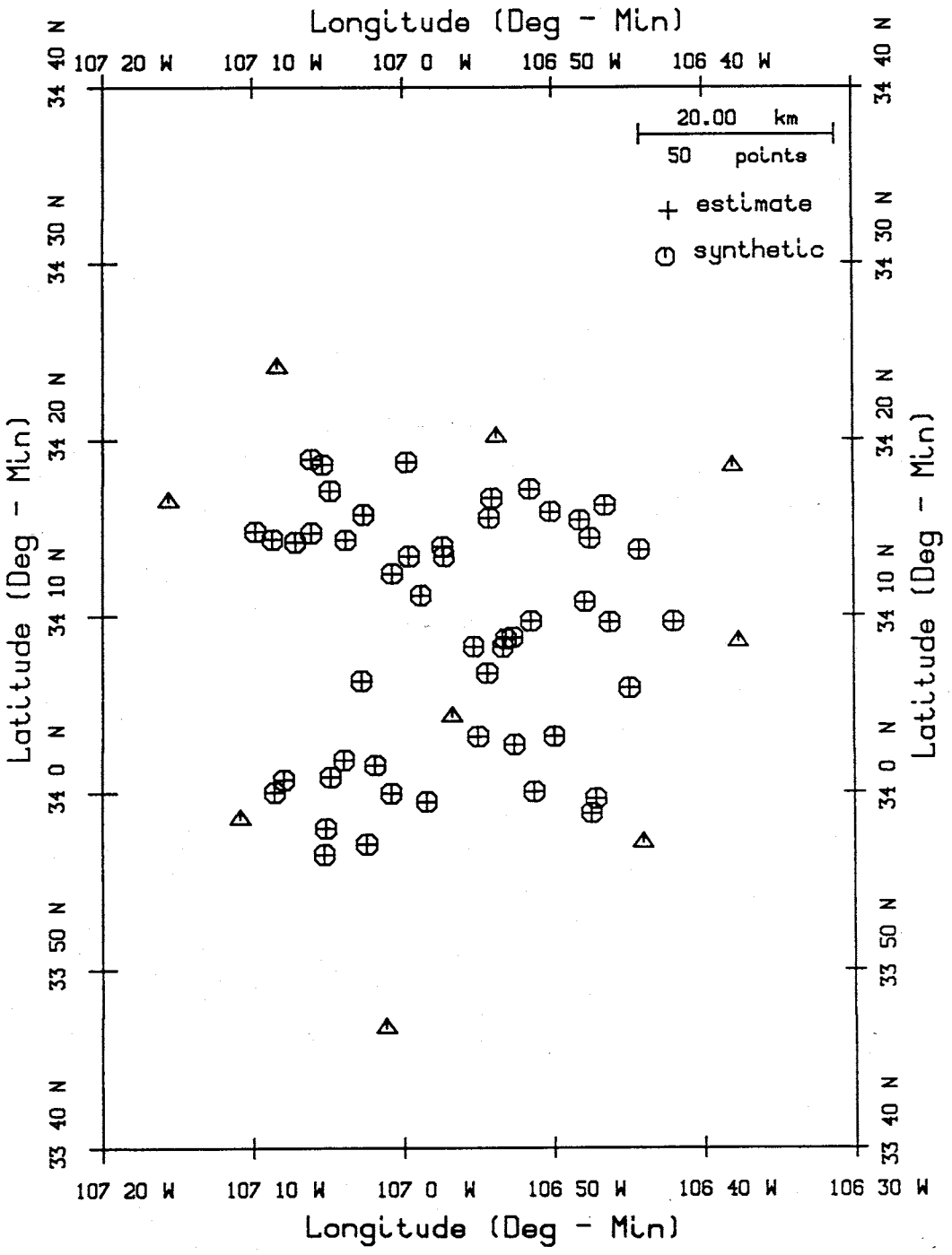

Fig. 5.2. Epicenters of 50 synthetic events (hexagons) and their inversion estimates (+'s) obtained with noise-free data.

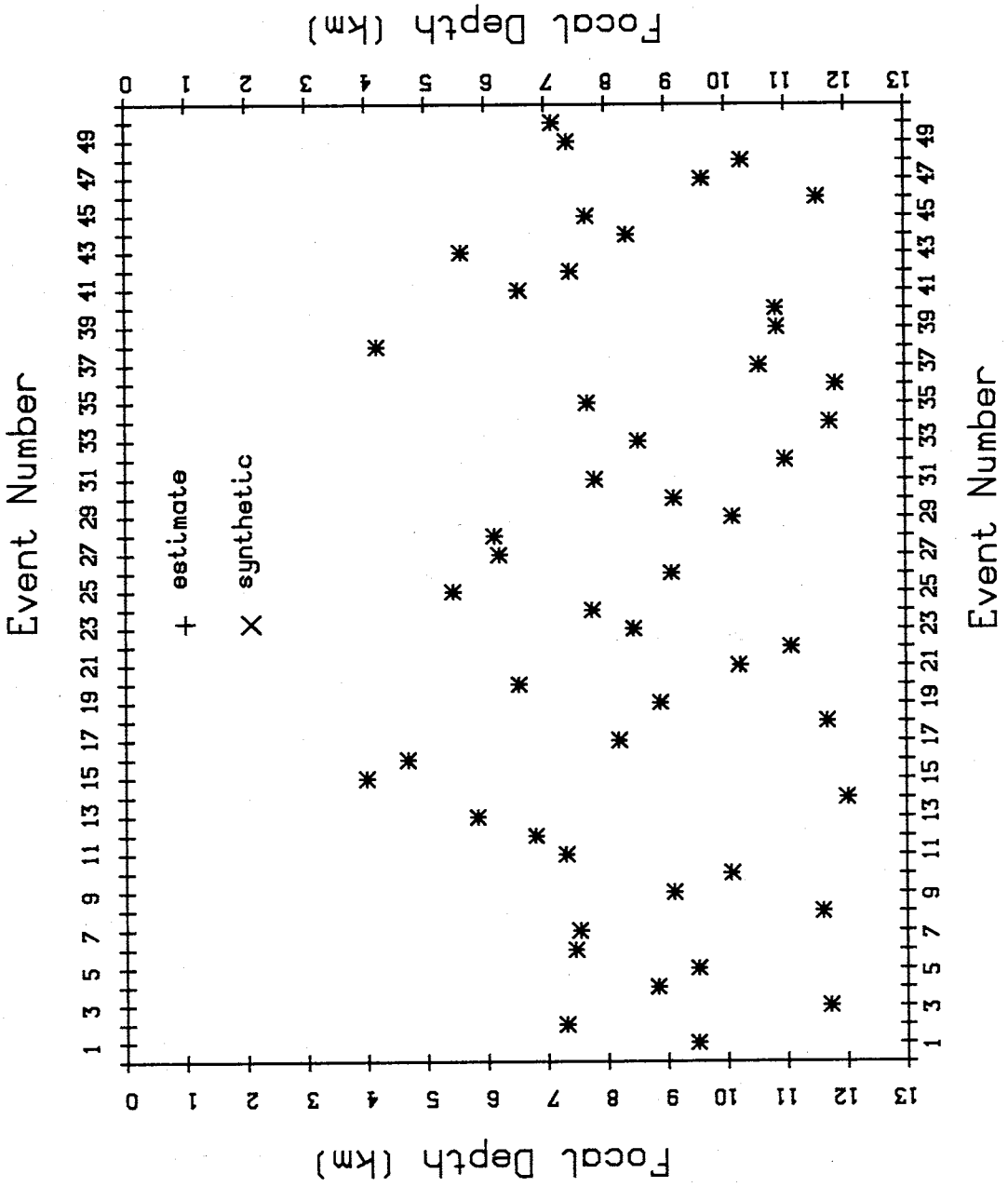

Fig. 5.3. Focal depths of 50 synthetic events (X's) and inversion estimates (+'s) obtained with noise-free data. Turn figure sideways for best viewing.

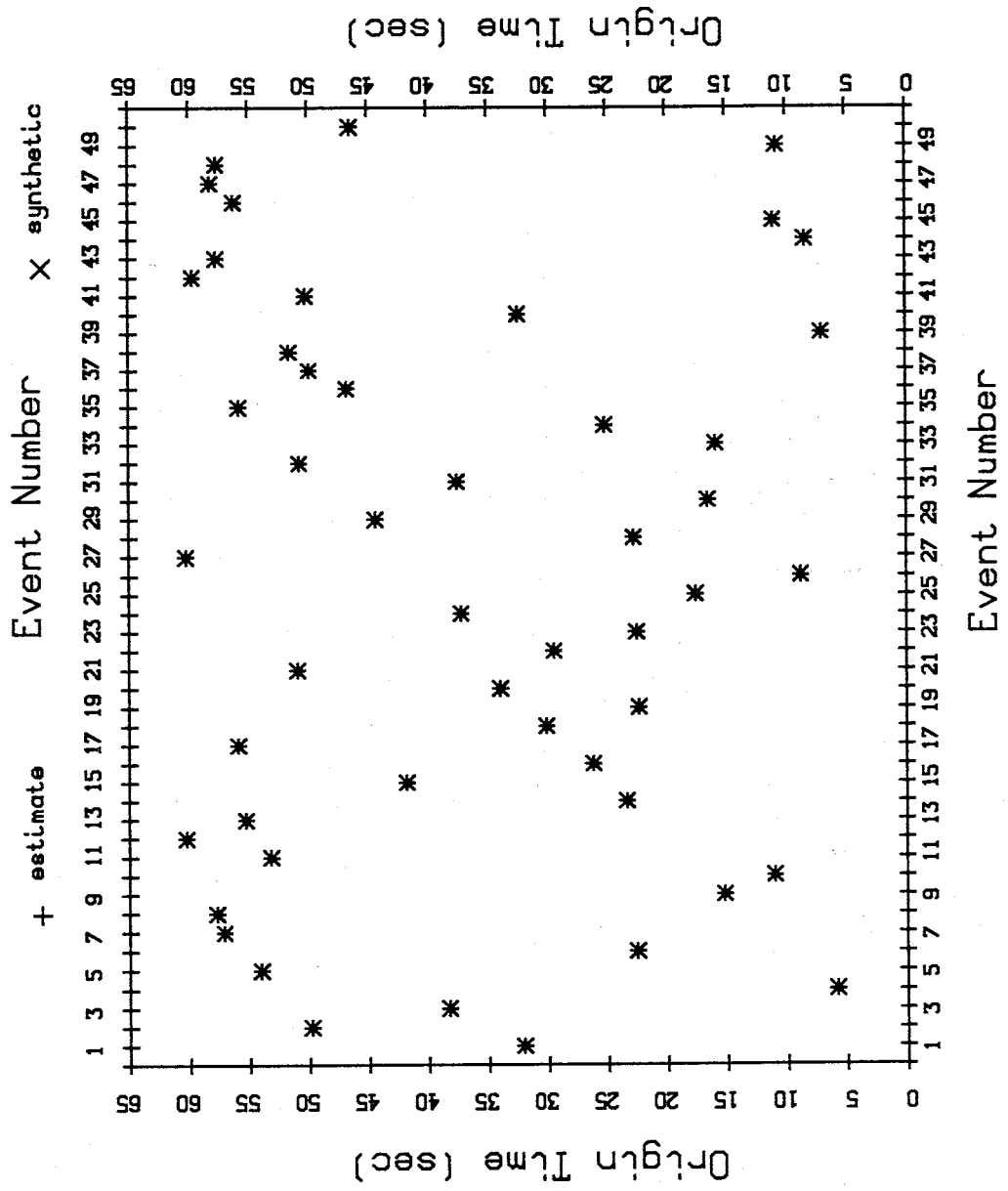

Fig. 5.4. Origin times of 50 synthetic events (X's) and inversion estimates (+'s) obtained with noise-free data. Turn figure sideways for best viewing.

TABLE 5.1. Model Parameter Estimation Using Noise-Free Data From 50 Synthetic Events				
713 Direct Arrivals - 246 Reflected Arrivals				
Parameter Type	Starting Model	Actual Value	Inversion Estimate	Difference
BAR	0.000	-0.030	-0.032	0.002
BMT	0.000	0.140	0.139	0.001
CAR	0.000	-0.080	-0.082	0.002
LAZ	0.000	0.040	0.040	0.000
LJY	0.000	0.560	0.561	0.001
LPM	0.000	-0.230	-0.231	0.001
SB	0.000	0.220	0.218	0.002
SMC	0.00	0.110	0.108	0.002
WTX	-0.080	-0.080	-0.080	0.000
V_{p1}	6.000	5.850	5.848	0.002
V_{p2}	6.000	5.960	5.958	0.002
ν_1	0.250	0.260	0.260	0.000
ν_2	0.250	0.250	0.250	0.000
Z_1	12.000	12.000	12.000	0.000
Z_2	20.000	19.200	19.201	0.001

Station correction values are given in sec, velocities in km s^{-1}, and depths in km. Station correction for WTX and depth to base of seismogenic zone (Z_1) were both held constant. Z_2 is depth to the magma body.

thus, are not shown here.

Each station correction was initially assumed to be 0.000 s, velocity in both layers was 6.0 km s^{-1}, Poisson's ratios were both 0.250, and magma body depth was assumed to be 20.0 km. The base of the seismogenic zone was held constant at 12.0 km and all initial hypocenter parameters were estimated in the same way as the first test; initial locations estimated from the nearest recording station, focal depths assigned at 7 km, and origin times estimated from $S-P$ intervals . However, before solving for the hypocenters and velocity model simultaneously, I first alternately solved for hypocenters and then station corrections while holding velocity and depth parameters constant. This was done to obtain starting hypocenters and station corrections which were much closer to their probable values than their rather approximate initial estimates. *Pavlis* [1982] points out that non-linear inversions can converge to parameters which may produce a local error minimum but may not converge to the true model parameters. Thus, relatively accurate hypocenter estimates were obtained before attempting to solve the joint problem to help prevent convergence to an incorrect solution representing such a local error minimum. I followed this procedure for all other synthetic and real data joint inversions.

Noise-Added Tests

After testing program correctness with noise-free data I ran several tests with noise-added data. These tests were intended to show that the proposed inversion was possible and individual model parameters could be resolved without convergence difficulties (most eigenvalues could be kept in the solution).

Table 5.2 shows velocity model results after adding noise to, and then inverting, the same data used in the noise-free tests. All velocity model parameter estimates, including station corrections, are within one standard deviation (obtained from Equation 10) of their true values. Convergence was reached in five iterations and all eigenvalues were kept in the solution. Convergence while resolving all

TABLE 5.2. Model Parameter Estimation Using Noise-Added Data From 50 Synthetic Events

713 Direct Arrivals - 246 Reflected Arrivals

Parameter Type	Starting Model	Actual Value	Inversion Estimate	Difference	1 Std
BAR	0.000	-0.030	-0.037	0.007	0.046
BMT	0.000	0.140	0.123	0.017	0.052
CAR	0.000	-0.080	-0.074	0.006	0.041
LAZ	0.000	0.040	0.029	0.011	0.057
LJY	0.000	0.560	0.543	0.017	0.039
LPM	0.000	-0.230	-0.232	0.002	0.058
SB	0.000	0.220	0.196	0.024	0.039
SMC	0.00	0.110	0.098	0.012	0.058
WTX	0.000	-0.080	-0.080	0.000	*
V_{p1}	6.000	5.850	5.834	0.016	0.053
V_{p2}	6.000	5.960	5.916	0.044	0.115
ν_1	0.250	0.260	0.259	0.001	0.003
ν_2	0.250	0.250	0.245	0.005	0.010
Z_1	12.000	12.000	12.000	0.000	*
Z_2	20.000	19.200	19.327	0.127	0.331

Station correction values are given in sec, velocities in km s^{-1}, and depths in km. Station correction for WTX and depth to base of seismogenic zone (Z_1) were both held constant. Z_2 is depth to the magma body.

model parameters was the most important result of this test. Previously, *Rinehart and Sanford* [1981] were unable to simultaneously invert for velocity and reflector depth. Because they used only the S_zS arrival the trade-off between reflector depth and velocity caused their inversion to be unstable. This first noise-added test demonstrates the trade-off between depth and velocity can be resolved when multiphase data (including mode-converted data such as S_zP) are simultaneously incorporated into an inversion.

Because all arrivals have traveled within the upper layer, more data have been used to estimate velocity and Poisson's ratio in the upper layer than in the lower layer. Also, because the direct P picks have been weighted with less uncertainty than the reflected picks, more better-quality data have been used to estimate parameters in the upper layer than in the lower layer. As expected, these two factors have contributed to lower standard deviations on parameter estimates in the upper layer.

Figure 5.5 shows focal depth results for this test. Of the 50 focal depths found, 45 estimates are within one standard deviation of their true value and the remaining five are within one and a half standard deviations. The average error on focal depth is only 0.60 km. The average focal depth error is quite low, but another important factor is that the standard deviation on these errors is only 0.10 km. The events range in nearest-station distance from 3.6 to 18.6 km and average 10.8 km. This small variation in focal depth error over a wide range of nearest-station distances indicates that reflections improve focal depth estimates over a wide range of recording geometries. Figure 5.6 shows focal depth estimates for the same 50 events when only direct arrivals are used in the locations. Average focal depth error is 1.37 km, and the standard deviation on these errors is 0.71 km. Average focal depth errors are more than twice as large as those obtained when reflections are included. Furthermore, errors vary much more widely for the direct-only case compared to the reflections-included case.

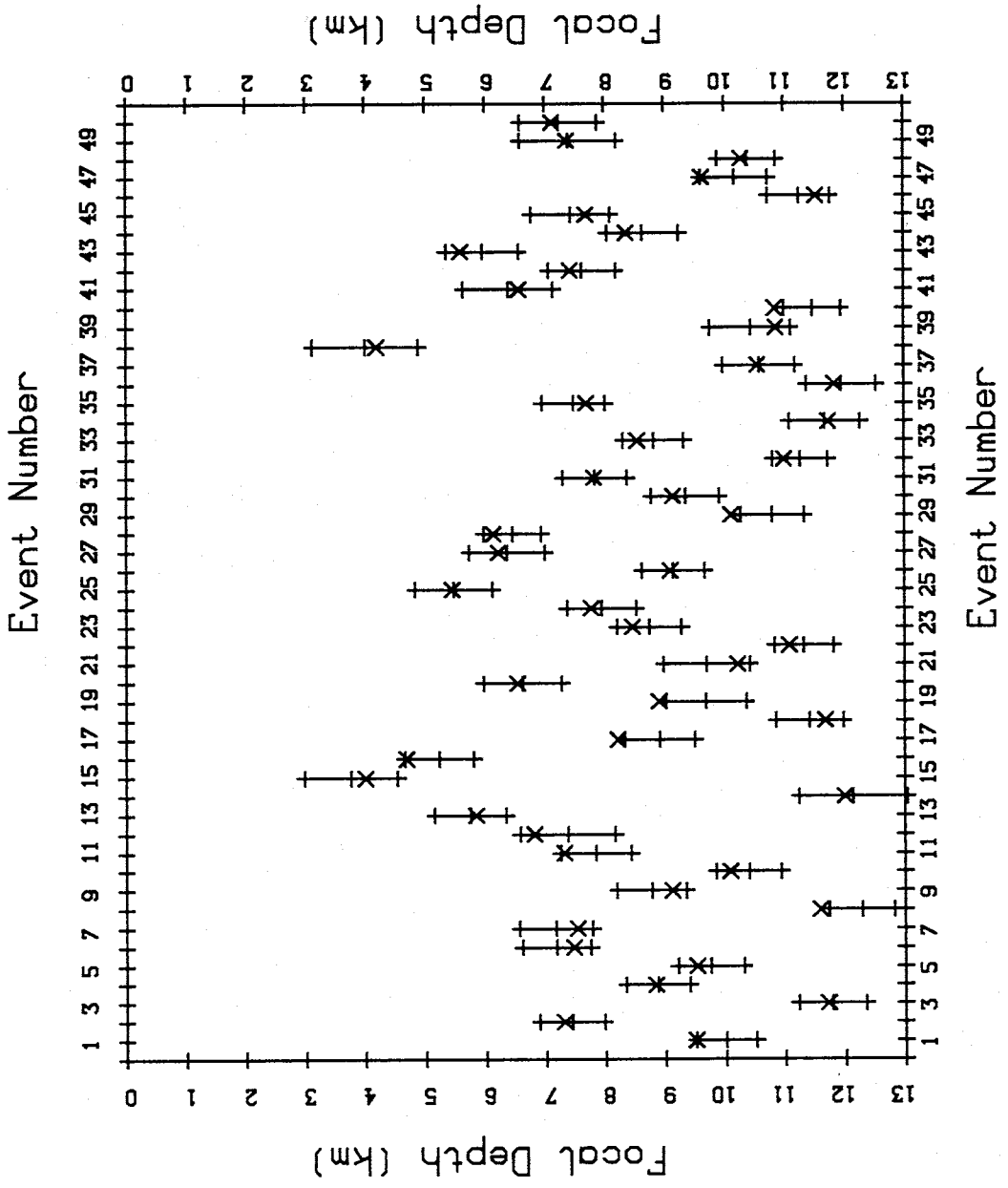

Fig. 5.5. Focal depths of 50 synthetic events (X's), inversion estimates (center cross bars) obtained with noise-added data, and error bars at one standard deviation (upper and lower cross bars). Turn figure sideways for best viewing.

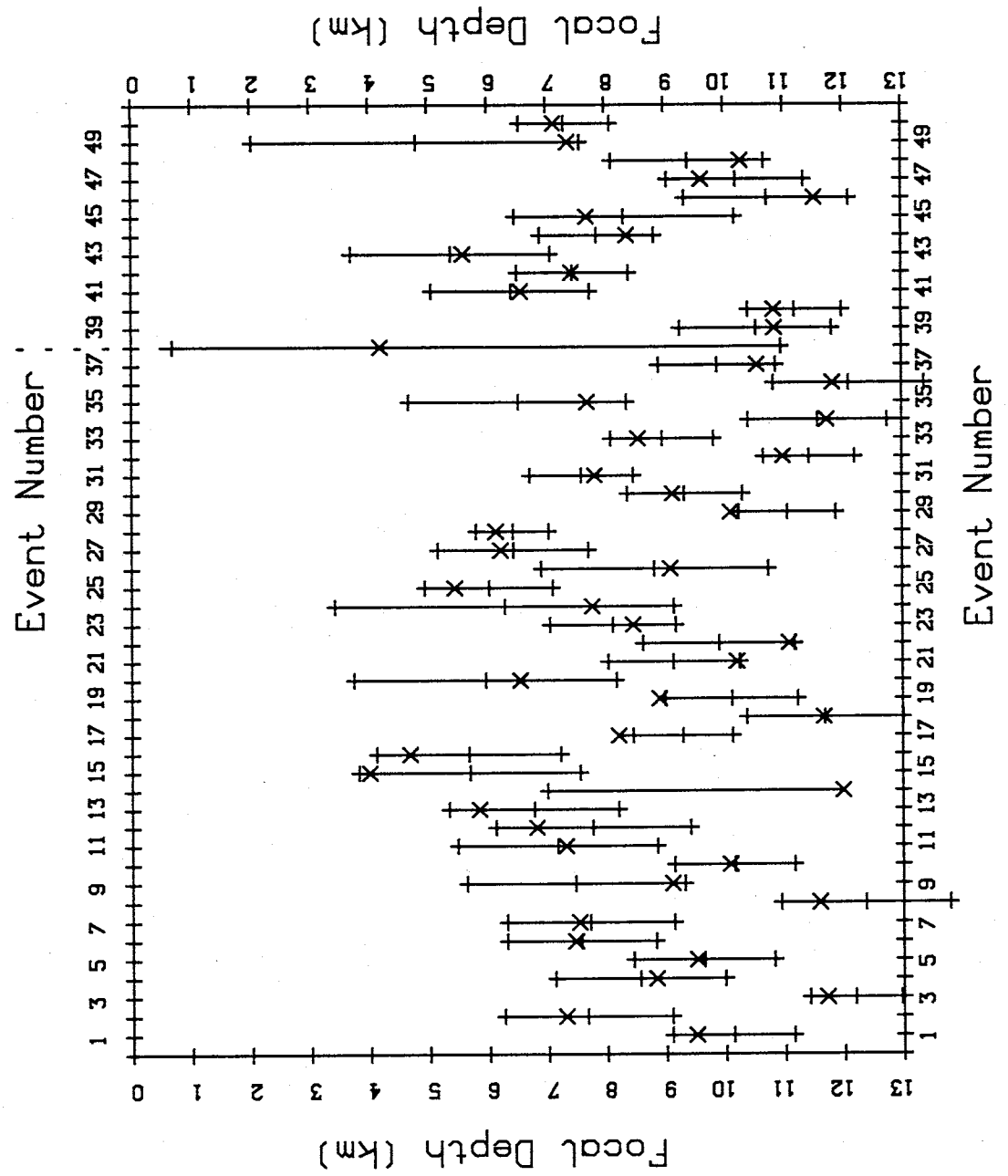

Fig. 5.6. Focal depths of 50 synthetic events (X's), inversion estimates (center cross bars) obtained with noise-added direct arrival data , and error bars at one standard deviation (upper and lower cross bars). No error bars are shown for event 14 because the focal depth defaulted to 7 km. Turn figure sideways for best viewing.

The first noise-added test demonstrates that convergence of the joint hypocenter-velocity model problem should be possible when multi-phase data, chosen from a high quality suite of events, are used. Most significantly, convergence was achieved while retaining all eigenvalues in the solution. The test also shows hypocenter estimates (especially focal depth estimates) can be significantly improved when reflected phases are included in the location process. I ran three more tests using more events and data to see if standard deviations on the velocity model estimates could be reduced. Table 5.3 summarizes results from the noise-added tests using 50, 60, 70, and 80 events. Most standard deviations were only reduced by a few thousandths of a unit when 60 events were used compared to the case of 50 events. The only notable change was for the magma body depth standard deviation, which was improved from 0.331 km for the 50-event case to 0.283 km for the 60-event case. Larger reductions in standard deviations occurred between 60 and 70 events, but improvements were again smaller between 70 and 80 events.

From these tests I concluded that a real data set of between 70 and 80 events composed of over 1000 direct arrivals and over 330 reflected arrivals would be most appropriate to solve a real joint inversion problem. I also concluded that as many S_zS - S_zP or P_zP - S_zP reflection pairs as possible should be included in the data set.

In all tests described above, I have known that the interface between the upper and lower layers of the velocity model was exactly 12 km deep, and I have held that boundary fixed at 12 km for each inversion. For a final synthetic test, I fixed the interface at 10 km and solved for hypocenters and the velocity model using the noise-added 50-event data set. Figure 5.7 shows the focal depth results and Table 5.4 shows the velocity model results. Results from when the interface was fixed at 12 km (Figure 5.5 and Table 5.2) are nearly identical to the results of this final test. Most importantly, the magma body depth and the focal depth estimates are nearly unchanged. This test shows that the focal depth estimates and the magma body depth estimate obtained from inverting real data will probably not change significantly if the choice of the velocity interface depth is changed.

TABLE 5.3. Synthetic Results Comparison - Standard Deviations on Parameter Esimates

Parameter Type	50 Events 713 Direct 246 Reflected	60 Events 852 Direct 289 Reflected	70 Events 1032 Direct 331 Reflected	80 Events 1178 Direct 377 Reflected
BAR	0.046	0.044	0.036	0.034
BMT	0.052	0.051	0.043	0.040
CAR	0.041	0.038	0.031	0.028
LAZ	0.057	0.056	0.047	0.044
LJY	0.039	0.038	0.033	0.031
LPM	0.058	0.055	0.046	0.042
SB	0.039	0.038	0.031	0.029
SMC	0.058	0.054	0.044	0.040
WTX	*	*	*	*
V_{p1}	0.053	0.050	0.040	0.037
V_{p2}	0.115	0.113	0.093	0.089
ν_1	0.003	0.002	0.002	0.002
ν_2	0.010	0.010	0.009	0.008
Z_1	*	*	*	*
Z_2	0.331	0.283	0.238	0.225

Station correction values are given in sec, velocities in km s^{-1}, and depths in km. Station correction for WTX and depth to base of seismogenic zone (Z_1) were both held constant. Z_2 is depth to the magma body.

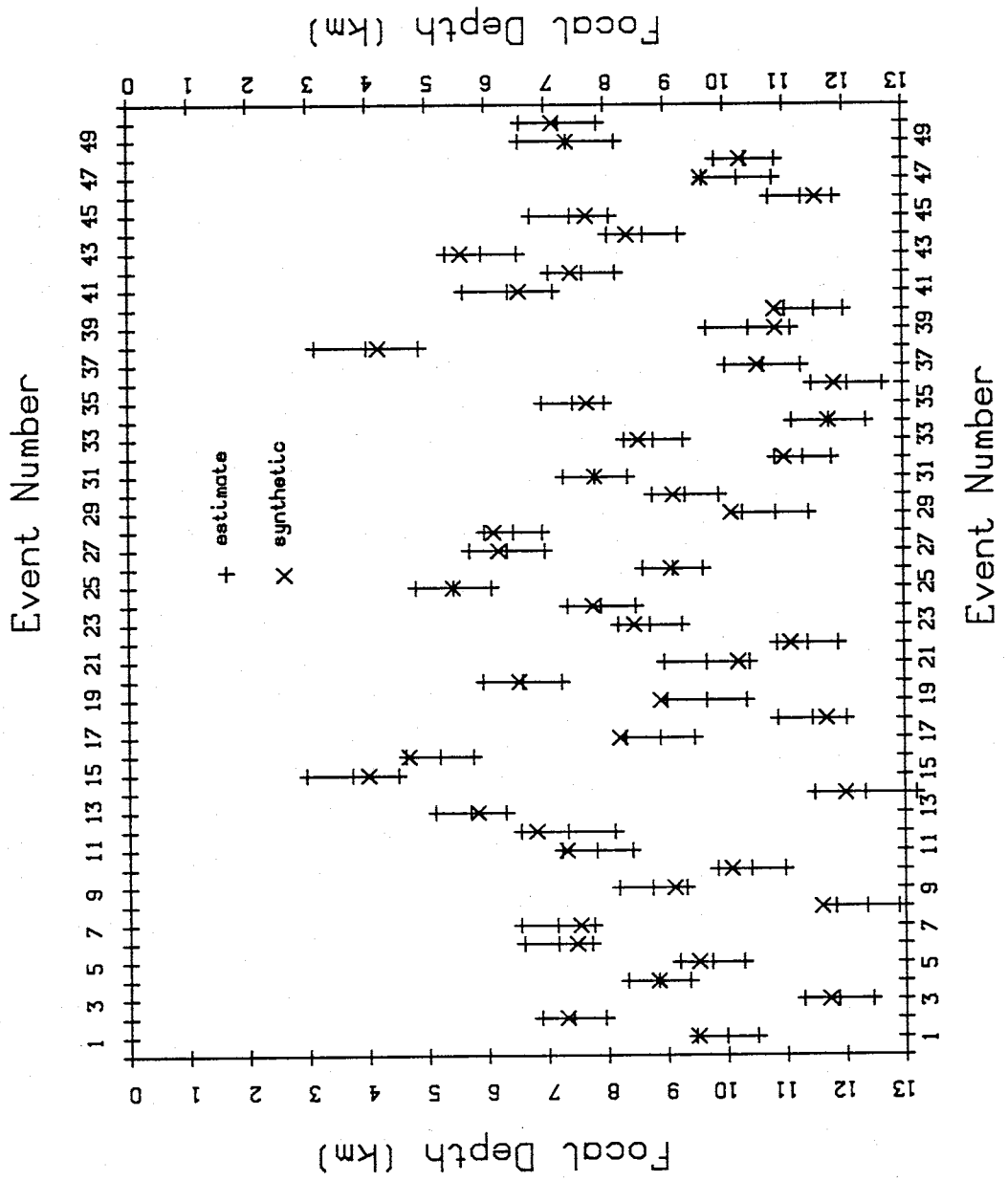

Fig. 5.7. Focal depths of 50 synthetic events (X's), inversion estimates (center cross bars) obtained with noise-added data, and error bars at one standard deviation (upper and lower cross bars). These results were obtained by holding constant the interface between the upper and lower layers of the velocity model at 10 km rather than 12 km. Turn figure sideways for best viewing.

TABLE 5.4. Model Parameter Estimation Using Noise-Added Data From 50 Synthetic Events - First Layer at 10 km -

713 Direct Arrivals - 246 Reflected Arrivals

Parameter Type	Starting Model	Actual Value	Inversion Estimate	Difference	1 Std
BAR	0.000	-0.030	-0.034	0.004	0.046
BMT	0.000	0.140	0.125	0.015	0.052
CAR	0.000	-0.080	-0.072	0.008	0.041
LAZ	0.000	0.040	0.032	0.008	0.057
LJY	0.000	0.560	0.545	0.015	0.039
LPM	0.000	-0.230	-0.228	0.002	0.058
SB	0.000	0.220	0.197	0.023	0.039
SMC	0.00	0.110	0.100	0.010	0.058
WTX	0.000	-0.080	-0.080	0.000	*
V_{p1}	6.000	5.850	5.834	0.016	0.053
V_{p2}	6.000	5.960	5.904	0.056	0.093
ν_1	0.250	0.260	0.260	0.000	0.003
ν_2	0.250	0.250	0.249	0.001	0.008
Z_1	10.000	12.000	10.000	0.000	*
Z_2	20.000	19.200	19.310	0.110	0.314

Station correction values are given in sec, velocities in km s^{-1}, and depths in km. Station correction for WTX and depth to base of seismogenic zone (Z_1) were both held constant. Z_2 is depth to the magma body.

6. Data

Overview

This section describes the data used in the study. This includes the microearthquake network which recorded the data, the criteria for selecting individual events, phase identification and timing, details of the direct and reflected phases, some general observations concerning the data set, and a comparison with other data sets previously used to study central New Mexico seismicity The phases used in this project are direct P, direct S, and mid-crustal magma body reflections S_zS, S_zP, and P_zP. Figure 6.1 shows an approximate velocity-depth model of the central Rio Grande rift and a raypath of each phase.

Seismic Network

The data used in this study come from seismograms recorded on the Socorro seismic network (Figure 6.2). This network has operated since 1981, and the seismograms used here were recorded between 1982 and 1990. None of the stations has operated continuously over this time period, but between 6 and 11 stations did record every event used in this study. Table 6.1 lists the latitude, longitude, and elevation of each station. The network covers the Socorro area, approximately 80 km north-south and 60 km east-west, and is centered about 34°10′ N, 106°58′ W near station LEM. Station MLM is about 35 km north of the network's northern limit and recorded eight events of my data set.

The network is a telemetered, analog system with central recording on the New Mexico Tech campus. The system's key field components for each station are a vertical-component seismometer (either 0.8 hz or 1 hz natural frequency), a preamplifier/voltage-controlled-oscillator, and a transmitter. In the observatory the key components for a single channel are a receiver, a discriminator, and a voltage-driven amplifier/helicorder. Figure 6.3 is the theoretical system response, derived from manufacturers specifications for individual components, plotted as magnification versus frequency. The records are written with a hot-wire stylus on

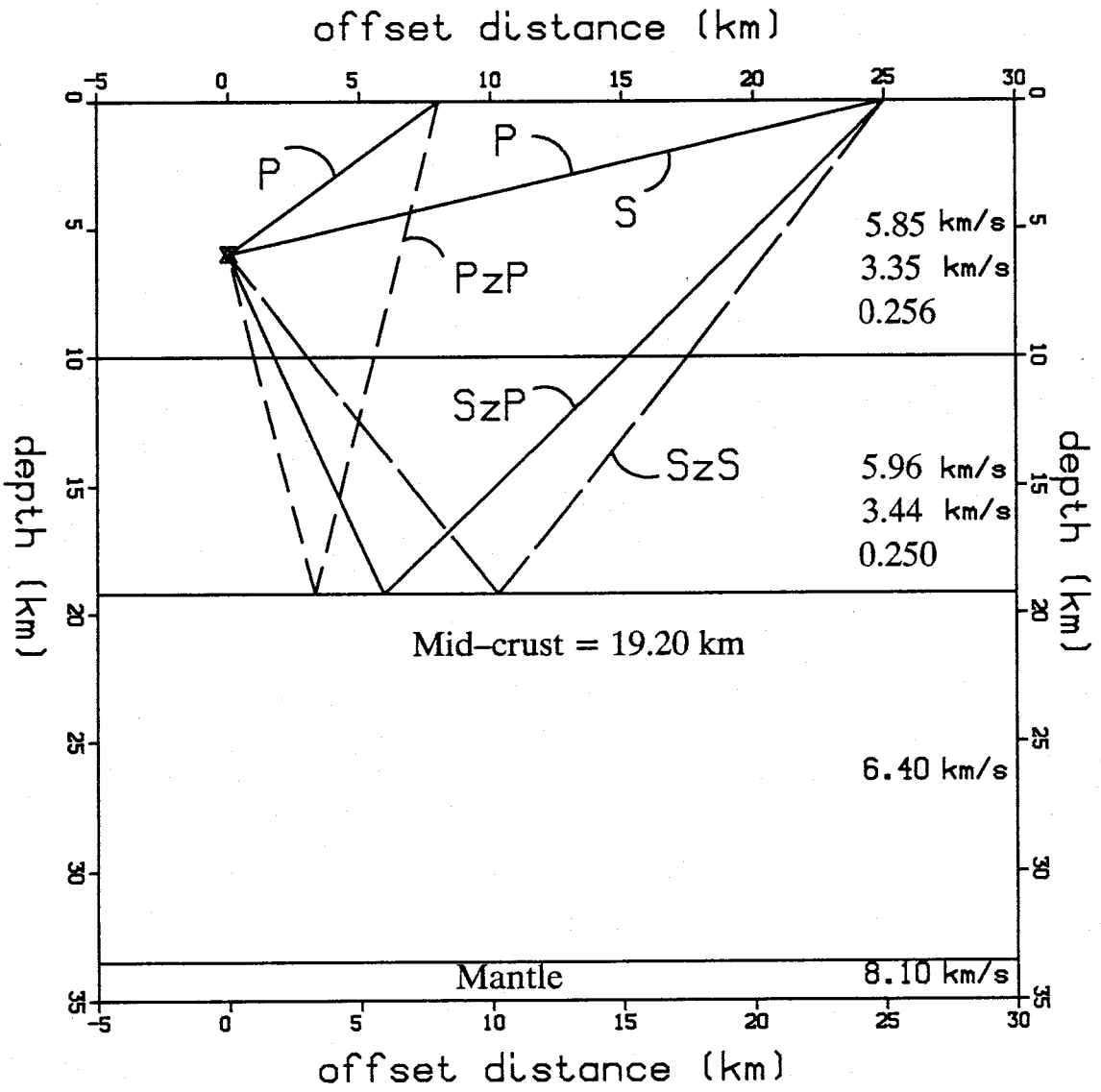

Fig. 6.1. Sample raypath of each arrival time phase used in this study.

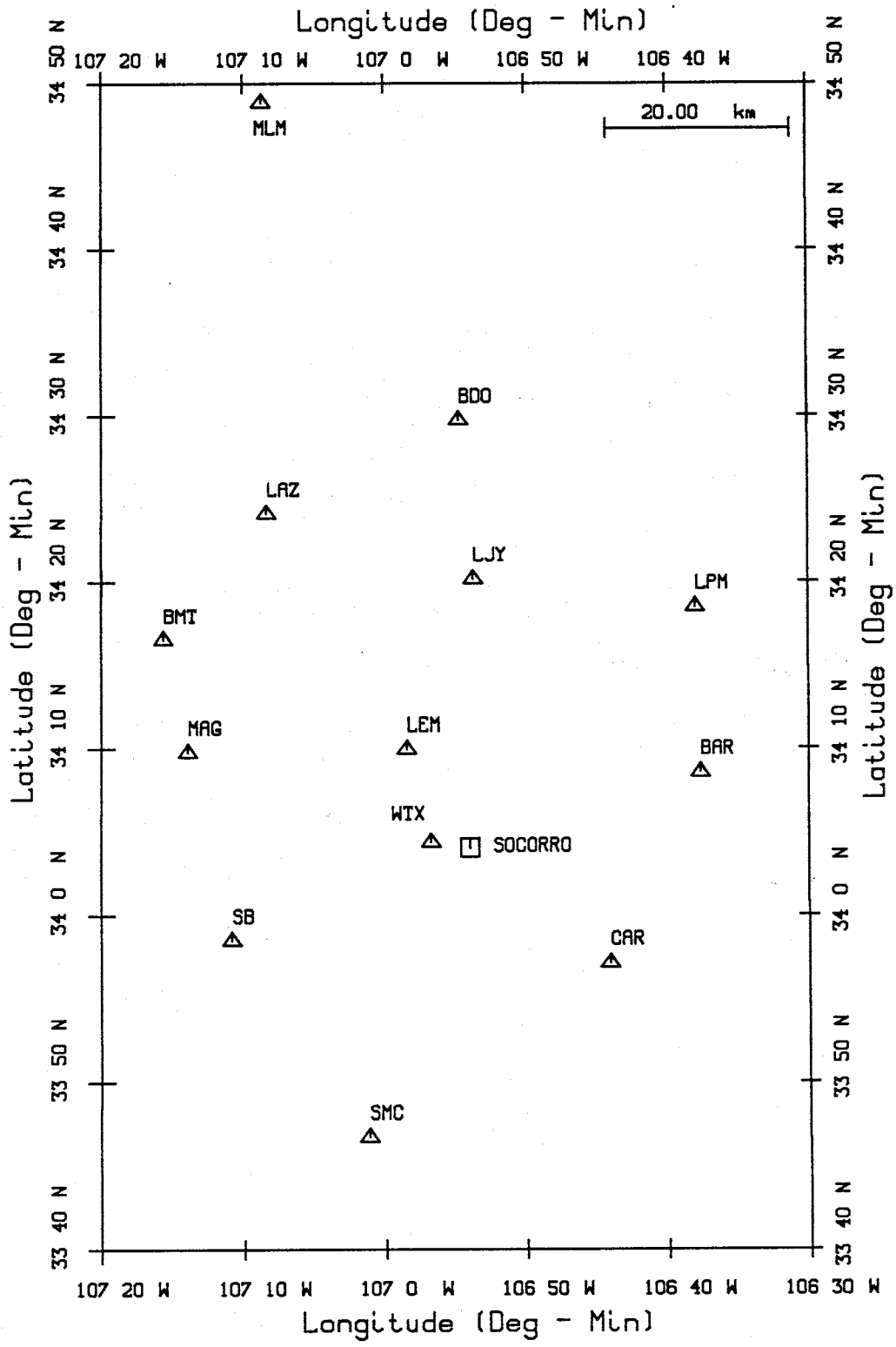

Fig. 6.2. Locations of stations which recorded data used in this study.

TABLE 6.1. Station Information

Station	Latitude (N)	Longitude (W)	Elevation (km)
BAR	34° 08.52′	106° 37.68′	2.120
BDO	34° 29.76′	106° 54.79′	1.505
BMT	34° 16.50′	107° 15.61′	1.972
CAR	33° 57.15′	106° 44.07′	1.662
LAZ	34° 24.12′	107° 08.36′	1.853
LEM	34° 09.93′	106° 58.45′	1.689
LJY	34° 20.19′	106° 53.75′	1.532
LPM	34° 18.77′	106° 38.03′	1.707
MAG	34° 09.75′	107° 13.92′	1.926
MLM	34° 48.85′	107° 08.70′	2.088
SB	33° 58.51′	107° 10.84′	3.230
SMC	33° 46.72′	107° 01.16′	1.560
SNM	34° 04.21′	106° 56.61′	1.511
WTX	34° 04.33′	106° 56.75′	1.555

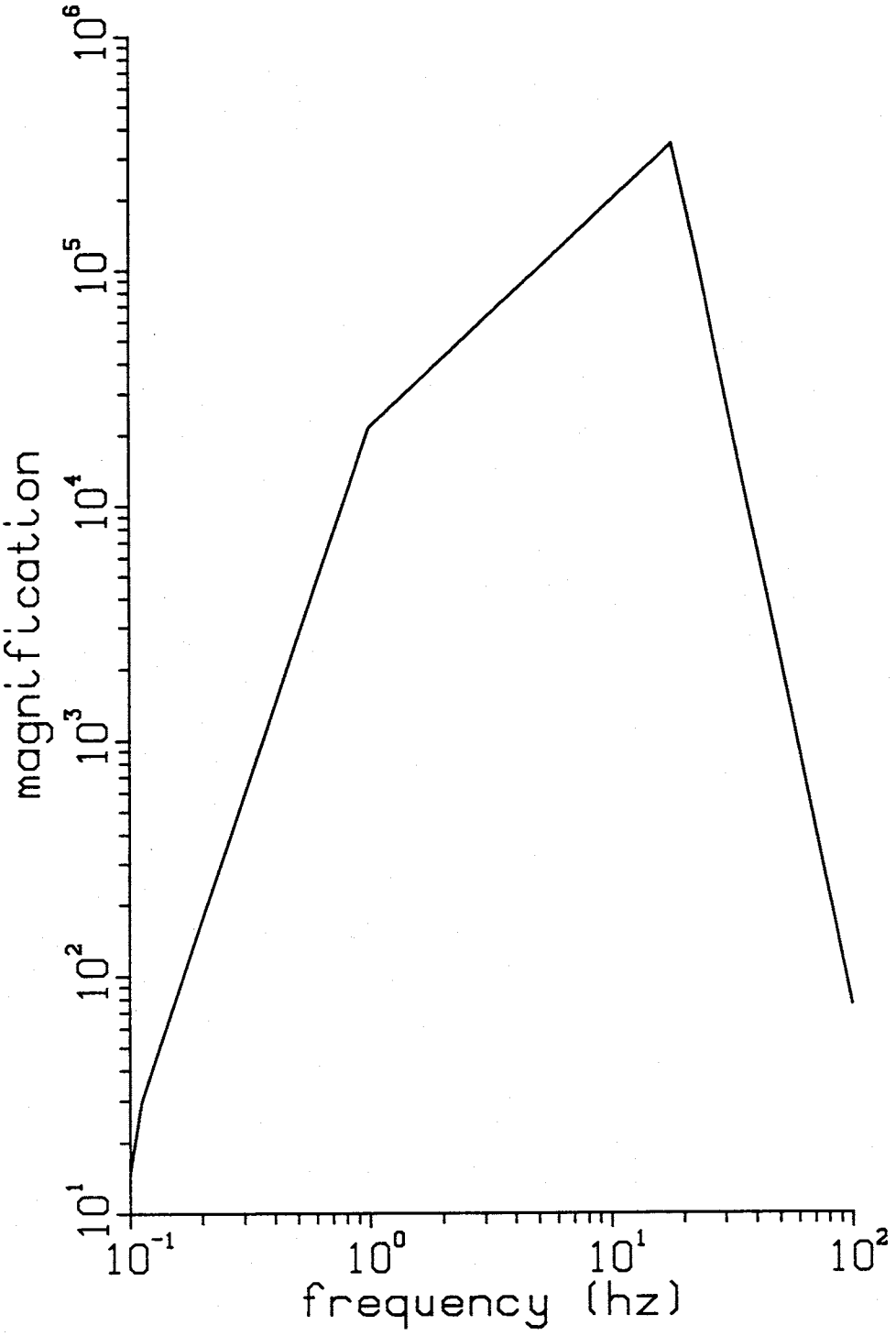

Fig. 6.3. System response of a typical Socorro seismic network station assuming an initial ground motion of 1×10^{-8} m.

heat sensitive paper. Recording speed is 1 mms^{-1}. Timing is controlled at the observatory and a clock is synchronized daily with WWV.

Event Selection

Events were selected which had good quality solutions, contained at least three reflections, and provided a wide epicentral and depth distribution across the Socorro area. The primary objective of these criteria was to obtain a data set which evenly sampled the crust in the study area to the depth of the magma body. Requiring three or more reflections per event was intended to help smooth possible magma body dip effects on each focal depth estimate. Also, requiring many reflections helped build a data set with both near and far offset reflections. A combination of near and far offset data are important in simultaneously resolving depth and velocity [*Braille*, 1973].

Since most of these events had previously been located using HYPO71 (Revised) [*Lee and Lahr*, 1975], only events with A or B composite qualities were considered. This eliminated events with large gaps, large near-station distances, and few recording stations. Figure 6.4 is an epicenter map for the 75 earthquakes in the final data set. The map shows that the criteria mentioned above require all events to fall inside the network.

A minimum of six stations were required to record each event. The most common number of stations recording an event was nine (Table 6.2). At least 12 picks were required for each event, and of those 12 picks at least three had to be reflections. The most common number of total picks per event was 20 (Table 6.3). A minimum of two stations per event were required to record reflections, provided at least one of the stations recorded a reflection pair (S_zP and either S_zS or P_zP). If no station recorded a reflection pair, then at least three stations were required to record reflections. Thirty-nine events recorded two or more reflection pairs, 31 events recorded at least one reflection pair, and only five events recorded no reflection pairs. Total reflection picks per event varied between three and 10 (Table

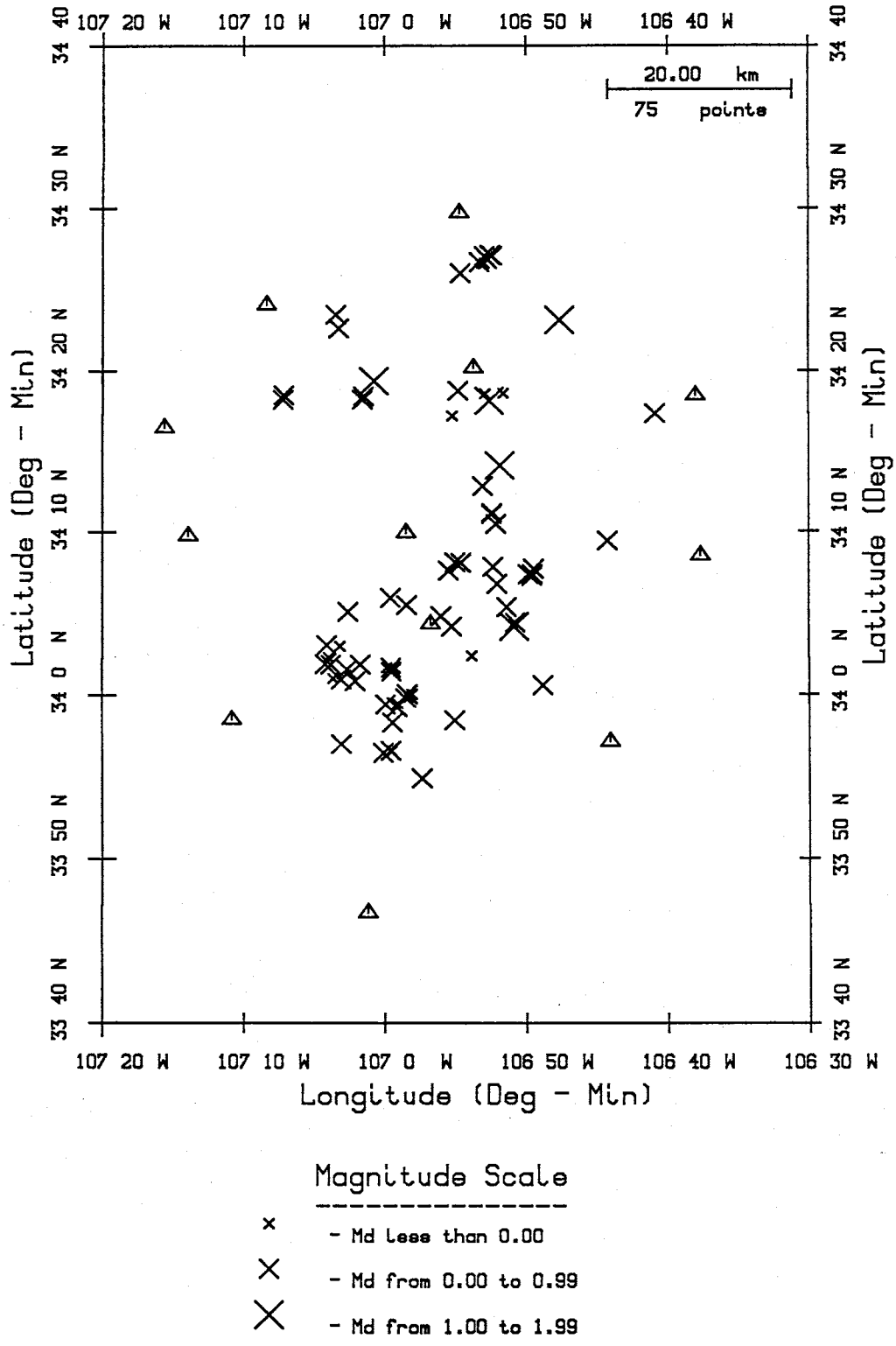

Fig. 6.4. Epicenters (X's) of the 75 earthquakes composing the data set. Also shown are the stations which recorded the data (triangles).

TABLE 6.2. Number of Events Recorded by Number of Stations

Stations	Events	Stations	Events
6	7	9	21
7	14	10	11
8	19	11	3

TABLE 6.3. Total Number of Arrivals Picked per Number of Events

Arrivals	Events	Arrivals	Events
12	1	20	18
13	0	21	7
14	1	22	4
15	4	23	1
16	8	24	1
17	9	25	2
18	8	26	5
19	5	27	1

TABLE 6.4. Number of Reflections Picked per Number of Events

Reflections	Events	Reflections	Events
3	7	7	12
4	14	8	4
5	25	9	2
6	10	10	1

6.4).

Phase Identification and Timing

Phase identification was based on the results of previous Socorro-area microearthquake investigations. *Sanford and Holmes* [1961] first recorded earthquakes in central New Mexico in the early 1960s. They identified P and S and also recognized four other phases. They postulated that two of these phases could be a matched $P_zP - S_zS$ reflected pair from a crustal discontinuity. *Sanford and Long* [1965] identified S_zS *and* S_zP reflections and *Sanford et al.* [1973] confirmed the earlier S_zS and S_zP identifications. Building on the work of these earlier investigations identification of reflected phases has almost become routine [*Sanford et al.*, 1977; *Rinehart et al.*, 1979; *Rinehart and Sanford*, 1981; *Ake and Sanford*, 1988; *Gridley*, 1989].

For this project a series of theoretical arrival time curves were constructed to aid in phase identification. Figure 6.5 shows a sample set of these curves for a focal depth of 8 km. The curves, plotting S-minus-P time versus phase-minus-P time, were generated for focal depths of 2, 4, 6, 8, 10, and 12 km and were based on the best known velocity model to the magma body [*Rinehart*, 1981]. At short epicentral distance all reflections arrive later than direct S. As epicenter distance increases P_zP and then S_zP arrive before direct S. However, S_zS never arrives before direct S. As a seismogram was timed these curves helped determine which phases were reflections and which phase was S.

All phases were carefully timed on a light table using a magnifying eyepiece which has a built-in scale with 0.1 millimeter gradations. Phases were read to the nearest 0.05 sec. Pick quality was assigned on a scale of 0 to 5. Zero represented a clear, sharp arrival where the first break of the phase could be easily distinguished. Thus, 0 weights were assigned only to the best P picks, and no other phases were ever weighted 0. A weight of 1 was assigned to P picks whose first breaks could not be positively identified but were still impulsive. A few S and S_zP

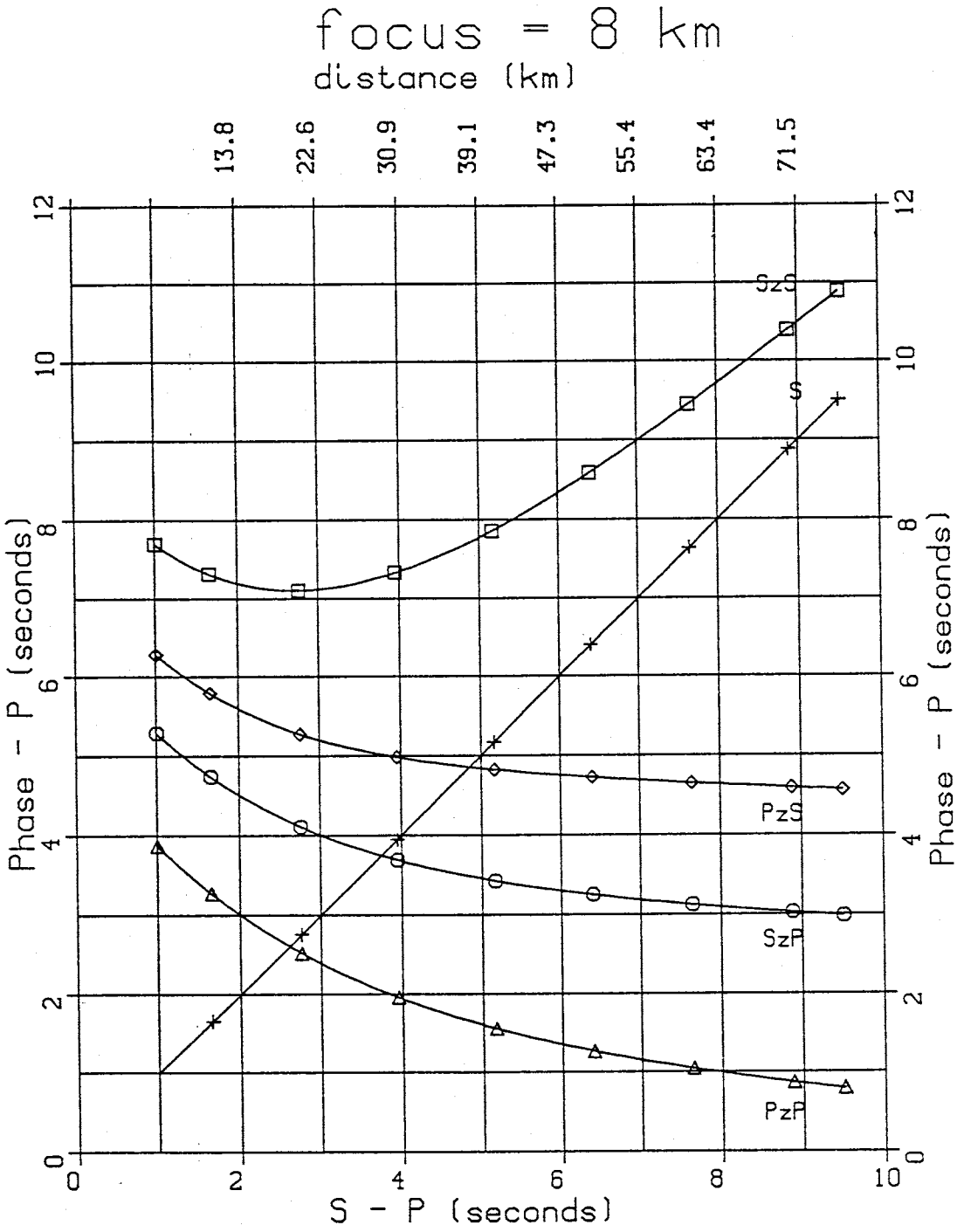

Fig. 6.5. Relative arrival time curves used to help identify secondary arrivals. These curves are based on the velocity model shown in Figure 6.1 and an event depth of 8 km.

picks were also weighted as 1. These were exceptionally impulsive secondary arrivals. Weights of 2 through 5 were assigned to the secondary phases, with a 2 being a clear pick, 3 a good pick, 4 a poor pick, and 5 a very poor pick. Table 6.5 lists the numbers of picks which were assigned various weights. The first column of this table lists the quality factor (0-5) and the assumed timing error in seconds associated with each factor. Thus, timing errors for this project vary between 0.075 and 0.450 sec. The necessity of assuming timing error is explained under **Method.**

Direct Arrivals

Direct P recorded on the Socorro network is generally clear and sharp. It is the most commonly recorded phase comprising the data set (Table 6.3). From a total of 564 P picks, 413 were weighted as 0 or 1. In addition to contributing to hypocenter estimation, P provides information on V_p within and above the seismogenic zone. Because P is by far the clearest pick of the data set, it also has the most influence on station correction estimation.

Direct S is generally a recognizable phase on Socorro-area seismograms. This data set contains 485 S picks of which 332 are weighted as 3. S is a valuable phase when estimating Poisson's ratio (ν) for the upper crust and for constraining event origin time. When origin time is constrained, then focal depth can also be constrained. This is especially true when an S can be combined with a P from a station with an epicentral distance less than one and a half times the focal depth [*Gomberg et al.,* 1989]. It should be noted that S is a common pick because these events have small magnitudes. Since all events here are less than magnitude 1.6, the P coda is quite small and does not overwrite the S arrival. The small events are also necessary for reflected phase identification. If events are too strong, both direct P and S codas will interfere with reflected arrivals.

TABLE 6.5. Phase and Pick Quality Information

Quality	P	S	S_2S	S_2P	P_2P
0 (0.075 s)	238	0	0	0	0
1 (0.150 s)	193	2	0	4	0
2 (0.225 s)	78	97	25	39	15
3 (0.300 s)	52	332	72	71	36
4 (0.375 s)	3	53	50	37	22
5 (0.450 s)	0	1	22	9	4
Totals	564	485	169	160	77

Reflected Phases

The strong reflected phases which have been well documented within the Socorro area provide unique information about the crust down to about 19 km depth. This includes information on velocity, Poisson's ratio, magma body depth, and event depths. The reflections are often of remarkably high amplitude (Figure 6.6) when considering they are analog recordings with no corrections for geometrical spreading or any other gain control applied to the data. *Sanford et al.* [1973] attributed these high amplitudes to asymmetrical radiation of energy from earthquake foci and the layer below the reflecting interface having zero rigidity.

The S_zS and S_zP phases are seen about equally often on Socorro-area seismograms (Table 6.5). The quality of S_zP is slightly better than S_zS, probably because of the vertical component seismometers comprising the network. However, S_zS always arrives later than all other phases, and the time separation from the direct S coda is often large which makes identification easy. P_zP is the least commonly identified reflected phase of the data set. This is partially because some P energy is transmitted through the magma body while virtually all S energy is reflected. Also, P_zP often arrives within the much stronger direct P and S codas. P_zP is most commonly seen on short offset records of small magnitude, where it arrives after direct S, and on long offset records of small magnitude where direct P is weak.

General Observations

By examining Table 6.6 several observations can be made concerning this data set. First, all stations comprising the network have recorded reflections. If reflections were seen only at a few stations, then an argument could be made that the energy seen as secondary arrivals is a function of those few stations. For instance, near-station diffractions or some type of near-surface multiple unique to a station could account for these phases. Since two or more stations record three or more reflections for every event in this data set, and the events are evenly

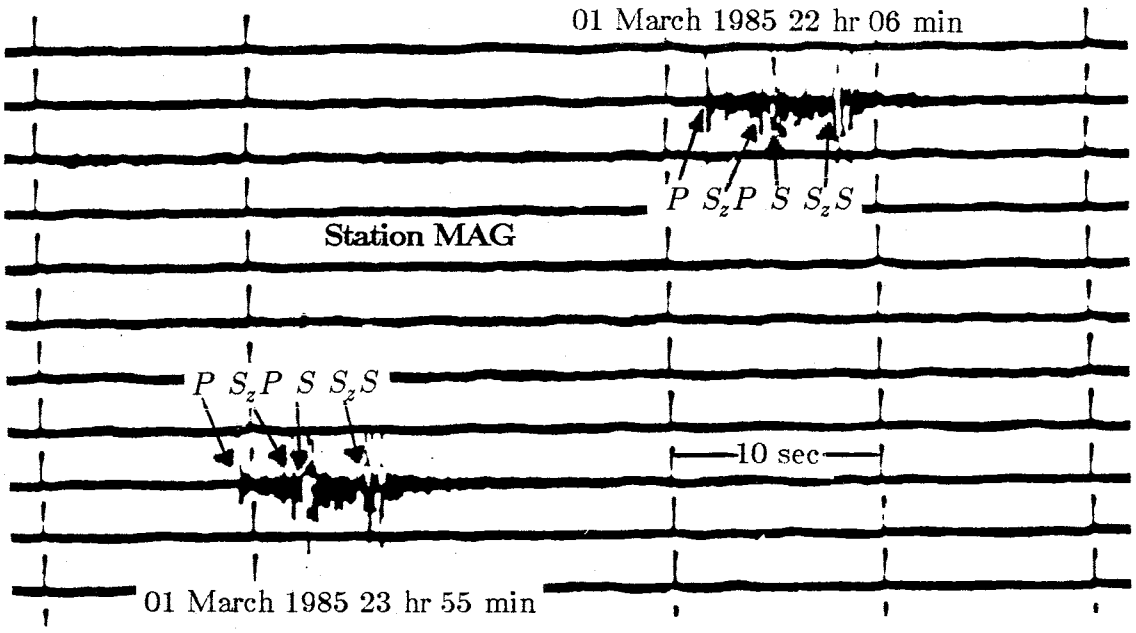

Fig. 6.6. Typical seismograms used to obtain the arrival time data set used in this study.

TABLE 6.6. Station and Pick Information

Station	P	S	S_zS	S_zP	P_zP	Total
BAR	72	62	9	17	9	169
BDO	10	0	0	3	0	13
BMT	40	34	23	25	13	135
CAR	64	55	3	9	2	133
LAZ	55	59	32	23	14	183
LEM	24	18	13	7	1	63
LJY	35	10	0	3	3	51
LPM	64	62	19	9	12	166
MAG	35	30	26	18	14	123
MLM	3	2	5	2	0	12
SB	42	42	12	12	4	112
SMC	49	50	0	15	1	115
SNM	14	10	2	1	0	27
WTX	57	51	25	16	4	153

distributed across the Socorro area, the phases must be reflections from an areally extensive reflector.

Second, stations BDO and MLM recorded few events. This is because BDO is a recently installed station (February, 1990), and MLM is north of the network and recorded few of the small events which comprise this data set. SNM also recorded few events. SNM and WTX have essentially the same location, except WTX is in a mine approximately 300 m inside Socorro Mountain. WTX has been operated more often than SNM because it is the quieter of the two locations.

LJY and BDO record few shear energy arrivals because these stations are on low-velocity valley fill, and S waves arriving from all offset distances are refracted to near vertical angles of incidence before arriving at these stations. All stations have vertical component seismometers, and therefore the vertically arriving shear waves are poorly recorded.

SMC recorded few S_zS and P_zP phases. Since SMC is the most southern station of the network, many potential S_zS and P_zP reflection points are between the southern limit of the mapped epicenters and station SMC (Figure 6.4). These reflections are not seen at SMC which suggests the southern limit of the magma body is around 33°55′ N. On the other hand, S_zP is often observed at SMC because reflection points for S_zP occur much closer to the epicenter than to the station.

Comparisons With Other Data Sets

This section compares the data types and quantities of this study with data sets for previous studies of the central Rio Grande rift. This comparison is limited to locally recorded earthquake data which was used to determine crustal velocity models, hypocenters, and map the magma body (Table 6.7). The data types considered here are P, S, S_zS, S_zP, P_zP.

Table 6.7 shows that this is the first central Rio Grande rift study to combine compressional and shear data to solve for velocity. This is also the first study to

TABLE 6.7. Data Set Comparisons of Selected Socorro-Area Earthquake Studies

Investigators	Year	Purpose	Data Type	Quantities
Rinehart, Sanford, and Ward	1979	Map the magma body	S_zS	220
Rinehart and Sanford	1981	Find V_s to magma body and find depth to magma body	S_zS	≈250
Ward, Schlue, and Sanford	1981	Find V_p in upper 10 km of crust and find hypocenters	P	262
Gridley	1989	Map the magma body	S_zS and P_zP	204
Present study	1991	Find V_p and ν to magma body, find depth to magma body, and find hypocenters	P, S, S_zS, S_zP, and P_zP	564, 485, 169, 160, and 77, (1455 total data)

combine both direct and reflected phases to solve for hypocenters and crustal structure simultaneously. Since the present study combines P and S data, this is the first study to solve for Poisson's ratio (ν) as part of the velocity model. Previously *Sakdejayont* [1974], *Caravella* [1976], and *Fender* [1976] studied ν in central New Mexico using S-minus-P intervals. This is the first study to use S_zP arrivals. This phase adds extra focal depth and reflector depth constraint, provides additional information on V_p and ν, and also adds more total reflection points which can be used to map the magma body.

The distribution of epicenters is better with the present study than previous studies. For instance *Rinehart et al.* [1979] used data from a temporary network which was often deployed closer to Socorro and the southern end of the magma body (Figure 6.7 compared to Figure 6.4). Since the present study used the permanent Socorro network, a wider distribution of epicenters and a more evenly distributed set of reflected phases could be assembled. Figures 6.8 and 6.9 compare the geographic distribution of reflection points between the current study and the study of *Rinehart et al.* [1979].

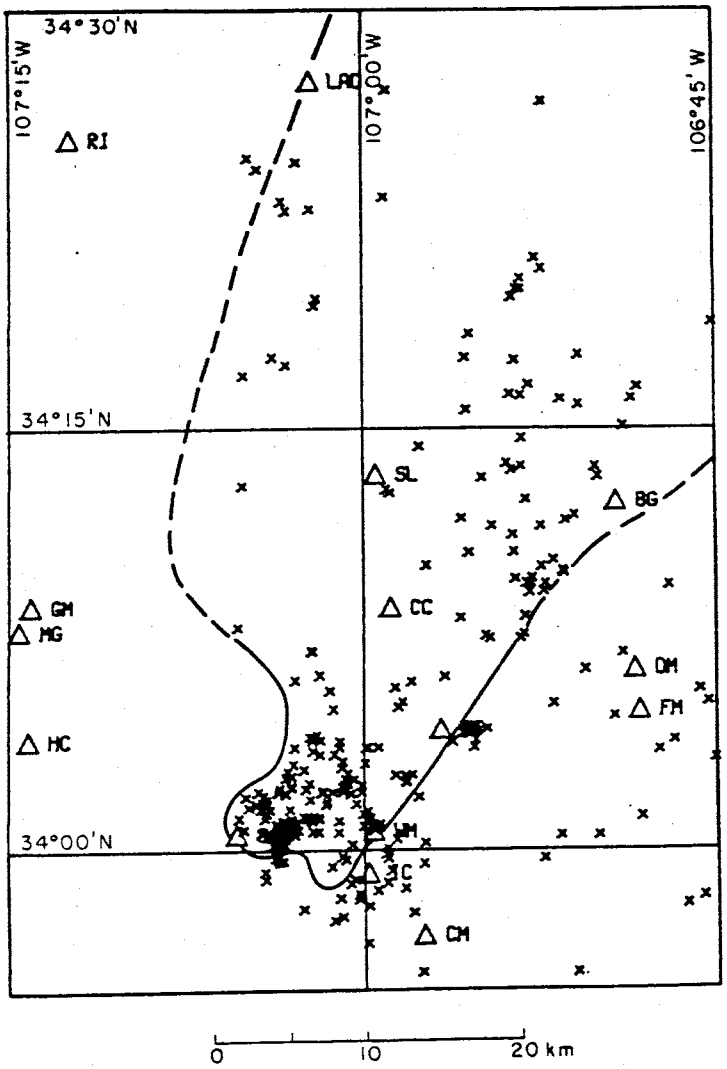

Fig. 6.7. Epicenter distribution and station locations from *Rinehart et al.* [1979].

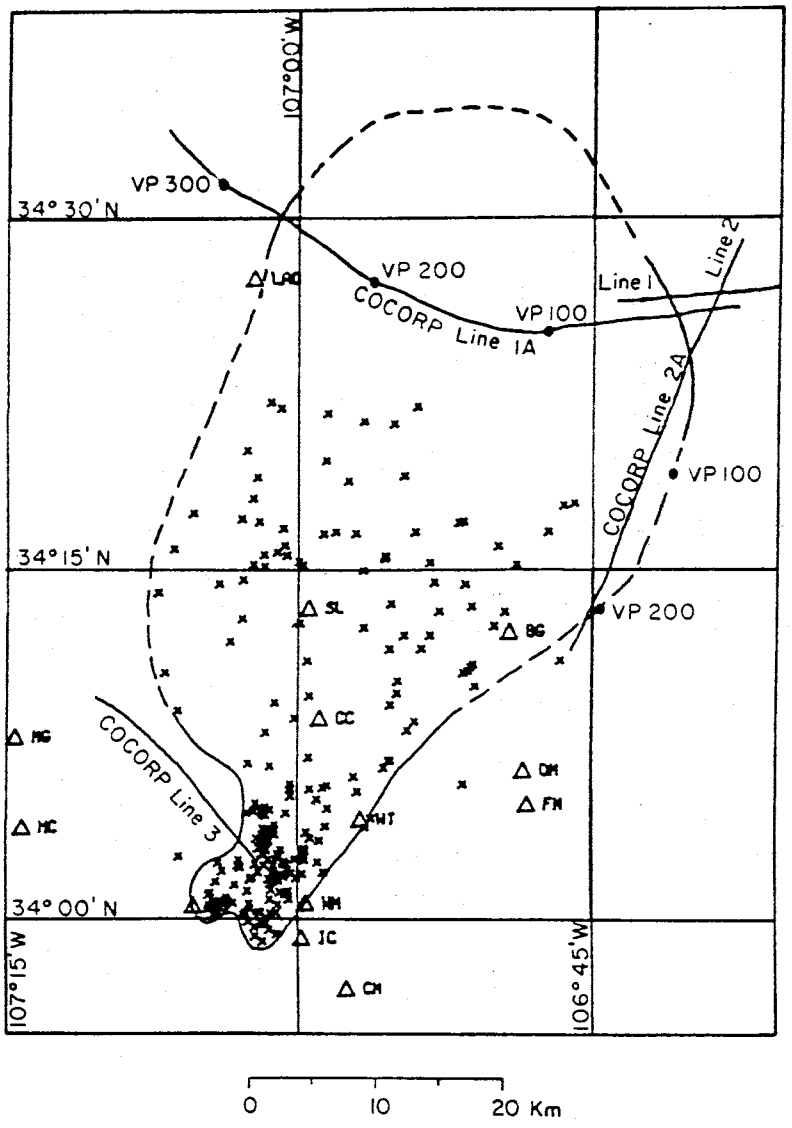

Fig. 6.8. Reflection point distribution from *Rinehart et al.* [1979].

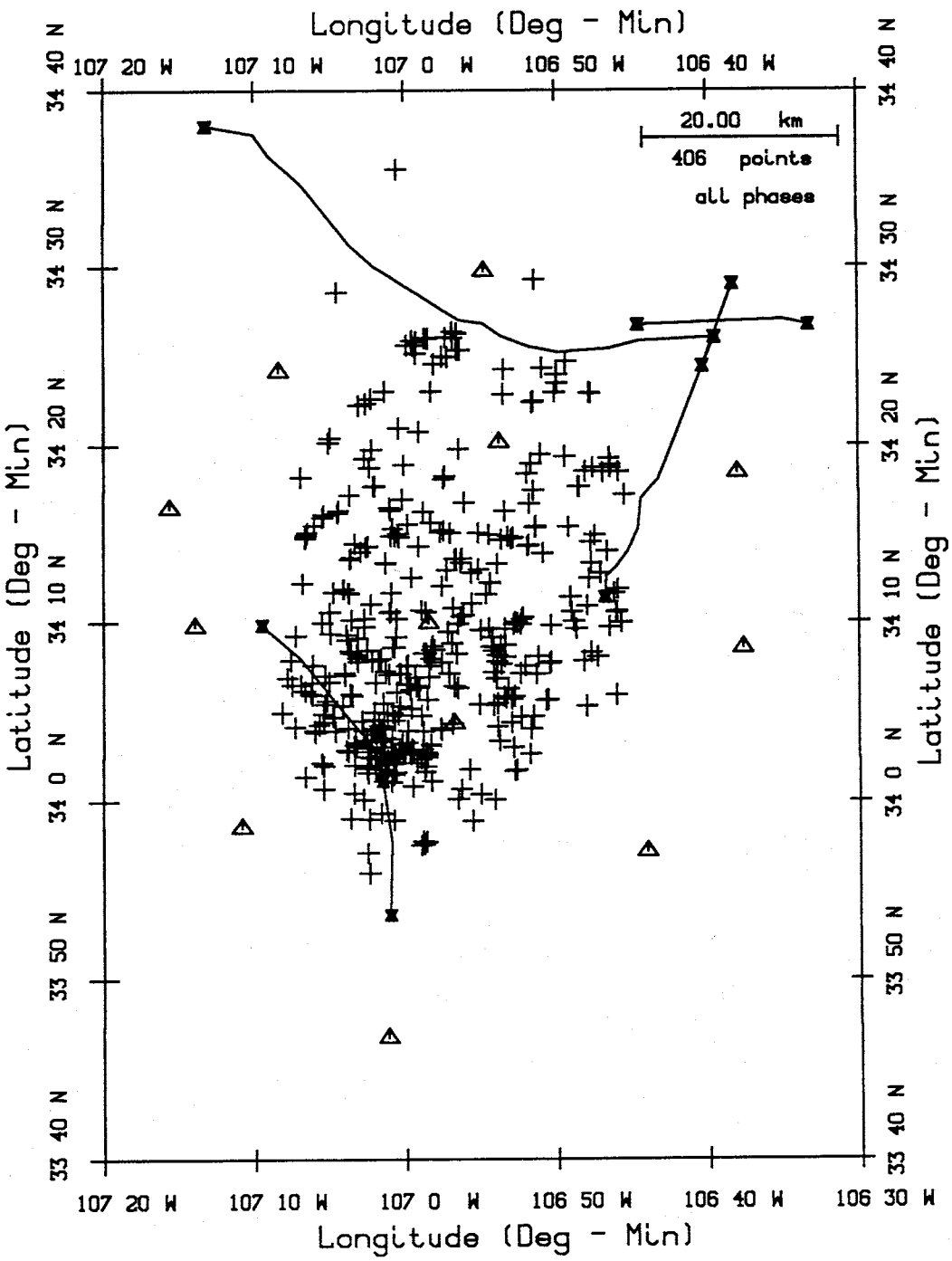

Fig. 6.9. Reflection point distribution from the present study and COCORP lines.

7. Results

Overview

After testing with synthetic data and then assembling a real data set, I solved for hypocenters and a velocity model. The model parameters treated as unknowns were the velocities and Poisson's ratios above and below the approximate base of the seismogenic zone, the depth to the upper surface of the magma body, and station corrections. Four hypocenter parameters, latitude, longitude, focal depth, and origin time, were associated with each earthquake of the 75 event data set. Thus, there were a total of 318 unknowns in this problem; two velocities, two Poisson's ratios, one reflector depth, 13 station corrections and the 300 hypocenter parameters. A total of 1455 arrival time data consisting of 564 P, 485 S, 169 S_zS, 160 S_zP, and 77 P_zP picks were used to solve for these unknowns.

The station correction for WTX was held constant for all inversions at a value of -0.080 s. WTX was selected because it is near the center of the network, operated nearly continuously while the data were acquired, and it is sited on Precambrian basement. The correction of -0.080 s is a value which has often been used by previous researchers. It has been considered the "standard" correction at WTX for locating local events using HYPO71 (revised) [*Lee and Lahr*, 1975], and it is close to the average value found by three previous investigators. *Ward* [1980] found a value of -0.110 s, *Ake* [1984] found -0.160 s, and *Singer* [1989] found a P_g time term of 0.060 s, for an average of -0.070 s. Selecting a slightly different correction value at WTX would only cause a relative shift in corrections at the other stations, and it would not affect the velocity or depth estimates.

I ran each inversion the same way the synthetic tests were run. Initial epicenters were estimated from the closest station recording an event, initial focal depths were all 7.0 km, and initial origin times were estimated from $S-P$ intervals. I assumed each station correction had a starting value of 0.0 s, both velocities were 6.0 km s^{-1}, both Poisson's ratios were 0.250, and magma body depth was 20.0 km. I first solved for hypocenters holding the initial velocity model fixed.

Then, I solved for station corrections holding velocities, Poisson's ratio, magma body depth, and the new hypocenter estimates constant. Finally, using the new station corrections and hypocenter estimates, I ran the inversion treating all parameters as unknowns. Each final inversion converged to reasonable parameters, standard deviations approximated results from synthetic tests, and all eigenvalues were kept in each solution. Velocity model parameters usually converged in five iterations while some hypocenter parameters took seven iterations to converge.

I ran two inversions to evaluate the most likely depth for the first layer. I ran an inversion where the depth to the base of the first layer was held constant at 12 km, and then I ran a second inversion where the depth was held constant at 10 km. To see how well a one-layer model could be fit to the observed data , I assumed a single-layer to the depth of the magma body and ran another joint inversion. Finally, to test if results were initial-model dependent, I ran inversions for the 10 km case using initial models which were extremely different from the starting model outlined above. Presented below are sub-sections on the possibility of head wave arrivals when solving a two-layer model, the most appropriate depth to the base of the first layer, the possible dip on the upper surface of the magma body, the improvement in hypocenter estimation when reflections are included in the location process, and the new velocity model I obtained from the inversions.

Possible Head Wave Arrivals

Assuming a two-layer model creates the possibility of head-waves arriving before direct phases, provided velocity increases from the upper to the lower layer and source-receiver distances are sufficiently large. Head wave arrivals from 10 to 18 km depth have never been previously detected for the Socorro area of the Rio Grande rift. Furthermore, the events represented by my data set all fall inside the network (Figure 6.4), limiting maximum possible source-receiver distances. However, because I invert my data while assuming they are either direct or reflected phases, it is necessary to examine the possibility of head wave arrivals.

Compressional velocity above 10 km depth has been estimated by *Ward et al.* [1981] at 5.85 km s^{-1}. Compressional velocity below the approximate base of the seismogenic zone has never before been estimated for the Socorro area, but the greatest V_p estimated within the rift just below 10 to 12 km depth is 6.1 km s^{-1} [*Sinno et al.*, 1986]. Figures 7.1 and 7.2 are time-distance curves for 12 and 10 km deep interfaces based on a 5.85 to 6.10 km s^{-1} velocity increase. The P curves represent the direct arrival and the P_g curves the head wave arrival for the cases where an earthquake occurs just above each interface (the shortest possible source-receiver distances with head waves arriving before direct phases will occur when earthquakes are just above the velocity interface). For both cases, distances must be greater than about 60 to 70 km for the head wave to arrive at a measurable time (assumed timing errors vary between 0.075 and 0.450 s) before the direct arrival. Figure 7.3, my real direct-arrival data plotted as traveltime versus distance, shows that all but 6 data arrive from distances less than 60 km. The deepest event associated with any of these 6 data is only 7.7 km, well above the 10 or 12 km interfaces. No changes in the slopes of either the P or S plots are noticeable, further demonstrating that head wave arrivals are not present in this data set. Hence, assuming a two-layer model with a 10 or 12 km velocity interface, it is not necessary to model potential head waves when inverting these data.

Depth of the First Layer

Because this data set contained no information which could uniquely resolve the trade-off between velocity and the depth to the base of the first layer of my model, I made no attempt to treat this depth as an unknown in any inversions. Instead, I fixed the depth of the first layer where the deepest earthquakes of the data set occurred. By using this approach I assumed that the approximate base of the seismogenic zone is a reasonable depth at which to expect a velocity change. For my first inversion, using a 12 km depth for the first layer, I solved the joint problem (Table 7.1 shows the new velocity model) and then examined focal depths (Figure 7.4). The deepest events found were just over 10 km, suggesting a more appropriate

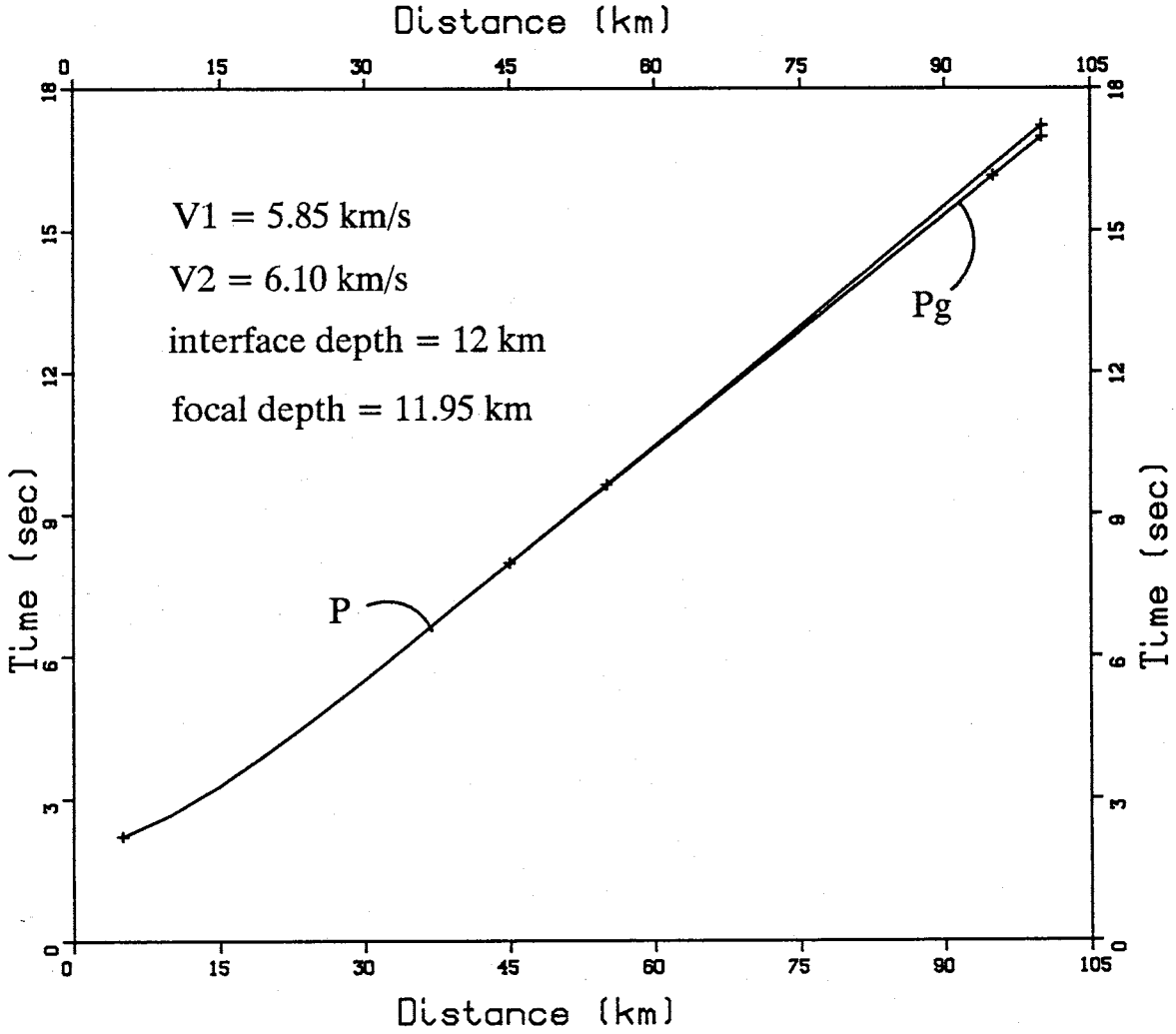

Fig. 7.1. Theoretical time versus distance curves for direct arrivals (P) and head wave arrivals (P_g). The velocities and interface depth (12 km) are typical values from the central Rio Grande rift.

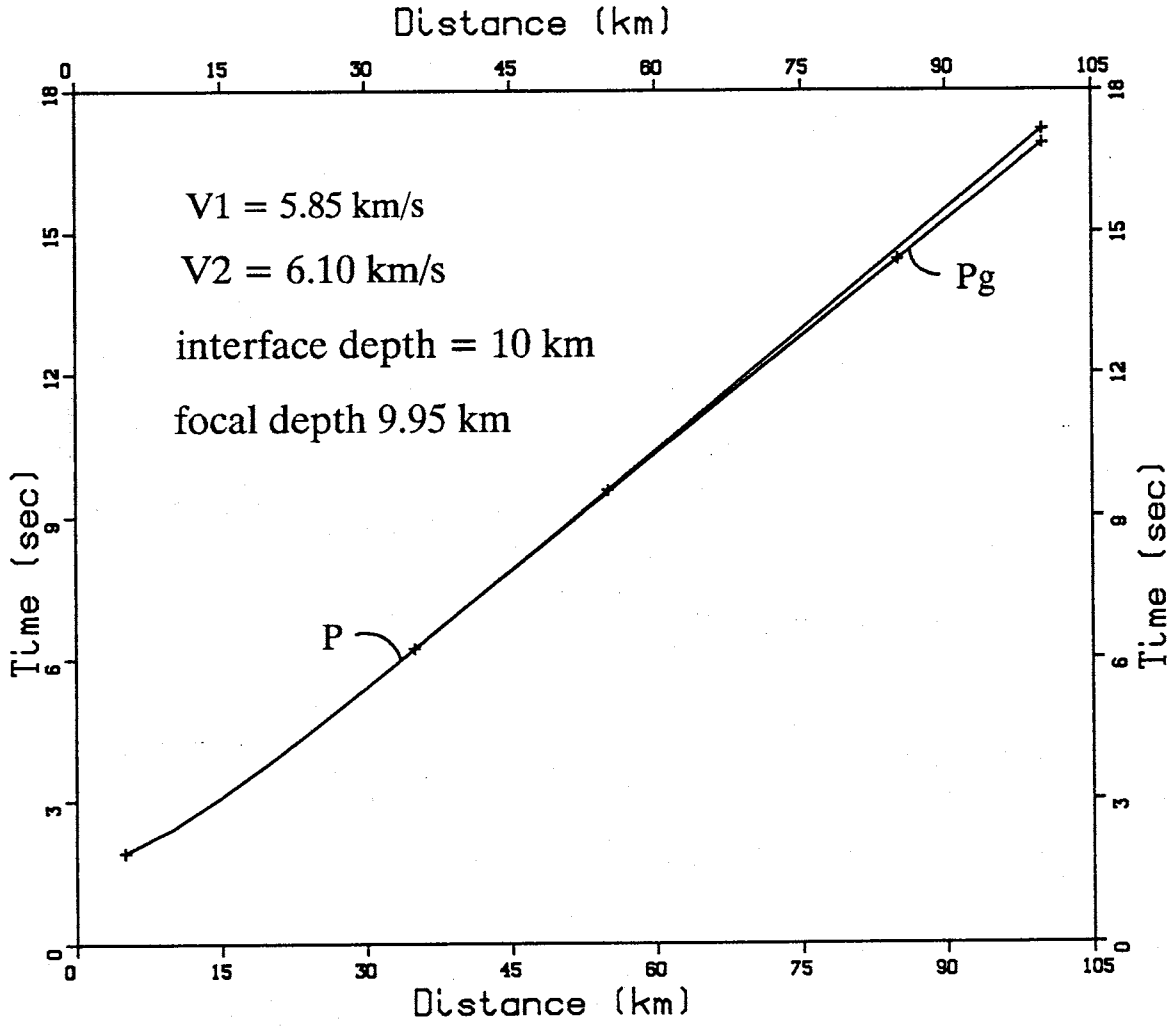

Fig. 7.2. Theoretical time versus distance curves for direct arrivals (P) and head wave arrivals (P_g). The velocities and interface depth (10 km) are typical values from the central Rio Grande rift.

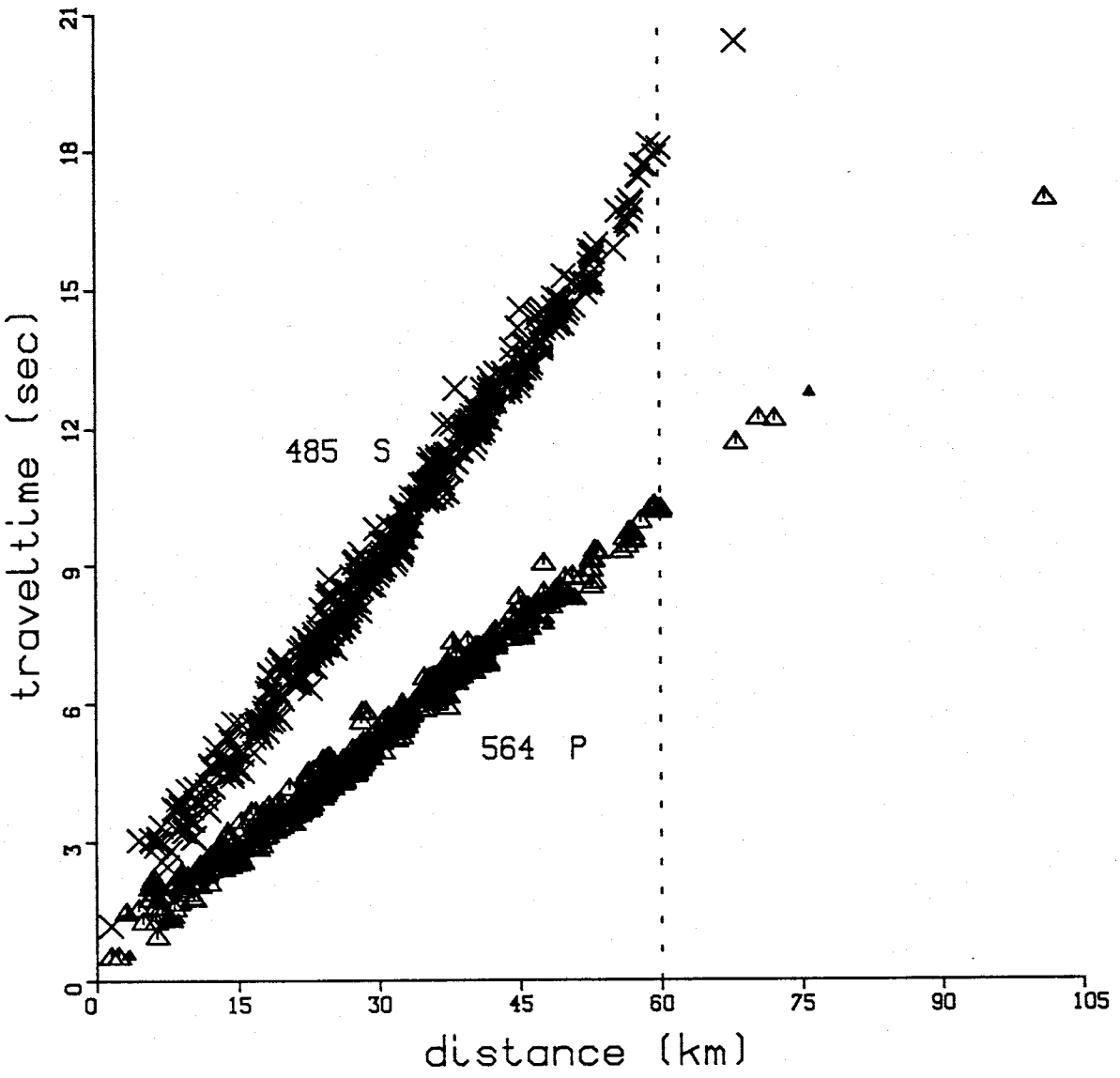

Fig. 7.3. Time versus distance plot of the direct arrival data set used in this study. Few data have been recorded at distances greater than 60 km and no head wave arrivals (change in slope with increasing distance) are apparent.

TABLE 7.1. Model Parameter Estimation Using Real Data From 75 Events - 12 km First Layer				
1049 Direct Arrivals - 406 Reflected Arrivals				
Parameter Type	Starting Model	Inversion Estimate	1 Std	**R** Matrix Diagonal
BAR	0.000	-0.027	0.044	1.00
BDO	0.000	0.666	0.084	1.00
BMT	0.000	0.160	0.051	1.00
CAR	0.000	0.001	0.043	1.00
LAZ	0.000	-0.008	0.053	1.00
LEM	0.000	-0.081	0.029	1.00
LJY	0.000	0.440	0.040	1.00
LPM	0.000	-0.191	0.052	1.00
MAG	0.000	-0.020	0.044	1.00
MLM	0.000	-0.215	0.168	1.00
SB	0.000	0.207	0.046	1.00
SMC	0.000	0.158	0.062	1.00
SNM	0.000	0.010	0.033	1.00
WTX	0.000	-0.080	*	*
V_{p1}	6.000	5.945	0.047	1.00
V_{p2}	6.000	5.760	0.091	1.00
ν_1	0.250	0.256	0.002	1.00
ν_2	0.250	0.220	0.009	1.00
Z_1	12.000	12.000	*	*
Z_2	20.000	18.695	0.282	1.00

Station correction values are given in sec, velocities in km s^{-1}, and depths in km. Station correction for WTX and depth to base of seismogenic zone (Z_1) were both held constant. Z_2 is depth to the magma body.

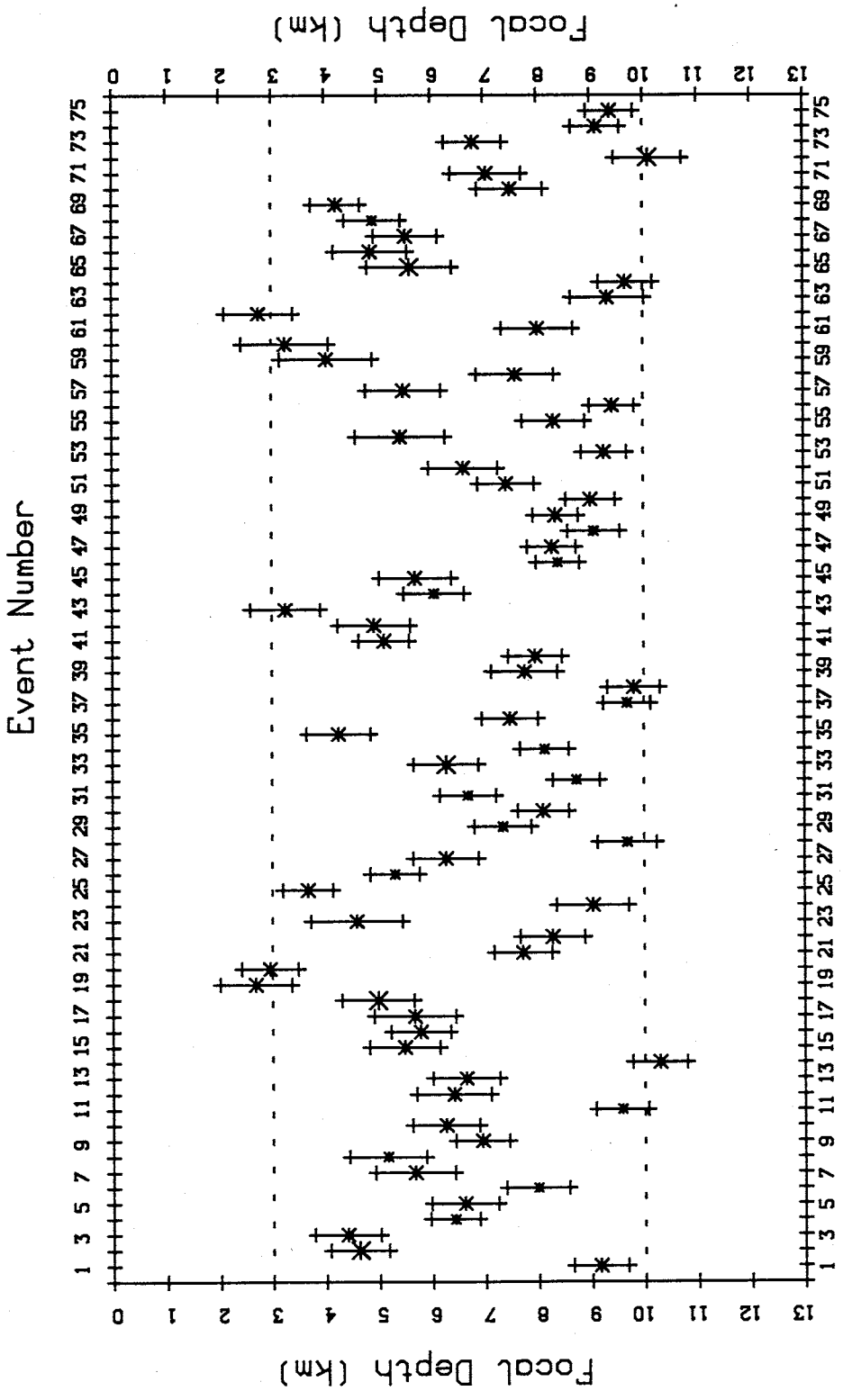

Fig. 7.4. Focal depth estimates (asterisks) and one standard deviation error bars for the case where depth of the first layer was fixed at 12 km. Dashed lines denote the approximate limits of shallowest and deepest events.

depth for the first layer is 10 km rather than 12 km.

I again solved the joint problem fixing depth to the first layer at 10 km. Focal depths (Figure 7.5) remained nearly the same when compared to the 12 km case (Figure 7.4). The velocity model (Table 7.2) changed slightly, but when the two models are compared all parameters overlap at one standard deviation. The R scalar value (how well residuals match assumed timing errors) for the 10 km case is 0.713 compared to 0.715 for the 12 km case. This means the 10 km model produces theoretical data which fit the observations slightly better than the 12 km model. From this slight improvement in fit, but primarily based on the sharp cut-off in focal depths below 10 km, I concluded that the 10 km interface was more appropriate than the 12 km interface.

To test if assuming a two-layer model is more appropriate than only a single layer, I solved for a one-layer case. Table 7.3 shows the velocity model results, Table 7.4 compares R and *RMS* values for the three different inversions, and Table 7.5 compares parameter estimates from all three inversions. The velocity and Poisson's ratio for the one-layer case are closer to the upper layer values from the two-layer cases. This is because more wave paths have sampled the upper 10 km of the single layer, causing the parameter values for the entire single layer to be weighted in favor of the values from the uppermost crust. For the direct arrivals, the differences in R between the three cases are slight, but for reflected phases R and RMS increase when only a single layer is considered. This also implies that the values found for the one-layer case are weighted in favor of the upper 10 km of crust. Furthermore, it implies that the velocity and Poisson's ratio beneath the approximate base of the seismogenic zone are indeed different than the same parameters in the upper crust.

The rather low R values (less than 1.0) for all three cases imply that my timing errors are actually smaller than I had assumed and, hence, standard deviations on parameter estimates are probably slightly larger than they should be. When testing with synthetic data I had also overestimated timing errors (I knew the size of

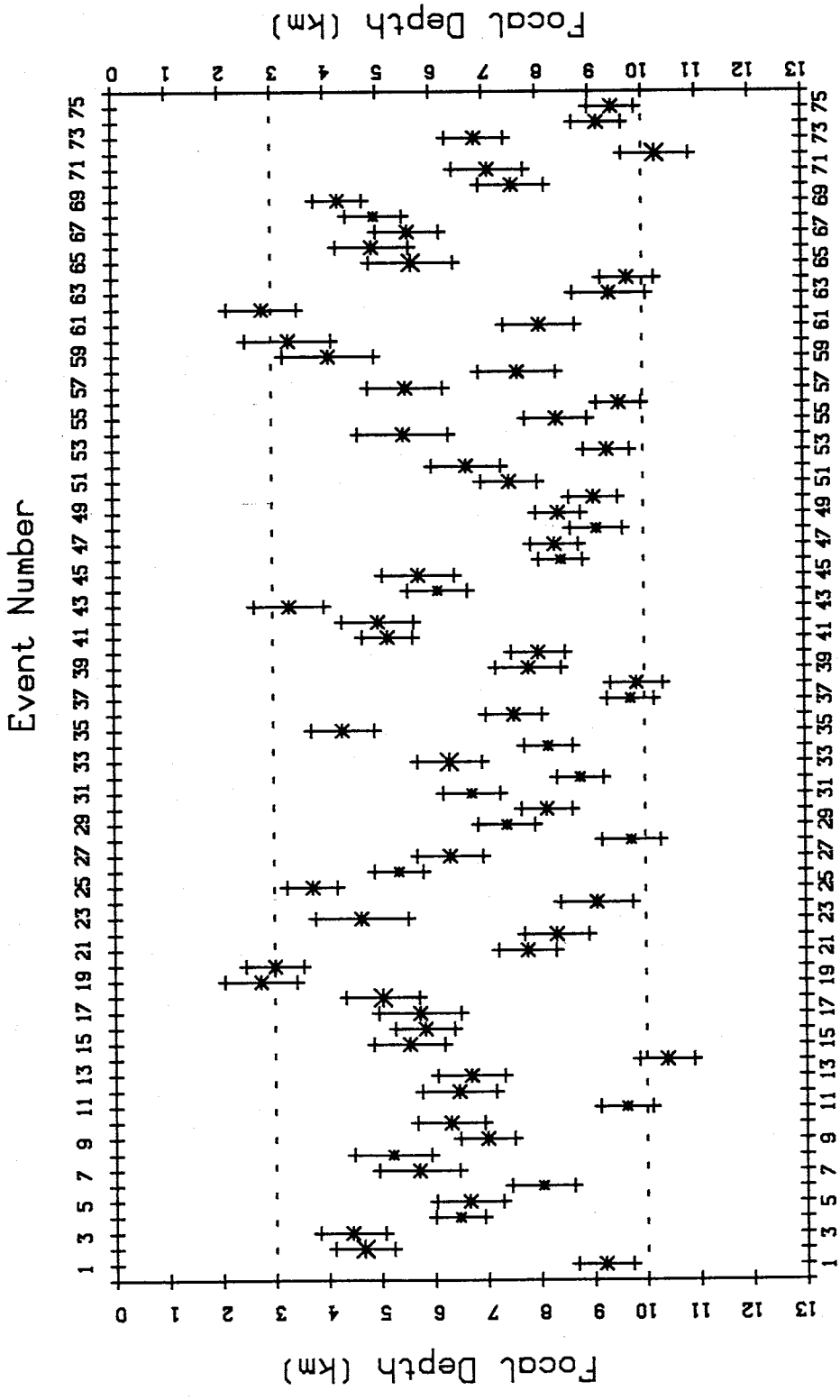

Fig. 7.5. Focal depth estimates (asterisks) and one standard deviation error bars for the case where depth of the first layer was fixed at 10 km. Dashed lines denote the approximate limits of shallowest and deepest events.

TABLE 7.2. Model Parameter Estimation Using Real Data From 75 Events - 10 km First Layer				
1049 Direct Arrivals - 406 Reflected Arrivals				
Parameter Type	Starting Model	Inversion Estimate	1 Std	**R** Matrix Diagonal
BAR	0.000	-0.023	0.044	1.00
BDO	0.000	0.672	0.084	1.00
BMT	0.000	0.165	0.051	1.00
CAR	0.000	0.005	0.043	1.00
LAZ	0.000	-0.004	0.053	1.00
LEM	0.000	-0.080	0.029	1.00
LJY	0.000	0.443	0.040	1.00
LPM	0.000	-0.187	0.052	1.00
MAG	0.000	-0.016	0.043	1.00
MLM	0.000	-0.204	0.168	1.00
SB	0.000	0.211	0.046	1.00
SMC	0.000	0.164	0.062	1.00
SNM	0.000	0.009	0.033	1.00
WTX	0.000	-0.080	*	*
V_{p1}	6.000	5.946	0.047	1.00
V_{p2}	6.000	5.804	0.075	1.00
ν_1	0.250	0.256	0.002	1.00
ν_2	0.250	0.228	0.007	1.00
Z_1	10.000	10.000	*	*
Z_2	20.000	18.748	0.282	1.00

Station correction values are given in sec, velocities in km s^{-1}, and depths in km. Station correction for WTX and depth to base of seismogenic zone (Z_1) were both held constant. Z_2 is depth to the magma body.

TABLE 7.3. Model Parameter Estimation Using Real Data From 75 Events - Single Layer				
1049 Direct Arrivals - 406 Reflected Arrivals				
Parameter Type	Starting Model	Inversion Estimate	1 Std	**R** Matrix Diagonal
BAR	0.000	-0.063	0.044	1.00
BDO	0.000	0.628	0.085	1.00
BMT	0.000	0.133	0.051	1.00
CAR	0.000	-0.035	0.043	1.00
LAZ	0.000	-0.036	0.053	1.00
LEM	0.000	-0.084	0.029	1.00
LJY	0.000	0.422	0.040	1.00
LPM	0.000	-0.230	0.052	1.00
MAG	0.000	-0.041	0.044	1.00
MLM	0.000	-0.327	0.161	1.00
SB	0.000	0.185	0.046	1.00
SMC	0.000	0.112	0.062	1.00
SNM	0.000	0.012	0.033	1.00
WTX	0.000	-0.080	*	*
V_{p1}	6.000	5.908	0.047	1.00
ν_1	0.250	0.255	0.002	1.00
Z_1	20.000	18.487	0.226	1.00

Station correction values are given in sec, velocities in km s^{-1}, and depths in km. Station correction for WTX was held constant. Z_1 is depth to the magma body.

TABLE 7.4. *R* and *RMS* Comparisons for Different Inversion Runs

Inversion Run	Total *R*	Total *RMS*	Direct *R*	Direct *RMS*	Reflected *R*	Reflected *RMS*
2-layer model - 10 km first interface	0.713	0.183	0.664	0.144	0.826	0.257
2-layer model - 12 km first interface	0.715	0.184	0.664	0.145	0.833	0.259
1-layer model	0.725	0.187	0.670	0.147	0.850	0.263

TABLE 7.5. Model Parameter Estimation Using Real Data From 75 Events - Results From Different Assumed Models

1049 Direct Arrivals - 406 Reflected Arrivals			
Parameter Type	12 km Model	10 km Model	Single Layer
BAR	-0.027 ±0.044	-0.023 ±0.044	-0.063 ±0.044
BDO	0.666 ±0.084	0.672 ±0.084	0.628 ±0.085
BMT	0.160 ±0.051	0.165 ±0.051	0.133 ±0.051
CAR	0.001 ±0.043	0.005 ±0.043	-0.035 ±0.043
LAZ	-0.008 ±0.053	-0.003 ±0.053	-0.036 ±0.053
LEM	-0.081 ±0.029	-0.080 ±0.029	-0.084 ±0.029
LJY	0.440 ±0.040	0.443 ±0.040	0.422 ±0.040
LPM	-0.191 ±0.052	-0.187 ±0.052	-0.230 ±0.052
MAG	-0.020 ±0.044	-0.016 ±0.043	-0.041 ±0.044
MLM	-0.215 ±0.168	-0.204 ±0.168	-0.327 ±0.161
SB	0.207 ±0.046	0.211 ±0.046	0.185 ±0.046
SMC	0.158 ±0.062	0.164 ±0.062	0.112 ±0.062
SNM	0.010 ±0.033	0.009 ±0.033	0.012 ±0.033
WTX	-0.080 ±0.000	-0.080 ±0.000	-0.080 ±0.000
V_{p1}	5.945 ±0.047	5.946 ±0.047	5.908 ±0.047
V_{p2}	5.760 ±0.091	5.804 ±0.075	*
ν_1	0.256 ±0.002	0.256 ±0.002	0.255 ±0.002
ν_2	0.220 ±0.009	0.228 ±0.007	*
Z_2	18.695 ±0.282	18.748 ±0.282	18.487 ±0.226

Station correction values are given in sec, velocities in km s^{-1}, and depths in km. Station correction for WTX was held constant. Z_2 is depth to the magma body.

the random noise which was added to the synthetic data) and had also probably calculated standard deviations which were slightly large. Because the synthetic tests suggest velocity model parameters can be obtained which are within one standard deviation of their true values when R is less than 1.0, and because error estimates from the real data case are nearly the same as the error estimates from the synthetic data case, I concluded that the new velocity model parameters were also reliable at one standard deviation.

Extreme Starting Models

A remarkable result of these inversions is that convergence occurred while all eigenvalues were retained for each solution. This means all diagonals of the resolution matrix are exactly 1.0, and thus, each parameter estimate is independent of the initial model. For nonlinear problems, however, convergence to a local minimum may occur rather than to the actual minimum even though there are no trade-offs between the parameter estimates (all eigenvalues retained) [*Pavlis,* 1982]. To test for such a possibility, I ran two more inversions holding the 10 km interface constant but starting with unreasonable velocities and magma body depth.

For one test I assigned both starting velocities values of 6.50 km s^{-1} and the initial magma body depth 25 km. No previous studies have ever found similar velocities for this depth range, and the magma body depth has never been estimated at greater than 20 km. Once again I solved first for locations, then station corrections, and finally solved for all parameters simultaneously. Considering I define convergence as when parameters vary between iterations by less than 0.005 times their unit values, these results are the same as the previous 10 km case (Table 7.6 compared to Table 7.2). For the second test I assumed another extreme model, with initial velocities of 5.30 km s^{-1} and magma body depth of 15.0 km. Again, such an extreme model has never before been estimated for central New Mexico. Parameter estimates were the same as the previous runs. (Table 7.7 compared to Tables 7.6 and 7.2). These tests demonstrate that my results are not biased by my

TABLE 7.6. Model Parameter Estimation Using Real Data From 75 Events - 10 km First Layer - High Velocity Starting Model -

1049 Direct Arrivals - 406 Reflected Arrivals

Parameter Type	Starting Model	Inversion Estimate	1 Std	**R** Matrix Diagonal
BAR	0.000	-0.023	0.044	1.00
BDO	0.000	0.672	0.084	1.00
BMT	0.000	0.165	0.051	1.00
CAR	0.000	0.005	0.043	1.00
LAZ	0.000	-0.003	0.053	1.00
LEM	0.000	-0.080	0.029	1.00
LJY	0.000	0.443	0.040	1.00
LPM	0.000	-0.187	0.052	1.00
MAG	0.000	-0.016	0.043	1.00
MLM	0.000	-0.205	0.168	1.00
SB	0.000	0.211	0.046	1.00
SMC	0.000	0.164	0.062	1.00
SNM	0.000	0.009	0.033	1.00
WTX	0.000	-0.080	*	*
V_{p1}	6.500	5.945	0.047	1.00
V_{p2}	6.500	5.806	0.075	1.00
ν_1	0.250	0.256	0.002	1.00
ν_2	0.250	0.228	0.007	1.00
Z_1	10.000	10.000	*	*
Z_2	25.000	18.752	0.281	1.00

Station correction values are given in sec, velocities in km s^{-1}, and depths in km. Station correction for WTX and depth to base of seismogenic zone (Z_1) were both held constant. Z_2 is depth to the magma body.

TABLE 7.7. Model Parameter Estimation Using Real Data From 75 Events - 10 km First Layer - Low Velocity Starting Model -

1049 Direct Arrivals - 406 Reflected Arrivals

Parameter Type	Starting Model	Inversion Estimate	1 Std	**R** Matrix Diagonal
BAR	0.000	-0.024	0.044	1.00
BDO	0.000	0.672	0.084	1.00
BMT	0.000	0.164	0.051	1.00
CAR	0.000	0.004	0.043	1.00
LAZ	0.000	-0.004	0.053	1.00
LEM	0.000	-0.080	0.029	1.00
LJY	0.000	0.442	0.040	1.00
LPM	0.000	-0.187	0.052	1.00
MAG	0.000	-0.017	0.043	1.00
MLM	0.000	-0.204	0.168	1.00
SB	0.000	0.211	0.046	1.00
SMC	0.000	0.163	0.062	1.00
SNM	0.000	0.009	0.033	1.00
WTX	0.000	-0.080	*	*
V_{p1}	5.300	5.945	0.047	1.00
V_{p2}	5.300	5.806	0.075	1.00
ν_1	0.250	0.256	0.002	1.00
ν_2	0.250	0.228	0.007	1.00
Z_1	10.000	10.000	*	*
Z_2	15.000	18.744	0.281	1.00

Station correction values are given in sec, velocities in km s^{-1}, and depths in km. Station correction for WTX and depth to base of seismogenic zone (Z_1) were both held constant. Z_2 is depth to the magma body.

choice of an initial model.

Dip Considerations

For all inversions I have assumed the upper surface of the magma body is a flat plane. If dip or any roughness on the reflector is significant, then the inclusion of the reflected phases in the earthquake location process could degrade focal depth estimates. Thus, possible dip on the upper surface of the magma body must be carefully examined before inclusion of reflected phases in the location process can be considered an appropriate procedure.

Before examining evidence for possible dip it is important to review the nature of the the data set. Figures 7.6 and 7.7 show locations of epicenters and reflection points. These figures are derived from the joint inversion results where I had assumed a 10 km depth to the first layer. Both the epicenters and reflection points in the data set are distributed over a wide area. Each event has between three and ten reflected phases recorded at between two and six stations. Thus, reflected phases from any single event sample the reflector at geographically well-distributed points. Another important consideration is that there are approximately 125 S_zP-S_zS or S_zP-P_zP reflection pairs contained in the data set. As Figure 1.4 demonstrates, each of these reflection pairs is associated with a unique focal depth and reflector depth. Finally, the reflections occur over a wide range of source-receiver distances (Figure 7.8).

By considering the nature of the data set and examining results from the inversions, strong evidence that the upper surface of the magma body is nearly flat can be obtained. First, R for only the reflected phases is 0.826 (Table 7.4), indicating the reflected phase residuals are smaller than the assumed reflected phase timing errors. If dip were significant, especially considering that the reflection points are from such a wide geographic distribution and are associated with many large (greater than 40 km) source-receiver distances, then residuals should exceed assumed timing error and, hence, R for reflections should exceed 1.0.

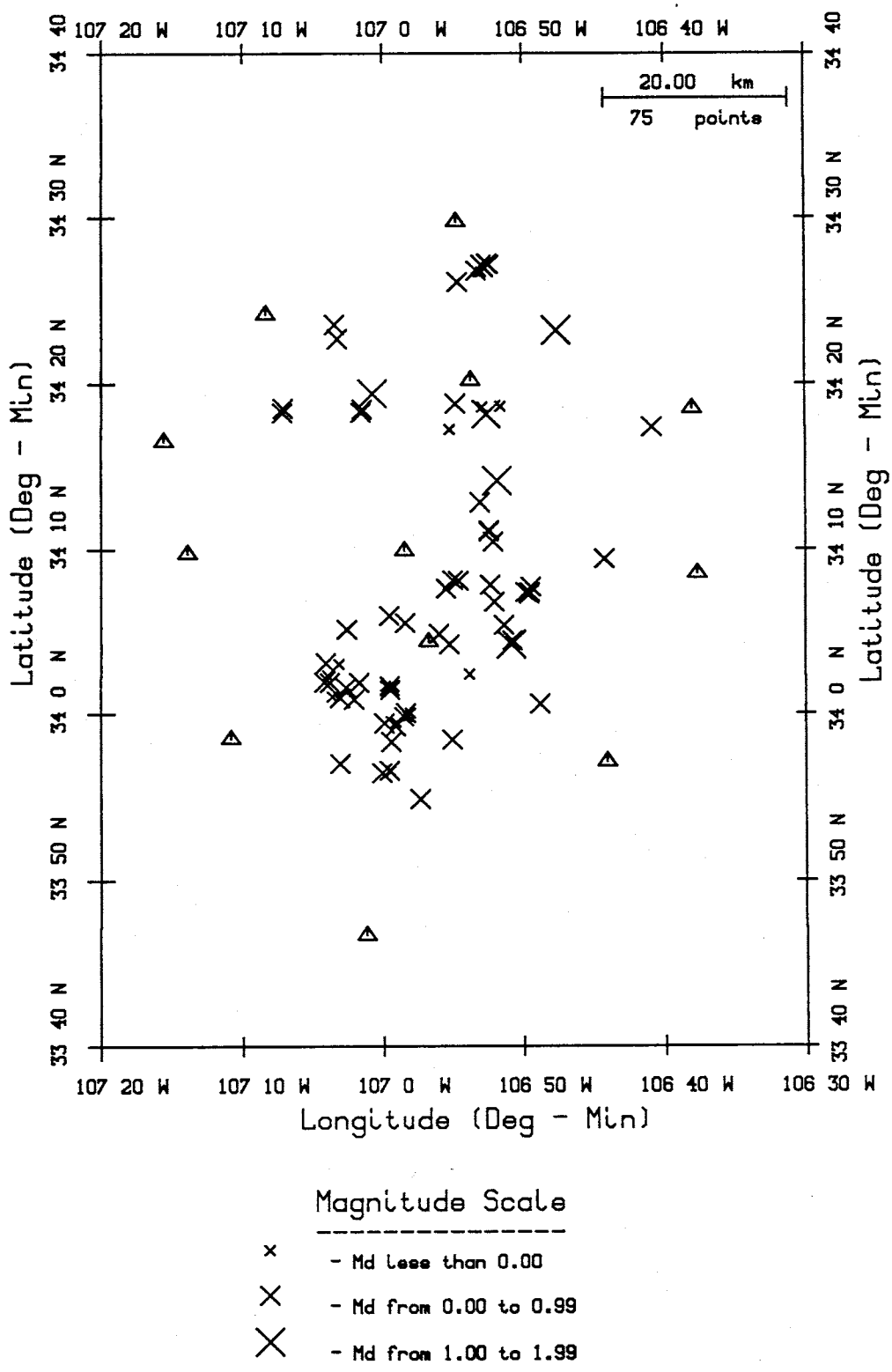

Fig. 7.6. Final epicenter estimates (X's) from the inversion where depth to the first layer was fixed at 10 km. Triangles are the network stations.

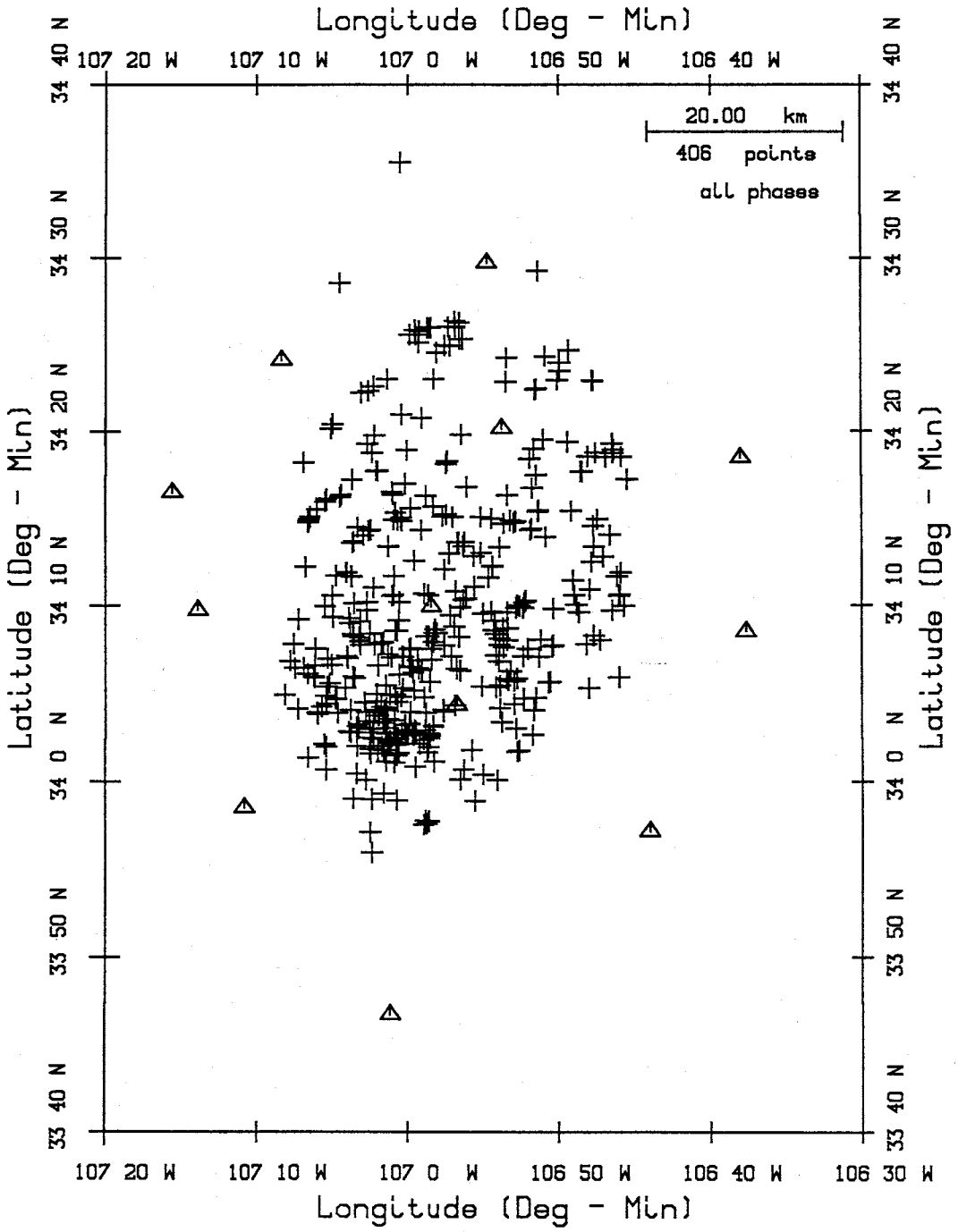

Fig. 7.7. Position of reflection points associated with the data used in this study. Positions are found using the velocity model shown in Table 7.2 and the hypocenter estimates shown in Figures 7.5 and 7.6. Triangles are the network stations.

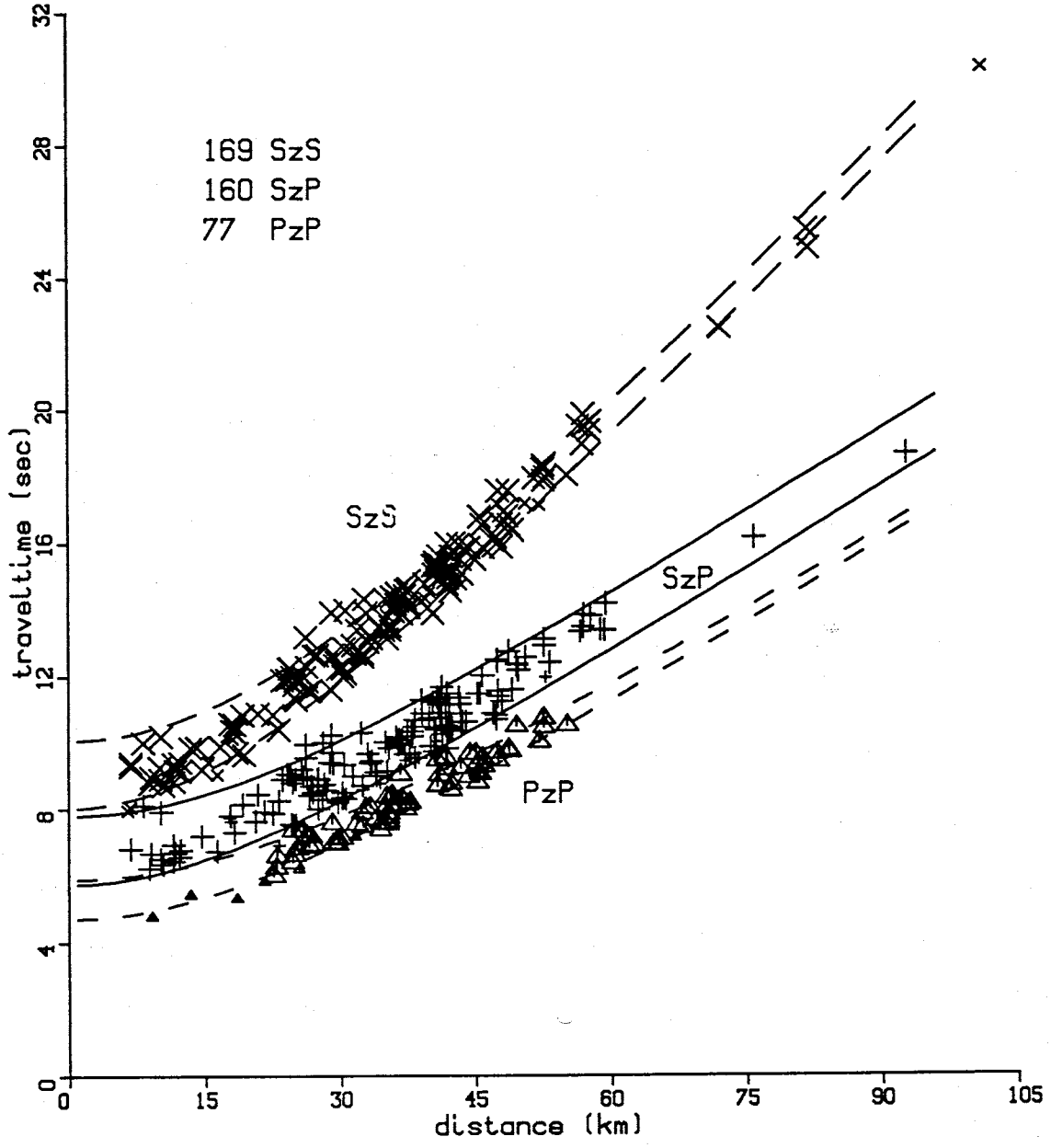

Fig. 7.8. Traveltime versus offset distance for the 406 reflected phases used in this study. The points are calculated using the model shown in Table 7.2 and the hypocenter estimates shown in Figures 7.5 and 7.6. Theoretical traveltimes for an event 3 km deep are shown by the three lines marking the upper limit of each phase type. Times for an event 10 km deep are shown by the lines marking the lower limit of each phase type.

The data in Figure 7.8 also support the argument for very little dip on the upper surface of the magma body. The large symbols represent observed reflection times whose residuals do not exceed assumed timing error. The small symbols represent observed times whose residuals do exceed assumed timing error. If dip were significant, more small symbols should be plotted at the greater offset distances. However, this is not the case; the small symbols are distributed over all distances, suggesting the residuals are caused by timing error rather than significant changes in reflector depth.

Another way to test for dip on the magma body is to examine the residuals associated with each reflection point. Figures 7.9 and 7.10 show the positions of reflection points that have positive and negative reflection time residuals. If the magma body displayed a regional dip, then one would expect the positive and negative reflection points to have separate geographic distributions. For instance, if dip were down to the north, then positive residuals should be more prevalent to the north and negative residuals more prevalent to the south (positive residuals imply later arrival times). No such patterns are apparent. In fact, comparing Figures 7.9 and 7.10 one sees that the positive and negative residuals each cover the same area, which is the entire region mapped by all reflection points (Figure 7.6). This too suggests dip is not significant and that reflection time residuals must be attributed to timing errors.

For residuals that actually exceed assumed timing error (Figure 7.11), a similar pattern is seen. Both positive and negative residuals are present over the entire mapped area. No pattern suggesting dip is apparent.

Hypocenters

One of the primary goals of this research was to develop an earthquake location tool which could accept all phases commonly seen on Socorro-area seismograms. Having accomplished this goal, and having established that dip is not significant enough to degrade hypocenter estimates when reflections are used in the

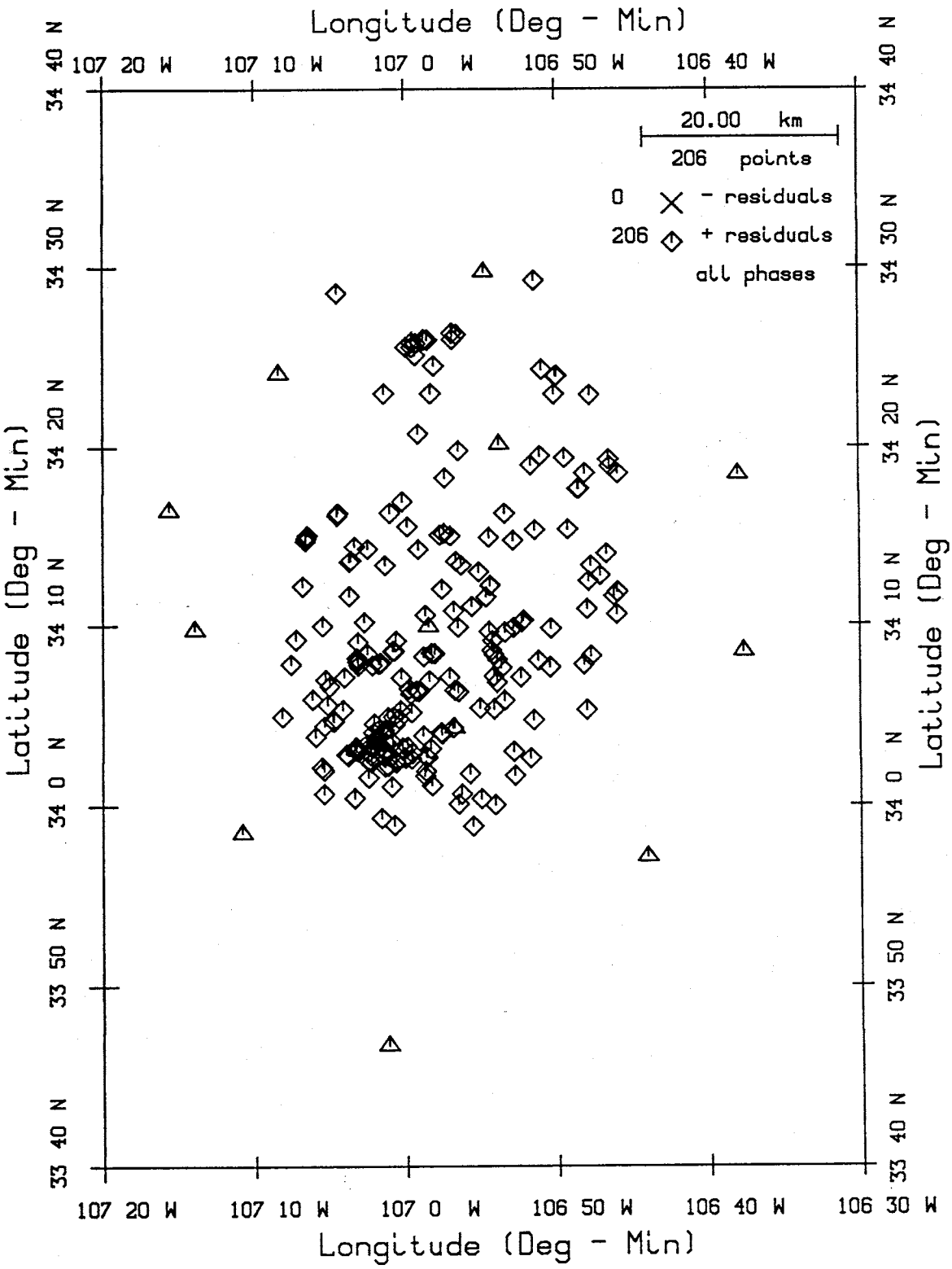

Fig. 7.9. Position of reflection points (diamonds) having positive arrival time residuals. Triangles are the network stations.

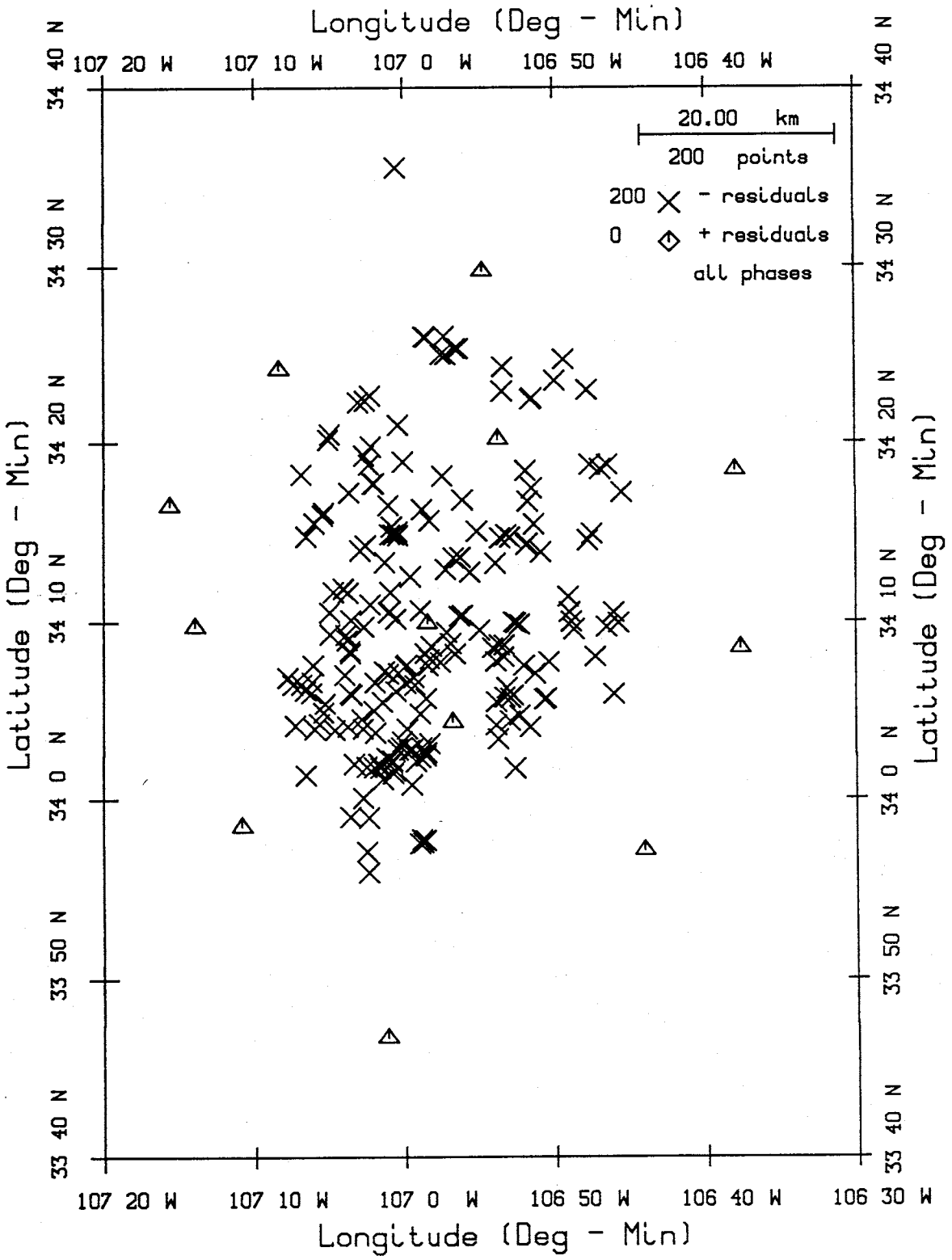

Fig. 7.10. Position of reflection points (X's) having negative arrival time residuals. Triangles are the network stations.

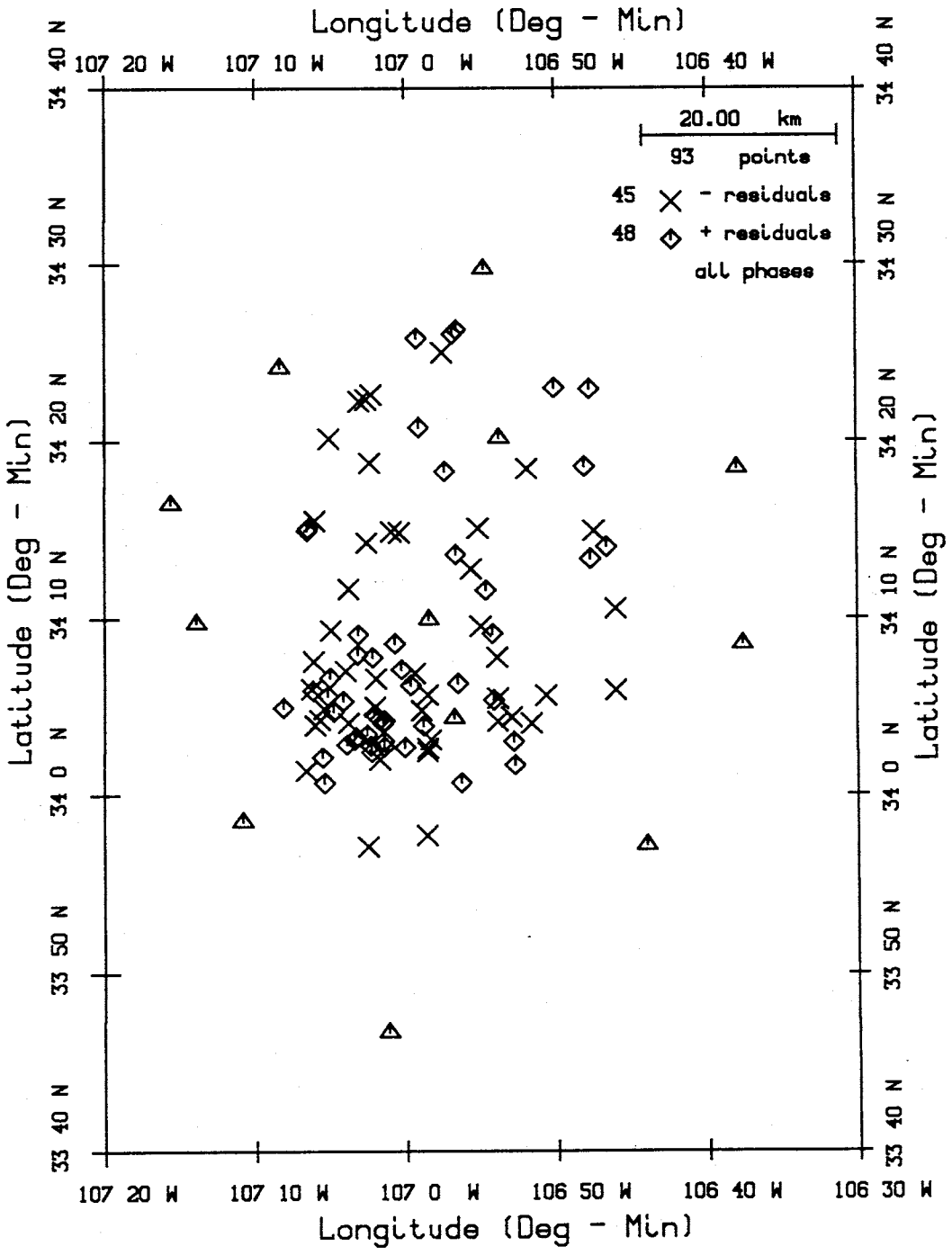

Fig. 7.11. Position of reflection points having negative (X's) and positive (diamonds) arrival time residuals which exceed assumed picking error. Triangles are the network stations.

location process, one can examine improvement in the locations when all phases are used. Figure 7.5 is a plot of focal depths (asterisks) and error bars at one standard deviation versus event number for the 10 km interface case. The average depth of these events is 6.9 km and the average near-station epicentral distance is 9.8 km, but the errors are quite small, averaging around 0.60 km. Also, both the deep-event and shallow-event depth errors are nearly the same. Thus, the inclusion of the reflection times now allows for relatively well-constrained focal depth estimates for both shallow and deep events.

Figure 7.12 is another focal depth plot, but for the case when only direct arrivals were used to locate the same 75 events. Superimposed on these solutions are the depth estimates (squares) found by including reflections (same depth estimates as shown in Figure 7.5). The errors on the direct-only depth estimates are much larger than the errors when reflections are used, averaging 1.9 km. The errors on the shallow events tend to be larger than errors on the deeper events because shallow depths can only be constrained by stations recording events at offset distances less than or equal to the focal depths. Because the Socorro network has a coarse station spacing relative to event depths, most of the near-station epicentral distances exceed the focal depths, resulting in poor constraint on focal depths. For four events, (numbers 2, 3, 20, and 43) the direct arrival data can not resolve focal depth, and event depth was held constant at 7 km. There is no systematic shift in the depth estimates when the two results are compared. About half of the events found with reflections are deeper than those found using only direct arrivals, and the other half are shallower.

Table 7.8 summarizes hypocenter results. The following points can be made about hypocenters estimated using reflected phases compared to those using only direct phases:

1. Focal depth error is reduced on average by a factor of three.

2. The origin time error is reduced by a factor of two. This should be expected because the trade-off between origin time and focal depth will be

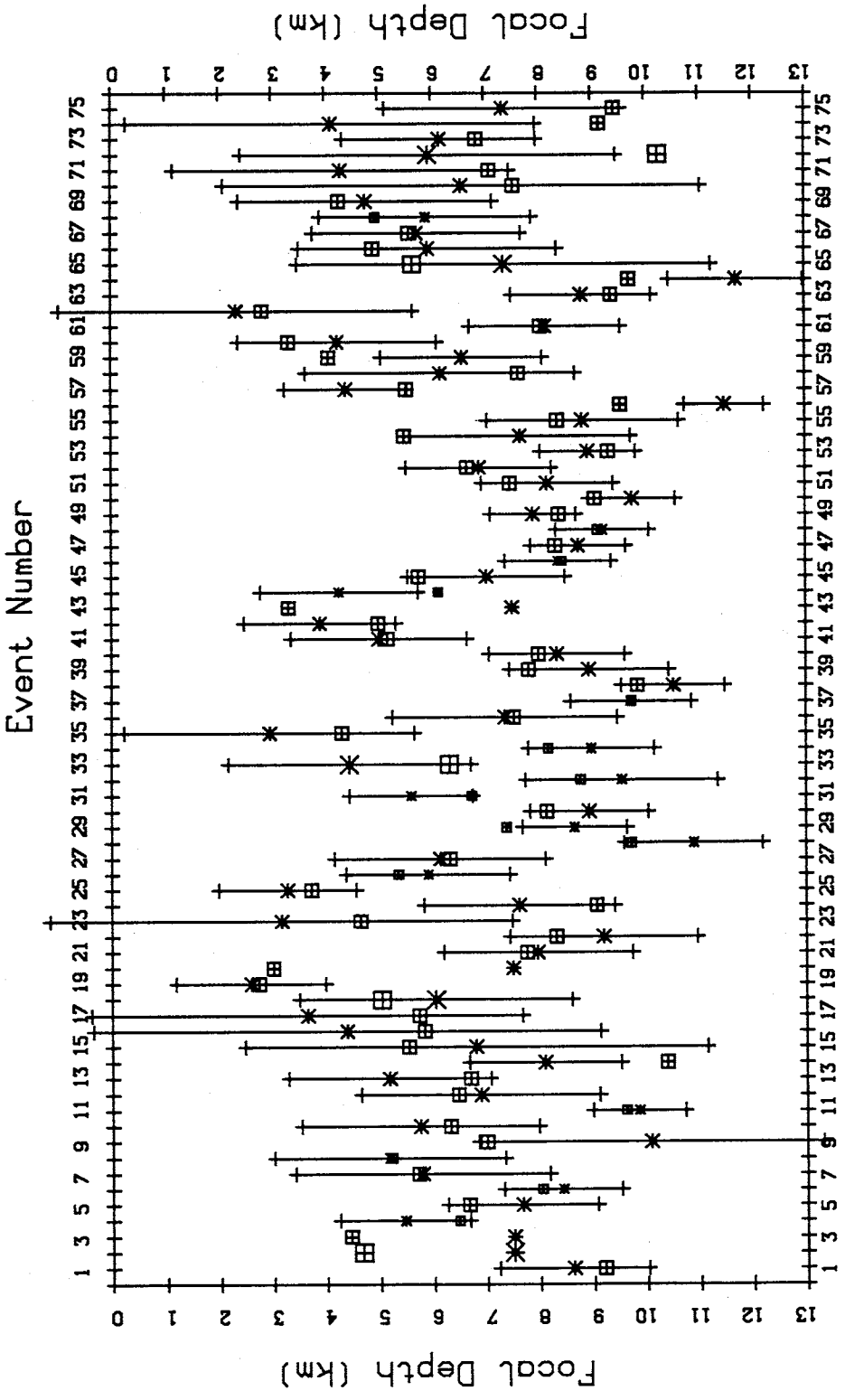

Fig. 7.12. Focal depth estimates (asterisks) and one standard deviation error bars obtained using only direct arrival data. The squares are the depth estimates obtained using direct and reflected data (same depth as shown in Figure 7.5).

TABLE 7.8. Hypocenter Comparison - Errors From Events Located With and Without Reflected Phases

	With Reflections	Direct Arrivals Only
Mean Longitude Error (km)	0.34 ±0.06	0.35 ±0.10
Mean Latitude Error (km)	0.45 ±0.11	0.47 ±0.19
Mean Focal Depth Error (km)	0.59 ±0.12	1.93 ±0.99
Mean Origin Time Error(sec)	0.06 ±0.01	0.11 ±0.04
Average "Deep" Event Depth Error (km)	0.53	1.45
Average "Shallow" Event Depth Error (km)	0.64	2.40

smaller when focal depths are better constrained.

3. Focal depth estimates on both shallow and deep events are improved. This means that focal depth constraint is not so dependent on near-station epicentral distance when reflections can be incorporated into the location procedure.

4. Epicenter estimates are neither improved or degraded.

Velocity Model

Figure 7.13 is a crustal profile showing the velocity model obtained when the base of the seismogenic zone was fixed at 10 km. With this figure I am not implying that there is an abrupt velocity change at exactly 10 km depth. Rather, Figure 7.13 is intended to show that the average values for P velocity and Poisson's ratio above 10 km depth are different (at 1 standard deviation) than the values between 10 km depth and the top of the magma body. The parameters in this figure are also listed in Table 7.2. Table 7.9 compares these results to the previous best-known model. Results which can be compared directly to previous findings are V_p in the upper layer, V_s in the lower layer, magma body depth, and Poisson's ratio in the upper layer. Parameters which had never been previously estimated are V_s in the upper layer, V_p in the lower layer, and Poisson's ratio in the lower layer.

The new model has a V_p in the upper layer now slightly higher than *Ward's* [1980] results. However, because *Ward's* data were limited to direct P arrivals, only the few deepest events (near 10 km depth) of his data set sampled the lowermost upper crust. But, every reflected phase from my data set samples the entire upper crust. Thus, assuming crustal velocity near 10 km depth is greater than velocity in the uppermost crust, one would expect my upper crustal velocity results to be higher than *Ward's*. *Singer* [1989] considered depth effects with time term analysis on P_g arrivals in the Socorro area. He found V_p increases from 5.7 km s^{-1} at the top of Precambrian to 6.0 km s^{-1} at a depth of near 10 km. Overall, his V_p for the upper crust was 5.95 km s^{-1}, identical to my result. It is interesting to note that *Singer* found P_g traveled to a maximum depth of near 10 km. Below

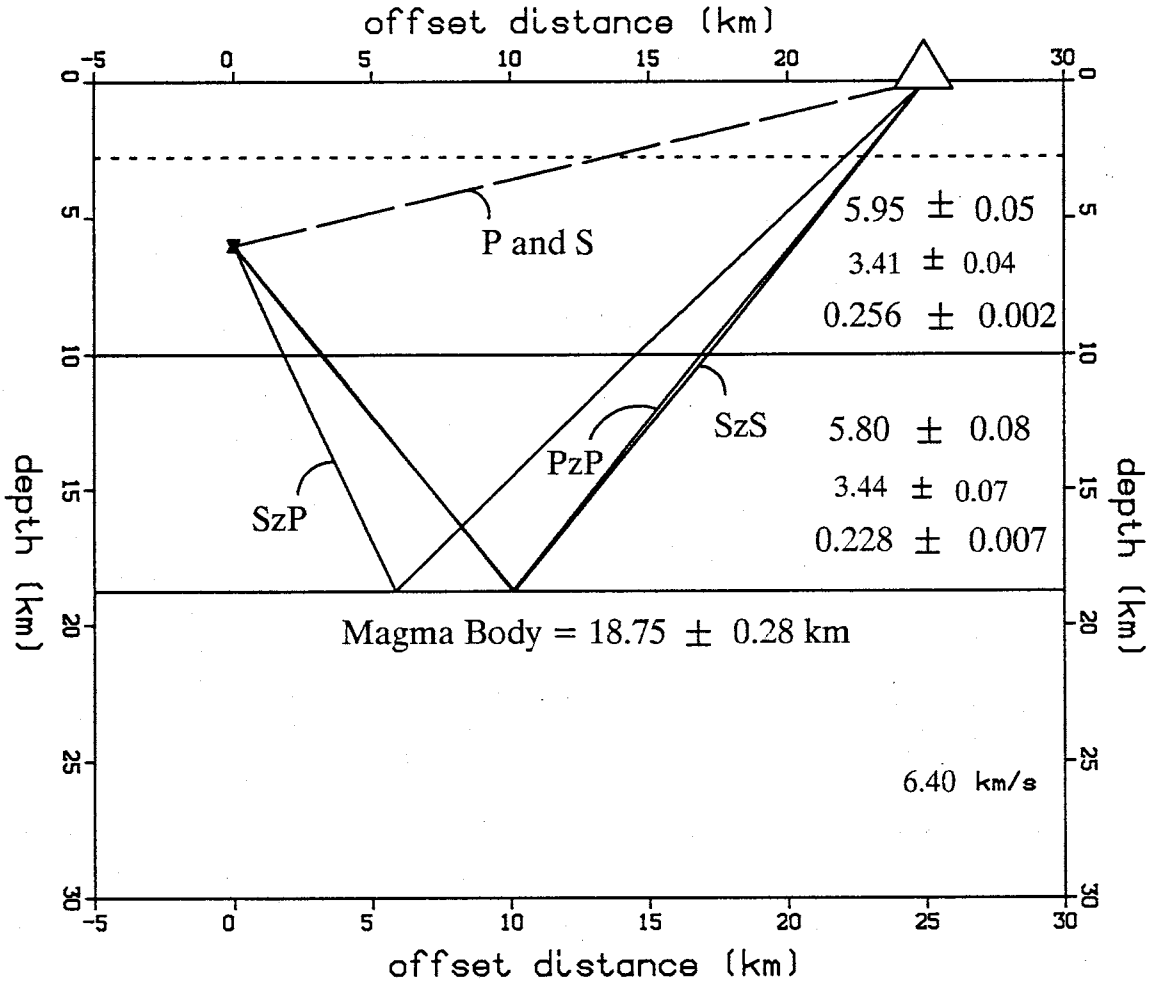

Fig. 7.13. Final velocity model and sample ray paths. The first layer is between 0 and 10 km and the second layer is between 10 km and the upper surface of the magma body. The dashed line denotes the approximate upper limit of the seismogenic zone. The approximate base of the seismogenic zone is at 10 km depth. Within each layer V_p is listed first, then V_s, and finally Poisson's ratio. Velocities are given in km s^{-1}. The V_s values and errors were calculated using V_p and Poisson's ratios values and errors.

TABLE 7.9. Velocity Model Comparison - Previous Studies and New Esitmates

Parameter	Previous Investigator	Old Estimate	New Estimate
V_{p1}	Ward, 1980	5.85 $\pm$0.020 km s^{-1}	5.95 $\pm$0.047 km s^{-1}
V_{p1}	Singer, 1989	5.95 $\pm$0.030 km s^{-1}	5.95 $\pm$0.047 km s^{-1}
V_{s1}	*	*	3.41 $\pm$0.036 km s^{-1}
V_{p2}	*	*	5.80 $\pm$0.075 km s^{-1}
V_{s2}	Rinehart and Sanford, 1981	3.44 $\pm$0.030 km s^{-1}	3.44 $\pm$0.073 km s^{-1}
ν_1	Caravella, 1976	0.262 $\pm$0.034	0.256 $\pm$0.002
ν_1	Fender, 1978	0.251 $\pm$0.052	0.256 $\pm$0.002
ν_2	*	*	0.228 $\pm$0.007
Z_2	Rinehart and Sanford, 1981	19.20 $\pm$0.60 km	18.75 $\pm$0.28 km

Poisson's ratios in the upper and lower layers are represented by ν_1 and ν_2. Z_2 is depth to the magma body. Shear velocity uncertainties from the present study are derived from the uncertainties on P velocity and ν. They are not estimated during the inversion.

10 km I have found a decrease in V_p (5.80 km s^{-1}) which may be the reason P_g travels no deeper than 10 km.

My value for Poisson's ratio in the upper layer is 0.256 $\pm$0.002. This is a well constrained result, and is extremely well constrained compared to the previous findings of *Caravella* [1976] and *Fender* [1978]. My estimate was obtained using carefully selected direct and reflected data, while the previous estimates were made using only direct arrivals. The fact that the previous estimates have large standard deviations suggests that some of the secondary arrivals used to make these estimates may have been mistakenly identified as direct S.

Using my new estimates for Poisson's ratio and V_p in the upper layer, produces a V_s of 3.41 km s^{-1}. Shear velocity in the upper layer for the immediate Socorro area had never been previously estimated from arrival time data, but *Rinehart and Sanford* [1981] had calculated V_s (3.35 km s^{-1}) by assuming Poisson's ratio is 0.25 and V_p is 5.8 km s^{-1}. North of the study area *Schlue et al.* [1986], using surface wave data, found alternating low and high shear velocity layers. Using their results, an average velocity calculated between 2.65 and 10.00 km is 3.31 km s^{-1}. My value for V_p in the lower layer is 5.80 km s^{-1}, and my estimate of Poisson's ratio is 0.228. Using these values to calculate V_s in the lower layer yields 3.44 km s^{-1}, the identical velocity reported by *Rinehart and Sanford* [1981].

My value for depth to the magma body is 18.75 $\pm$0.28 km. This is slightly less than the depth obtained by *Rinehart and Sanford* [1981] of 19.20 $\pm$0.6 km. Considering errors at one standard deviation, the two values could be the same. But, *Rinehart and Sanford* estimated magma body depth by holding shear velocity constant when solving for depth. Hence, their depth value depended on their velocity estimate while both depth and velocity were independent parameters in my inversions. The smaller standard deviation from my study, only half that reported by *Rinehart and Sanford*, can be explained by the data types and quantities used in each inversion. *Rinehart and Sanford* used approximately 250 S_zS arrival times

while I used over 400 times from all three reflected phases, including many S_zS - S_zP and P_zP - S_zP reflection pairs.

Station correction results are more difficult to compare with previous researcher's findings than other model parameters. Station corrections account for the combined effects of near-surface geology at each station, receiver elevation, and velocity inhomogeneities along ray paths. Separating these three factors, and even defining a datum on which the corrections are based, is difficult. Hence, the discussion below should only be considered an interpretation.

Many researchers have estimated corrections for specific Socorro-area swarms. For instance, *Ake* [1984] solved for corrections at many of the same stations I used, but his corrections were tailored for a swarm beneath the Socorro Mountain block and not for a general suite of events spread across the Socorro area. *Ward* [1980], using 40 well-distributed Socorro-area events, inverted for station corrections while solving for a P velocity model, but his data were from a different network than the network used in my study. The only station which was the same for both investigations was WTX.

A set of "standard", best-fitting station corrections have slowly evolved over the years the present network has operated. The evolution of these corrections is poorly documented, but I have included the values in Table 7.10, along with the values found by *Ake* [1984], and my results. To actually compare results, I have normalized all three sets of corrections so that each value at WTX is 0.000 (Table 7.11). In general, the "standard" corrections match my results quite well. The new corrections also generally match surface geology at each station location. The negative correction I found for LPM and a normalized value of 0.000 at LEM are reasonable as both stations are sited on Precambrian basement rocks. Likewise, the large positive corrections at LJY and BDO are the result of thick, low-velocity basin fill beneath those stations. Most corrections for stations sited on Tertiary volcanics, generally ash flows, are positive but not as large as the corrections sited on the basin fill. The corrections for stations sited on Paleozoic limestones, stations

TABLE 7.10. Station Correction Comparisons and Surface Geology at Each Station

Station	*Ake* [1984] Corrections	"Standard" Corrections	Present Study	Elev (km)	Surface Geology
BAR	0.060	-0.030	-0.023	2.120	Permian limestone
BDO	*	0.650	0.672	1.505	Synrift fill
BMT	*	0.140	0.165	1.972	Tertiary ash flow tuffs
CAR	0.090	-0.080	0.005	1.662	Permian limestone
LAZ	-0.010	0.040	-0.004	1.853	Permian limestone
LEM	*	0.060	-0.080	1.689	Precambrian basement
LJY	*	0.560	0.443	1.532	Synrift fill
LPM	-0.330	-0.230	-0.187	1.707	Precambrian basement
MAG	*	0.080	-0.016	1.926	Tertiary ash flow tuffs
MLM	-0.230	-0.100	-0.204	2.088	Quaternary basalt
SB	0.280	0.220	0.211	3.230	Tertiary ash flow tuffs
SMC	0.200	0.110	0.164	1.560	Tertiary volcanics
SNM	-0.040	0.000	0.009	1.511	Tertiary moat deposits
WTX	-0.160	-0.080	-0.080	1.555	Precambrian basement

TABLE 7.11. Station Correction Comparisons - Corrections Normalized at WTX

Station	*Ake* [1984] Corrections	"Standard" Corrections	Present Study	Elev (km)	Surface Geology
BAR	0.220	0.050	0.057	2.120	Permian limestone
BDO	*	0.730	0.752	1.505	Synrift fill
BMT	*	0.220	0.245	1.972	Tertiary ash flow tuffs
CAR	0.250	0.000	0.085	1.662	Permian limestone
LAZ	0.015	0.120	0.076	1.853	Permian limestone
LEM	*	0.140	0.000	1.689	Precambrian basement
LJY	*	0.640	0.523	1.532	Synrift fill
LPM	-0.170	-0.150	-0.107	1.707	Precambrian basement
MAG	*	0.160	0.064	1.926	Tertiary ash flow tuffs
MLM	-0.070	-0.020	-0.124	2.088	Quaternary basalt
SB	0.440	0.300	0.291	3.230	Tertiary ash flow tuffs
SMC	0.360	0.190	0.244	1.560	Tertiary volcanics
SNM	0.120	0.080	0.017	1.511	Tertiary moat deposits
WTX	0.000	0.000	0.000	1.555	Precambrian basement

BAR, CAR, and LAZ, have small, positive values. These values are also reasonable as limestones often have velocities equal to and sometimes even slightly greater than granites [*Dobrin,* 1976]. The small correction at MAG is unexpected when considering it is sited on Tertiary volcanics. This may indicate Precambrian basement is at a shallow depth beneath MAG. The nearest Precambrian outcrop is 4.6 km southeast of the station site [*Osborn,* 1984].

Summarizing model results, when considering that I have treated all velocity model parameters (except depth of the first interface) as unknowns, it is somewhat surprising that many of the new parameter estimates are more tightly constrained than the earlier findings. My new estimate for Poisson's ratio in the upper layer is much better constrained, and the error on magma body depth is now less than one half the previous error. Equally surprising is the fact that all parameters could be estimated without any damping, even when starting the inversions with extreme high-velocity and low-velocity initial models. These results demonstrate the exceptional resolving power obtained when multiple phases, and especially mode-converted phases such as S_zP, are inverted simultaneously.

In general, the velocity model I estimated is quite similar to the composite model assembled from previous investigator's findings. The most unexpected findings from the new velocity model are the low values for V_p and Poisson's ratio in the lower layer, two parameters which had not been estimated prior to this study. The new values indicate a decrease in P velocity (from 5.95 to 5.80 km s^{-1}) beneath the seismogenic zone while S velocity increases slightly (from 3.41 to 3.44 km s^{-1}). *Holbrook et al.* [1988] have detected a similar mid-crustal velocity relationship in sections of the Rhinegraben. The possible causes for these unexpected findings are presented under **Discussion.**

8. Case Study - Arroyo del Coyote Sequence

This case study compares hypocenter parameters, and especially focal depths, estimated with three different data sets for a well-recorded earthquake sequence. First, the events were located using direct arrivals recorded with Socorro network stations. Next, the events were located by combining direct arrivals recorded with Socorro network stations and direct arrivals recorded with supplemental portable stations. Finally, the events were located by combining direct and reflected arrivals recorded with Socorro network stations. The velocity model and station corrections used for all three location runs are shown in Table 7.2. This study demonstrates that reflected and direct arrivals recorded at source-to-receiver distances greater than event depths can constrain locations as well as direct arrivals recorded close to an epicentral area.

The Arroyo del Coyote sequence began with a small foreshock at 2 hours 43 minutes (Universal Time) on August 16, 1985 (M_D 0.2). About 12 hours later, at 14 hours 56 minutes, the main shock occurred (Figure 8.1). Duration magnitude for this event was estimated at 3.8, and 10 km southwest of the epicenter the intensity at Socorro was VI. Activity continued to at least January, 1986, but most aftershocks occurred within the first 48 hours following the main event.

Around 50 aftershocks were located by New Mexico Tech investigators using direct arrivals recorded with the Socorro network in 1985 and 1986. The nearest network station to record the sequence was WTX, approximately 12 km to the southwest. Although no stations were close to the epicentral area (recording distances less than the event focal depths), most locations had maximum station gaps of fewer than 90°. Hence, event epicenters were generally well constrained by network data, but focal depths could not be well constrained when using only direct arrivals. About 6 hours after the main shock portable recorders were deployed (Figure 8.2). These recorders were kept in the field for about 70 hours from August 17 to August 20.

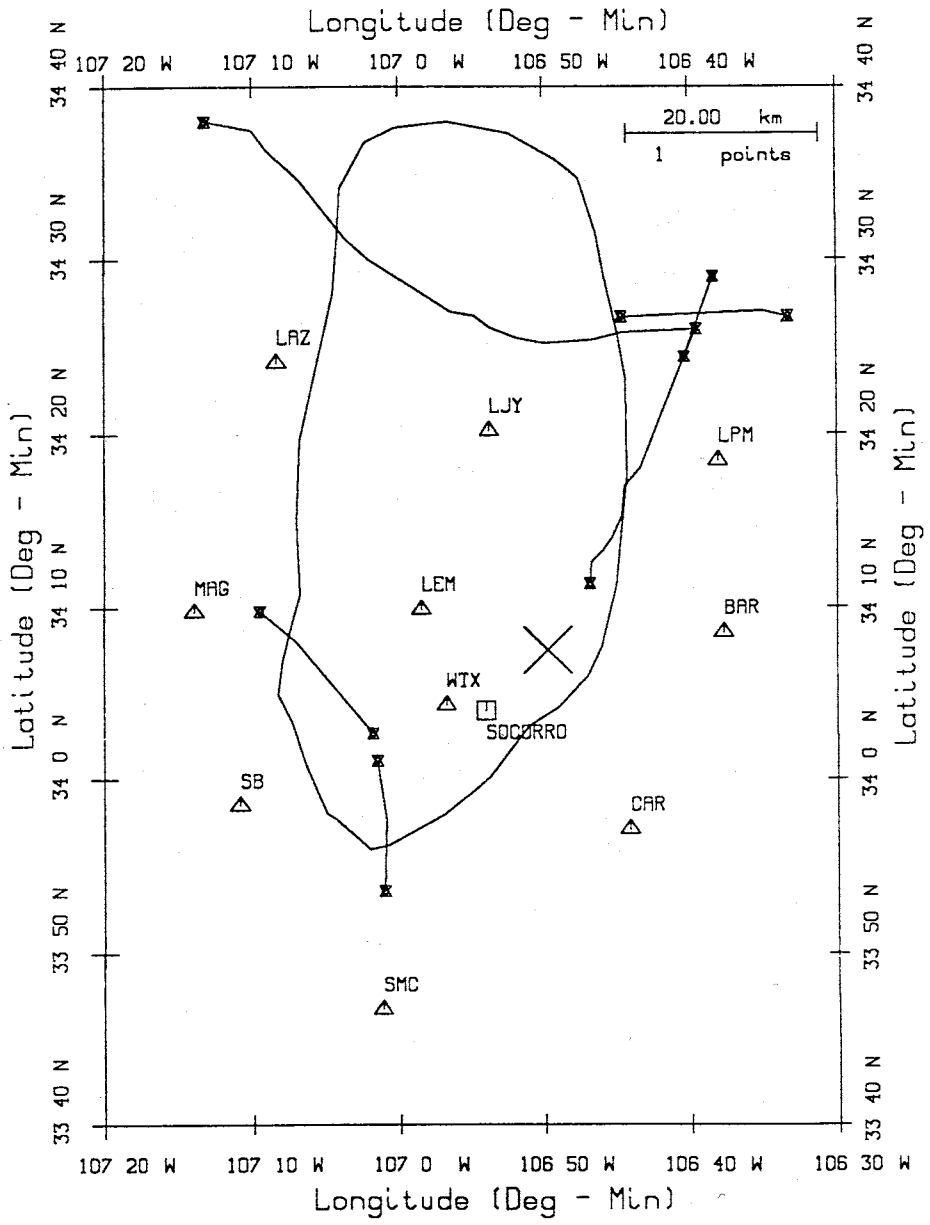

Fig. 8.1. Location of Arroyo del Coyote main shock (large X) relative to network stations, magma body outline, and COCORP lines.

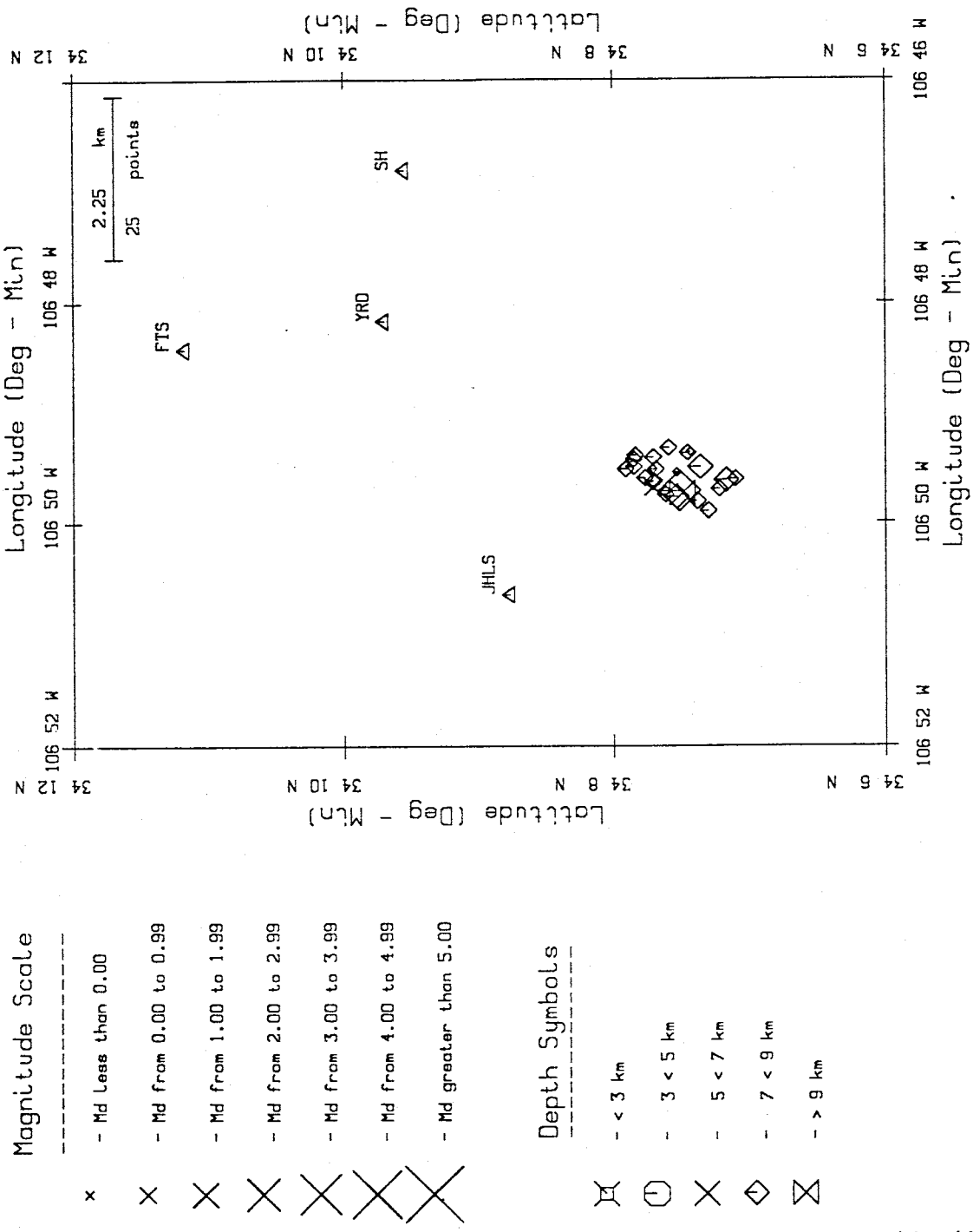

Fig. 8.2. Location of the four portable stations and the 25 events used in this case study.

I studied the foreshock, the main shock, and 23 aftershocks of this sequence. Table 8.1 provides details on all 25 events. Each value listed under the P heading of Table 8.1 corresponds to the number of portable stations which recorded an event. The value under each R heading indicates the total number of reflections picked for each event. All reflected arrivals were picked from network records, and many of these phases were clear enough that I often assigned them weights of 2 or 3. In addition to their clarity, they often could be picked as S_zP - S_zS pairs, especially at stations MAG and LAZ. Only events 2 and 23, the strongest events of the sequence, have no identifiable reflections.

For my first location estimates, I assumed that only direct arrivals from the network stations were available. Focal depth estimates and error bars at one standard deviation are shown in Figure 8.3. All focal depths could be estimated by the direct arrivals, but errors are large. My second location run (Figure 8.4) used the same data from the first run and the P arrivals from the portable records. The focal depths and errors for events 1 to 8 and 23 to 25 are identical to those shown in Figure 8.3, because no portable recorders were deployed when these events occurred. However, for events 9 to 22 portable recorders were deployed and errors range from only 0.5 to 1.0 km.

For my final location run (Figure 8.5), I used all arrival times (direct and reflected) which could be picked from the network records, but assumed the portable recorders had never been deployed. The number listed directly beneath each lower error bar is the number of reflections used in the solution. When three or more reflections are used errors are small, but as fewer reflections are used focal depth errors increase.

When Figure 8.5 is compared to Figure 8.3, only the focal depths and errors for events 2 and 23 are the same because no reflections were picked for these events. However, all other errors are reduced, even for events 18, 19, 20, and 25 where only one reflection time was available. Comparing events 9 to 22 in Figures 8.4 and 8.5 shows that when three or more reflections are available, errors are

TABLE 8.1. Arroyo del Coyote Events

	Time	Lat	Long	Depth	Mag	R	P
1.	16024306.36	34 7.11	106 49.61	8.68	0.18	6	0
2.	16145652.76	34 7.52	106 49.72	8.17	3.77	0	0
3.	16153154.09	34 7.91	106 49.52	8.06	0.45	5	0
4.	16153531.55	34 7.37	106 49.50	7.29	1.643	3	0
5.	16154223.09	34 7.60	106 49.32	7.33	0.39	3	0
6.	16154726.61	34 7.70	106 49.63	8.27	0.46	7	0
7.	16155905.68	34 7.71	106 49.41	7.96	0.39	4	0
8.	16160025.78	34 7.71	106 49.64	8.63	0.29	4	0
9.	17012422.22	34 7.31	106 49.90	7.68	0.32	4	2
10.	17051446.68	34 7.18	106 49.62	8.10	1.52	2	2
11.	17180424.81	34 7.39	106 49.81	7.68	0.14	7	2
12.	17194924.72	34 7.85	106 49.43	8.01	0.13	5	2
13.	17213411.03	34 7.71	106 49.69	6.29	0.71	4	3
14.	18002802.02	34 7.85	106 49.50	8.12	0.00	4	4
15.	18035711.57	34 7.69	106 49.52	7.47	0.00	4	4
16.	18062429.66	34 7.71	106 49.52	8.43	-0.42	3	4
17.	18102908.62	34 7.44	106 49.36	8.23	-0.12	4	4
18.	18130341.18	34 7.54	106 49.55	8.77	-0.35	1	4
19.	18144705.05	34 7.46	106 49.37	7.66	0.90	1	4
20.	18154815.74	34 7.54	106 49.77	7.12	1.61	1	4
21.	18165444.05	34 7.77	106 49.60	7.55	0.48	4	4
22.	18221427.59	34 7.84	106 49.39	8.11	0.26	5	4
23.	19193533.95	34 7.50	106 49.74	9.35	1.82	0	0
24.	20022603.56	34 7.23	106 49.70	8.68	0.22	4	0
25.	20073611.74	34 7.62	106 49.75	8.84	0.11	1	0

All events are from August, 1985. Under the *Time* heading is the day, hour, minute, and second of each event. The *R* heading lists the total number of reflections picked for each event. The *P* heading lists the total number of portable stations recording each event.

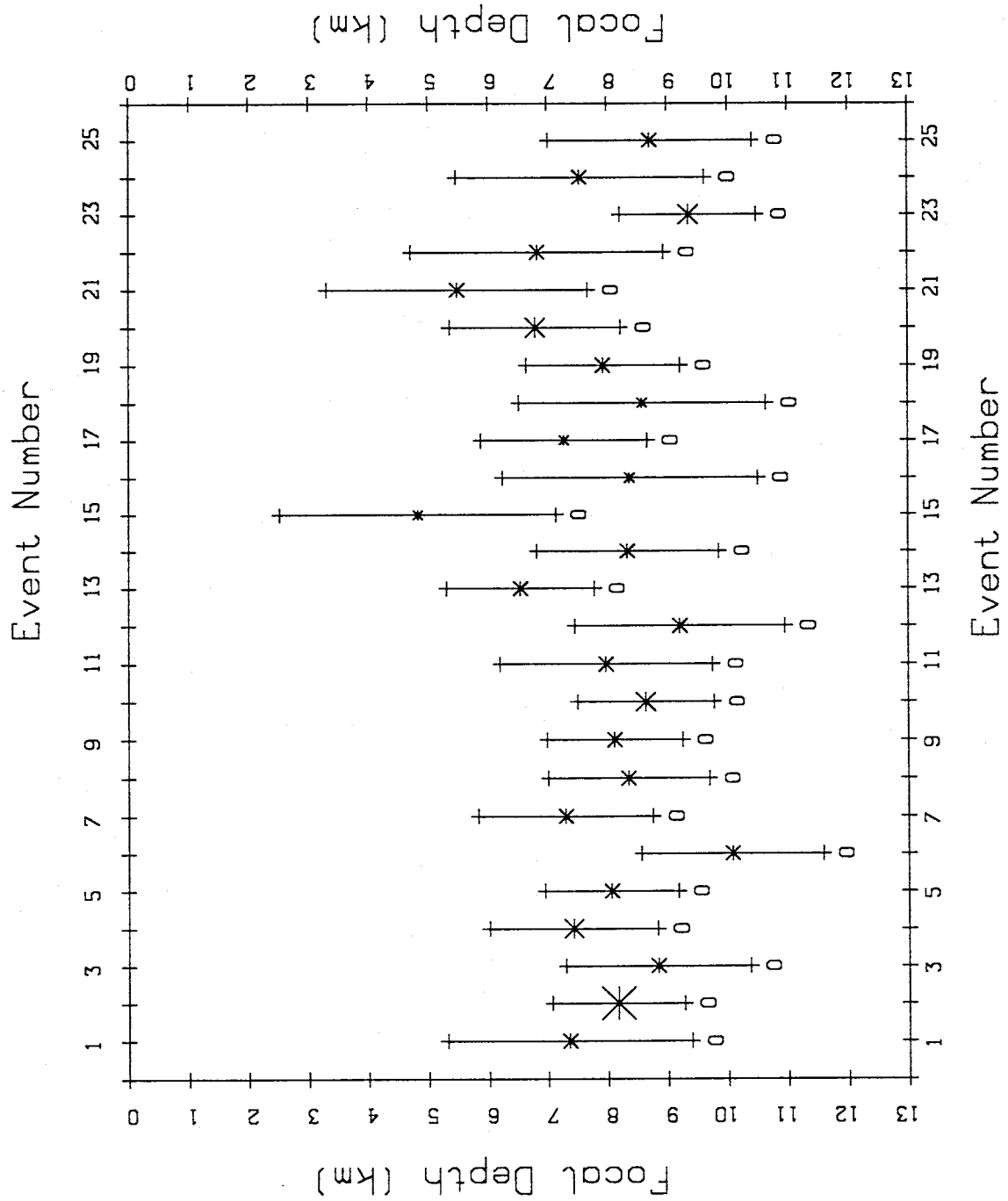

Fig. 8.3. Focal depths (asterisks) and one standard deviation error bars obtained using direct arrivals from only the network stations.

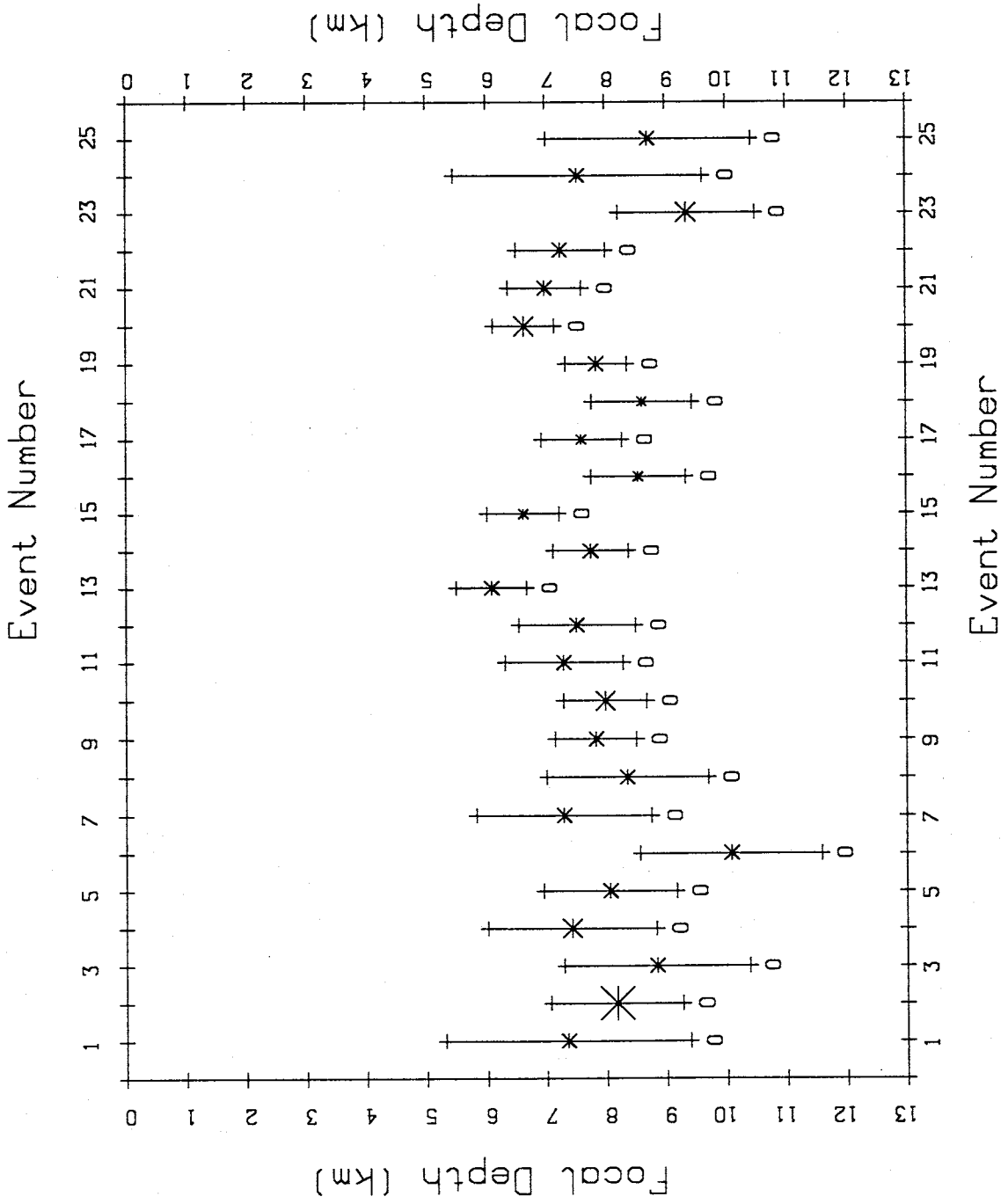

Fig. 8.4. Focal depths (asterisks) and one standard deviation error bars obtained using only direct arrivals from both the network stations and the portable recorders.

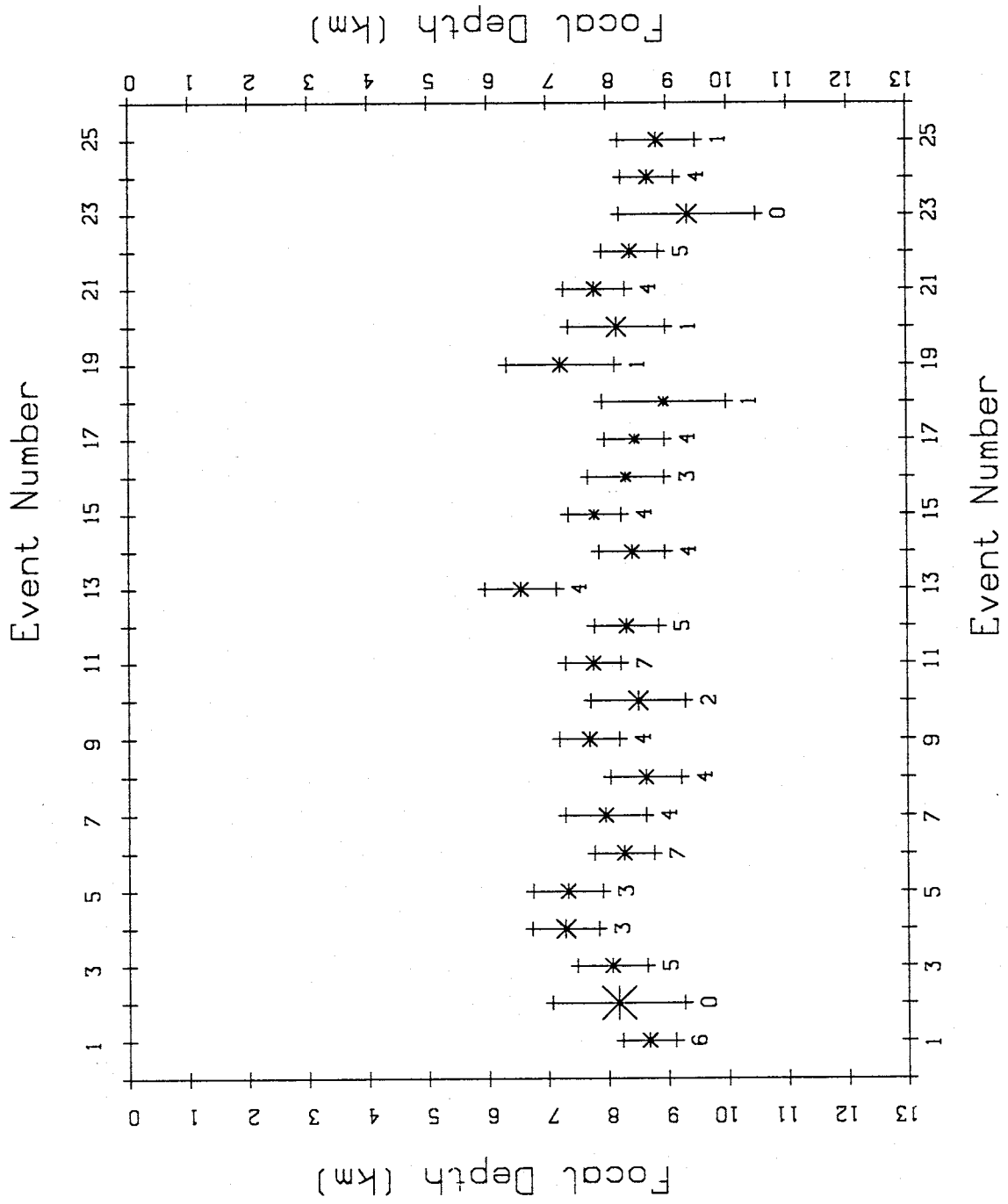

Fig. 8.5. Focal depths (asterisks) and one standard deviation error bars obtained using direct and reflected arrivals from only the network stations. The numbers below each event depth indicate the number of reflections used in each solution.

actually slightly smaller than when the portable data have been used. Using two reflections errors are about the same, and when only one reflection is available, then the portable data constrain focal depths better.

Tables 8.2, 8.3, 8.4, and 8.5 compare hypocenter parameters obtained with location runs two and three. Only the events which occurred when the portable recorders were deployed (events 9 to 22) are listed. The purpose of these tables is to see if reflections have caused locations to shift significantly relative to high-quality solutions obtained with only direct arrivals. All latitudes, longitudes, and origin times agree within one standard deviation. Except for events 15 and 20, all focal depths agree within one standard deviation. For these two cases the differences between overlap at one standard deviation is slight, and the focal depths easily overlap at two standard deviations.

The importance of reflected phases, and especially S_zP, can be quantified by the information density matrix, **S** (Equation 9). For example, Table 8.6 displays detailed station and phase information for event 11 of the Arroyo del Coyote sequence. The diagonals of **S** vary between 0.69 and 0.05. The largest values are associated with direct P arrivals at stations BAR, CAR, and LAZ because these phases have the smallest assumed timing errors (pick qualities of 0). All the secondary phases from this event have pick qualities of 3, but their **S** diagonals are not the same. At stations LAZ and MAG the S_zP diagonals are near 0.30, the S_zS diagonals are slightly less than 0.20, and the direct S diagonals are less than 0.10. This indicates that S_zP provides about 1.5 times more information to the solution than S_zS, and S_zP provides about 3 times more information than direct S. S_zP even provides between 2 and 3 times more information than direct P with pick quality 1 (compare P at WTX and LEM with S_zP at MAG and LAZ). Summarizing, this example shows that S_zP (even with pick quality 3) is the second most important phase, after direct P (with pick quality 0), for locating earthquakes.

This case study shows that reflected phases, even when recorded at source-receiver distances greater than 35 km, can constrain focal depths as well as, and

TABLE 8.2. Latitudes Found Using Network and Portable Direct Data Compared to Using Only Network Direct and Reflected Data

	Direct Data	Reflections		
	Lat (km)	Lat (km)	R	P
9.	5.77 ±0.23	5.74 ±0.24	4	2
10.	5.48 ±0.25	5.42 ±0.26	2	2
11.	5.78 ±0.33	5.81 ±0.34	7	2
12.	6.62 ±0.49	6.44 ±0.51	5	2
13.	6.42 ±0.30	6.43 ±0.31	4	3
14.	6.65 ±0.31	6.69 ±0.32	4	4
15.	6.38 ±0.28	6.21 ±0.33	4	4
16.	6.49 ±0.55	6.69 ±0.59	3	4
17.	5.93 ±0.25	5.87 ±0.26	4	4
18.	6.13 ±0.38	6.15 ±0.41	1	4
19.	5.98 ±0.30	6.03 ±0.32	1	4
20.	6.11 ±0.24	5.98 ±0.27	1	4
21.	6.63 ±0.32	6.41 ±0.35	4	4
22.	6.71 ±0.44	6.68 ±0.47	5	4

TABLE 8.3. Longitudes Found Using Network and Portable Direct Data Compared to Using Only Network Direct and Reflected Data

	Direct Data	Reflections		
	Long (km)	Long (km)	R	P
9.	10.29 ±0.22	10.31 ±0.22	4	2
10.	10.74 ±0.27	10.70 ±0.28	2	2
11.	10.39 ±0.30	10.44 ±0.30	7	2
12.	11.01 ±0.26	11.00 ±0.26	5	2
13.	10.63 ±0.24	10.65 ±0.25	4	3
14.	10.96 ±0.24	10.91 ±0.25	4	4
15.	10.85 ±0.27	10.68 ±0.33	4	4
16.	10.90 ±0.27	10.94 ±0.28	3	4
17.	11.13 ±0.21	11.13 ±0.22	4	4
18.	10.87 ±0.33	10.86 ±0.35	1	4
19.	11.15 ±0.22	11.23 ±0.23	1	4
20.	10.43 ±0.26	10.43 ±0.28	1	4
21.	10.65 ±0.33	10.56 ±0.38	4	4
22.	11.10 ±0.34	11.05 ±0.37	5	4

TABLE 8.4. Focal Depths Found Using Network and Portable Direct Data Compared to Using Only Network Direct and Reflected Data

	Direct Data	Reflections		
	Depth (km)	Depth (km)	R	P
9.	7.83 ±0.68	7.70 ±0.50	4	2
10.	7.98 ±0.69	8.51 ±0.79	2	2
11.	7.30 ±0.99	7.76 ±0.47	7	2
12.	7.51 ±0.98	8.32 ±0.54	5	2
13.	6.09 ±0.59	6.55 ±0.60	4	3
14.	7.75 ±0.63	8.41 ±0.55	4	4
15.	6.61 ±0.61	7.79 ±0.44	4	4
16.	8.55 ±0.79	8.32 ±0.63	3	4
17.	7.60 ±0.67	8.46 ±0.50	4	4
18.	8.61 ±0.83	8.95 ±1.03	1	4
19.	7.85 ±0.51	7.23 ±0.90	1	4
20.	6.63 ±0.52	8.17 ±0.81	1	4
21.	6.99 ±0.62	7.80 ±0.52	4	4
22.	7.25 ±0.76	8.39 ±0.47	5	4

TABLE 8.5. Origin Times Found Using Network and Portable Direct Data Compared to Using Only Network Direct and Reflected Data

	Direct Data	Reflections		
	Time (sec)	Time (sec)	R	P
9.	22.21 ±0.05	22.22 ±0.04	4	2
10.	46.70 ±0.06	46.67 ±0.05	2	2
11.	24.84 ±0.07	24.82 ±0.04	7	2
12.	24.76 ±0.08	24.72 ±0.05	5	2
13.	11.05 ±0.05	11.03 ±0.04	4	3
14.	2.06 ±0.06	2.01 ±0.05	4	4
15.	11.66 ±0.06	11.59 ±0.05	4	4
16.	29.65 ±0.10	29.66 ±0.06	3	4
17.	8.68 ±0.06	8.62 ±0.04	4	4
18.	41.20 ±0.09	41.17 ±0.08	1	4
19.	5.03 ±0.05	5.06 ±0.06	1	4
20.	15.78 ±0.05	15.72 ±0.05	1	4
21.	44.11 ±0.07	44.07 ±0.05	4	4
22.	27.69 ±0.09	27.60 ±0.06	5	4

TABLE 8.6. **S** Matrix Details From Event 11 of the Arroyo del Coyote Case Study

Station Name	Phase Type	Pick Quality	**S** Matrix Diagonal	Distance (km)	Azimuth (deg)
WTX	p	1	0.20	12.0	243
LEM	p	1	0.15	14.1	290
LEM	s	3	0.12	14.1	290
BAR	p	0	0.66	18.8	83
BAR	s	3	0.10	18.8	83
CAR	p	0	0.69	20.8	155
LJY	p	1	0.16	24.6	346
LPM	p	3	0.05	27.5	41
MAG	p	1	0.14	37.3	277
MAG	s	3	0.09	37.3	277
MAG	szp	3	0.31	37.3	277
MAG	szs	3	0.19	37.3	277
SMC	s	3	0.16	41.8	205
LAZ	p	0	0.46	42.2	318
LAZ	s	3	0.08	42.2	318
LAZ	szs	3	0.16	42.2	318
LAZ	szp	3	0.29	42.2	318

sometimes even better than, direct arrivals recorded close to an earthquake. Ideally, three or more reflections should be used, but even two reflections will constrain focal depth about as well as near-event direct data. Furthermore, this study shows that reflections will not significantly change locations relative to high-quality solutions found using only direct data.

9. Discussion

Flatness of the Magma Body's Upper Surface

COCORP Line 2A, (Figures 9.1 and 9.2) has been interpreted by *Brown et al.* [1979] as evidence that the magma body dips to the north by as much as 6 degrees. However, the reflected phase arrival time residuals from my data set indicate the magma body is essentially flat (Figures 7.9 and 7.10). The reflections points from my study do not reach as far north and east as Line 2A (Figure 6.9), and it is possible that significant dip could begin north of my reflection point map. However, because I find no evidence of north dip for the large portion of the magma body I have mapped, it may also be possible that Line 2A displays apparent dip caused by near-surface lateral velocity changes. As low-velocity basin fill thickens and thins along a seismic line, velocity pullup creates apparent dip on deeper reflectors. *Rinehart et al.* [1979] proposed that low-velocity basin fill was responsible for apparent magma body dip on Line 1A. Later, *de Voogd et al.* [1988] modeled Line 1A and confirmed the earlier interpretation. As with Line 1A, the north dip of the magma body on Line 2A may be caused by thickening low-velocity basin fill.

Line 2A and its northern extension, Line 2, are in a graben between the Los Pinos Mountains on the east and the Hubbell-Joyita Bench on the west. On Line 1 (Figure 9.3), the east-west line which intersects Line 2, *Cape et al.* [1983] have identified the boundary faults of this graben. Their interpretation of Line 1 shows that it is between 2.5 km deep (from their depth-converted seismic section) and 4 km deep (from their line drawing). On Line 2A the magma body reflection time increases by 0.8 s from south to north. To cause an 0.8 s increase in reflection time, low-velocity (3.0 km s^{-1}) fill would need to thicken to 2.5 km, displacing high-velocity (5.90 km s^{-1}) basement rocks. If the fill thickens to 4.0 km, then its velocity would have to average 3.7 km s^{-1}. Apparent dip would not show up on my reflection point maps because station corrections compensate for any low-velocity material beneath each station site.

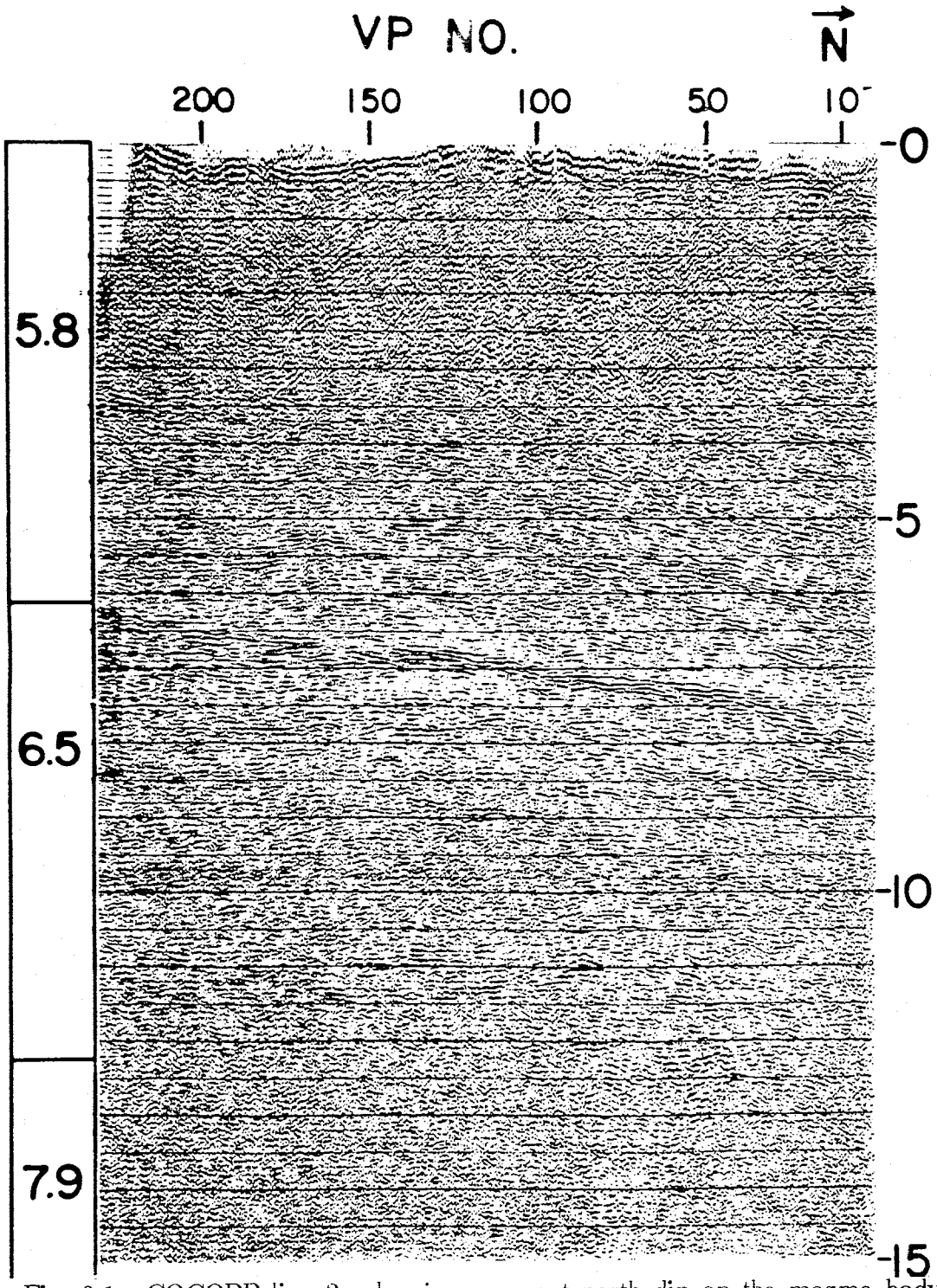

Fig. 9.1. COCORP line 2a showing apparent north dip on the magma body. Numbers on right are time in seconds. Magma body is near 7 seconds. From *Brown et al.* [1979].

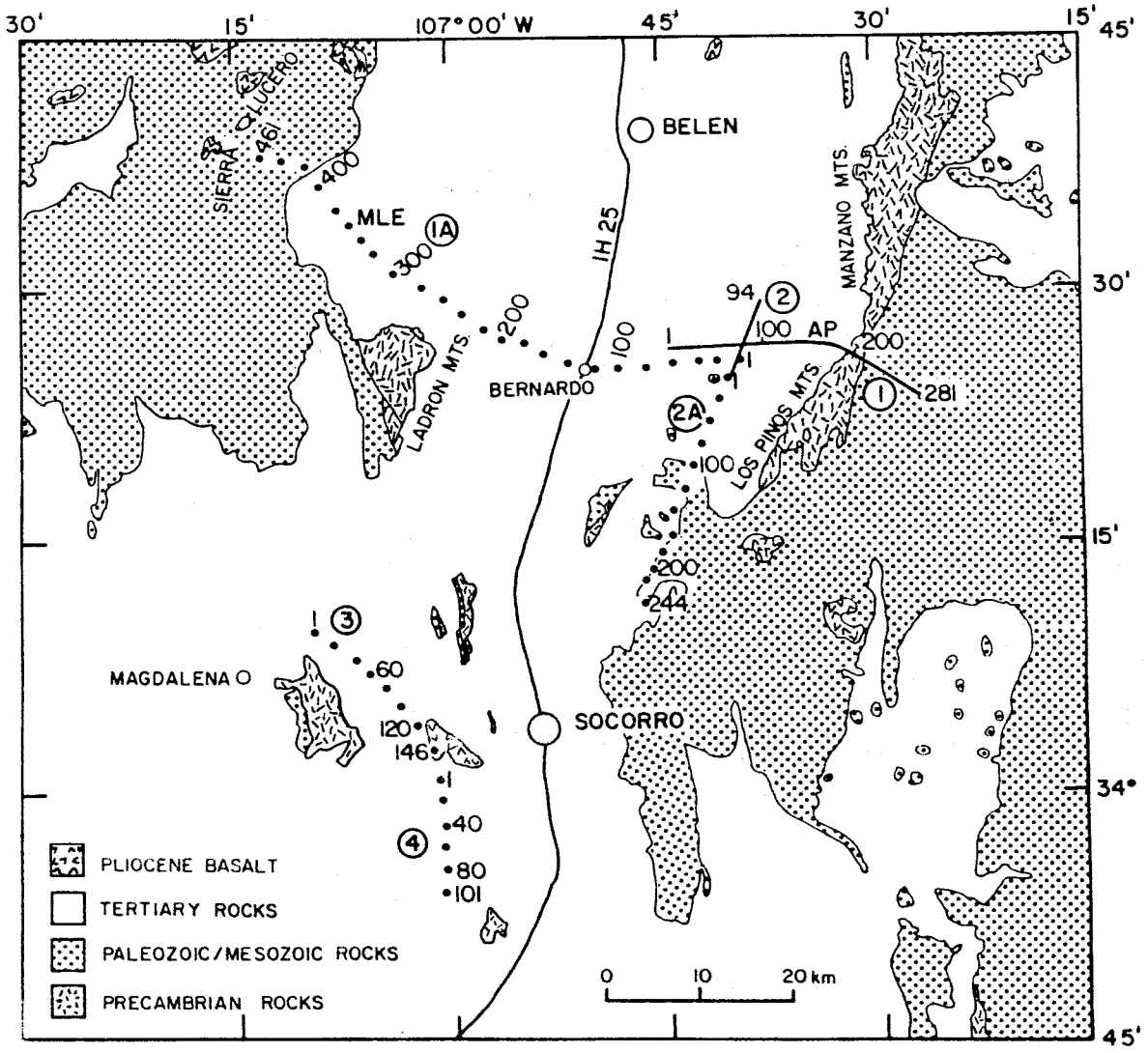

Fig. 9.2. Map of COCORP lines and general Socorro-area geology. From *Brown et al.* [1979].

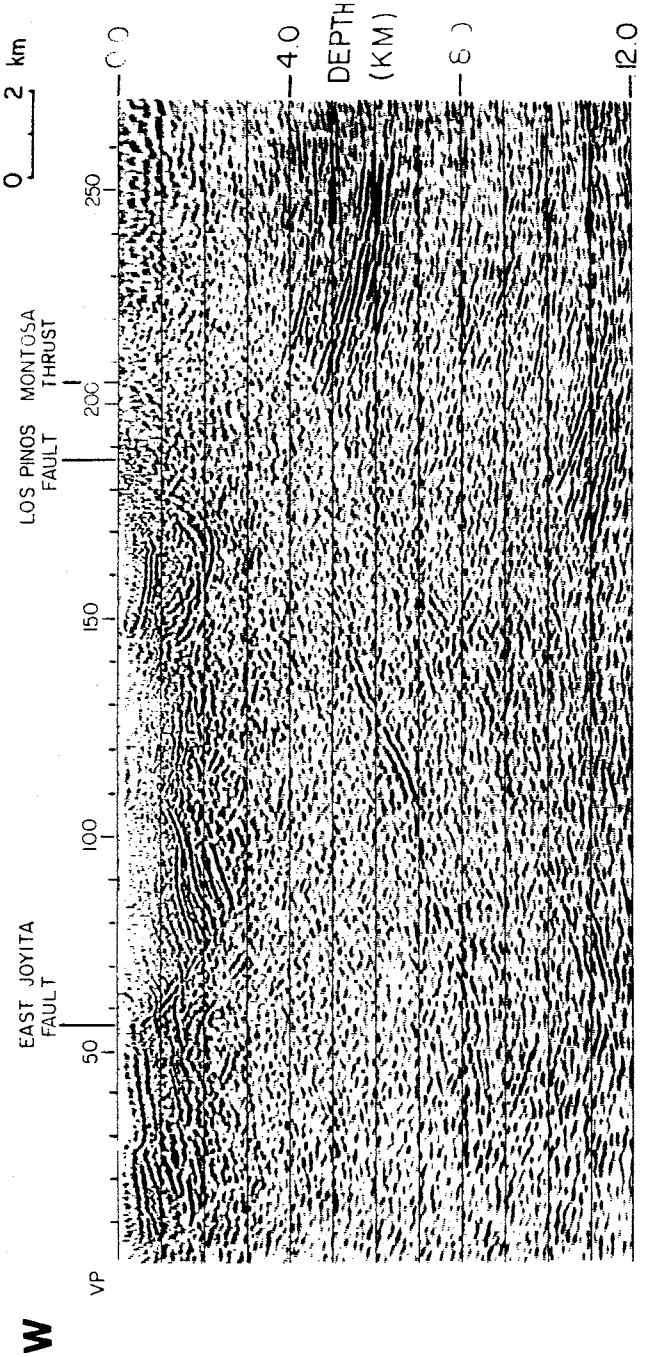

Fig. 9.3. COCORP Line 1 (top) and interpretation of Line 1 showing a graben structure (centered near shotpoint 100) at the intersection with Line 2. From *Cape et al.* [1983].

The flatness of the magma body's upper surface suggests the trapping mechanism for the magma exists over a broad area and must also be quite flat. One possible explanation for such a mechanism is buoyancy [*Glazner and Ussler* 1988]. Low density magma will ascend through higher density mantle and lower crust material until it reaches a level of neutral buoyancy. When the magma ceases to rise it spreads laterally to form a sill-shaped body [*Lister and Kerr*, 1991].

Such a level of neutral buoyancy could occur at mid-crustal levels where P velocity increases by about 0.6 km s^{-1}. Figure 9.4 shows the relationship between density and V_p, and Figure 9.5 shows density of a basalt magma under varying pressures. My results indicate V_p above the magma body is 5.80 km s^{-1}, and *Singer* [1989], using time-term analysis, estimated V_p below the magma body to be 6.40 km s^{-1}. From Figure 9.4 this velocity change corresponds to a density change from 2.68 g cm^{-3} above the magma body to 2.77 g cm^{-3} below the magma body. From Figure 9.5 the density of basalt magma at 500 MPa (approximate lithostatic pressure at 19 km depth) is also 2.68 g cm^{-3}. Thus, beneath the Socorro area magma could rise to the mid-crustal velocity discontinuity where it would then spread out and form a flat, sill-shaped reflector.

Lateral Extent of the Magma Body

The position of reflection points can be used to establish the lateral extent of the magma body. Figure 9.6 shows the reflection points from my data set. Clearly, reflection point coverage to the north is too sparse to define the limit of the magma. A figure that can be used to help determine which segments of the boundary are well constrained is a map of hypothetical reflection points. Figure 9.7 was made by assuming all earthquakes of my data set could have S_zS and S_zP reflections at every station that recorded each event. When the outline of the magma body based on the real reflection points is compared to the distribution of the hypothetical reflection points, only the southeast side of the magma body is well constrained. To better constrain the boundaries elsewhere, my data set would have to be

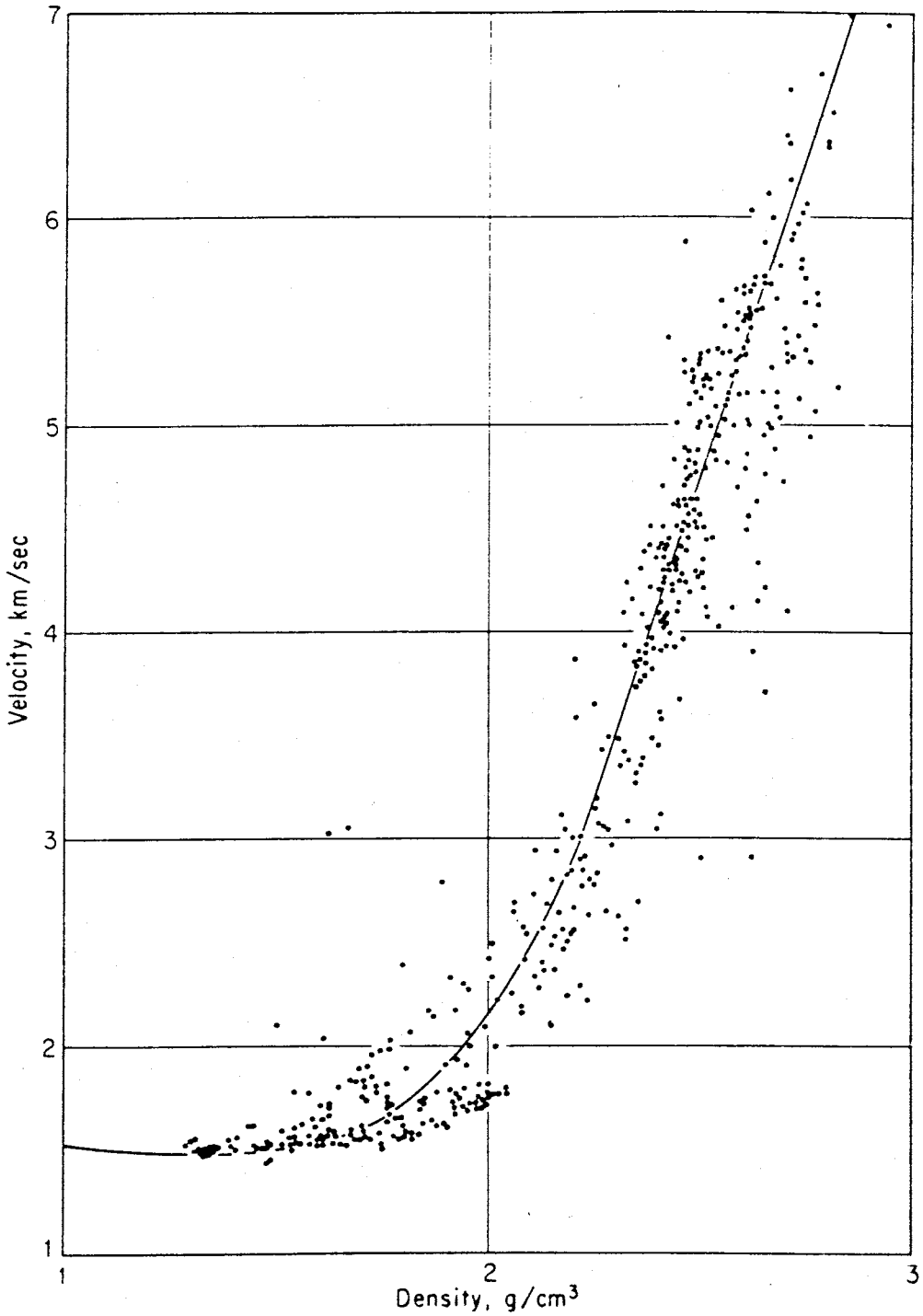

Fig. 9.4. Relationship between density and compressional velocity. From *Grant and West* [1965].

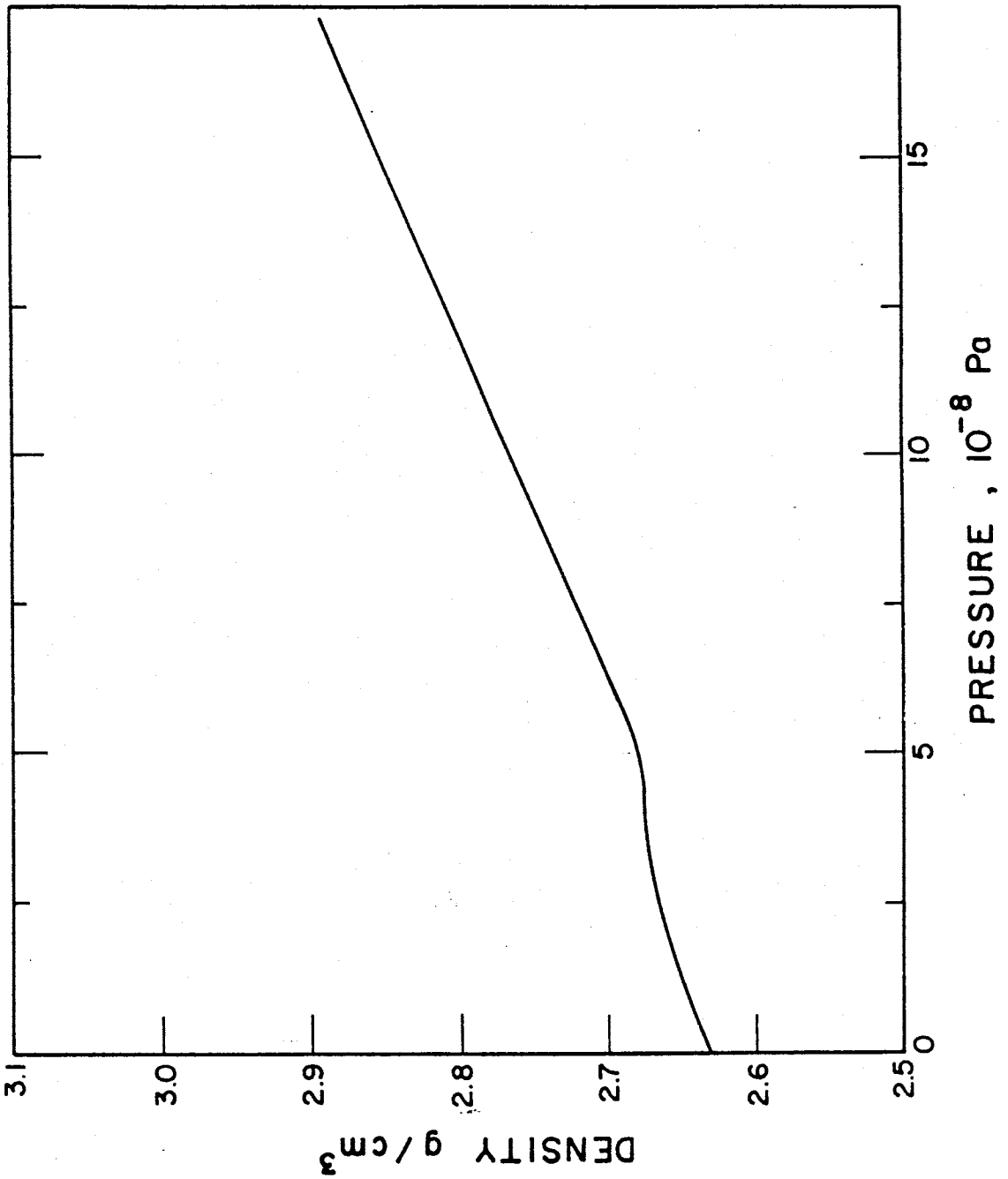

Fig. 9.5. Relationship between density and pressure for an olivine tholeiite magma. From *Mysen* [1981].

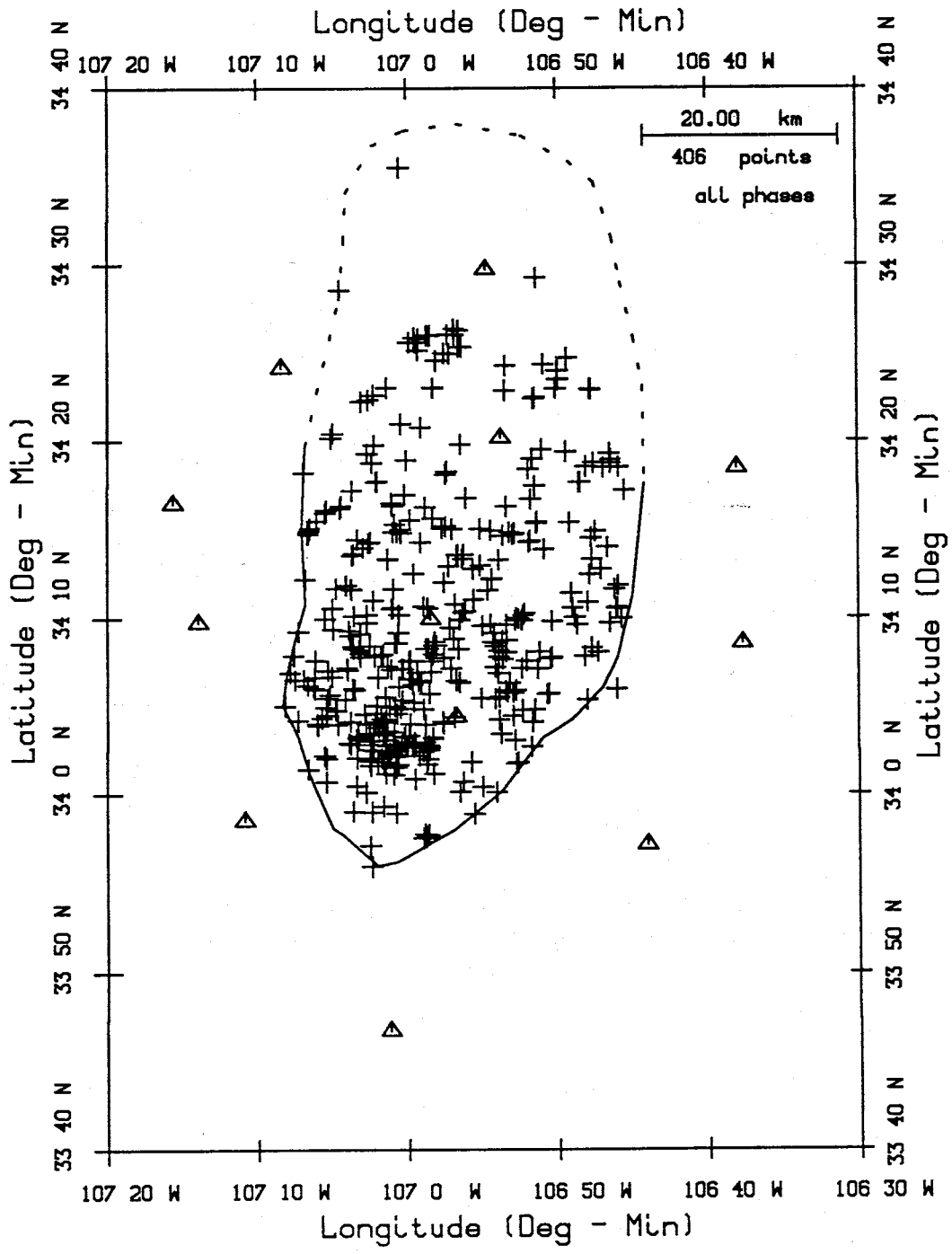

Fig. 9.6. Outline of magma body based on observed reflection points for S_zP, S_zS, and P_zP. Stations are represented by triangles.

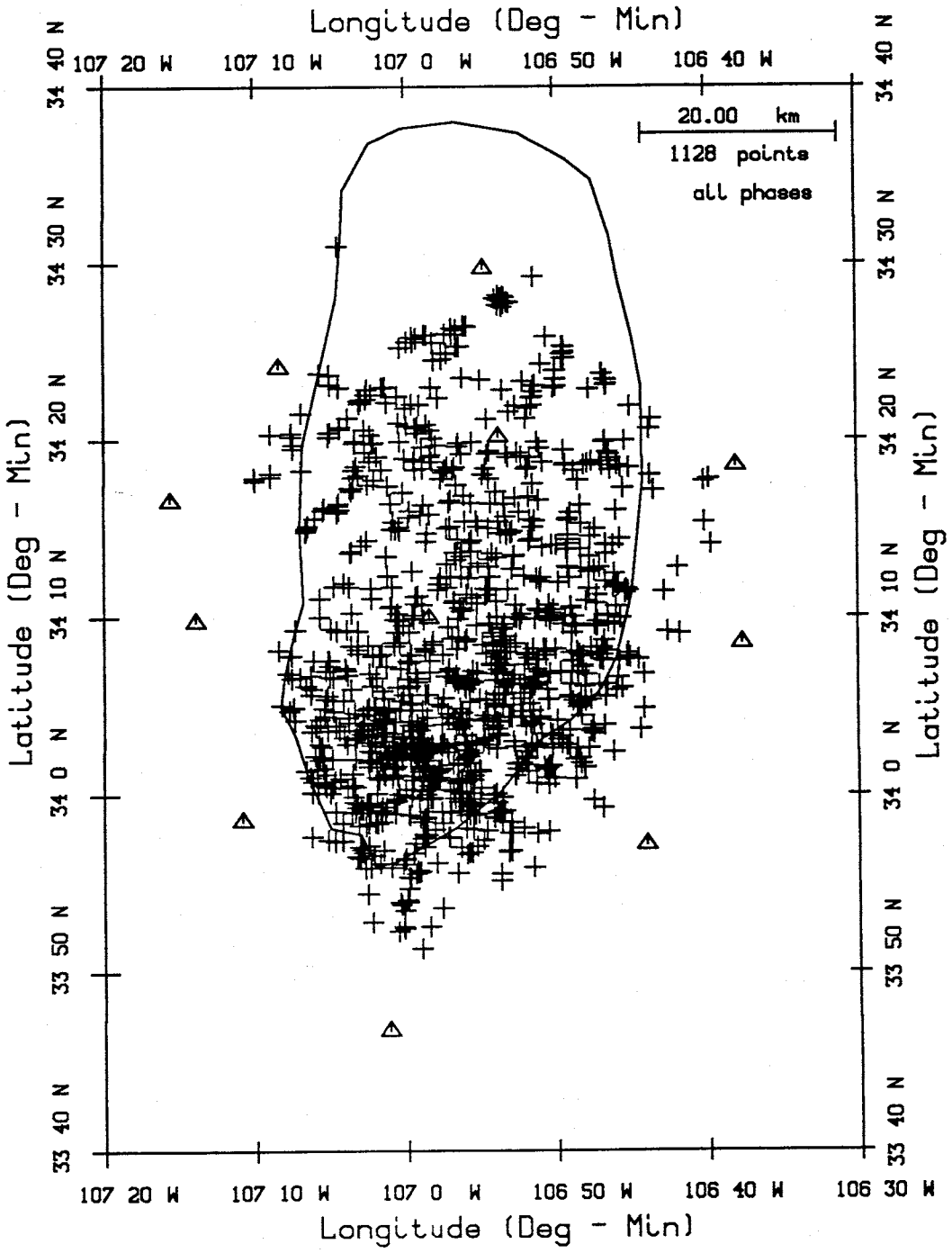

Fig. 9.7. Hypothetical S_2P and S_2S reflection points based on the data set used in this study. Solid line is the mapped outline of the magma body. Stations are represented by triangles.

expanded to include events over a broader epicentral distribution, and therefore include real and hypothetical reflection points over a larger area.

Figure 9.8 shows the magma body outline of *Rinehart et al.* [1979] and the outline from my study. The new outline now extends south and southeast of previous mapping and also covers a previously unmapped area on the west side of the magma body. These new areas had probably not been previously mapped because the present network is now configured differently than stations deployed in the 1970's. However, if the older data did constrain the outline on the west and southeast sides of the magma body, then my mapping may indicate that the magma body has expanded in the last 15 years. A detectable change in the lateral extent of the magma body seems unlikely, especially over such a short time period, but the older data set should still be re-examined to determine how well the 1979 outline was constrained.

The one region where my mapping should overlap with the older map, but does not, is just west of station LPM. Here the older map extends farther east than my map (Figure 9.8). *Rinehart et al.* [1979] based this portion of their map on the COCORP lines, and especially Line 2A. I relied only on microearthquake reflections for my outline. Figure 9.7 shows that my data include only four hypothetical reflections within the area of no overlap. Thus, this disagreement can be completely attributed to the limits of my data set.

Seismogenic Zone

The limits of the seismogenic zone for the central Rio Grande rift can be estimated from the earthquakes located in this study. Because the focal depths have errors which average 0.6 km and never exceed 0.9 km, they represent the best-constrained focal depth information ever gathered in central New Mexico. However, my results are based on only 75 small-magnitude events, and therefore the interpretation discussed below should be considered preliminary until many more events have been located using reflected phases. Previously *King* [1986] used over 500

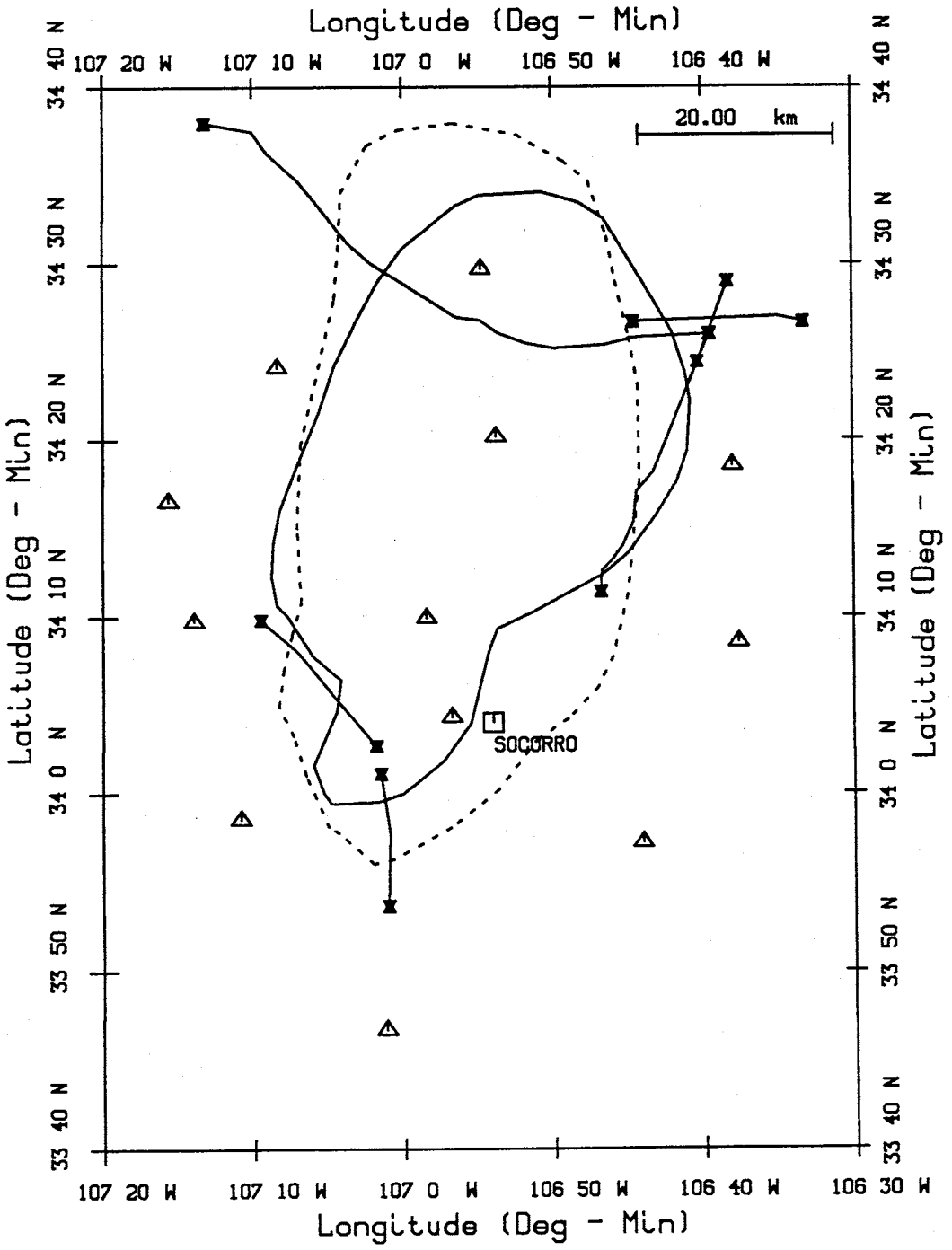

Fig. 9.8. Magma body outlines from the present study (dashed line) and *Rinehart et al.* [1979]. COCORP lines and seismic stations are also shown.

events to study the seismogenic zone in the Socorro area, but they were located using only direct arrivals. Although he used the best HYPO71 solutions available *King* still used many focal depth estimates which had errors of nearly 2 km.

Before comparing depth results between my study and *King's*, Figure 9.9, an epicenter map of *King's* events, can be compared to Figure 7.6, the epicenters from my study. Although *King* used many more events, the epicentral distribution of his events is similar to mine. Nearly all events from both studies fall within the network, and both studies reveal an absence of events in the west-central portion of the network. This comparison shows that the histograms presented below are derived from events with epicentral distributions which are nearly the same.

A focal depth histogram from my results (Figure 9.10), shows a sharp cutoff in event depths at 10 km. Less than 3 percent of all events are deeper than 10 km, and these deepest events are all less than 10.5 km. Figure 9.11 shows the focal depth histogram obtained by *King* [1986]. His deepest events, around 12 km, could be the result of greater uncertainties in focal depth.

The rather shallow and sharp cutoff at the base of the seismogenic zone shown in Figure 9.10 could have several causes. *Sibson* [1984] considers factors which influence the transition from frictional deformation (faulting) to ductile deformation. The most important factors are:

1. Temperature. High temperatures cause rocks to deform ductilely when subjected to deviatoric stress. Thus, regions of high heat flow are expected to have shallower transitions than areas of low heat flow.

2. Composition. Quartz is the first mineral to deform ductilely (at around $300°C$). Feldspars do not begin to deform ductilely until temperatures of around $450°C$. Thus, quartz-rich granitoids will deform ductilely at shallower depths than more intermediate or basic rocks.

Secondary factors are:

3. Strain rate. High strain rates cause faulting to occur at greater depths than low strain rates.

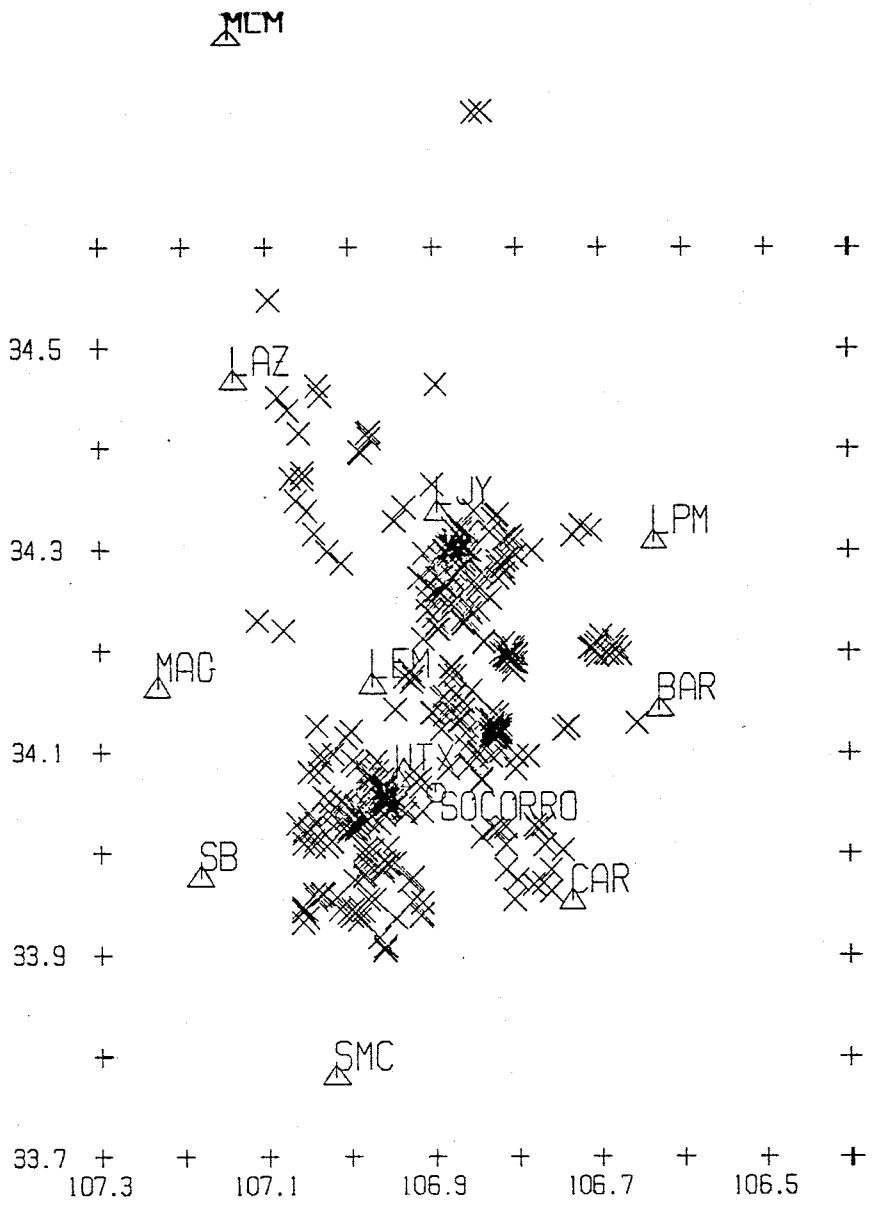

Fig. 9.9. Epicenter distribution of the events used by *King* [1986] to study the limits of the seismogenic zone in the Socorro area.

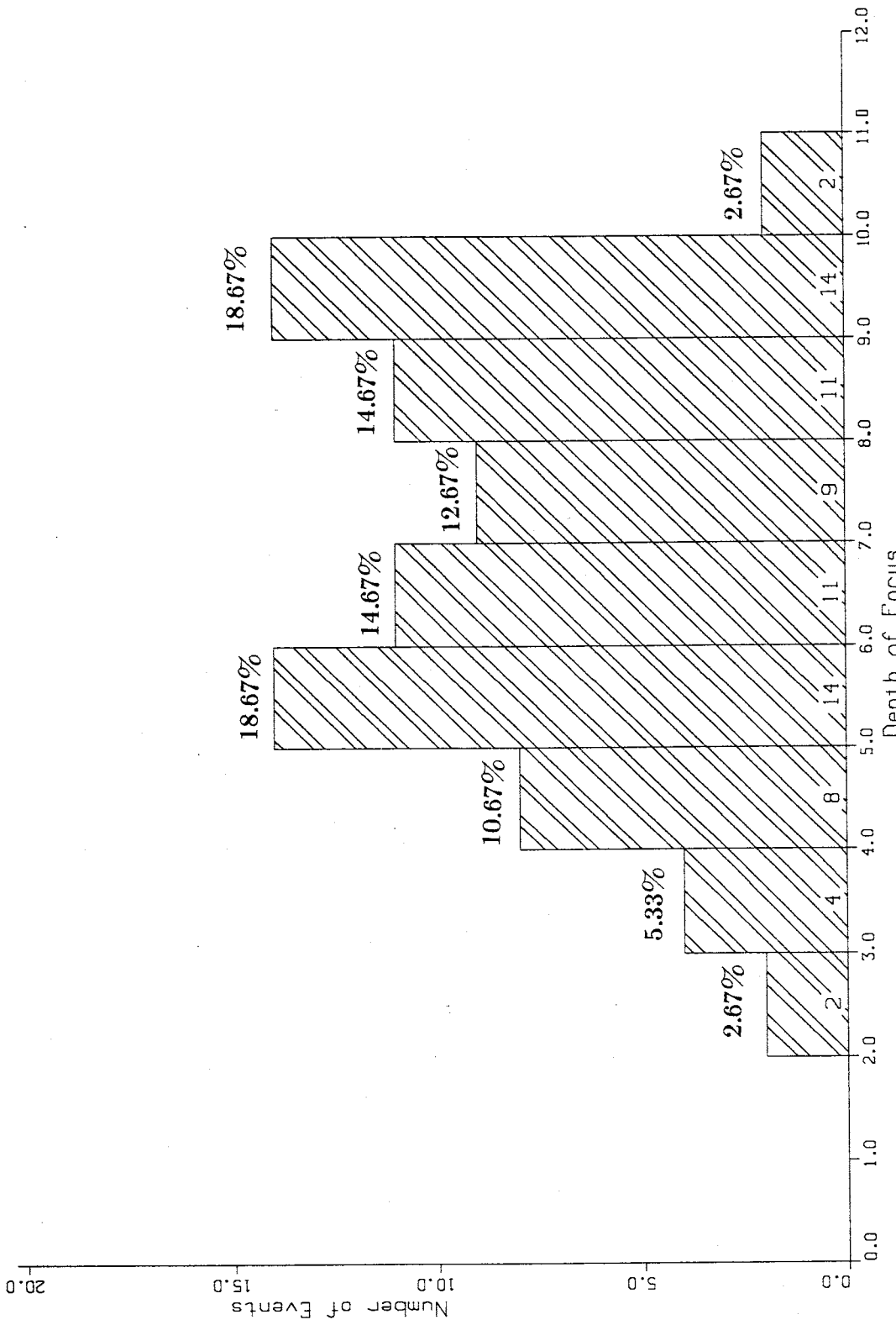

Fig. 9.10. Focal depth histogram of the 75 events used in this study.

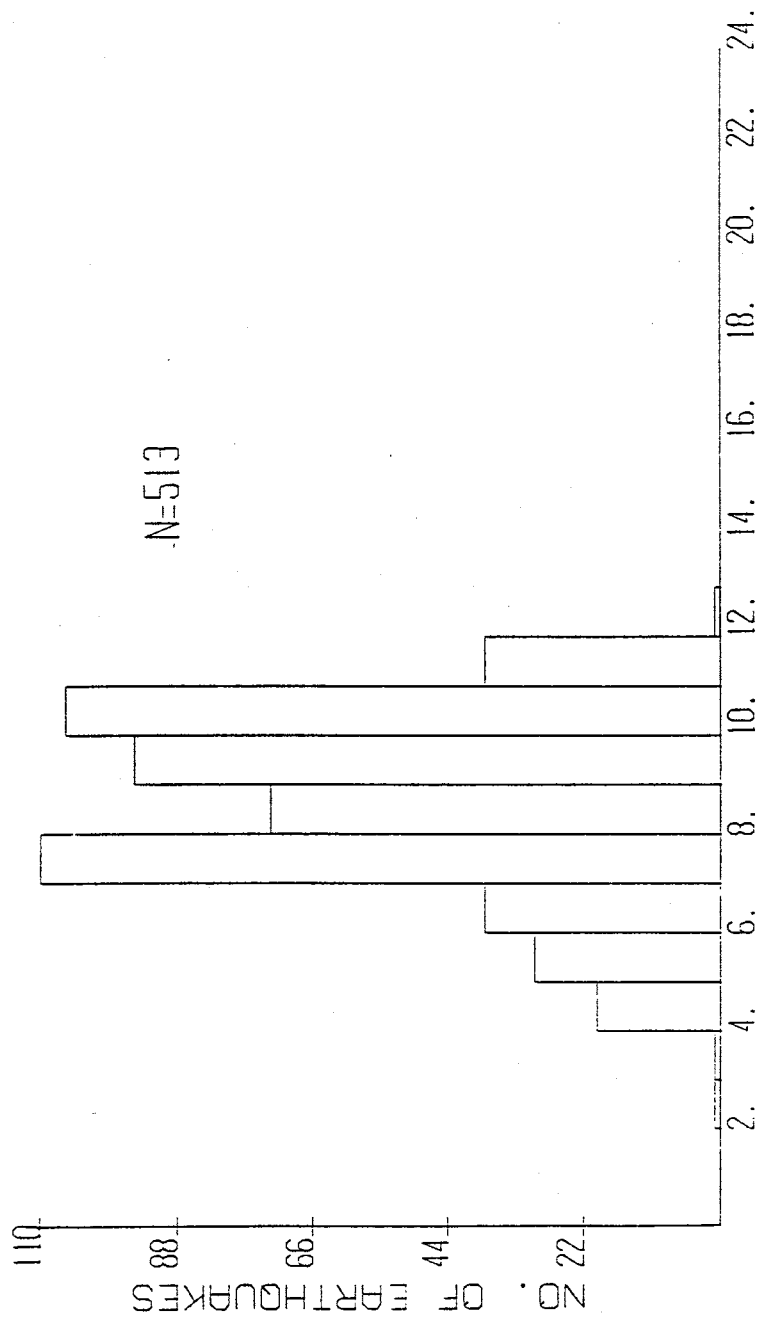

Fig. 9.11. Focal depth histogram of the 513 events used by *King* [1986].

4. Fluids within the ductile crust. The presence of fluids may cause rocks to deform ductilely at shallower depths than rocks where fluids are absent. The nature and even the presence of fluids in the ductile crust is poorly understood. Thus, I choose not to speculate on the influence of fluids on the brittle-ductile transition in the Socorro area.

The average heat flow in the Socorro area is approximately 90 mW m^{-2} *Reiter et al.* [1986]. If the brittle-ductile transition occurs where quartz reaches temperatures of around 300° C, then the base of the seismogenic zone and the 300° C temperature should occur at the same depth. Figure 9.12, a temperature-depth plot based on surface heat flow, shows that when heat flow is 90 mW m^{-2}, the 300° C depth matches the 10 km base of the seismogenic zone. The sharpness of the transition could be related to a compositional change at near 10 km depth (a slight increase in quartz content). Thus, the abrupt absence of earthquakes below 10 km depth is probably caused by the combined effects of temperature and compositional change.

The upper limit of the seismogenic zone from my findings is not as sharp as the lower limit. Most events are deeper than 4 km (92 percent) and over 97 percent of all events are deeper than 3 km. However, nearly 19 percent of my events occur between 5 and 6 km depth, and over 35 percent of my events are less than 6 km deep. This contrasts with *King's* histogram which shows only 10 percent of Socorro-area earthquakes less than 6 km deep. The lack of shallow events in *King's* distribution is probably caused by using only events with A or B quality HYPO71 solutions. To be ranked as an A solution the nearest recording station must be within an epicentral distance less than or equal to the focal depth of the event. To be ranked as a B solution the nearest station must be within an epicentral distance of two times the focal depth. Because station spacing for the Socorro network is coarse relative to average event depth, mostly deeper events examined by *King* qualified as A or B quality events. I have shown that by using reflected phases in the location process both deep and shallow events are located nearly equally well. Thus, a greater percentage of high quality shallow focal depths is

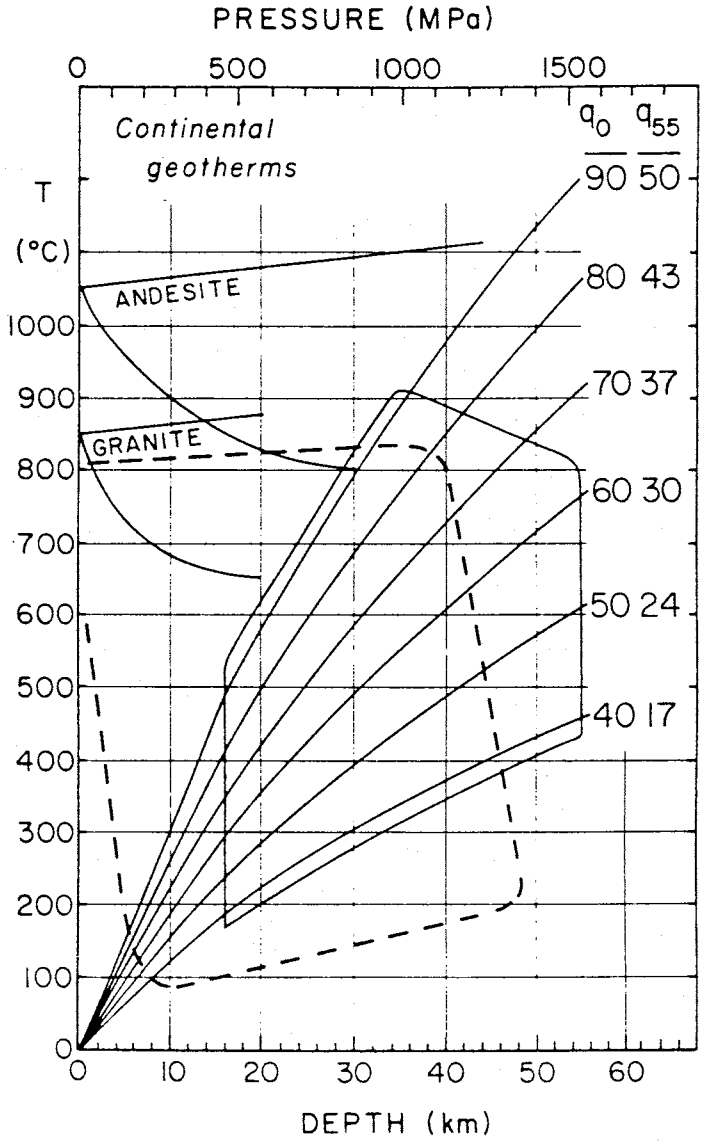

Fig. 9.12. Temperature versus depth based on different surface heat flow values (denoted by q_0). From *Chapman* [1986].

included in my histogram in than *King's.*

Velocities and Poisson's Ratio

The velocity and Poisson's ratio I obtained for the upper 10 km of crust (V_p of 5.95 km s^{-1} and ν of 0.256) are similar to previous researcher's findings for the Socorro area of the Rio Grande rift. For the lower part of the upper crust (between the approximate base of the seismogenic zone and the upper surface of the magma body) I found that V_p decreases to 5.80 km s^{-1} while ν decreases to 0.228. These parameters had never before been estimated for the Socorro area, but they are similar to Rhinegraben crustal structure as determined by *Holbrook et al.* [1988]. Their velocity model has V_p increasing to near 6.0 km s^{-1} at around 9 km depth and then decreasing to 5.8 km s^{-1} for the next 8 km. Their Poisson's ratio values are near 0.25 in the uppermost crust and decrease to near 0.23 within the low velocity zone.

Spencer and Nur [1976] investigated the effects of several factors on V_p and V_s and, hence, ν. These factors and their effects are:

1. Pressure. As pressure increases with depth, fractures and voids close, and both V_p and V_s increase. They found that increasing pressure tends to increase V_p more rapidly than V_s, suggesting bulk modulus is affected by pressure more than shear modulus.

2. Temperature. Increasing temperature retards both V_p and V_s. *Spencer and Nur* found V_s is affected by temperature more than V_p, suggesting that shear modulus is more sensitive to temperature than bulk modulus.

3. Generally the net effect of pressure and temperature increasing with depth is to increase V_p more rapidly than V_s, resulting in an increase in ν. If the temperature gradient is high, then V_p and V_s will both decrease. However, V_s will decrease more rapidly than V_p, once again resulting in an increase in ν.

4. Composition. Replacing a small percentage of feldspar (ν of 0.25 to 0.30) with quartz (ν of only 0.08 *Christiansen* [1982]) will lower Poisson's ratio. The changes in ν I have detected could occur by replacing about 5% of feldspar with quartz.

5. Fluid pressure. A high pore fluid pressure will cause V_s to decrease more rapidly than V_p, resulting in an increase in Poisson's ratio. However, a low pore fluid pressure will not change V_s while decreasing V_p, resulting in a decrease in Poisson's ratio.

Factors 4 or 5 could possibly cause a decrease in V_p and ν beneath the seismogenic zone in the Socorro area. However, *Holbrook et al.* [1988] suggest that low pressure fluids should cause Poisson's ratio to decrease from normal values of around 0.25 to rather low values of around 0.15. Because I have found Poisson's ratio decreases from only 0.256 to 0.228, low pressure fluid seems to be an unlikely cause. This leaves compositional change (a small increase in quartz content) as the simplest reason for the decrease in both V_p and ν near 10 km depth. An increase in quartz content is also a more reasonable explanation because the sharpness of the base of the seismogenic zone is is also apparently related to a compositional change.

Using Reflected Phases to Locate Earthquakes

It appears that there are no significant problems with using reflected phases to better constrain earthquake hypocenters in the Socorro area. The upper surface of the magma body is quite flat and improvements in location estimates are significant. Small events (less than about M_D 1) are routinely recorded on the Socorro network, and these small magnitude events often produce clear reflections which can be picked as accurately as direct S. The greatest weakness of using reflections is that they are not always identifiable for every event. This is especially true for events larger than about M_D 1.5. High-quality digital recordings, showing clear, sharp reflected phases, have been recorded and interpreted in the past [*Ake and Sanford,*

1988]. In the future, digital recording and signal processing will almost certainly make routine use of reflected phases more common, helping to increase the numbers of both small and larger events which can be located using magma body reflections.

Using three or more reflected phases recorded at two or more stations best constrains focal depths, but even a single reflection will improve a depth estimate over the case where no reflections are available (compare Figures 7.5 and 7.12, and Figures 8.3 and 8.5). My results indicate that the reflections primarily contribute to focal depth and origin time estimates (Table 7.8). For poorly recorded events where station gaps are large and epicenters can not be tightly constrained, any additional data (such as reflections) will also help to slightly improve epicenter estimates. For, example Tables 9.1 and 9.2 show location results using modified pick files from event 11 of the Arroyo del Coyote sequence (see Chapter 8). Table 9.1 shows parameter errors when only direct P arrivals are left in the solution, and all arrivals at stations SB, SMC, and CAR have been removed from the pick file. This creates an extremely poor solution due to a large station gap (see Figure 8.1) and lack of S data to help constrain arrival time. Table 9.2 shows errors when S_zP and S_zS at MAG and LAZ have been added to the solution, but the large station gap and absence of direct S remains. The addition of the reflections has significantly reduced focal depth and origin time error. The reflections have also helped reduced epicenter error, but only by a few tenths of a kilometer.

When using relative arrival time curves (**Appendix B**) as a guide, correct reflected phase identification is nearly always possible. With an S_zP - S_zS or S_zP - P_zP pair recorded at a single station, or individual reflections recorded at two or more stations, the phases will only match relative arrival time curves for a narrow focal depth range. Even when only one reflection is available and it is misidentified, the location solution usually will be poor and the error will be obvious. The one extreme case where a misidentified phase could go undetected is when the following occur together: (1) only one reflection is picked, (2) the station which recorded the reflection is between about 0 and 25 km from the event, and (3) the event focal

TABLE 9.1. Error Information From Event 11 of the Arroyo del Coyote Case Study - *P* Arrivals Only

parameter type	error at 1 std	rmatrx
lat	0.91	1.0
lon	0.33	1.0
depth	6.48	1.0
orig	0.19	1.0

TABLE 9.2. Error Information From Event 11 of the Arroyo del Coyote Case Study - *P* Arrivals and Reflected Arrivals

parameter type	error at 1 std	rmatrx
lat	0.68	1.0
lon	0.35	1.0
depth	0.60	1.0
orig	0.06	1.0

depth is either deep (around 10 km) or shallow (around 3 km). Over this 0 to 25 km distance range, P_zP from a shallow event could be identified as S_zP from a deep event, and S_zP from a deep event could be identified as P_zP from a shallow event. This potential overlap can be seen on Figure 7.8, where the 3 km P_zP curve and the 10 km S_zP curve have a similar time-distance relationship from 0 to 25 km. In most situations these three conditions will not occur together. As a precaution, when only one reflection is available, I recommend first locating the event using direct arrivals and then identifying the reflection based on the preliminary location.

10. Summary and Conclusions

Because earthquakes occur in the Socorro area at shallow depths relative to network station spacing, constraining focal depths using only direct arrival data is often difficult. However, reflected phases from a sill-shaped mid-crustal magma body, commonly identified on Socorro-area microearthquake seismograms, provide an exceptional opportunity to improve location estimates, and especially depth of focus estimates. Not only do the reflected phases help constrain focal depth estimates, they also help constrain estimates of crustal velocities and the depth to the magma body.

The primary goals of my research were to (1) develop a generalized least squares inversion technique to solve the joint hypocenter-velocity model problem while simultaneously utilizing arrival times from both the direct and reflected phases commonly seen on Socorro-area seismograms and (2) solve the joint problem using arrival times from a suite of well distributed earthquakes to find a velocity model most appropriate for locating Socorro-area events. This project has resulted in the development of a new and more powerful single-event earthquake location tool which can now be routinely applied to seismology problems in central New Mexico. Other goals of the research were to (3) evaluate the inversion results for possible dip on the magma body's upper surface, (4) compare solutions for events located with and without reflected phases, (5) interpret the inversion results with respect to crustal composition and temperature, and (6) redefine the limits of the seismogenic zone in the central Rio Grande rift using the new, well-constrained focal depths obtained from the inversion.

After writing a generalized least squares inversion program and testing the program for correctness with synthetic data, I assembled over 1000 direct P and S arrival times and over 400 reflected phase S_zS, S_zP, and P_zP arrival times from 75 earthquakes recorded on the Socorro seismic network. This was the first Socorro-area study to use the S_zP phase in an inversion, and the first study to combine direct and reflected phases simultaneously. Events were selected which had

epicenters surrounded by the network stations. Thus, all epicenters from my data set were well constrained using only direct P and S arrivals, and the reflections primarily contributed to focal depth estimates.

While inverting for the event hypocenters, I solved for a two-layer velocity model consisting of the unknowns V_p and Poisson's ratio in an upper layer, V_p and Poisson's ratio in a lower layer, the depth to the base of the lower layer (depth to the magma body), and station corrections. Because my data set contained no information which could constrain the base of the first layer, I ran two different inversions. For the first run I held constant the base of the upper layer at 12 km. For the second run I held constant the base of the top layer at 10 km. The 10 km depth approximates the base of the seismogenic zone and also resulted in a model which fit the observed data the best. Thus, the most geologically reasonable and best-fitting model I obtained was for the case with a 10 km thick first layer. Each inversion converged to physically reasonable parameters, and all eigenvalues were retained in each solution. Thus, all parameters were uniquely resolved and did not depend on starting models, even when extreme initial models were used.

The upper layer of the new velocity model is similar to the findings of previous researchers. Compressional velocity is 5.95 ± 0.05 km s^{-1} and Poisson's ratio is 0.256 ± 0.002, resulting in a shear velocity of 3.41 ± 0.04 km s^{-1}. In the lower layer V_p drops to 5.80 ± 0.08 km s^{-1} and Poisson's ratio is 0.228 ± 0.007, resulting in V_s of 3.44 ± 0.07 km s^{-1}. V_p and Poisson's ratio within the lower layer had never before been estimated for central New Mexico. They are both lower than expected, but V_s in the lower layer is identical to previous findings. Depth to the magma body is 18.75 ± 0.28 km.

The low values for V_p and Poisson's ratio in the lower layer are most likely caused by a small increase in quartz content near 10 km depth. High temperature alone is not a likely cause for this velocity distribution because, if composition remains constant, both V_p and V_s will decrease with increasing temperature. The base of the seismogenic zone is also near 10 km depth, and the cutoff in focal

depths is abrupt (less than 3% of events are deeper than 10 km). This sharp cutoff is most likely caused by the increase in quartz content and a high geothermal gradient in the Socorro area . The 10 km base of the seismogenic zone matches the depth for a 300° C temperature (the temperature at which quartz begins to deform ductilely) predicted by an average Socorro-area heat flow of 90 mW m^{-2}.

The results of the inversion indicate the upper surface of the magma body is quite flat. The primary reasons for this conclusion are the exceptionally good fit between observed and theoretical reflection times and the even distribution of both positive and negative reflected-phase residuals across the entire mapped surface of the magma body. Apparent magma body dip seen on some Socorro-area COCORP lines is most likely caused by near-surface lateral velocity variations.

The absence of dip on the upper surface of the reflector suggests a flat, area-wide barrier to rising magma. A likely barrier is crustal density contrast at near 19 km depth. If the rising magma is basalt, then its density will be less than upper mantle and lower crustal rocks. At the mid-crustal discontinuity velocity increases from near 5.80 km s^{-1} to near 6.40 km s^{-1}, corresponding to a density increase from 2.68 g cm^{-3} to 2.77 g cm^{-3}. At this depth rising magma would reach a point of neutral buoyancy and could form a flat sill.

The hypocenter estimates obtained when reflections are used in the location process are significantly improved relative to the case of using only direct arrivals. Average error on focal depth for the 75 events is 0.60 km, an improvement by more than a factor of three over using only direct arrival times. Similarly, origin time error was reduced by a factor of two when reflections were used. Latitude and longitude error remained nearly the same, indicating the reflections provide almost no constraint on epicenters comprising my data set. However, for events where station gaps are large and direct arrivals alone do not constrain epicenters, the reflections will also contribute to epicenter estimates.

11. Suggestions for Further Studies

There are several Socorro-area projects which can be pursued using the improved earthquake location procedure I have developed. First, more events could be located using reflections to build a larger set of well-constrained focal depths. This would better define the limits of the seismogenic zone.

The nature of the southeastern limit of the magma body could be examined more closely. The magma body map of *Rinehart et al.* [1979] was made using only S_zS reflection points. A hypothetical reflection point map using S_zP, P_zP, and S_zS from the 1979 data set could be made to better determine how well the southeastern boundary was constrained in 1979. When the extra reflection points are used, the upgraded map may match my magma body map more closely. If the two maps still fail to overlap, then the possibility that the magma body has expanded in the past 15 years will have to be considered.

The northern limit of the magma body could be investigated by searching for events which occurred in the northern section of my study area and have reflections recorded at stations MLM, ALQ, and ANMO. The recent Bernardo swarm has produced reflections at ALQ and ANMO and could be a useful source of data.

Digital data acquisition could lead to more routine reflected phase identification (for both small and large events) and more accurate timing. With more data and better timing, complex models could possibly be solved to investigate three-dimensional velocity variations.

A logical extension of this project is to solve the joint earthquake location-velocity model problem by including head wave arrivals from regional events. A good starting point for regional data studies would be to combine *Singer's* [1989] P_n data set with my data set in a joint inversion. The local data (direct and reflected arrivals) would constrain the upper crust velocity model, and the P_n data would constrain the lower crust and upper mantle velocity.

Before combining primary and secondary regional phases two factors should be carefully considered. First, identification of regional phases must be

investigated. When *Singer* [1989] used head wave data for time-term analysis, he was careful to pick only first-arriving P_g, P^*, and P_n phases. Secondary phases, such as P_g arriving after P_n, can often be identified, but for some events it is not clear whether secondary arrivals are head waves or possibly Moho reflections (P_mP, S_mP, and S_mS).

The second problem with regional work is understanding the relationship between origin time and velocity model estimation when multi-phase data are used to solve the joint problem. When solving the joint problem using only one regional phase, such as P_n, any travel time residuals due to differences between the velocity model beneath a network and the model from the source to the edge of the network will be compensated for in the origin time estimate. It is not clear what will happen to velocity and origin time estimates when secondary head wave arrivals are included in the problem. Hence, an important project before inverting primary and secondary regional arrivals would be to invert multi-phase, regional synthetic data to study the affects of combining arrival times generated with varying velocity-depth models.

12. References

Ake, J. P., and A. R. Sanford, New evidence for the existence and internal structure of a thin layer of magma at mid-crustal depths near Socorro, New Mexico, *Bull. Seismol. Soc. Am., 78,* 1335-1359, 1988.

Ake, J. P., An analysis of the May and July, 1983 Socorro Mountain earthquake swarms, *Geophysics Open-File Report 49,* N. M. Inst. of Mining and Technol., Socorro, New Mexico, 107 PP, 1986.

Aki, K., and W. H. Lee, Determination of three-dimensional velocity anomalies under a seismic array using first P arrival times from local earthquakes, 1, A homogeneous initial model, *J. Geophys. Res., 81,* 4381-4399, 1976.

Aldrich, M. J., C. E. Chapin, and A. W. Laughlin, Stress history and tectonic development of the Rio Grande rift, New Mexico, *J. Geophys. Res., 91,* 6199-6211, 1986.

Barroll, M. W., and M. R. Reiter, Analysis of the Socorro hydro-geothermal system; central New Mexico, *J. Geophys. Res., 95,* 21949-21963, 1990.

Braile, L. W., Inversion of crustal seismic refraction and reflection data, *J. Geophys. Res., 78,* 7738-7744, 1973.

Brocher, T. M., Geometry and physical properties of the Socorro, New Mexico, magma bodies, *J. Geophys. Res., 86,* 9420-9432, 1981.

Brown, L. D., C. E. Chapin, A. R. Sanford, S. Kaufman, and J. Oliver, Deep structure of the Rio Grande rift from seismic reflection profiling, *J. Geophys. Res., 85,* 4773-4800, 1980.

Brown, L. D., P. A. Krumhansl, C. E. Chapin, A.R. Sanford, F. A. Cook, S. Kaufman, J. Oliver, and F. S. Schilt, COCORP seismic reflection studies of the Rio Grande rift, in *Rio Grande Rift: Tectonics and Magmatism,* edited by R. E. Riecker, pp. 169-184, AGU, Washington, D.C., 1979.

Cape, C. D., S. McGeary, and G. A. Thompson, Cenozoic normal faulting and the shallow structure of the Rio Grande rift near Socorro, New Mexico, *Geol. Soc. Am. Bull., 94,* 3-14, 1983.

Caravella, F. J., A study of Poisson's ratio in the upper crust of the Socorro, New Mexico area, M. S. Indep. Study, 80 pp., N. M. Inst. of Mining and Technol., Socorro, 1976.

Carlson, D., A crustal structure study in the Socorro, New Mexico area using the time-term method, M. S. Indep. Study, 30 pp., N. M. Inst. of Mining and Technol., Socorro, 1983.

Carpenter, P. J., and D. J. Cash, Poisson's ratio in the Valles caldera and Rio Grande rift of northern New Mexico, *Bull. Seismol. Soc. Am., 78,* 1826-1829, 1988.

Carpenter, P. J., and A. R. Sanford, Apparent Q for upper crustal rocks of the central Rio Grande rift, *J. Geophys. Res., 90,* 8661-8674, 1985.

Chapin, C. E., R. M. Chamberlin, et al., Exploration framework of the Socorro geothermal area, New Mexico, *N. Mex. Geol. Soc. Spec. Pub. 7,* pp. 114-129, 1978.

Chapin, C. E., Evolution of the Rio Grande rift - a summary, *Rio Grande Rift: Tectonics and Magmatism,* edited by R. E. Riecker, pp. 1-5, AGU, Washington, D.C., 1979.

Chapin, C. E., Volcanism along the Socorro accomodation zone, Rio Grande rift, New Mexico, *Field Excursions to Volcanic Terranes in the Western United States, Volume 1: Southern Rocky Mountain Region,* edited by C. E. Chapin and J. Zidek, New Mexico Bureau of Mines and Mineral Resources, Mem. 46, pp. 46-57, 1989.

Chapman, D. S., Thermal gradients in the continental crust, *The Nature of the Lower Continental Crust,* edited by J. B. Dawson, D. A. Carswell, J. Hall, and K. H. Wedepohl, pp. 63-70, Geol. Soc. Am. Sp. Publ. 24.

Christiansen, N. I., Chapter 1: Seismic Velocities, *Handbook of Physical Properties of Rocks Volume II,* edited by R. S. Carmicheal, CRC Press Inc., Boca Raton, Florida, 1982.

Cordell, L., Regional geophysical setting of the Rio Grande rift, *Geol. Soc. Am. Bull., 89,* 1073-1090, 1978.

Crosson, R. S., Crustal structure modeling of earthquake data. 1. Simultaneous least squares estimation of hypocenter and velocity parameters, *J. Geophys. Res., 81,* 3036-3046, 1976.

Crosson, R. S., Crustal structure modeling of earthquake data. 2. Velocity structure of the Puget Sound region, Washington, *J. Geophys. Res., 81,* 3047-3054, 1976.

de Voogd, B., L. Serpa, and L. Brown, Crustal extension and magmatic processes: COCORP profiles from Death Valley and the Rio Grande rift, *Geol. Soc. Am. Bull., 100,* 1550-1567, 1988.

Dee, M., A crustal and *P*-wave velocity study of portions of southwest New Mexico and southeast Arizona using open pit mining explosions, M. S. Indep. Study, 30 pp., N. M. Inst. of Mining and Technol., Socorro, 1973.

Dobrin, M. B., *Introduction to Geophysical Prospecting,* 630 pp., McGraw-Hill, New York, 1976.

Eaton, G. P., A tectonic redefinition of the southern Rocky Mountains, *Tectonophsyics, 132,* 163-194, 1986.

Fender, J. J., A study of Poisson's ratio in the upper crust in the Socorro, New Mexico area, M. S. Indep. Study, 57 pp., N. M. Inst. of Mining and Technol., Socorro, 1978.

Gish, D. W., G. R. Keller, and M. L. Sbar, A refraction study of deep crustal structure in the Basin and Range: Colorado plateau of eastern Arizona, *J. Geophys. Res., 86,* 6029-6038, 1981.

Glazner, A. F., and W. Ussler III, Trapping of magma at midcrustal density discontinuities, *Geophys. Res. Let., 15* 673-675, 1988.

Gomberg, J. S., K. M. Shedlock, and S. T. Roecker, The effect of *S*-wave arrival times on the accuracy of hypocenter estimation, *Bull. Seismol. Soc. Am., 80,* 1605-1628, 1990.

Grant, F. S., and G. F. West, *Interpretation Theory in Applied Geophysics,* McGraw-Hill Book Company, New York, 584 pp., 1965.

Gridley, J., Microearthquake reflection phases of a mid-crustal magma body in the Socorro area, New Mexico, M. S. Indep. Study, 25 pp., N. M. Inst. of Mining and Technol., Socorro, 1989.

Hawley, B. W., G. Zandt, and R. B. Smith, Simultaneous inversion for hypocenters and lateral velocity variations: an iterative solution with a layered model, *J. Geophys. Res., 86,* 7073-7086, 1981.

Holbrook, S. W., D. Gajewski, A. Krammer, and C. Prodehl, An interpretation of wide-angle compressional and shear wave data in southwest Germany: Poisson's ratio and petrological implications, *J. Geophys. Res., 93,* 12081-12106, 1988.

Jackson, D. D., Interpretation of inaccurate, insufficient, and inconsistent data, *Geophys. J. Roy. Astron. Soc., 28,* 97-109, 1972.

Jaksha, L. H., and A. R. Sanford, Earthquakes near Albuquerque, New Mexico, 1976-1981, *J. Geophys. Res., 91,* 6293-6303, 1986.

Jaksha, L. H. and D. H. Evans, Reconnaissance seismic refraction-reflection surveys in northwestern New Mexico, *Bull. Seismol. Soc. Am., 74,* 1263-1274, 1984.

Jaksha, L. H., Reconnaissance seismic refraction-reflection surveys in southwestern New Mexico, *Geol. Soc. Am. Bull., 93,* 1030-1037, 1982.

Keller, G. R., L. W. Braile, and J. W. Schlue, Regional crustal structure of the Rio Grande rift from surface wave dispersion measurements, *Rio Grande Rift: Tectonics and Magmatism,* edited by R. E. Riecker, pp. 115-126, AGU,

Washington, D.C., 1979.

King, K. M., Investigation of the seismogenic zone in the vicinity of Socorro, New Mexico, from an analysis of focal depth distributions, M. S. Indep. Study, 124 pp., N. M. Inst. of Mining and Technol., Socorro, 1986.

Kreyszig, D., *Advanced Engineering Mathematics,* John Wiley & Sons, New York, 1979.

Lanczos, C., *Linear Differential Operators,* D. Van Nostrand, Princeton, N. J., 1961.

Larsen, S., R. Reilinger, and L. Brown, Evidence of ongoing crustal deformation related to magmatic activity near Socorro, New Mexico, *J. Geophys. Res., 91,* 6283-6292, 1986.

Lee, W. H. K., and S. W. Stewart, *Principles and Applications of Microearthquake Networks,* Advances in Geophysics, Supplement 2, edited by B. Saltzman, 293 pp., Academic Press, New York, 1981.

Lee, W. H. K., and J. C. Lahr, HYPO71 (Revised): A computer program for determining hypocenter, magnitude, and first motion pattern of local earthquakes, U.S. Geological Survey Open-File Report 75-311, 1975.

Lister, J. R., and R. C. Kerr, Fluid-mechanical models of crack propagation and their application to magma-transport in dykes, *J. Geophys. Res., 96,* in press, 1991.

Mysen, B. O., Chapter 11: Melting Curves of Rocks and Viscosity of Rock-forming Minerals, *Physical Properties of Rocks and Minerals, Volume II-2,* edited by Y. S. Toultoukian,W. R. Judd, and R. F. Roy, McGraw-Hill., New York, 1981.

Murdock, J. N. and L. H. Jaksha, The *P* wave velocity of the uppermost mantle of the Rio Grande rift region of north central New Mexico, *J. Geophys. Res., 86,* 7055-7063, 1981.

Olsen, K. H., G. R. Keller, and J. N. Stewart, Crustal structure along the Rio Grande rift from seismic refraction profiles, *Rio Grande Rift: Tectonics and*

Magmatism, edited by R. E. Riecker, pp. 127-143, AGU, Washington, D. C., 1979.

Osborn, G. R., Geologic map of Socorro County, New Mexico Bureau of Mines and Geology, 1984.

Ouchi, S., Effects of uplift on the Rio Grande over the Socorro magma body, New Mexico, *Field Conf. Guideb. N. M. Geol. Soc., 34,* 54-56, 1983.

Pavlis, G. L., Progressive inversion, Ph.D. dissertation, 295 pp., U. of Washington, 1982.

Press, W. H., B. P. Flannery, S. A. Teukolsky, and W. T. Vetterling, *Numerical Recipes, The Art of Scientific Computing,* Cambridge University Press, Cambridge, 1986.

Pujol, J., Comments on the joint determination of hypocenters and station corrections, *Bull. Seismol. Soc. Am., 78,* 1179-1189, 1988.

Reid, H. F., Remarkable earthquakes in central New Mexico in 1906 and 1907, *Bull. Seismol. Soc. Am., 1,* 10-16, 1911.

Reiter, M. J., B. R. Eggleston, B. R. Broadwell, and J. Minier, Estimates of terrestrial heat flow from deep petroleum tests along the Rio Grande rift in central and southern New Mexico, *J. Geophys. Res., 91,* 6225-6245, 1986.

Rinehart, E. J., and A. R. Sanford, Upper crustal structure of the Rio Grande rift near Socorro, New Mexico, from inversion of microearthquake S-wave reflections, *Bull. Seismol. Soc. Am., 71,* 437-450, 1981.

Rinehart, E. J., A. R. Sanford, and R. M. Ward, Geographic extent and shape of an extensive magma body at mid-crustal depths in the Rio Grande rift near Socorro, New Mexico, in *Rio Grande Rift: Tectonics and Magmatism,* edited by R. E. Riecker, pp. 237-251, AGU, Washington, D. C., 1979.

Roller, J. C., Crustal structure in the eastern Colorado Plateau province from seismic refraction measurements, *Bull. Seismol. Soc. Am., 55,* 107-119, 1965.

Sakdejayont, K., A study on Poisson's ratio and V_p/V_s ratio in the Rio Grande rift, M. S. Indep. Study, 28 pp., N. M. Inst. of Mining and Technol., Socorro, 1974.

Sanford, A. R., L. H. Jaksha, and D. J. Cash, Seismicity of the Rio Grande rift, *Neotectonics of North America,* edited by D. B. Slemmons, E. R. Engdahl, D. Blackwell, and D. Schwartz, Geol. Soc. Amer., Boulder, Colorado, 1990.

Sanford, A. R. and P. Einarsson, Magma chambers in rifts, *Continental and Oceanic Rifts, Geodynamics Series, Vol. 8,* pp. 147-168, AGU, Washington, D. C., 1982.

Sanford, A. R., K. H. Olsen, and L. H. Jaksha, Earthquakes in New Mexico, 1849-1977, New Mexico Bureau of Mines and Mineral Resources Circular *171,* 20 pp., 1981.

Sanford, A. R., K. H. Olsen, and L. H. Jaksha, Seismicity of the Rio Grande rift, in *Rio Grande Rift: Tectonics and Magmatism,* edited by R. E. Riecker, pp. 237-251, AGU, Washington, D. C., 1979.

Sanford, A. R., R. P. Mott, P. J. Shuleski, E. J. Rinehart, F. J. Caravella, R. M. Ward, and T. C. Wallace, Geophysical evidence for a magma body in the vicinity of Socorro, New Mexico, *The Earth's Crust: Its Nature and Physical Properties, Geophys. Monogr. Ser., Vol 20,* edited by J. G. Heacodk, pp. 385-404, AGU, Washington, D. C., 1977.

Sanford, A. R., O. Alptekin, and T. R. Topozada, Use of reflection phases on microearthquake seismograms to map an unusual discontinuity beneath the Rio Grande rift, *Bull. Seismol. Soc. Am., 63,* 2021-2034, 1973.

Sanford, A. R., and L. T. Long, Microearthquake crustal reflections, Socorro, New Mexico, *Bull. Seismol. Soc. Am., 55,* 579-586, 1965.

Sanford, A. R., and C. R. Holmes, Note on the July 1960 earthquakes in central New Mexico, *Bull. Seismol. Soc. Am., 51,* 311-314, 1961.

Schlue, J. W., P. J. Singer, and C. L. Edwards, Shear wave structure of the upper crust of the Albuquerque-Belen basin from Rayleigh wave phase velocities, *J. Geophys. Res., 91,* 6277-6281, 1986.

Sibson, R. H., Roughness at the base of the seismogenic zone: contributing factors, *J. Geophys. Res., 89,* 5791-5799, 1984.

Singer, P. J., Crustal structure in the Socorro area of the Rio Grande rift from time-term analysis, Ph.D. dissertation, 206 pp., N. M. Inst. of Mining and Technol., 1989.

Sinno, Y. A., P. H. Dagget, G. R. Keller, P. Morgan, and S. H. Harder, Crustal structure of the southern Rio Grande rift from seismic refraction profiling, *J. Geophys. Res., 91,* 6143-6156, 1986.

Sinno, Y. A., and G. R. Keller, Rayleigh wave dispersion study between El Paso, Texas and Albuquerque, New Mexico, *J. Geophys. Res., 91,* 6168-6174, 1986.

Spencer, J. W., and A. M. Nur, the effects of pressure, temperature, and pore water on velocities in Westerly granite, *J. Geophys. Res., 81,* 899-904, 1976.

Stewart, S. W. and L. C. Pakiser, Crustal structure in the eastern New Mexico interpreted from the GNOME explosion, *Bull. Seismol. Soc. Am., 52,* 1017-1030, 1962.

Stuart, W. D., and M. J. S. Johnson, Intrusive origin of the Matsushiro earthquake swarm, *Geology, 3,* 63-67, 1975.

Toppozada, T. R. and A. R. Sanford, Crustal structure in central New Mexico interpreted from the Gasbuggy explosion, *Bull. Seismol. Soc. Am., 66,* 877-886, 1976.

Ward, R. M., J. W. Schlue, and A. R. Sanford, Three-dimensional velocity anomalies in the upper crust near Socorro, New Mexico, *Geophys. Res. Letters, 8,* 553-556, 1981.

Ward, R. M., Determination of three-dimensional velocity anomalies within the upper crust in the vicinity of Socorro, New Mexico, using P arrival times from

local mircroearthquakes, Ph.D. dissertation, 146 pp., N. M. Inst. of Mining and Technol., 1980.

Appendix A - Program User's Guide

Introduction

This appendix describes programs written to analyze or facilitate the analysis of arrival time data. The programs fall under four categories. First is the hypocenter-velocity model inversion program, *seismos*, and its associated programs (Table A1). Next are some useful programs for creating data files in proper formats and transforming existing files into different formats (Table A2). The plotting programs (Table A3) compose the third category. They use *Grafix* Fortran subroutines, a New Mexico Tech in house plotting package similar to *Calcomp* software. Finally, there are synthetic data generating programs (Table A4). Some of the formatting programs were written by Rod Flores and James Lakings (note the credits at the bottom of Table A2). All other programs were written by Hans Hartse.

The programs are written in Fortran 77 and will compile and run on Sun's *Unix* operating systems. I have not attempted to compile the programs on any other systems, but I have written them so they should be fairly machine and operating system independent. When output is written to the screen it is through unit 6, and when input is read from the screen it is through unit 5. If using an operating system other than *Unix*, it may be necessary to change these unit numbers. At the end of this appendix I briefly describe how to compile the programs on a *Unix* system.

Programs Related to Hypocenter and Velocity Model Inversion

Overview. The main program for earthquake location and velocity model estimation is known as *seismos* (Table A1). This program can use direct, reflected, and critically refracted (head wave) arrival times to solve for individual earthquake and explosion locations, or it can simultaneously solve for event hypocenters and a one-dimensional velocity model. Hence, the program can find event latitude, longitude, focal depth, and origin time, and it can solve for compressional velocities, layer depths, Poisson's ratio within each layer, and station corrections. The specific arrival time phases the program can use are: direct P and S; mid-crustal reflections

TABLE A1. Programs Used in Earthquake Location

Program	Purpose	Files Read	Files Written
seismos	Earthquake location and velocity model estimation using inverse methods.	velmod.dat stacrd.dat jparam.dat picfil.dat newloc.dat	refloc.dat newloc.dat eigen.dat
no_ref	Remove all reflected phases from a pick file.	*	no_ref.dat
no_direct	Remove all direct phases from a pick file.	*	no_direct.dat
no_magma	Remove all magma body reflections from a pick file.	*	no_magma.dat
no_moho	Remove all moho reflections from a pick file.	*	no_moho.dat
no_phase	Remove any user specified phase from a pick file.	*	no_phase.dat
no_statn	Remove any user specified station from a pick file.	*	no_statn.dat
ev_stats	Compile general statistics on location solutions.	newloc.dat picfil.dat picfil.dat	stats.dat

* means the user is to provide the name of a file in *picfil.dat* format.

TABLE A2. Useful Input and Formatting Programs

Program	Purpose	Files Read	Files Written
velmod	Helps user develop a velocity model.		velmod.dat
chvmod	Helps user to modify a velocity model.	velmod.dat	velmod.dat
hansin[a]	Prompts user in constructing a pick file readable by satan.		+
hyp2hans[a]	Changes a HYPO71 pick file into a satan pick file	* stnid.new	+
hans2hyp[a]	Changes a satan pick file into a HYPO71 pick file	+ stnid.new	*
distance	Changes a station location file from lat-lon coords into km coords.	sta.dat pit.dat %	coords.dat
chopshop[b]	Constrains a location file by applying windows for time, epicenter, and errors	@ constpar.dat	@

* file must be (or will end up being) in the format of a *HYPO71* pick file.

+ file must be (or will end up being) in *picfil.dat* format.

% file must be a list of station names.

@ file must be (or will end up being) in *HREGQK* format.

[a] Program written by Rod Flores.

[b] Program written by James Lakings.

TABLE A3. Plotting Programs

Program	Purpose	Files Read	Files Written
headplt	Change newloc.dat into a file readable by NMT plotting programs.	newloc.dat picfil.dat	HREGQK refpnt.dat
epiplot	Plot epicenters or reflection points.	pltpar.dat * refpnt.dat stacrd.dat velmoc.dat optional files@	map.plt
dep_plot	Plot focal depths or origin times with error bars.	newloc.dat synloc.dat	depth.plt
refvsx	Plot traveltime versus offset distance for magma body reflections.	* refpnt.dat stacrd.dat velmod.dat	tvd.plt
curvfnd	Find theoretical traveltimes for all phases at multiple offset distances	velmod.dat	tdpairs.dat
timdis	Plot theoretical traveltime versus offset distance for all phases	+	all.plt
phsminp	Plot theorectical phase-minus-P versus S-minus-P times	+	phs.plt
xzfind	Find focal depth-reflector depth pairs for S_cS and S_cP		xzfind.dat hzcurv.dat
hzcurv	Plot focal depth-reflector depth pairs for S_cS and S_cP	hzcurv.dat	hzcr.plt

* means the user is to provide the name of a file in *HREGQK* format.

@ the optional files provide geographic information such as city loctions, COCORP line locations, and magma body outlines.

+ means the user is to provide the name of a file in *tdpairs.dat* format.

TABLE A4. Programs Used to Generate Synthetic Data

Program	Purpose	Files Read	Files Written
syngen	Generate multiple events of synthetic direct and reflected data.	velmod.dat stacrd.dat station.list	synloc.dat synpic.dat
synrfr	Generate a single event of synthetic head wave and direct data.	velmod.dat stacrd.dat sta_phs.list	picfil.dat
add_nois	Add random noise to a synthetic pick file.	*	add_nois.dat
no_rannois	Remove random noise from a synthetic pick file.	*	no_rannois.dat

* means the user is to provide the name of a file which is in *picfil.dat* format.

S_zP, S_zS, P_zP, and P_zS; head wave arrivals P_g, S_g, P^*, S^*, P_n, and S_n; Moho reflections S_mP, S_mS, P_mP, and P_mS.

Seismos is based on generalized least squares (GLS) theory. GLS essentially involves decomposing a matrix of partial derivatives (changes in arrival times with respect to model parameters) into eigenvalues and associated eigenvectors. The inverse of the matrix is found using eigenvalues which are greater than 0. Next, using the inverse of the matrix, new parameter estimates are then found. The process is repeated using the new estimates until the parameter values no longer change. The most important parts of my inverse program are the ray tracing algorithms which solve the forward problem and the inversion algorithm which decomposes the derivative matrix into eigenvalues and eigenvectors. The inversion algorithm uses IMSL subroutines. Because IMSL is not provided on all systems, I have made available the subroutines *tred2* (reduce a real-symmetric matrix to tridiagonal form) and *tqli* (find eigenvalues and eigenvectors of a real-tridiagonal matrix). The subroutines are presented in *Numerical Recipes* [*Press et al.*, 1986]. For more details on GLS theory, and how it is applied to the joint earthquake location-velocity problem, users should refer to the **Method** section.

Event, Interface, and Phase Codes. *Seismos* uses numerical codes to identify the type of event to be located, each interface used in the velocity model, and each arrival time phase composing the data set (Tables A5, A6, and A7). An event code is specified on the header line of an event pick file, interface codes are specified with the velocity model, and phase codes are specified with every time entered in a pick file. The details of these data files are presented below. The codes are necessary to ensure that theoretical arrival times are derived from appropriate ray paths while using correct velocities. For example, proper phase codes for mid-crustal reflections (8, 9, and 10) and the proper code for the mid-crustal reflector (9) will instruct *seismos* to find theoretical times and derivatives for the phases S_zS, P_zP, and S_zP.

TABLE A5. Event Codes	
Event Type	Code Number
Local Earthquake	1
Regional Earthquake	2
Local Explosion	3
Regional Explosion	4

TABLE A6. Layer Codes	
Layer	Code Number
Phanerozoic-Precambrian boundary (P_g, S_g)	3
Mid-crust (S_zS, S_zP, P_zP, P_zS, P^*, and S^*)	9
Moho (S_mS, S_mP, P_mP, P_mS, P_n, and S_n)	12
Half-space	13
Any other layer	1

TABLE A7. Phase Codes	
Phase Type	Code Number
P	0
S	1
P_g	2
S_g	3
P^*	4
S^*	5
P_n	6
S_n	7
S_zS	8
P_zP	9
S_zP	10
P_zS	11
S_mS	12
P_mP	13
S_mP	14
P_mS	15
DUR	31

In most cases the program will not make its own decisions about correct phase identification based on relative arrival times or the velocity model. For instance, if a user picks a mid-crustal reflection but assigns a Moho phase code to the pick, then *seismos* will always treat that pick as a Moho arrival. The only exception is for the case of head waves. The program does check for critical distance and a velocity increase at a refracting interface. If a source-to-receiver distance for a head wave phase is less than the critical distance, or if velocity does not increase at the assigned layer, then the program will treat the phase as a direct arrival.

Input Files. There are four input data files which are necessary to run *seismos.* These are *velmod.dat* (an input velocity model), *stacrd.dat* (station coordinates and associated station corrections), *jparam.dat* (instructions which control the execution of *seismos),* and *picfil.dat* (the arrival times used by the program). The program does not ask for these files by name, rather it assumes the files exist and will attempt to read them upon execution. Below are sample input files.

Velmod.dat (Figure A1) can be created with the program *velmod,* modified with *chvmod* (see Table A2), or created and edited with any screen editor. The first line of *velmod.dat* (format: i2) specifies the number of layers in the model. The next three lines (format: f8.3,1x,f8.3,1x,f8.3,1x,f5.1,i3) list the depth to a layer interface, the velocity above the interface, Poisson's ratio above the interface, the dip of the interface, and the layer code. Although dip is listed as a variable in *velmod.dat,* it should always set to 0.0 as the ray tracing programs presently used by *seismos* will not trace through dipping interfaces. The final line (format: f8.3,1x,f8.3,1x,i3) lists the velocity, Poisson's ratio, and the layer code of the half-space. Thus, the model shown consists of three layers and a half-space (see Figure A2). The mid-crust (at 18.75 km) has layer code 9 and the Moho (at 33.5 km) has layer code 12. A Phanerozoic layer is not specified for this model, and, hence, the Phanerozoic-Precambrian boundary (layer code 3) is not included in the model. The arrays used by these programs are presently dimensioned so a maximum of 7 layers can describe a velocity model.

```
3
 10.000     5.946     0.256    0.0  1
 18.748     5.804     0.228    0.0  9
 33.500     6.500     0.250    0.0 12
  8.100     0.250 13
```

Fig. A1. Sample velocity model input file *velmod.dat*. The "3" at the top of the file denotes the number of layers in the model, and columns (from left to right) denote layer depth, P velocity, Poisson's ratio, layer dip, and the layer code.

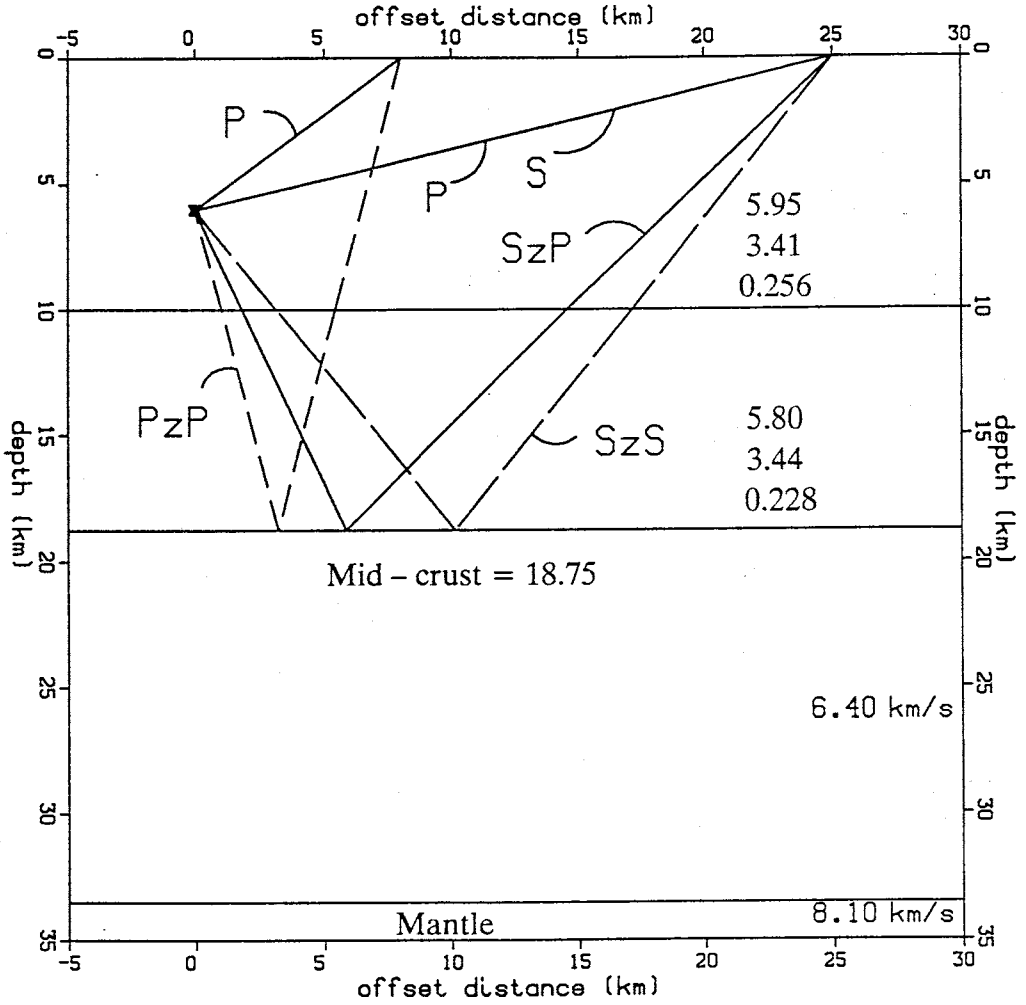

Fig. A2. Crustal cross section of the velocity model defined in Figure A1.

The station locations (*stacrd.dat*) used by *seismos* are defined in x and y coordinates. The station coordinates are in km relative to a grid center with coordinates (500.0,500.0). The x is the east-west direction and the y is the north-south direction. A file of station locations given in latitude and longitude can be transformed into *stacrd.dat* format (Figure A3) using the program *distance* (Table A2). Each line of *stacrd.dat* consists of a station name abbreviation, x, y, and a station correction (format: a4,2f8.2,f7.3).

The control file, *jparam.dat*, (Figure A4) provides instructions to *seismos*. Table A8 describes the meanings and formats for each line of *jparam.dat*. The first five headings: *hypo, vel, dep, pois*, and *sta* designate which parameters are to be treated as unknowns and which parameters are to be held fixed during an inversion. Switches are set at either 1 or 0 for "yes, treat this parameter as an unknown", or "no, leave this parameter fixed". For the case shown, only the hypocenter parameters are to be treated as unknowns. Hence, the instructions shown will cause *seismos* to operate as a single-event location program. If model parameters are set to 1, then *seismos* will operate as a joint hypocenter-velocity model program.

The numbers next to each switch are initial estimates on parameter uncertainty. The uncertainties are in km for distances and depths, sec for time, and km s^{-1} for velocity. These uncertainty estimates are necessary for the inversion. They can be adjusted as required by the particular problem.

Below the parameter switches are values which provide other controls and instructions. Before the switch for *jrpevl* can be set to 1, the file *newloc.dat* must be created by setting the switch for *jwnevl* to 1 and then running *seismos*. The variable *dlxcut* defines convergence. From one iteration to the next, if every parameter being estimated changes by more than *dlxcut*, then the program will continue iterating. If every parameter changes by less than *dlxcut*, then convergence has occurred and the program will quit iterating. Thus, when *dlxcut* is set at 0.0049, if x, y, and focal depth change by less than 0.0049 km (4.9 m), and if origin time changes by less than 0.0049 sec (4.9 msec), then the program will stop iterating.

```
BAR    529.11   507.96 -0.023
BDO    502.87   547.17  0.672
BMT    470.81   522.72  0.165
CAR    519.31   486.94  0.005
FTS    512.59   512.88  0.030
JHLS   509.18   508.41  0.080
LAZ    481.96   536.80 -0.004
LEM    497.17   510.57 -0.080
LJY    504.40   529.54  0.443
LPM    528.56   526.34 -0.187
MAG    473.38   510.24 -0.016
MLM    481.48   582.53 -0.204
SB     478.09   489.46  0.211
SH     515.06   509.85 -0.090
SMC    492.99   467.67  0.164
SNM    500.00   500.00  0.009
WTX    499.79   500.22 -0.080
YRD    512.98   510.13 -0.040
```

Fig. A3. Sample station coordinate input file *stacrd.dat*. The columns from left to right are station abbreviations, X coordinates (km), Y coordinates (km), and station corrections.

```
hypo
1  5.10
1  5.10
1  3.10
1  0.50
vel
0  0.10
0  0.10
0  0.10
0  0.50
dep
0  2.50
0  1.00
0  1.50
pois
0  0.10
0  0.10
0  0.10
0  0.10
sta
0  0.05
maxitr   07
jrpevl    0
jwnevl    1
jstats    0
rlitcut  0.101
jtoss    000
wtfc     0.075
dlxcut   0.0049
offmax   150.0
depmax    33.0
depmin    00.2
depstrt   07.5
xnear     40.0
xfactor   0.50
```

Fig. A4. Sample earthquake location controller file *jparam.dat*. See Table A8 for an explanation.

TABLE A8. The Conroller File *jparam.dat*

Entry	Meaning	Format
hypo	start listing hypocenter switches	(a4)
1 5.10	find longitude - initial error 5.10 km	(i1,1x,f5.2)
1 5.10	find latitude - initial error 5.10 km	(i1,1x,f5.2)
1 3.10	find focal depth - initial error 3.10 km	(i1,1x,f5.2)
1 0.50	find origin time - initial error 0.50 sec	(i1,1x,f5.2)
vel	start listing velocity switches	(a4)
0 0.10	do not find velocity 1 - initial error 0.10 km s^{-1}	(i1,1x,f5.2)
0 0.10	do not find velocity 2 - initial error 0.10 km s^{-1}	(i1,1x,f5.2)
0 0.10	do not find velocity 3 - initial error 0.10 km s^{-1}	(i1,1x,f5.2)
0 0.50	do not find velocity 4 - initial error 0.50 km s^{-1}	(i1,1x,f5.2)
dep	start listing depth switches	(a4)
0 2.50	do not find depth 1 - initial error 2.50 km	(i1,1x,f5.2)
0 1.00	do not find depth 2 - initial error 1.00 km	(i1,1x,f5.2)
0 1.50	do not find depth 3 - initial error 1.50 km	(i1,1x,f5.2)
pois	start listing Poisson's ratio switches	(a4)
0 0.10	do not find Poisson 1 - initial error 0.10 km	(i1,1x,f5.2)
0 0.10	do not find Poisson 2 - initial error 0.10 km	(i1,1x,f5.2)
0 0.10	do not find Poisson 3 - initial error 0.10 km	(i1,1x,f5.2)
0 0.10	do not find Poisson 4 - initial error 0.10 km	(i1,1x,f5.2)
sta	list station correction switch	(a4)
0 0.05	do not find station corrections - initial error 0.05 sec	(i1,1x,f5.2)
maxitr 07	maximum of 7 iterations allowed	(a8,1x,i2)
jrpevl 0	do not read previous event locations	(a8,1x,i2)
jwnevl 1	write new event locations into file *newloc.dat*	(a8,1x,i2)
jstats 1	write residual statistics onto *refloc.dat*	(a8,1x,i2)
rlitcut 0.101	control on eigenvalues kept in the solution	(a8,1x,f5.3)
jtoss 000	remove exactly 000 eigenvalues from each iteration	(a8,1x,i3)
wtfc 0.075	time in seconds which corresponds to a "0" weight	(a8,1x,f5.3)
dlxcut 0.0049	control on when to stop iterating	(a8,1x,f6.4)
offmax 150.0	maximum station-to-event distance allowed	(a8,1x,f5.1)
depmax 33.0	maximum focal depth allowed	(a8,1x,f5.1)
depmin 00.2	minimum focal depth allowed	(a8,1x,f5.1)
depstrt 00.2	starting focal depth estimate	(a8,1x,f5.1)
xnear 40.0	maximum range (km) without distance weighting	(a8,1x,f5.1)
xfactor 0.50	distance weighting - time in sec per 100 km	(a8,1x,f5.2)

The variable *rlitcut* controls the number of eigenvalues kept in a solution. It can be set at values between 0.0 and 1.0. Essentially, this variable controls the amount of damping which is applied to an inversion. If *rlitcut* is set near 0.0, then no damping will occur and all parameters will be uniquely resolved. When the data used by the inversion can not resolve all parameters, convergence may not be possible using only slight damping. It may then be necessary to increase *rlitcut* to greater than 0.5. The *jtoss* option allows the user to remove a fixed number of eigenvalues from every iteration of *seismos*. When *jtoss* is greater than 000 it overrides *rlitcut*, and the number of eigenvalues removed from each iteration will always equal the value specified with *jtoss*, even if damping values exceed what has been specified with *rlitcut*. It is important to understand that increased damping means the final solution produced by *seismos* will be dependent on the starting model.

Picfil.dat consists of a single header line followed by a separate line for each arrival time (Figure A5). This means there is a new data line for each phase, even if more than one phase has been picked at a particular station. When many events are to be located at once, many separate pick files can be combined into one large *picfil.dat*. Presently, the fastest way to do this is with the *Unix* command "cat".

Listed in order on the header line are: number of picks, year, month, day, hour, minute of origin time, seconds of origin time, and the event code (format: i2,1x,i4,1x,i2,1x,i2,1x,i2,1x,i2,1x,f5.2,1x,i1). The seconds need only be approximated as *seismos* will automatically estimate origin time once the program is started. Each data line specifies a phase code, station, pick quality, arrival time minute, and arrival time second (format (i2,1x,a4,1x,i1,1x,i2,1x,f5.2). The only exception is for a phase code of 31, which specifies a signal duration (for magnitude estimation). The minutes and seconds entries for a duration line are the signal duration time in minutes and seconds. This example is of a small magnitude event, and, hence, all minute durations are 0.

Pick qualities (or weights) can vary from 0 (best quality) to 9 (worst quality). A 0 weight should only be assigned to a first-arrival pick when the first motion is

```
23 1982  9 19 22 25 35.00 1
 0 BAR   1 25 43.10
 1 BAR   3 25 48.70
31 BAR   0  0 30.00
 0 BMT   1 25 41.80
 1 BMT   2 25 46.10
10 BMT   2 25 44.40
 8 BMT   4 25 48.40
31 BMT   0  0 19.00
 0 CAR   1 25 41.35
 1 CAR   3 25 45.20
31 CAR   0  0 50.00
 1 LPM   3 25 50.30
31 LPM   0  0 21.00
 0 SB    2 25 38.60
 1 SB    3 25 40.90
31 SB    0  0 20.00
 0 SMC   1 25 41.00
31 SMC   0  0 47.00
 0 WTX   1 25 38.10
 1 WTX   2 25 40.10
 8 WTX   3 25 45.00
10 WTX   3 25 42.50
31 WTX   0  0 27.00
```

Fig. A5. Sample earthquake location arrival time input file *picfil.dat*. See text for details.

clear. The pick error (in seconds) which corresponds to a weight of 0 can be set in *jparam.dat* using the variable *wtfc*. For the example shown in Figure A4, *wtfc* is set at 0.075 sec. This means a weight of 0 will correspond to a pick error of 0.075 sec, a weight of 1 will correspond to an error of 0.150 sec, and a weight of 9 will correspond to an error of 0.75 sec.

Sample Program Run. Below is a sample program run (Figure A6) using the input files which have been listed above. For this example Roman characters are written to the screen by the computer and underlined characters are entered by the user. When only a single event is to be located, as in this case, *seismos* will ask if an initial hypocenter is to be entered by the user. If the user desires to specify an initial hypocenter, then a prompt will appear for x and y coordinates and a focal depth. Otherwise, the initial location will be estimated by the program using the coordinates of the station which recorded the earliest P arrival time, and the initial focal depth will be the depth specified in *jparam.dat*. Initial origin time is always estimated within the program by using $S-P$ intervals. If S times are not available, then the origin time from the pick file header will be used.

For the example shown convergence occurred in four iterations. For each iteration parameters were estimated when using 4 eigenvalues (this is the case where all possible eigenvalues are kept in the solution), and then parameters were estimated while retaining 3 eigenvalues. The *rlitcut* set at 0.101 caused *seismos* to reject the parameter estimates found for each three-eigenvalue case, and start the next iteration using the parameters estimated from the four-eigenvalue case.

Solution files. There are three files which are written by *seismos*: *refloc.dat*, *newloc.dat*, and *eigen.dat*. *Refloc.dat* is a detailed solution file, providing information on every iteration. *Newloc.dat* contains summary information about locations which is useful for plotting. It will be written only if the switch *jwnevl* in the file *jparam.dat* is set to 1. *Eigen.dat* contains details on the GLS process.

Refloc.dat always consists of at least four pages; a title page with information about instructions which had been specified in *jparam.dat*, a page specifying the

```
sirius% seismos
 printout title: Sample run - single event
 *** working on event:   1

 to estimate hypocenter manually type "1": 2
 there are   16 data and   4 parameters
 iteration  1 considering the case of   4 eigenvalues . . .
 iteration  1 considering the case of   3 eigenvalues . . .
 there are   16 data and   4 parameters
 iteration  2 considering the case of   4 eigenvalues . . .
 iteration  2 considering the case of   3 eigenvalues . . .
 there are   16 data and   4 parameters
 iteration  3 considering the case of   4 eigenvalues . . .
 iteration  3 considering the case of   3 eigenvalues . . .
 there are   16 data and   4 parameters
 iteration  4 considering the case of   4 eigenvalues . . .
```

Fig. A6. Sample run (what the user sees on the terminal screen) of *seismos*, the earthquake location program. Underlined characters are entered by the user.

velocity model used, a page specifying station corrections used, and a separate page of information for every event located. The first three pages have been condensed into Figure A7. The location information is shown in Figure A8. The location information can be broken down into three categories; (1) general event and iteration information, (2) station and phase information, and (3) event location information. Table A9 explains the abbreviations found in Figure A8. If the user has requested summary residual information (by setting the switch for *wrstats* found in *jparam.dat* to 1), then additional information will be included on the end of *refloc.dat.*

Dimensioning. Array dimensioning is controlled with Fortran *parameter* statements. When using *seismos* only as a location program arrays need not be dimensioned as large as is required for the joint problem. There are three Fortran files where dimensioning is critical. In *seismos.f* the values for *mdinv* (maximum number of data to be inverted) can be set at the maximum number of picks expected for a single event when only hypocenter parameters are to be found. The value of *mdata* must always equal the total number of picks from all events. The value for *mpar* (the number of parameters being found for a single event) can be set at 4. If the joint problem is to be solved, then *mdinv* must equal *mdata*, the total number of arrival times used in the problem. The value for *mpar* must also be increased to equal the total number of unknowns being found. The value for *mevnts* must always be set to the total number of events listed in a pick file.

The subroutine *sorta.f* must always have *mpar* set to equal the value of *mpar* in *seismos.* The final file, *eigen.f*, must have its value for *mdata* set to be exactly equal to the value of *mdinv* found in *seismos*, and its value for *mpar* must be equal to the *mpar* in *seismos.*

Other Location-Related Programs. The other programs listed in Table A1 can sometimes be useful when locating earthquakes. The "no_*" programs can be used to remove phases and stations from a pick file. This helps avoid screen editing pick files when studying such things as the influence of a particular station or phase on a

Page 1

output from program SEISMOS Seismic Arrival Time ANalysis:

day and time of this run: Mon Jun 3 20:21:55 1991

Sample run - single event

some program parameters from jparam.dat:

maximum number of possible iterations: 7

read previous locations: 0, write new locations: 1 write residual statistics: 1 [1=yes, 0=no]

cutoff criteria for small r: 0.101, cutoff criteria for delta x: 0.0049

data weight factor: 0.075

ray trace constraints:
max offset: 150.0, max depth: 33.0, min depth: 0.2

starting depth of focus estimate: 7.5

xnear: 40.0, xfactor: 0.50 sec per 100 km

Page 2

initial depth-velocity model:

depths:	10.00	18.75	33.50	
velocities:	5.95	5.80	6.50	8.10
dips:	0.00	0.00	0.00	
poisson's ratio:	0.256	0.228	0.250	0.250

this run holds velocity-depth model constant

Page 3

intitial station corrections:

BAR	-0.023
BMT	0.165
CAR	0.005
LPM	-0.187
SB	0.211
SMC	0.164
WTX	-0.080

station corrections held constant on this run

Fig. A7. Sample earthquake location output file *refloc.dat*, pages 1 to 3.

Page 4

general iteration results for event 1:

itr	R	RMS
1	2.067	0.435
2	0.820	0.217
3	0.819	0.218
4	0.819	0.218

year	month	day	hour	minute
1982	9	19	22	25

number of stations: 7 total number of picks: 16 number of reflections: 4

starting hypocenter estimate: x= 496.79 y= 503.22 h= 7.50 orig=35.75

itr	x	adj	y	adj	h	adj	orig	adj	rms
1	489.13	-7.66	495.77	-7.45	10.18	2.68	36.18	0.43	0.43
2	488.95	-0.19	495.71	-0.06	9.21	-0.96	35.83	-0.35	0.22
3	488.95	0.01	495.69	-0.02	9.21	-0.01	35.82	-0.01	0.22
4	488.95	0.00	495.69	0.00	9.21	0.00	35.82	0.00	0.22

sta	phs	qual	wt	delta	azm	ain	obs-arv	obs-trv	theo-trv	resid	sta-cor
WTX	p	1	0.21	11.7	67	52	25 38.10	2.28	2.51	-0.15	-0.08
WTX	s	2	0.24	11.7	67		25 40.10	4.28	4.38	0.03	-0.14
WTX	szs	3	0.24	11.7	67		25 45.00	9.18	8.93	0.38	-0.14
WTX	szp	3	0.25	11.7	67		25 42.50	6.68	6.42	0.33	-0.08
SB	p	2	0.22	12.5	240	54	25 38.60	2.78	2.61	-0.05	0.21
SB	s	3	0.27	12.5	240		25 40.90	5.08	4.56	0.14	0.37
SMC	p	1	0.52	28.3	172	72	25 41.00	5.18	5.01	0.01	0.16
CAR	p	1	0.23	31.6	106	74	25 41.35	5.53	5.53	-0.01	0.00
CAR	s	3	0.13	31.6	106		25 45.20	9.38	9.66	-0.30	0.01
BMT	p	1	0.36	32.6	326	74	25 41.80	5.98	5.69	0.12	0.17
BMT	s	2	0.38	32.6	326		25 46.10	10.28	9.94	0.05	0.29
BMT	szp	2	0.39	32.6	326		25 44.40	8.58	8.80	-0.39	0.17
BMT	szs	4	0.13	32.6	326		25 48.40	12.58	12.57	-0.29	0.29
BAR	p	1	0.18	42.0	73	78	25 43.10	7.28	7.23	0.07	-0.02
BAR	s	3	0.13	42.0	73		25 48.70	12.88	12.62	0.29	-0.04
LPM	s	3	0.12	50.1	52		25 50.30	14.48	14.95	-0.15	-0.33

lat	1std	2std	rmatrx	rsubk	lon	1std	2std	rmatrx	rsubk
34 1.88	0.50	1.00	1.000	0.000	107 3.79	0.40	0.80	1.000	0.000

depth	1std	2std	rmatrx	rsubk	orig	1std	2std	rmatrx	rsubk
9.21	0.45	0.89	1.000	0.000	35.82	0.06	0.12	1.000	0.000

1std epi	2std epi	rms	gap	dmag	nmag
0.64	1.28	0.22	86	0.43	7

Fig. A8. Page 4 of a sample earthquake location output file *refloc.dat*. This page lists iteration results, station information, and the event location.

TABLE A9. Abbreviations From Output File *refloc.dat* - Event Identification and Iteration Results

Name	Meaning
itr	iteration number
R	R scalar value
rms	root-mean-square of residuals in sec
x	x coordinate in km
y	y coordinate in km
h	focal depth in km
orig	origin time in sec
adj	adjustment on a parameter over one iteration

TABLE A9. Abbreviations From Output File *refloc.dat* - Continued - Station and Phase Results

Name	Meaning
sta	station name
phs	name of phase picked
qual	pick quality
wt	relative weight a pick has in a solution (diagonal of the S matrix)
delta	epicentral distance in km
azm	azimuth from event to station
ain	angle of incidence - upper focal sphere
obs-arv	observed arrival time in min and sec
obs-trv	observed travel time in min and sec
theo-trv	theoretical travel time in min and sec
resid	difference between observed time and (theoretical time +station correction) in sec
sta-cor	station correction in sec adjusted for velocity of arriving phase

TABLE A9. Abbreviations From Output File *refloc.dat* - Continued - Solution Information

Name	Meaning
lat	solution latitude in degrees and minutes
lon	solution longitude in degrees and minutes
depth	solution focal depth in km
orig	solution origin time in sec
1std	parameter error at one standard deviation
2std	parameter error at two standard deviations
1std epi	epicenter error at one standard deviation
2std epi	epicenter error at two standard deviation
rmatrx	diagonal of the resolution matrix
rsubk	another measure of parameter resolution
rms	root-mean-square of residuals in sec
gap	maximum gap between stations in deg
dmag	duration magnitude estimate
nmag	number of durations used to estimate dmag
*	indicates an unknown was not solved

large number of event locations. Ev_stats will compile general statistics for location runs of many events. The file *stats.dat* will contain information about average parameter errors, the numbers of different phases used, and the qualities of the phases used.

Useful Input And Formatting Programs

The programs summarized in Table A2 are especially useful for building data files into correct formats, transforming pick files between *HYPO71* format and *seismos* format, and modifying location plot files. The programs *velmod* and *chvmod* are useful for entering and then modifying a velocity model. However, once a user becomes familiar with the file *velmod.dat*, then using a screen editor to modify a velocity model will probably be more efficient than using these two programs. The programs dealing with pick file formats, especially the two which transform formats, can save a user much effort. When *hans2hyp* is executed, any reflected phase arrival times will not be transformed into *HYPO71* format as *HYPO71* can not use reflected phases.

Chopshop will take an *HREGQK* plot file and remove any events which do not meet the time-window, epicenter, or parameter error criteria set by the user. Thus, this program is a pre-processor to any other plotting or histogram program which can read *HREGQK* format. It is extremely useful for sifting out poor quality locations before plotting. The program *distance* reads a file of station names, latitudes, and longitudes (*sta.dat*) and transforms the locations into x and y coordinates measured in km. The center of the coordinate system is designated in the file *pit.dat*. It's location is also specified in latitude and longitude, but upon transformation its coordinates will be 500.0, 500.0. Both *pit.dat* and *sta.dat* must have latitudes and longitudes listed in decimal degrees, not degrees and minutes. The output file *coords.dat* will be similar to *stacrd.dat*, the station coordinate file read by *seismos*, but station corrections will have to be provided by the user.

Plotting Programs

The most important plotting program I have written is *epiplot* (Table A3). It can be used to plot epicenters or reflection points. Before using *epiplot* the user first runs *seismos*, obtains locations (stored in *newloc.dat*), and then processes the data files *newloc.dat* and *picfil.dat* using the program *headplt*. This creates a file in *HREGQK* format, the standard data plotting format used by the New Mexico Tech Geophysics Program.

There are several controlling parameters which the user must set before running *epiplot*. Figure A9 is a sample controlling file, *pltpar.dat*, and Table A10 explains the meaning of most options found in this file. The switches are the same as those found in other controlling files, 1 means yes and 0 means no. For instance, the first option, *manual axis selection?*, is set to 1. This means that the user, rather than the program, will decide on the latitude and longitude limits of the plot dimensions. If this option were set to 0, then the user would not be prompted for input on the plot area, and the program would decide on appropriate limits.

In *pltpar.dat* the entry *neg-pos-normal resids?* refers to options when reflection points are to be plotted. If the switch for *plot ref points?* has not been set to 1, then the options will be ignored. When plotting reflection points the user is asked to specify whether a *normal* residual is defined as a residual which is within either one or two times the assumed timing error. If a user chooses not to classify a residual with respect to assumed timing error, then all theoretical arrival times will end up being defined as either positive or negative. If a user sets all three options to 0, but still sets the *plot ref points?* switch to 1, then all reflection points will be plotted without preference to residual sign or timing error.

The other programs listed in Table A3 can be used to produce many of the plots found in this dissertation. The programs *dep_plot* and *refvsx* use data from earthquakes located using *seismos*. *Timdis* can plot either standard or reduced time-distance curves for all the phases listed in Table A7. If plotting reduced times, then the user is prompted for a reducing velocity. *Curvfnd* and *xzfnd* are not plotting

```
 depth limits
1   0.0000  15.0000
 magnitude limits
1  -1.0000   5.0000
 longitude limits
1 105.0000 108.0000
 latitude limits
1  32.0000  36.0000
manual axis selection?
1
plot station symbols?
1
plot station labels?
1
draw lat-lon lines?
0
plot synthetic locs?
0
number each event?
0
large plot?
1
diff dep symbols?
0
plot ref points?
0
neg-pos-normal resids
0 0 0
plot epicenters?
1
plot cocorp lines?
1
plot provinces?
0
plot new mexico?
0
plot mag bod outline?
1
plot uplift contours?
0
plot cities?
1
plot studies?
0
n stations / list
11
BAR
MAG
CAR
LAZ
LPM
LJY
LEM
SB
SMC
WTX
MLM
```

Fig. A9. Sample epicenter plotting controller file *pltpar.dat*. This file is read by ***epiplot***.

TABLE A10. Epicenter Plotting Instructions - *pltpar.dat*	
Entry	Meaning
manual axis selction?	user selects axis limits
plot station symbols?	plot a triangle for each station location
plot station labels?	post the station abbreviations
draw lat-lon lines?	add a lat-lon grid to the plot
plot synthetic locs?	plot locations from *synloc.dat*
number each event?	number the events as they are listed in the *HREGQK* file
large plot?	controls orientation of plot
diff dep symbols?	use different symbols for different focal depth ranges
plot ref points?	plot reflection points
neg-pos-normal resids?	when reflection points are to be plotted show points associated with positive, negative, or normal residuals
plot epicenters?	plot event epicenters
plot cocorp lines?	plot the COCORP lines near Socorro
plot provinces?	plot the physiographic provinces of New Mexico
plot New Mexico?	plot a map of New Mexico
plot mag bod outline?	plot the magma body outline
plot uplift contours?	plot the uplift contours over the magma body
plot cities?	plot cities in New Mexico
plot studies?	plot various study area outlines
n stations - list	number of stations in list followed by the name of each station to be plotted

programs, but they generate data files used by *timdis, phsminp*, and *hzcurv.*

Synthetic Data Generating Programs

The data generating program I emphasize in this appendix is *syngen* (Table A4). It can create single-event pick files or pick files of many events. Random noise can be added to the synthetic times using *add_nois.* Synthetic data are useful for testing location program correctness and the affects of recording geometry on the earthquake location problem. Possible phases which can be generated are direct P and S, P_zP, S_zP, and S_zS. The controlling file for *syngen* is *station.list* (Figure A10). Table A11 describes more details of this file. The user controls how many km in the x and y directions epicenters can vary from a specified central point, the possible depth range of the events, the proportions of various phases comprising the data set, and the possible stations which will record synthetic data.

If an S_zP arrival is "recorded" at a station, then an S_zS arrival will automatically occur at the same station. Thus, this program builds an arrival time file of S_zP - S_zS pairs, not individual S_zP or S_zS arrivals. Half of these reflections will have a weight of 3 and the half a weight of 4. The P weighting is controlled by the user through an option to specify which proportion of these arrivals will be weighted 0 and which will be weighted 1. For the case of direct S arrivals, half will have a weight of 2 and half a weight of 3. The P_zP arrivals are weighted the same as the other reflected arrivals, half with weights of 3 and half with weights of 4. If a P arrival is not selected for a particular station, then no other arrivals will be chosen for that station.

All phases, weights, epicenters, focal depths, and origin times are chosen with Sun's uniform random number generator. Station names are chosen from the stations listed in, *station.list*, and the station locations are read from the file *stacrd.dat.* Whether or not a station is actually chosen to "record" an event is done with the random number generator. Normally distributed random noise can be added to a synthetic data pick file using *add_nois.* The random noise is generated by summing

```
nev l h    x      y    cenx ceny    dmax    dmin    scut  rcut pwtcut pcut pzpcut
 10 3 8   25.0   30.0 500.0 500.0   12.0     4.0    0.70  0.25  0.80  0.90  0.10
09 1990 04 15 12 1
BAR
BMT
CAR
LAZ
LJY
LPM
SB
SMC
WTX
```

Fig. A10. Sample synthetic data generation controller file *station.list*. This file is read by *syngen*.

TABLE A11. Synthetic Data Generating Instructions - *station.list*

Entry	Meaning	Format
nev	number of synthetic events to generate	i3
l	minimum number of reflections per event	i2
h	maximum number of reflections per event	i2
x	the maximum x epicenter distance from the origin	f6.1
y	the maximum y epicenter distance from the origin	f6.1
cenx	coordinate for x marking center of grid	f6.1
ceny	coordinate for y marking center of grid	f6.1
dmax	maximum depth of any event	f6.1
dmin	minimum depth of any event	f6.1
scut	proportion of stations with direct S arrivals	f6.2
rcut	proportion of stations with reflected S_zP and S_zS arrivals	f6.2
pwtcut	proportion of direct P arrivals with a "0" weight	f6.2
pcut	proportion of stations with direct P arrivals	f6.2
pzpcut	proportion of stations with reflected P_zP arrivals	f6.2

12 uniform random numbers. The random noise can be removed from a synthetic pick file using *no_rannois*. The amplitude of the random noise is controlled by the weight assigned to each synthetic arrival time.

The program *synrfr* can generate synthetic regional-event data. It reads the controller file *sta_phs.list* (similar to *station.list*), but it generates only one pick file per program run. The event location is selected by the user rather than being chosen with the random number generator. The program will only generate head wave arrivals.

Compiling the Programs

I have organized my programs into several parallel directories (Table A12). I recommend using this directory structure or something similar to help keep the source code organized. The *Makefile*, available with the source code, provides compiling and linking instructions for a *Unix* operating system. To compile a program, move the *Makefile* into the directory storing the necessary source code and type: *make program_name.*

The start of the *Makefile* lists options for the floating point accelerator (*fpa*) or the standard (*f68881*) *Sun* compiler. I recommend using the *fpa* option when solving the joint problem. *Seismos* will run much faster, however, at New Mexico Tech the floating point accecerator is only available three machines (*jupiter, titan, sirius*). When using a system where *IMSL* subroutines are available, then link *seismos* with either the *imsl* or the *imsl-fpa* option, depending on whether *f68881* or *fpa* is being used. If *IMSL* is being used, then check the source code, *eigen.f*, to make sure it calls the subroutine *eigfnd1*. If *IMSL* is not being used, then check to make sure the subroutine *eigfnd* is being called. The compiling option *r8* can be used if double precision is necessary. Using this option does not require any modification of source code.

The directory *Shared* contains subroutines which are used by more than one program. For instance, the ray-tracing subroutines are all stored in *Shared*. The

TABLE A12. Recommened Directory Structure

Directory	Purpose
Shared	store all source code (subroutines) shared by many of the programs
Hypo_source	store all source code related to *seismos*
Chng_pics	store all source code related to modifying pick files
Epi_plot	store all source code related to *epiplot* and *dep_plot*
Time_curv	store all source code related to plotting time or distance curves
Syngen	store all source code related to synthetic data generation
Distance	store all source code related to converting latitudes and longitudes to distances in km

Makefile contains directions for the compiler to automatically look into the directory *Shared* if a needed subroutine is stored there.

Appendix B - Final Relative Arrival Time Curves

This appendix contains relative arrival time curves based on the velocity model shown in Table 7.2 and Figure 7.13. The curves are for focal depths of 2 to 12 km. They can be used to help identify reflected phases.

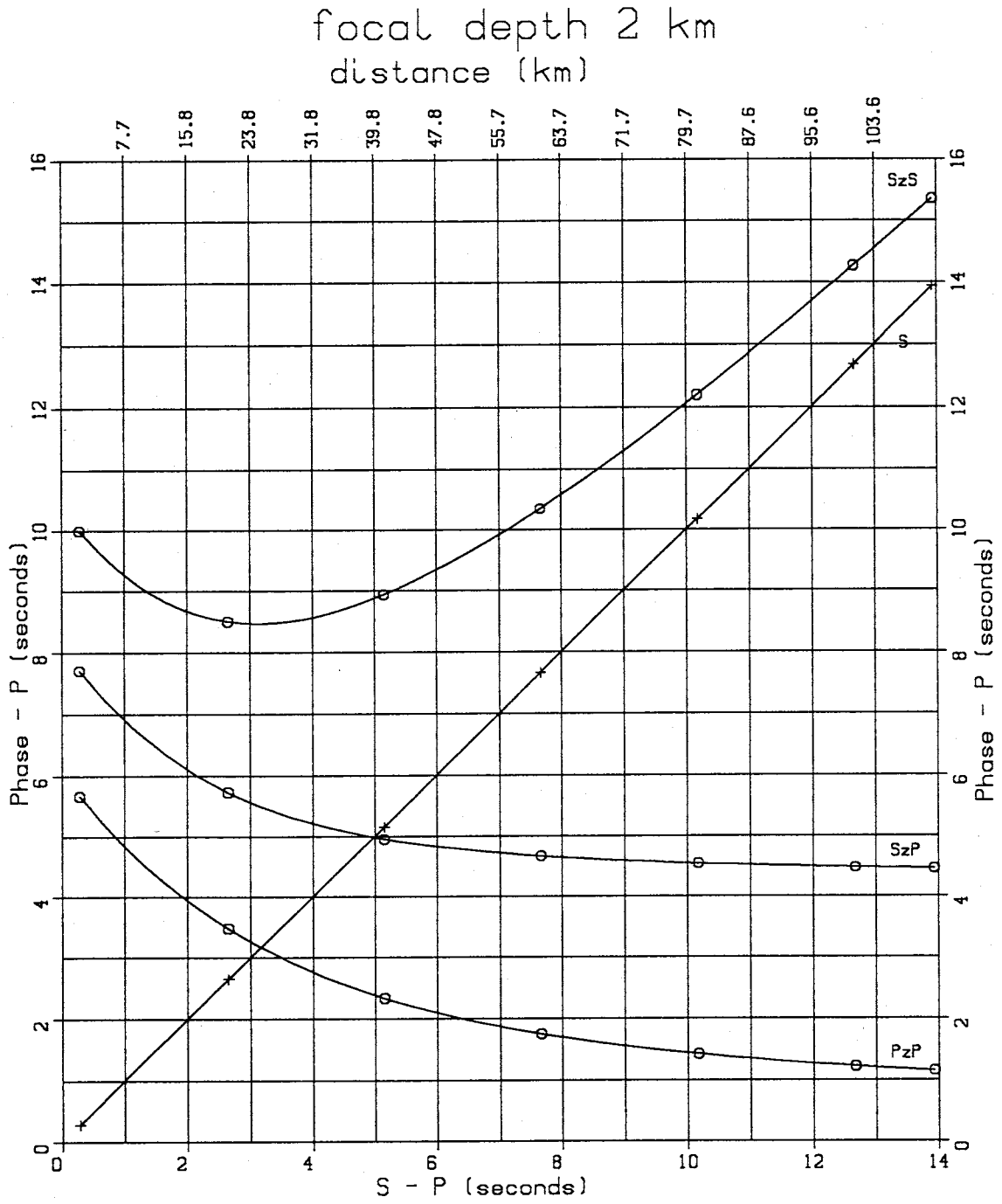
focal depth 2 km
distance (km)
7.7
15.8
23.8
31.8
39.8
47.8
55.7
63.7
71.7
79.7
87.6
95.6
103.6
SzS
S
SzP
PzP
Phase - P (seconds)
Phase - P (seconds)
S - P (seconds)
0
2
4
6
8
10
12
14
16

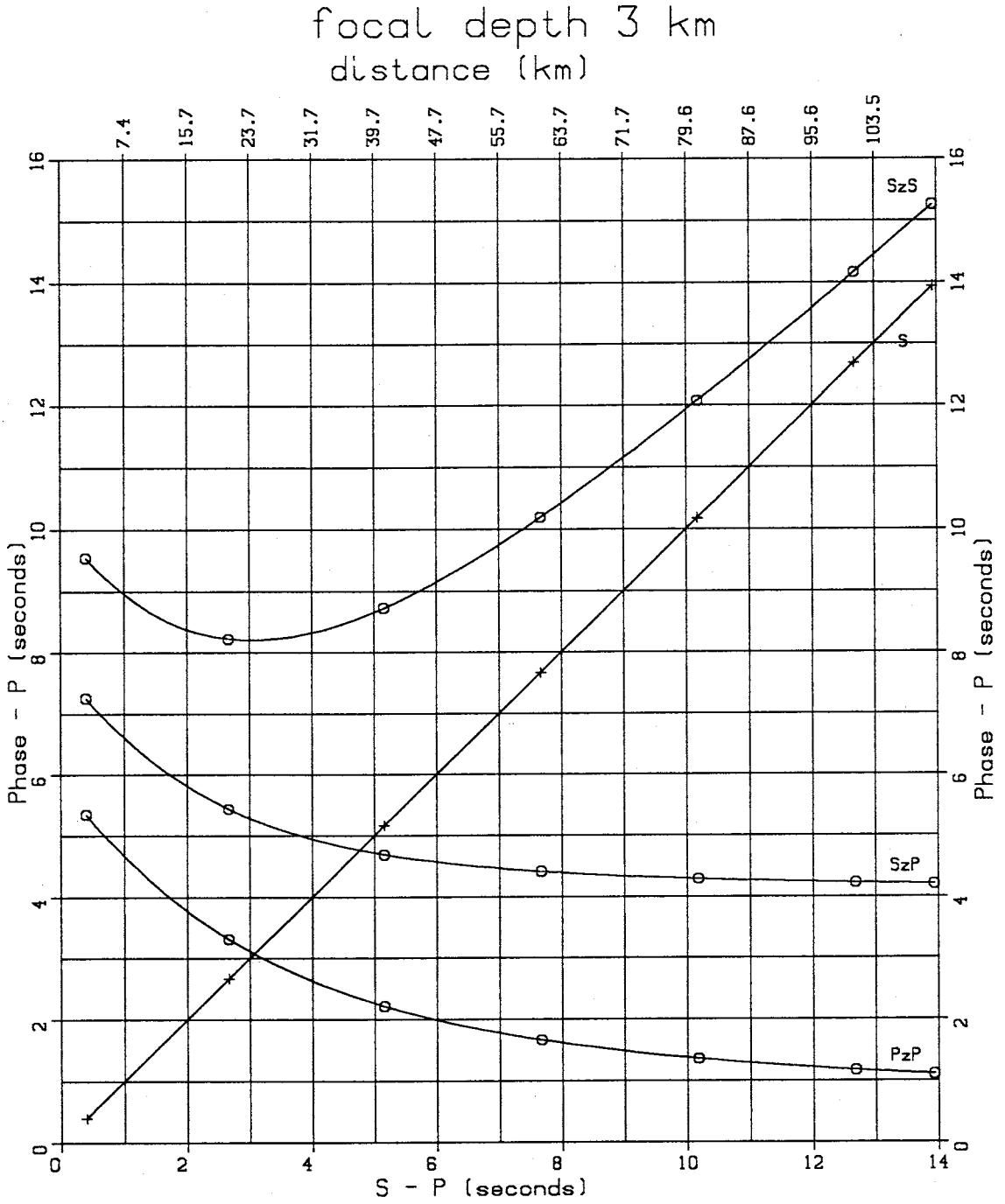
focal depth 3 km
distance (km)
7.4
15.7
23.7
31.7
39.7
47.7
55.7
63.7
71.7
79.6
87.6
95.6
103.5
SzS
S
SzP
PzP
Phase - P (seconds)
Phase - P (seconds)
S - P (seconds)
0
2
4
6
8
10
12
14
16

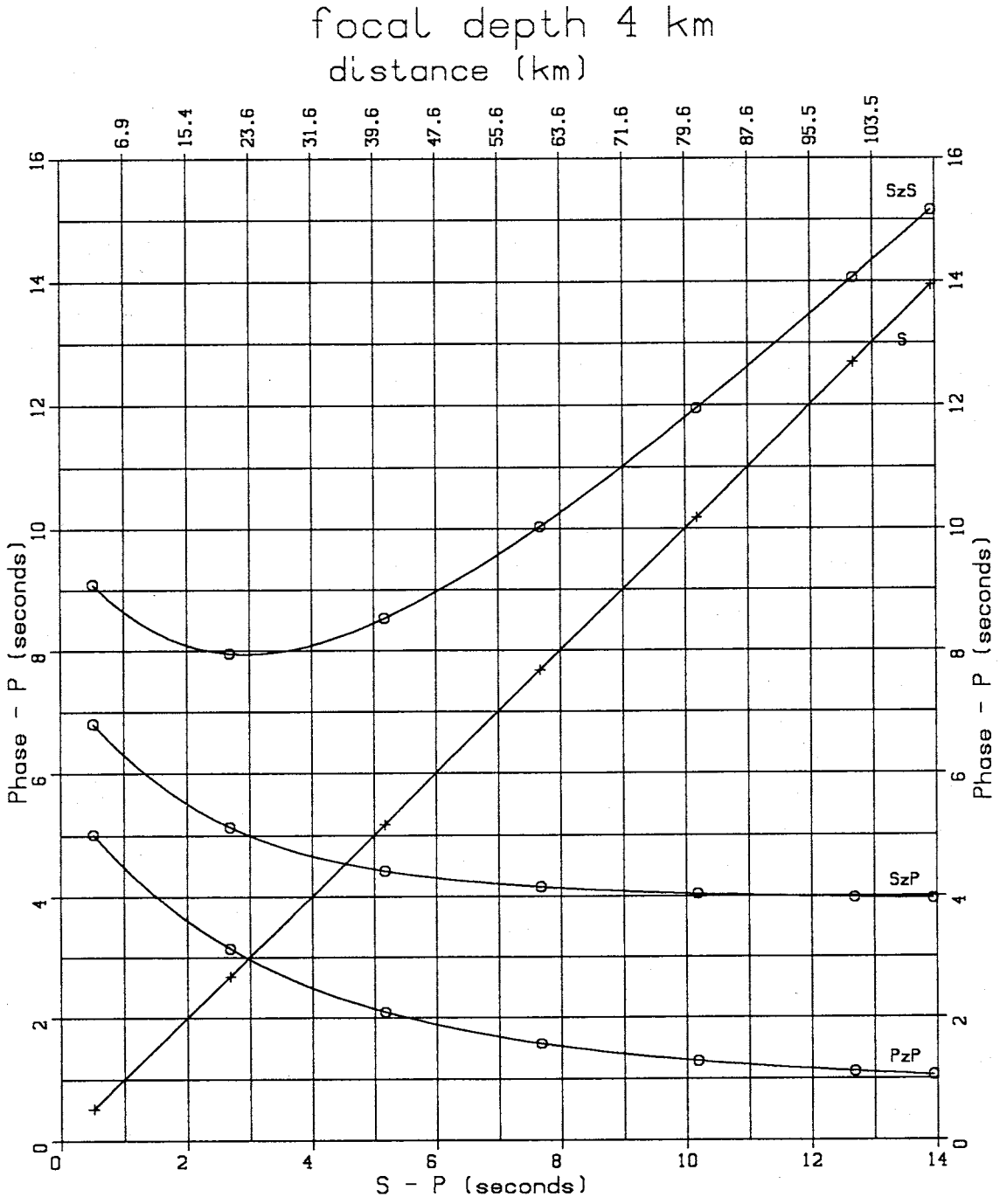
focal depth 4 km
distance (km)
6.9
15.4
23.6
31.6
39.6
47.6
55.6
63.6
71.6
79.6
87.6
95.5
103.5
SzS
S
SzP
PzP
Phase - P (seconds)
Phase - P (seconds)
S - P (seconds)
0
2
4
6
8
10
12
14
16

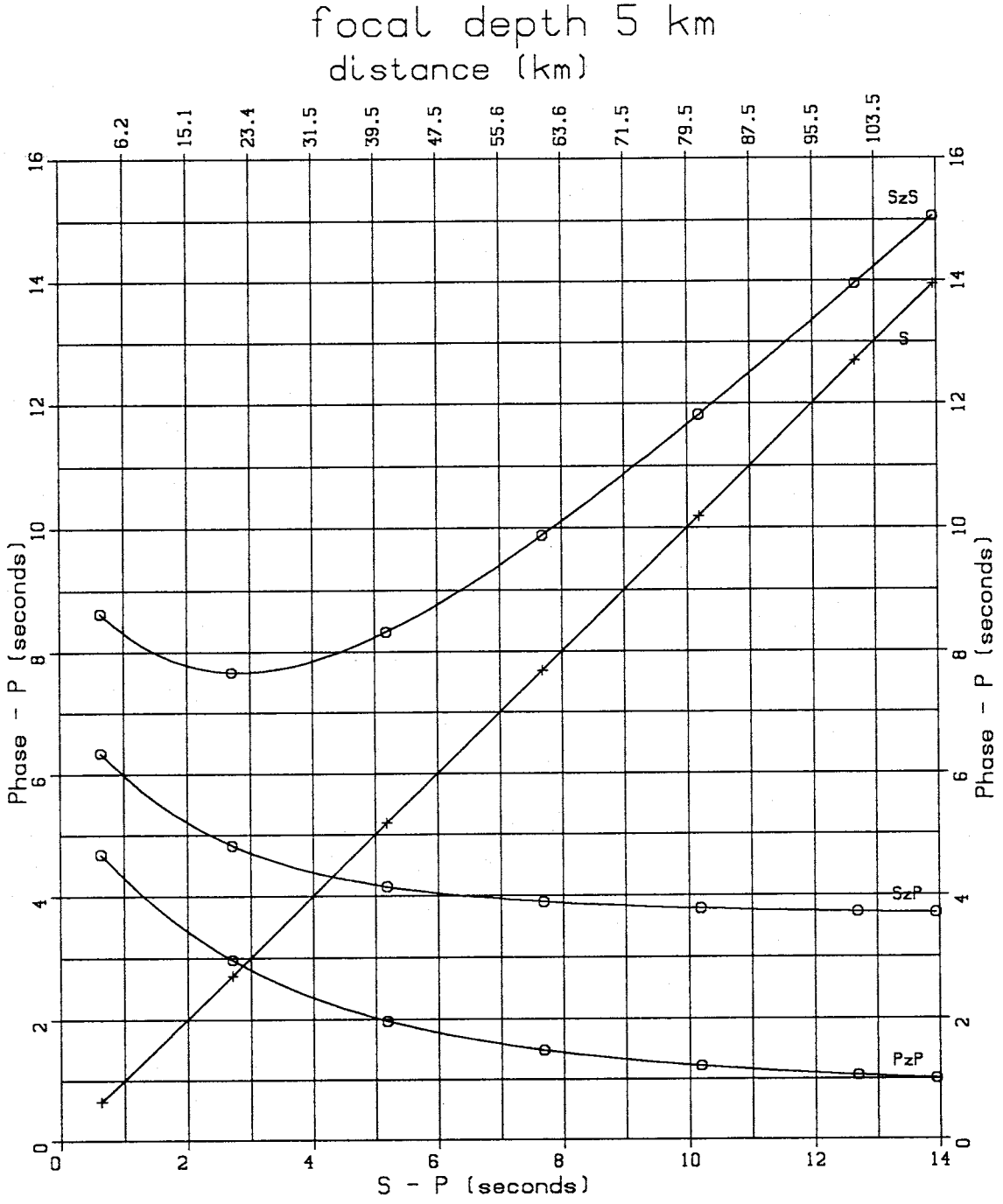
focal depth 5 km
distance (km)
6.2
15.1
23.4
31.5
39.5
47.5
55.6
63.6
71.5
79.5
87.5
95.5
103.5
SzS
S
SzP
PzP
Phase - P (seconds)
S - P (seconds)
0
2
4
6
8
10
12
14
16

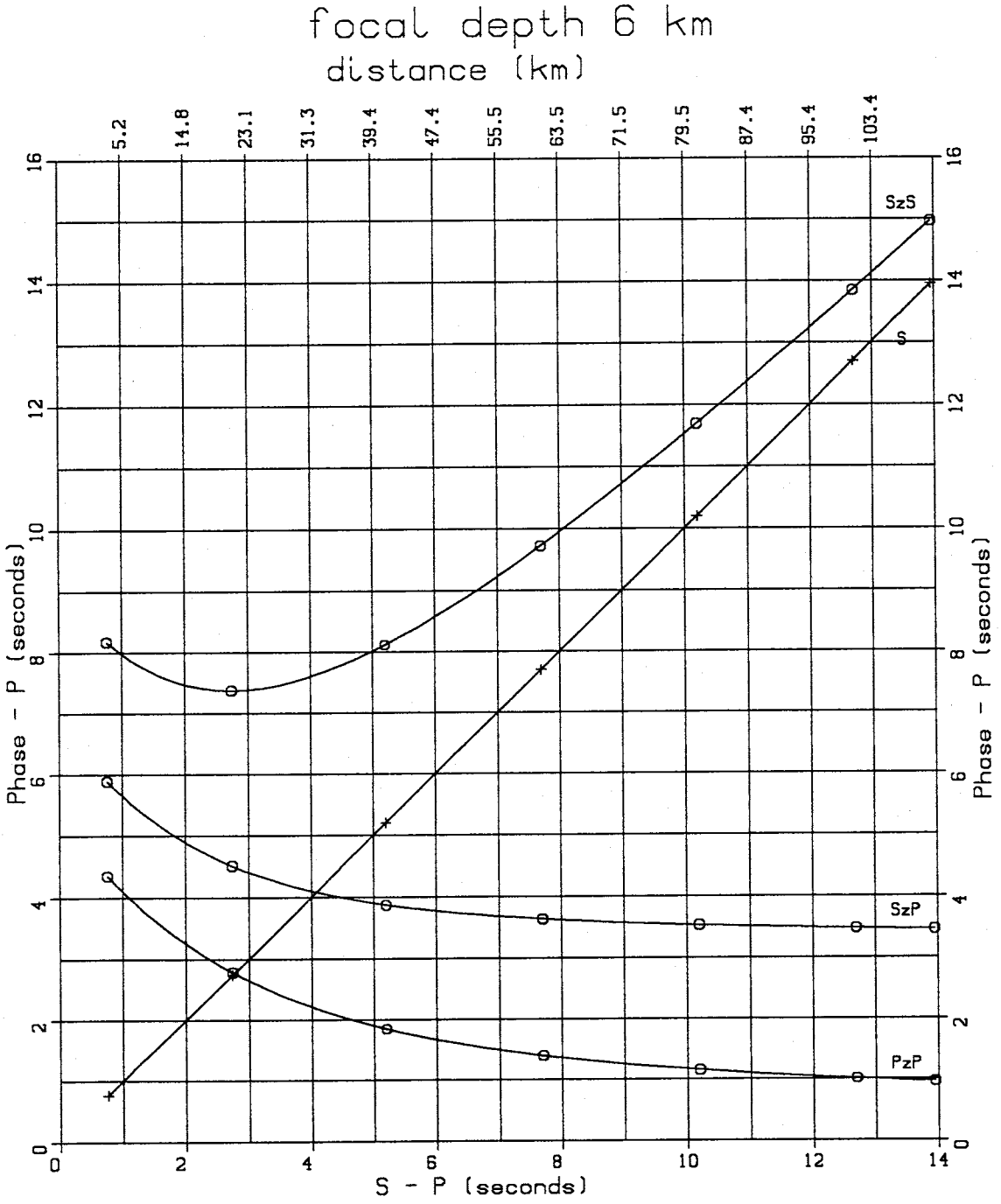
focal depth 6 km
distance (km)
5.2
14.8
23.1
31.3
39.4
47.4
55.5
63.5
71.5
79.5
87.4
95.4
103.4
SzS
S
SzP
PzP
Phase - P (seconds)
S - P (seconds)
0
2
4
6
8
10
12
14
16

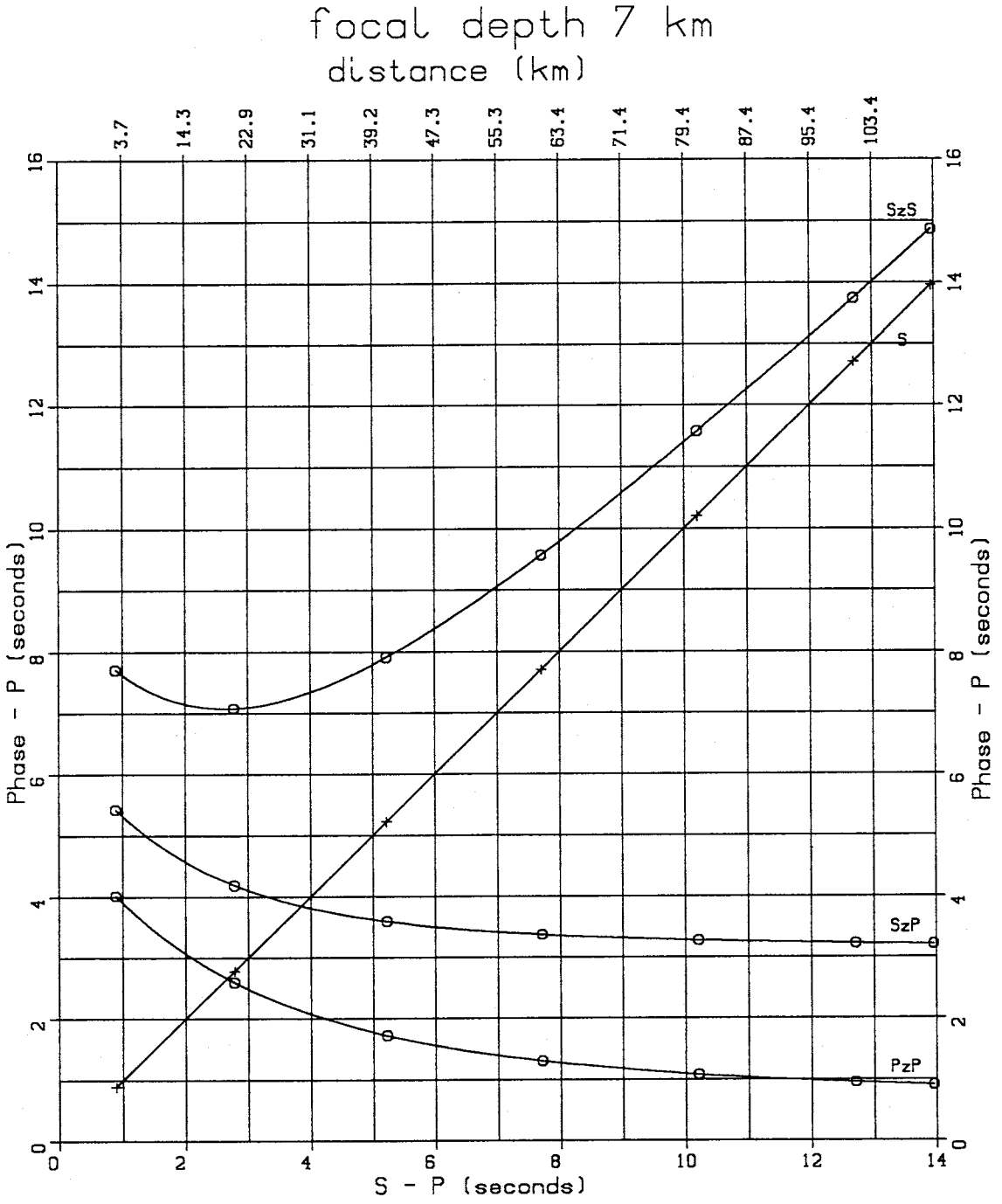
focal depth 7 km
distance (km)
3.7
14.3
22.9
31.1
39.2
47.3
55.3
63.4
71.4
79.4
87.4
95.4
103.4
SzS
S
SzP
PzP
Phase - P (seconds)
Phase - P (seconds)
S - P (seconds)
0
2
4
6
8
10
12
14
16

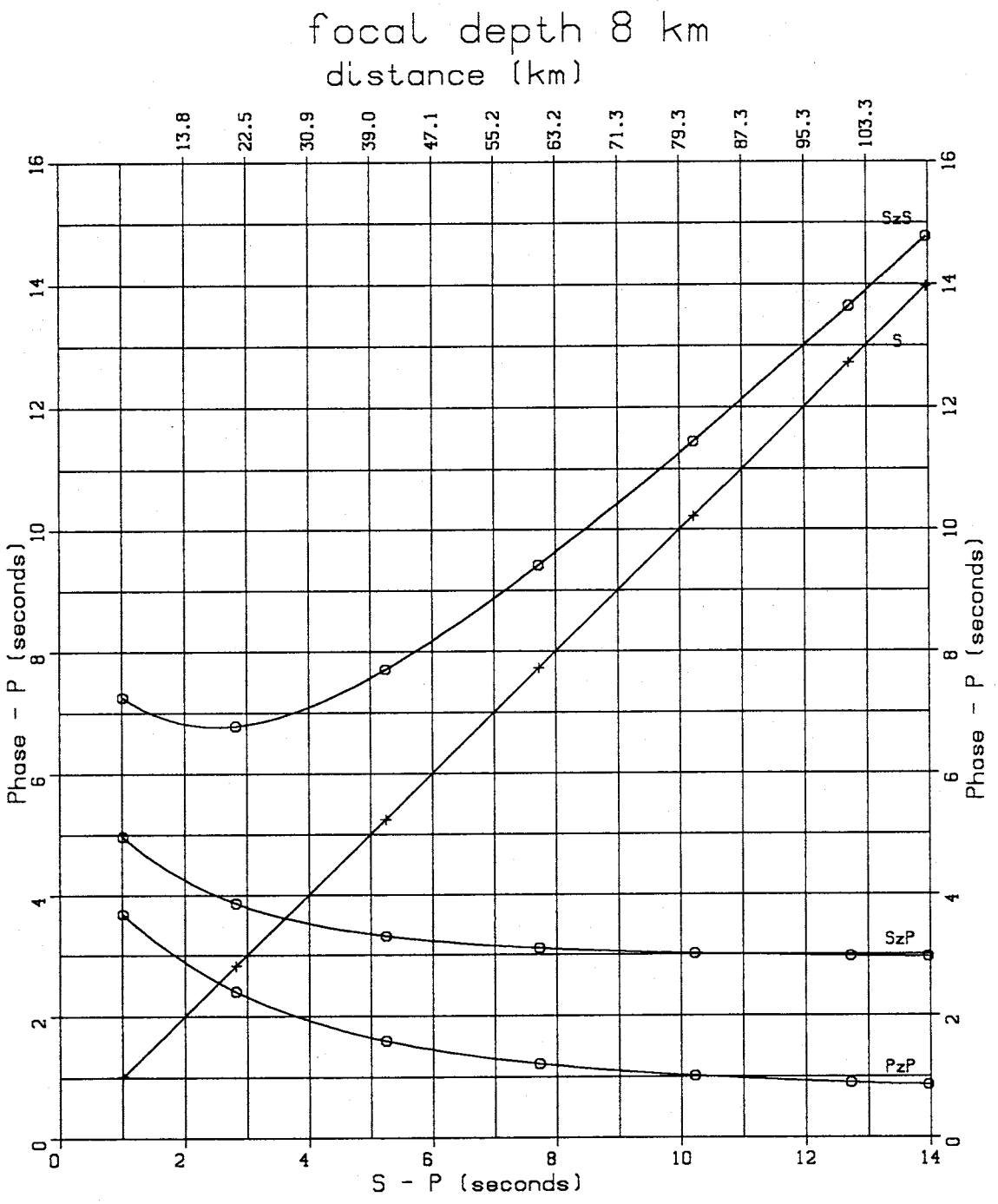
focal depth 8 km
distance (km)
13.8
22.5
30.9
39.0
47.1
55.2
63.2
71.3
79.3
87.3
95.3
103.3
SzS
S
SzP
PzP
Phase - P (seconds)
Phase - P (seconds)
S - P (seconds)
0
2
4
6
8
10
12
14
16

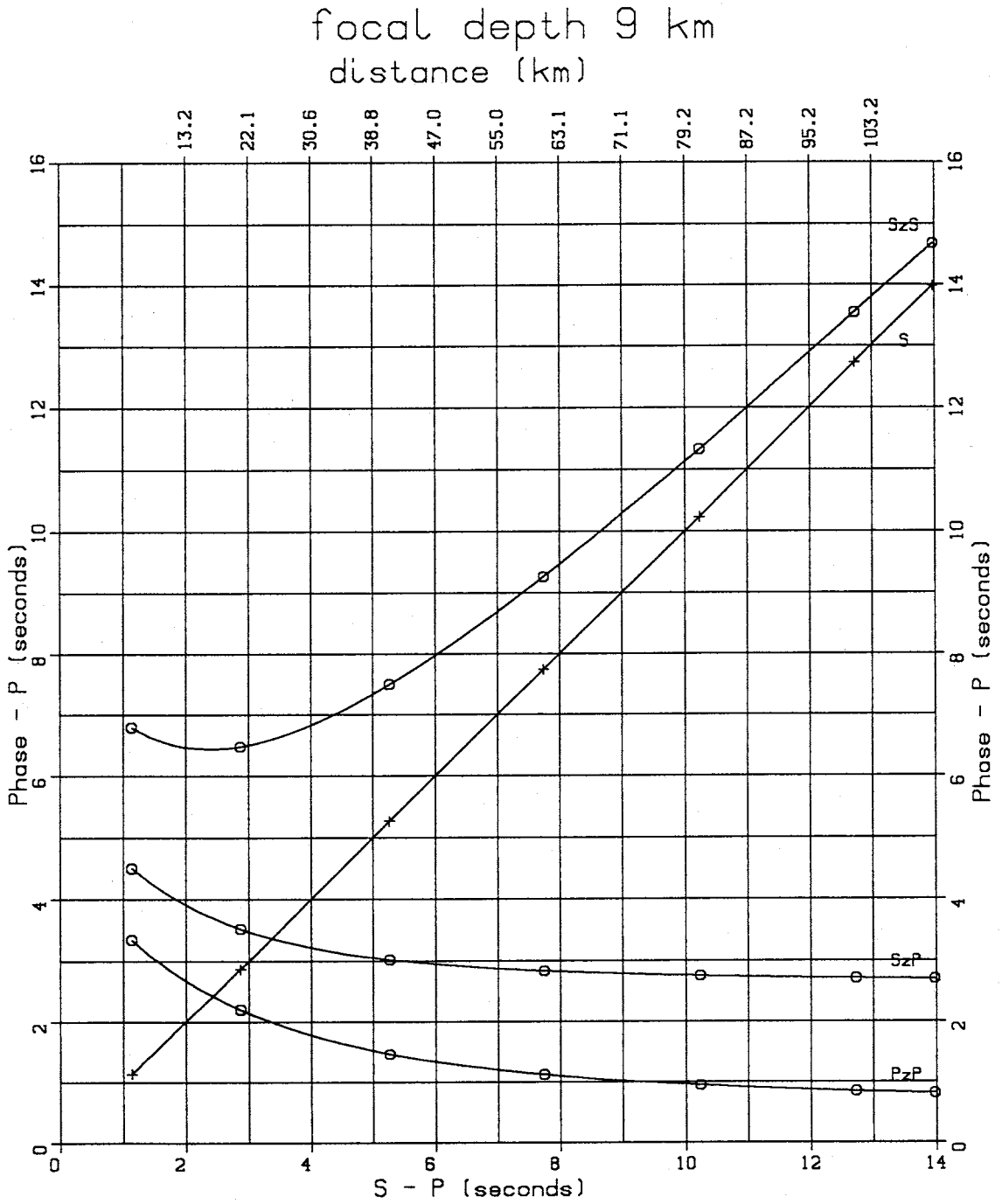
focal depth 9 km
distance (km)
13.2
22.1
30.6
38.8
47.0
55.0
63.1
71.1
79.2
87.2
95.2
103.2
SzS
S
SzP
PzP
Phase - P (seconds)
Phase - P (seconds)
S - P (seconds)
0
2
4
6
8
10
12
14
16

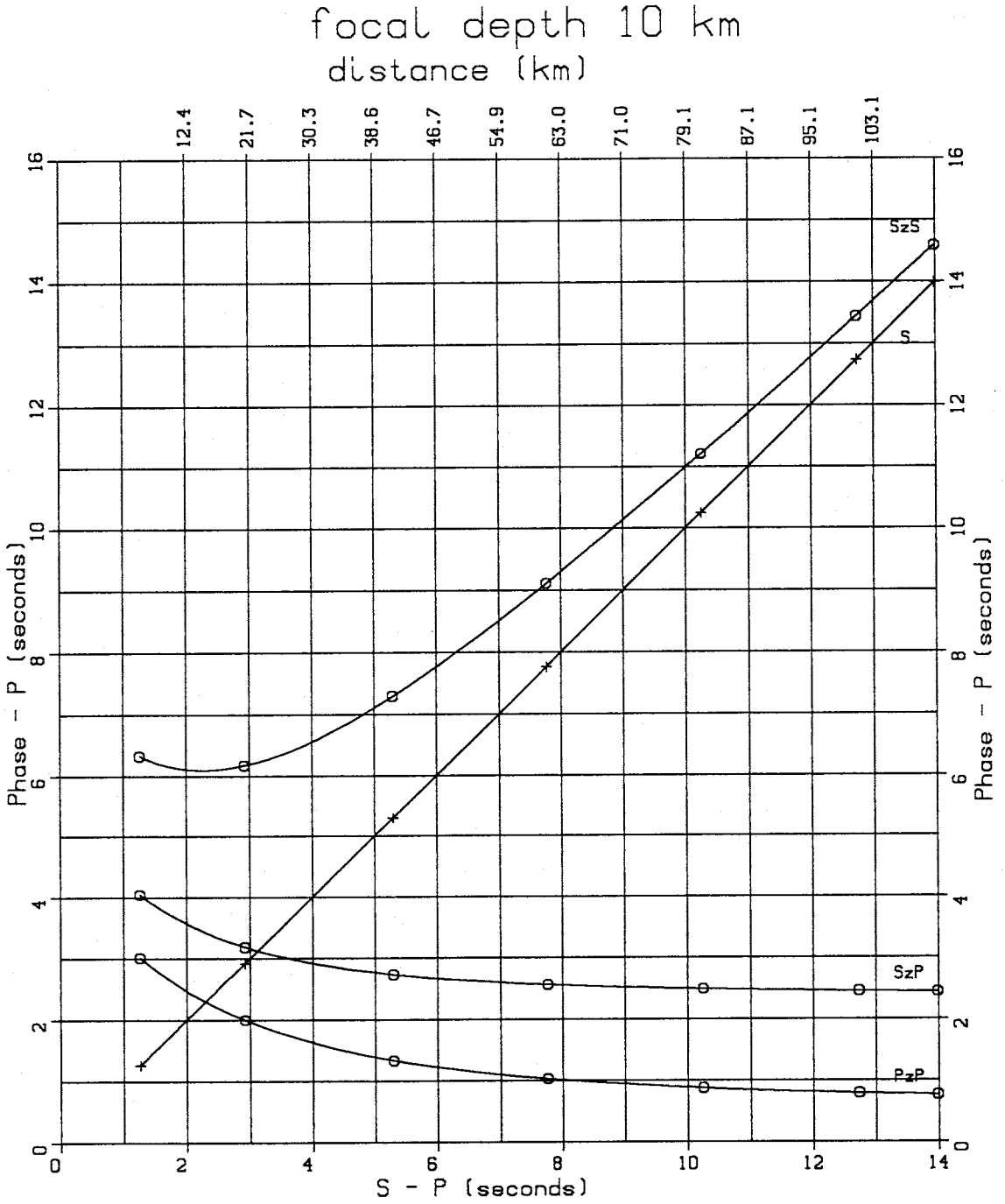
focal depth 10 km
distance (km)
12.4
21.7
30.3
38.6
46.7
54.9
63.0
71.0
79.1
87.1
95.1
103.1
SzS
S
SzP
PzP
Phase - P (seconds)
S - P (seconds)
0
2
4
6
8
10
12
14
16

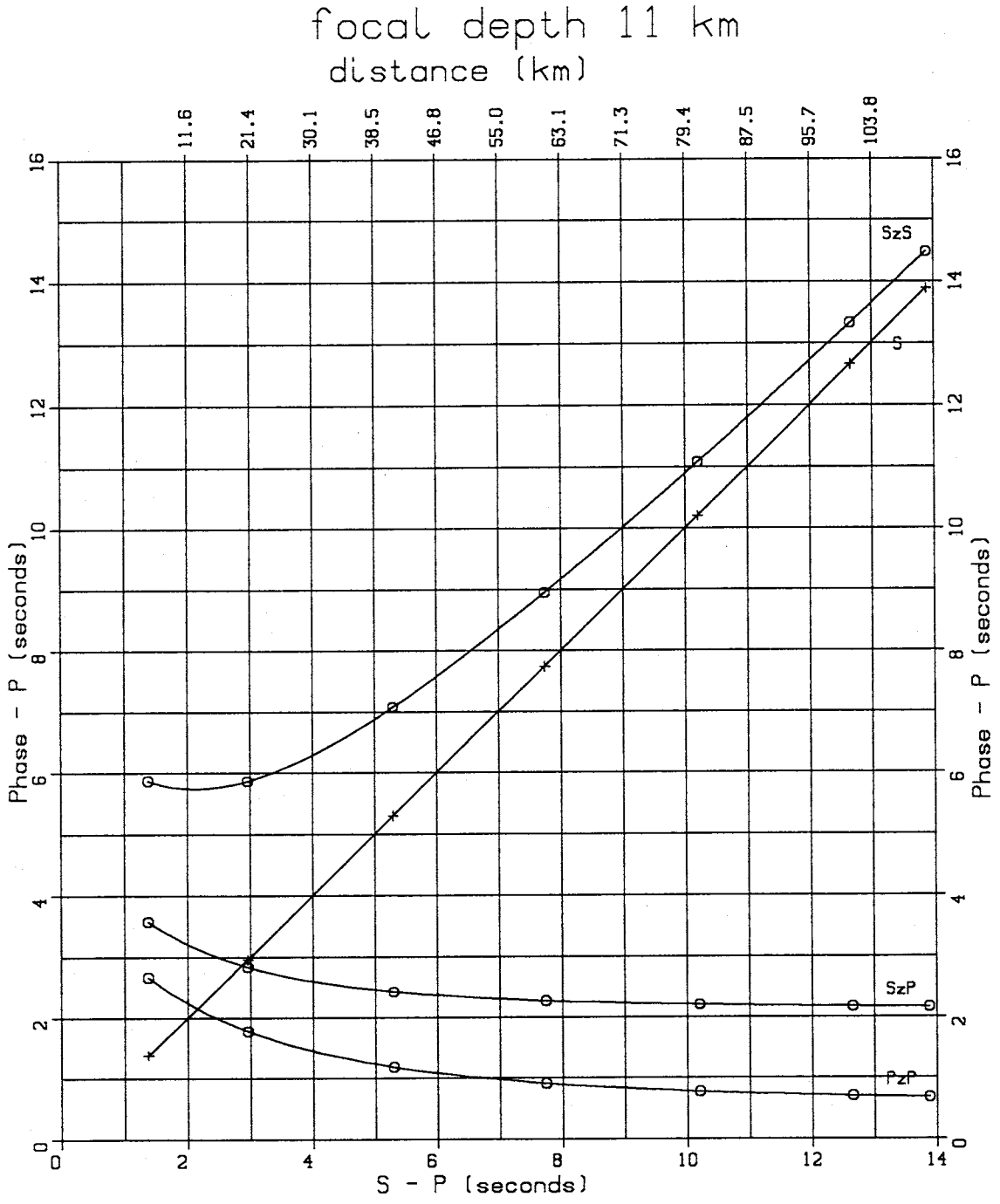
focal depth 11 km
distance (km)
11.6
21.4
30.1
38.5
46.8
55.0
63.1
71.3
79.4
87.5
95.7
103.8
SzS
S
SzP
PzP
Phase - P (seconds)
S - P (seconds)
0
2
4
6
8
10
12
14
16

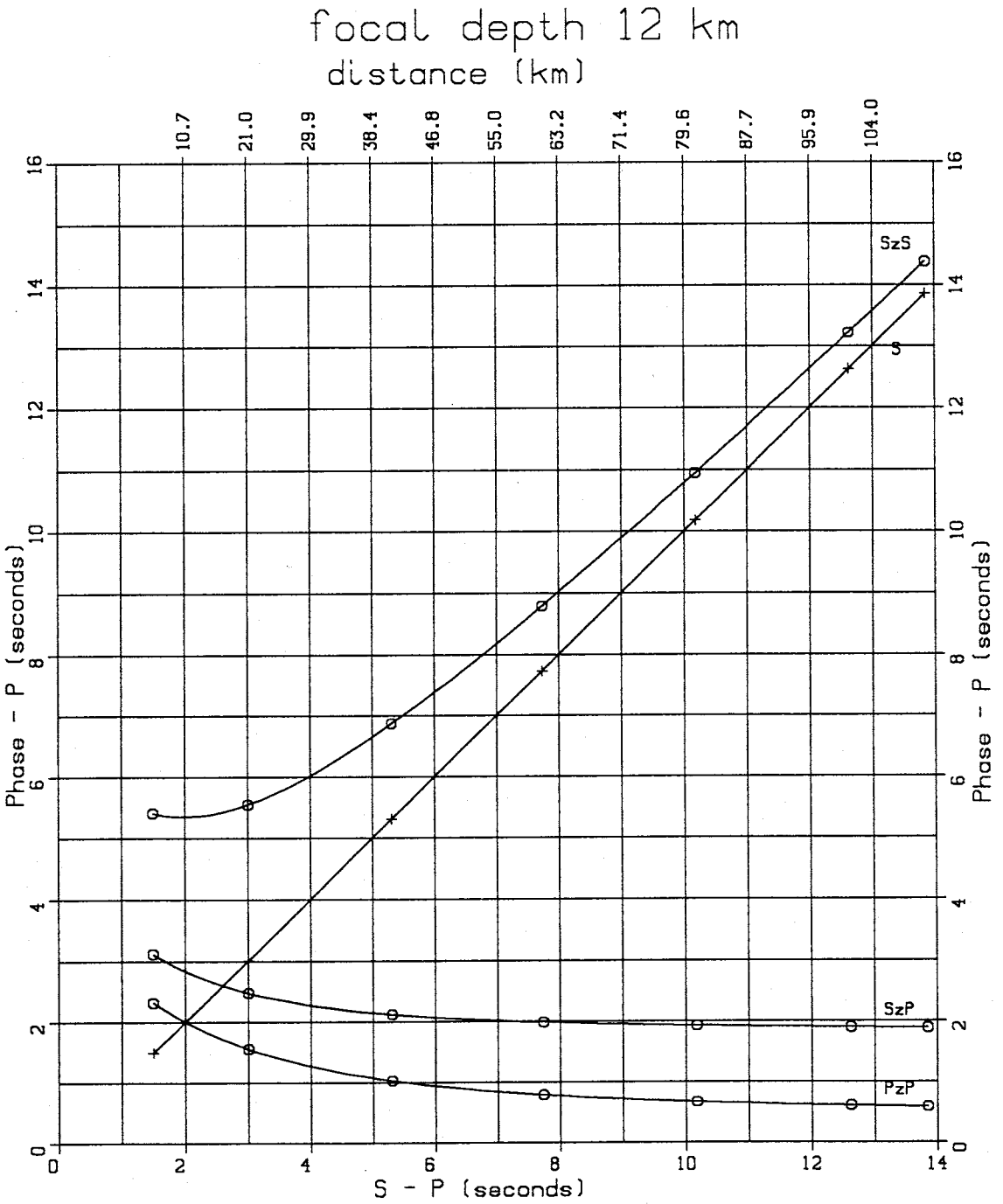
focal depth 12 km
distance (km)
10.7
21.0
29.9
38.4
46.8
55.0
63.2
71.4
79.6
87.7
95.9
104.0
SzS
S
SzP
PzP
Phase - P (seconds)
S - P (seconds)
0
2
4
6
8
10
12
14
16

Appendix C - Locations and Data

Table C1 lists the locations of the 75 earthquakes used in the joint hypocenter-velocity model inversion. The origin time listings include year, month, day, hour, minute, second, and error in seconds. The latitude and longitude listings are in degrees and minutes, but the errors are in kilometers. The depth listings and errors are in kilometers. All errors are for one standard deviation. The locations were estimated along with the velocity model listed in Table 7.2. The locations of the Arroyo del Coyote events are listed in Table 8.1.

The arrival time pick files follow Table C1. Listed first are 75 pick files composing the main data set, followed by the 25 pick files of the Arroyo del Coyote sequence. **Appendix A** explains the pick file format.

TABLE C1. Final Event Locations - Main Data Set

	OriginTime	Lat	Long	Depth	Mag
1	8209192225 35.82 ±0.07	34 01.89 ±0.51	107 03.79 ±0.41	9.20 ±0.51	0.43
2	8303041820 06.91 ±0.05	34 18.14 ±0.46	106 52.61 ±0.29	4.68 ±0.55	1.21
3	8304280210 21.66 ±0.05	34 06.80 ±0.35	106 52.05 ±0.33	4.45 ±0.62	0.57
4	8402270102 06.91 ±0.06	34 01.67 ±0.55	106 59.84 ±0.40	6.47 ±0.46	-0.07
5	8407161612 15.61 ±0.06	34 04.41 ±0.34	106 50.77 ±0.32	6.66 ±0.62	0.04
6	8407221655 38.09 ±0.06	34 04.43 ±0.35	106 50.81 ±0.27	8.04 ±0.59	-0.20
7	8409022157 39.87 ±0.07	33 56.60 ±0.44	106 59.55 ±0.33	5.71 ±0.76	0.01
8	8409100630 03.87 ±0.06	33 56.58 ±0.31	106 59.46 ±0.40	5.22 ±0.72	-0.08
9	8409220515 16.65 ±0.06	34 10.46 ±0.59	106 52.13 ±0.36	7.00 ±0.50	0.02
10	8410071148 43.32 ±0.05	34 11.07 ±0.34	106 52.45 ±0.31	6.32 ±0.63	0.77
11	8410071349 05.75 ±0.06	34 00.06 ±0.40	106 58.06 ±0.30	9.62 ±0.49	-0.17
12	8410132055 00.56 ±0.06	34 11.17 ±0.46	106 52.42 ±0.28	6.47 ±0.70	0.05
13	8410290908 25.26 ±0.06	34 07.82 ±0.37	106 52.36 ±0.32	6.70 ±0.63	0.25
14	8503012206 07.60 ±0.06	34 05.94 ±0.51	106 59.56 ±0.28	10.38 ±0.51	0.22
15	8503210917 51.33 ±0.09	34 26.05 ±0.72	106 54.68 ±0.39	5.54 ±0.67	0.07
16	8503241105 47.11 ±0.07	34 18.24 ±0.52	107 01.55 ±0.39	5.84 ±0.55	0.32
17	8503290913 06.40 ±0.06	34 18.43 ±0.50	107 01.46 ±0.33	5.74 ±0.77	0.33
18	8504070028 44.68 ±0.05	34 14.13 ±0.36	106 51.86 ±0.31	5.04 ±0.69	1.02
19	8505011219 26.10 ±0.05	34 04.19 ±0.33	106 55.28 ±0.30	2.73 ±0.68	0.52
20	8507080434 18.59 ±0.07	34 05.50 ±0.56	106 58.40 ±0.58	3.00 ±0.54	0.35
21	8508171804 24.82 ±0.05	34 07.36 ±0.36	106 49.82 ±0.32	7.77 ±0.54	0.14
22	8508171949 24.72 ±0.06	34 07.70 ±0.53	106 49.46 ±0.30	8.32 ±0.61	0.13
23	8508192223 50.83 ±0.07	33 56.46 ±0.46	107 00.07 ±0.37	4.65 ±0.88	0.41
24	8510131223 34.16 ±0.09	34 22.66 ±0.51	107 03.21 ±0.47	9.07 ±0.68	0.03
25	8510140421 28.40 ±0.08	34 04.82 ±0.58	106 56.00 ±0.51	3.72 ±0.48	0.09
26	8510180616 05.66 ±0.07	34 18.60 ±0.56	106 51.60 ±0.34	5.36 ±0.46	-0.35
27	8511030240 24.14 ±0.06	34 05.35 ±0.56	106 51.36 ±0.36	6.33 ±0.61	0.34
28	8602190732 51.46 ±0.08	33 59.49 ±0.47	106 59.05 ±0.43	9.73 ±0.55	-0.24
29	8602201444 41.87 ±0.08	34 01.65 ±0.56	106 59.24 ±0.38	7.39 ±0.53	-0.08
30	8602221158 06.84 ±0.06	34 01.91 ±0.33	107 04.19 ±0.33	8.15 ±0.48	0.87
31	8603100458 30.66 ±0.06	34 17.20 ±0.44	106 55.25 ±0.29	6.74 ±0.53	-0.53
32	8603250902 09.67 ±0.06	34 02.33 ±0.51	107 03.93 ±0.43	8.77 ±0.44	-0.23
33	8604051452 20.91 ±0.06	34 19.37 ±0.62	107 00.75 ±0.34	6.32 ±0.61	1.13
34	8605310031 08.16 ±0.06	34 01.02 ±0.43	107 03.62 ±0.30	8.18 ±0.46	-0.03
35	8608080708 00.39 ±0.05	33 59.44 ±0.28	106 59.90 ±0.30	4.31 ±0.60	0.15
36	8608310101 10.81 ±0.05	34 12.84 ±0.33	106 53.08 ±0.31	7.53 ±0.53	0.31
37	8611031236 57.09 ±0.06	33 59.89 ±0.41	106 58.25 ±0.33	9.73 ±0.44	-0.10

TABLE C1. Final Event Locations - Main Data Set (Continued)

	Origin Time	Lat	Long	Depth	Mag
38	8611061857 59.91 ±0.06	34 00.05 ±0.31	106 58.36 ±0.32	9.85 ±0.49	0.16
39	8708221049 44.21 ±0.06	34 09.41 ±0.27	106 44.25 ±0.33	7.81 ±0.62	0.62
40	8711030211 15.24 ±0.05	33 59.28 ±0.29	106 59.12 ±0.26	8.00 ±0.51	0.55
41	8711240352 01.86 ±0.05	33 58.32 ±0.34	106 59.41 ±0.26	5.16 ±0.48	0.12
42	8712180125 45.03 ±0.06	34 08.10 ±0.35	106 55.04 ±0.34	4.99 ±0.68	0.22
43	8712272211 55.84 ±0.06	34 23.52 ±0.49	107 03.44 ±0.29	3.31 ±0.66	0.70
44	8801211519 26.97 ±0.07	34 18.56 ±0.47	106 52.91 ±0.37	6.11 ±0.56	-0.31
45	8801250318 49.63 ±0.06	33 57.02 ±0.31	107 03.06 ±0.32	5.75 ±0.68	0.05
46	8801271359 26.01 ±0.05	34 03.01 ±0.31	107 03.12 ±0.28	8.44 ±0.41	-0.22
47	8801281749 54.92 ±0.05	34 00.98 ±0.29	107 03.06 ±0.29	8.32 ±0.46	0.81
48	8802042354 26.44 ±0.06	34 02.37 ±0.47	106 53.85 ±0.30	9.11 ±0.50	-0.10
49	8803010759 16.80 ±0.07	34 01.67 ±0.46	106 59.53 ±0.37	8.39 ±0.43	0.04
50	8803060419 16.95 ±0.05	34 01.45 ±0.37	106 59.49 ±0.27	9.05 ±0.46	0.19
51	8803170815 53.98 ±0.06	34 03.06 ±0.49	107 04.08 ±0.37	7.47 ±0.53	0.28
52	8804162123 54.52 ±0.07	34 00.60 ±0.44	106 48.80 ±0.34	6.67 ±0.65	0.33
53	8804240918 39.80 ±0.06	34 01.56 ±0.38	107 02.63 ±0.33	9.31 ±0.43	0.24
54	8804281613 18.16 ±0.06	33 58.46 ±0.35	106 55.09 ±0.32	5.48 ±0.85	0.48
55	8805032134 03.87 ±0.06	34 07.37 ±0.38	106 49.55 ±0.33	8.36 ±0.59	0.10
56	8805161521 07.23 ±0.05	34 01.87 ±0.31	107 01.69 ±0.29	9.55 ±0.42	0.28
57	8806181658 13.14 ±0.07	34 18.78 ±0.50	106 54.83 ±0.34	5.53 ±0.70	0.28
58	8807220811 00.13 ±0.10	34 17.35 ±0.59	106 40.90 ±0.58	7.63 ±0.73	0.51
59	8808181623 04.19 ±0.07	33 54.91 ±0.44	106 57.34 ±0.35	4.07 ±0.87	0.67
60	8809301428 27.19 ±0.05	34 08.08 ±0.34	106 54.61 ±0.32	3.31 ±0.82	0.39
61	8810030103 10.45 ±0.07	34 05.11 ±0.49	107 02.57 ±0.41	8.05 ±0.67	0.54
62	8810270426 49.46 ±0.06	34 07.61 ±0.49	106 55.50 ±0.36	2.82 ±0.66	0.04
63	8909272343 08.30 ±0.07	34 00.86 ±0.46	107 02.07 ±0.29	9.37 ±0.69	0.31
64	8910270650 51.26 ±0.05	33 59.83 ±0.34	106 58.51 ±0.28	9.71 ±0.50	0.68
65	9004192215 28.56 ±0.07	34 23.15 ±0.53	106 47.62 ±0.38	5.65 ±0.79	1.59
66	9005052055 55.41 ±0.09	34 27.10 ±0.79	106 52.96 ±0.32	4.92 ±0.69	0.45
67	9005060711 59.45 ±0.08	34 26.94 ±0.60	106 52.80 ±0.30	5.59 ±0.60	0.44
68	9006030008 08.24 ±0.07	34 26.65 ±0.56	106 52.95 ±0.29	4.96 ±0.53	-0.06
69	9006031114 14.01 ±0.07	34 26.71 ±0.54	106 53.32 ±0.28	4.27 ±0.47	0.16
70	9006040729 41.42 ±0.05	34 07.26 ±0.36	106 49.59 ±0.32	7.55 ±0.61	0.68
71	9006131236 06.80 ±0.09	34 27.11 ±0.69	106 52.41 ±0.32	7.10 ±0.67	0.33
72	9006200122 29.79 ±0.06	34 04.19 ±0.29	106 50.86 ±0.29	10.25 ±0.62	1.14
73	9006211554 46.24 ±0.08	34 27.16 ±0.61	106 52.55 ±0.30	6.85 ±0.55	0.65
74	9009010841 23.91 ±0.06	34 18.49 ±0.42	107 07.12 ±0.41	9.16 ±0.46	0.33
75	9009011047 32.89 ±0.06	34 18.24 ±0.39	107 07.18 ±0.34	9.43 ±0.44	0.98

Main Data Set

```
23 1982  9 19 22 25 35.00 1
 0 BAR  1 25 43.10
 1 BAR  3 25 48.70
31 BAR  0  0 30.00
 0 BMT  1 25 41.80
 1 BMT  2 25 46.10
10 BMT  2 25 44.40
 8 BMT  4 25 48.40
31 BMT  0  0 19.00
 0 CAR  1 25 41.35
 1 CAR  3 25 45.20
31 CAR  0  0 50.00
 1 LPM  3 25 50.30
31 LPM  0  0 21.00
 0 SB   2 25 38.60
 1 SB   3 25 40.90
31 SB   0  0 20.00
 0 SMC  1 25 41.00
31 SMC  0  0 47.00
 0 WTX  1 25 38.10
 1 WTX  2 25 40.10
 8 WTX  3 25 45.00
10 WTX  3 25 42.50
31 WTX  0  0 27.00


22 1983  3  4 18 20  5.00 1
 0 BAR  0 20 11.75
 1 BAR  3 20 15.45
31 BAR  0  0 58.00
 0 BMT  0 20 13.00
31 BMT  0  0 50.00
 0 CAR  0 20 13.90
10 CAR  3 20 18.05
31 CAR  0  0 55.00
 0 LAZ  0 20 11.50
 1 LAZ  3 20 14.80
31 LAZ  3  0 69.00
 0 LPM  0 20 10.60
31 LPM  0  0 60.00
 0 SMC  1 20 17.15
 1 SMC  3 20 24.80
10 SMC  1 20 21.10
31 SMC  0  0 40.00
 0 WTX  2 20 11.45
10 WTX  4 20 15.80
 8 WTX  3 20 19.20
 9 WTX  4 20 14.10
31 WTX  0  0 53.00
```

```
27 1983  4 28  2 10 25.00 1
 0 BAR  0 10 25.45
 1 BAR  3 10 28.50
31 BAR  0  0 46.00
 0 BMT  1 10 28.85
 8 BMT  3 10 37.00
10 BMT  3 10 32.90
31 BMT  3  0 28.00
 0 CAR  0 10 25.40
 1 CAR  3 10 28.30
31 CAR  3  0 42.00
 1 LAZ  3 10 33.90
 8 LAZ  4 10 37.10
 0 LPM  0 10 26.60
 1 LPM  3 10 30.55
 8 LPM  2 10 34.50
10 LPM  3 10 31.00
31 LPM  3  0 27.00
 8 MIM  4 10 47.10
 0 SB   2 10 27.30
 1 SB   4 10 31.50
 8 SB   5 10 36.00
31 SB   4  0 25.00
 0 SMC  2 10 28.70
 1 SMC  4 10 33.70
31 SMC  4  0 36.00
 0 WTX  1 10 23.00
31 WTX  4  0 26.00


26 1984  2 27  1  2  6.00 1
 0 BAR  3  2 13.10
 1 BAR  3  2 18.00
 0 BMT  1  2 13.45
 1 BMT  2  2 18.20
10 BMT  2  2 17.00
 8 BMT  4  2 20.70
31 BMT  4  0 20.00
 0 CAR  0  2 11.35
 1 CAR  2  2 14.55
10 CAR  3  2 16.10
31 CAR  2  0 18.00
 1 LPM  3  2 20.20
 0 MAG  1  2 11.50
 1 MAG  2  2 14.90
 8 MAG  2  2 18.50
31 MAG  2  0 15.00
 1 SMC  3  2 15.60
 0 SNM  0  2  8.50
```

```
 1 SNM  3  2  9.50
10 SNM  4  2 13.70
 8 SNM  4  2 16.20
31 SNM  4  0 20.00
 0 WTX  1  2  8.35
 1 WTX  3  2  9.50
 8 WTX  4  2 16.30
31 WTX  3  0 22.00


27 1984  7 16 16 12 15.00 1
 0 BAR  0 12 19.35
 1 BAR  4 12 22.75
31 BAR  0  0 23.00
 0 CAR  0 12 18.60
 1 CAR  3 12 21.20
31 CAR  0  0 25.00
 0 LAZ  1 12 23.35
 1 LAZ  2 12 28.75
 9 LAZ  4 12 25.00
10 LAZ  3 12 27.10
31 LAZ  3  0 21.00
 0 LPM  0 12 21.05
 1 LPM  2 12 25.00
 8 LPM  5 12 28.20
31 LPM  0  0 24.00
 0 MAG  1 12 21.90
 1 MAG  4 12 26.40
 9 MAG  3 12 23.90
10 MAG  3 12 25.70
 8 MAG  4 12 29.50
31 MAG  4  0 18.00
 0 SMC  2 12 22.00
 1 SMC  3 12 27.00
31 SMC  0  0 15.00
 0 WTX  2 12 17.75
 1 WTX  2 12 18.85
31 WTX  0  0 21.00


28 1984  7 22 16 55 38.00 1
 0 BAR  0 55 42.00
 1 BAR  2 55 45.00
 9 BAR  4 55 43.90
10 BAR  3 55 46.00
31 BAR  3  0 20.00
 0 CAR  0 55 41.20
 1 CAR  3 55 43.60
31 CAR  3  0 26.00
 0 LAZ  3 55 45.60
 1 LAZ  3 55 51.40
31 LAZ  3  0 15.00
 0 LPM  0 55 43.50
 1 LPM  2 55 47.40
31 LPM  2  0 26.00
 0 MAG  0 55 44.45
 1 MAG  2 55 49.00
 9 MAG  3 55 46.40
 8 MAG  3 55 52.00
31 MAG  3  0 15.00
 0 SMC  2 55 44.45
 1 SMC  3 55 49.40
31 SMC  3  0 15.00
 0 SNM  1 55 40.10
31 SNM  1  0 15.00
 0 WTX  1 55 40.20
 1 WTX  2 55 41.50
 9 WTX  3 55 42.85
31 WTX  3  0 10.00


27 1984  9  2 21 57 57.00 1
 0 BAR  1 57 46.80
 1 BAR  3 57 51.90
31 BAR  0  0 20.00
 0 CAR  1 57 43.90
 1 CAR  3 57 47.00
31 CAR  3  0 27.00
 0 LAZ  2 57 48.75
 1 LAZ  3 57 55.40
 8 LAZ  2 57 58.10
 9 LAZ  4 57 50.60
31 LAZ  3  0 19.00
 1 LPM  4 57 55.00
 8 LPM  3 57 57.00
31 LPM  3  0 16.00
 0 MAG  0 57 45.45
 1 MAG  3 57 49.50
 9 MAG  3 57 47.90
31 MAG  4  0 29.00
 0 SB   0 57 43.20
 1 SB   3 57 45.70
10 SB   4 57 47.60
31 SB   4  0 15.00
 0 SMC  1 57 43.30
 1 SMC  4 57 46.20
 0 WTX  1 57 42.45
 1 WTX  3 57 44.50
31 WTX  4  0 19.00
```

```
31 1984  9 10  6 30  5.00 1
 0 BAR  1 30 10.75
 1 BAR  3 30 16.00
31 BAR  3  0 16.00
 0 CAR  1 30  8.00
31 CAR  3  0 28.00
 0 LAZ  1 30 12.75
 1 LAZ  3 30 19.20
 9 LAZ  5 30 14.60
10 LAZ  5 30 16.80
 8 LAZ  3 30 22.20
31 LAZ  3  0 20.00
 1 LPM  4 30 18.80
 9 LPM  3 30 13.90
31 LPM  3  0 18.00
 0 MAG  2 30  9.70
 1 MAG  2 30 13.90
 8 MAG  4 30 17.80
31 MAG  3  0 19.00
 0 SB   1 30  7.05
 1 SB   3 30  9.80
10 SB   4 30 11.50
31 SB   3  0 14.00
 0 SMC  0 30  7.25
 1 SMC  3 30 10.10
31 SMC  3  0 27.00
 0 SNM  0 30  6.50
 1 SNM  2 30  8.50
31 SNM  2  0  9.00
 0 WTX  0 30  6.40
 1 WTX  3 30  8.50
31 WTX  3  0 28.00

23 1984  9 22  5 15 15.00 1
 0 BAR  0 15 20.60
 1 BAR  3 15 23.60
10 BAR  3 15 24.50
 8 BAR  3 15 27.50
31 BAR  0  0 30.00
10 CAR  3 15 25.55
 0 LAZ  1 15 22.75
 1 LAZ  3 15 27.50
10 LAZ  3 15 26.50
 9 LAZ  3 15 24.50
31 LAZ  3  0 20.00
 0 LPM  3 15 21.00
 1 LPM  4 15 24.30
31 LPM  3  0 18.00
 0 MAG  2 15 22.10
 1 MAG  4 15 26.80
10 MAG  3 15 26.10
 8 MAG  4 15 29.80
31 MAG  4  0 20.00
 0 WTX  1 15 19.05
 1 WTX  3 15 21.10
 8 WTX  3 15 26.50
31 WTX  4  0 16.00

29 1984 10  7 11 48 45.00 1
 0 BAR  1 48 47.40
31 BAR  3  0 40.00
 0 CAR  1 48 48.35
31 CAR  1  0 63.00
 0 LAZ  1 48 49.20
 1 LAZ  3 48 53.80
 8 LAZ  3 48 56.80
31 LAZ  3  0 35.00
 0 LJY  1 48 46.80
31 LJY  1  0 48.00
 0 LPM  0 48 47.60
 1 LPM  3 48 51.00
 8 LPM  5 48 55.30
31 LPM  3  0 22.00
 0 MAG  0 48 49.00
 1 MAG  4 48 53.40
10 MAG  4 48 53.00
 8 MAG  2 48 56.40
31 MAG  3  0 32.00
 0 SB   2 48 49.80
 1 SB   3 48 54.30
31 SB   3  0 25.00
 0 SMC  1 48 51.50
 1 SMC  3 48 57.70
31 SMC  3  0 46.00
 0 WTX  0 48 45.80
 1 WTX  3 48 47.85
 8 WTX  4 48 53.20
31 WTX  3  0 47.00

24 1984 10  7 13 49  5.00 1
 0 BAR  0 49 11.90
31 BAR  3  0 22.00
 0 CAR  0 49  9.80
 1 CAR  3 49 12.85
31 CAR  3  0 36.00
 0 LJY  0 49 12.65
```

```
31 LJY  1  0 11.00
 0 LPM  1 49 13.50
 1 LPM  3 49 19.20
31 LPM  3  0 12.00
 0 MAG  0 49 11.10
 1 MAG  3 49 14.95
10 MAG  2 49 14.10
 8 MAG  2 49 18.00
31 MAG  3  0 19.00
 1 SB   2 49 12.50
31 SB   3  0 12.00
 0 SMC  1 49 10.50
 1 SMC  4 49 13.90
10 SMC  3 49 13.30
31 SMC  3  0 22.00
 0 WTX  0 49  7.80
 1 WTX  3 49  9.50
31 WTX  3  0 16.00


25 1984 10 13 20 55  0.00 1
 0 BAR  0 55  4.55
 1 BAR  3 55  7.60
10 BAR  3 55  8.80
31 BAR  0  0 26.00
 0 CAR  1 55  5.55
 1 CAR  4 55  9.40
31 CAR  3  0 18.00
 1 LAZ  3 55 11.00
 0 LJY  3 55  4.20
31 LJY  3  0 24.00
 0 LPM  1 55  4.85
 1 LPM  3 55  8.10
31 LPM  3  0 17.00
 0 MAG  0 55  6.20
 1 MAG  3 55 10.40
 8 MAG  2 55 13.60
31 MAG  4  0 22.00
 0 SB   2 55  7.20
 1 SB   3 55 11.45
 9 SB   3 55  9.60
31 SB   3  0 19.00
 1 SMC  3 55 15.05
 0 WTX  1 55  3.15
 1 WTX  2 55  5.00
31 WTX  4  0 22.00


29 1984 10 29  9  8 25.00 1
 0 BAR  0  8 29.15
 1 BAR  4  8 32.60
31 BAR  3  0 28.00
 0 CAR  1  8 29.40
31 CAR  3  0 44.00
 0 LAZ  2  8 31.90
 1 LAZ  3  8 36.75
31 LAZ  3  0 18.00
 0 LJY  1  8 29.80
31 LJY  1  0 21.00
 0 LPM  2  8 30.20
 1 LPM  3  8 33.80
31 LPM  3  0 22.00
 0 MAG  1  8 31.00
 1 MAG  3  8 35.15
 9 MAG  2  8 33.30
10 MAG  4  8 34.65
 8 MAG  2  8 38.50
31 MAG  3  0 23.00
 0 SB   2  8 31.05
 1 SB   3  8 35.40
31 SB   3  0 17.00
 0 SMC  0  8 32.50
 1 SMC  3  8 38.10
10 SMC  3  8 35.70
31 SMC  3  0 32.00
 0 WTX  1  8 26.90
 1 WTX  3  8 28.50
31 WTX  3  0 26.00


20 1985  3  1 22  6  8.00 1
 0 BAR  0  6 13.55
 1 BAR  4  6 18.00
10 BAR  4  6 16.70
31 BAR  3  0 22.00
 0 CAR  0  6 12.80
 1 CAR  2  6 16.50
31 CAR  2  0 31.00
 0 LAZ  3  6 14.00
 1 LAZ  3  6 18.50
31 LAZ  3  0 29.00
 1 LPM  3  6 19.30
 8 LPM  3  6 21.50
 0 MAG  0  6 11.90
 1 MAG  2  6 15.00
10 MAG  2  6 14.50
 8 MAG  2  6 18.00
31 MAG  2  0 17.00
 0 SB   3  6 12.00
 1 SB   2  6 15.00
```

```
 1 WTX  3  6 10.50


22 1985  3 21  9 17 55.00 1
 0 BAR  2 17 58.15
 1 BAR  3 17 63.70
 8 BAR  3 17 66.40
31 BAR  0  0 25.00
 0 CAR  2 17 60.60
31 CAR  3  0 26.00
 0 LAZ  2 17 54.70
 1 LAZ  2 17 57.80
31 LAZ  3  0 20.00
 0 LPM  0 17 56.15
 1 LPM  3 17 59.90
 9 LPM  3 17 58.30
10 LPM  4 17 60.70
 8 LPM  3 17 64.00
31 LPM  3  0 22.00
 0 MAG  3 17 58.80
 1 MAG  3 17 64.30
10 MAG  4 17 62.50
 8 MAG  4 17 66.50
31 MAG  4  0 15.00
 1 MLM  4 17 65.40
 8 MLM  3 17 67.50


28 1985  3 24 11  5 45.00 1
 0 BAR  1  5 54.00
 1 BAR  4  5 59.00
 9 BAR  3  5 55.80
31 BAR  3  0 28.00
 0 CAR  1  5 55.25
 1 CAR  4  5 61.00
31 CAR  4  0 21.00
 0 LAZ  1  5 49.80
31 LAZ  1  0 34.00
 0 LJY  1  5 49.90
31 LJY  1  0 27.00
 0 LPM  3  5 53.10
31 LPM  3  0 33.00
 0 MAG  0  5 51.35
 1 MAG  5  5 54.50
 9 MAG  5  5 53.50
 8 MAG  4  5 59.10
10 MAG  3  5 55.90
31 MAG  3  0 24.00
 1 SB   3  5 58.80
10 SB   2  5 58.00
31 SB   2  0 23.00
 1 SMC  3  5 64.80
 0 WTX  3  5 51.90
 1 WTX  3  5 55.00
10 WTX  3  5 55.80
 8 WTX  4  5 58.70
31 WTX  4  0 21.00


24 1985  3 29  9 13  5.00 1
 0 BAR  2 13 13.30
 1 BAR  3 13 18.50
 9 BAR  2 13 15.10
31 BAR  3  0 34.00
 0 LAZ  0 13  9.10
 1 LAZ  4 13 11.10
31 LAZ  3  0 35.00
 0 LJY  0 13  9.10
31 LJY  4  0 26.00
 0 LPM  1 13 12.50
 1 LPM  3 13 16.90
 9 LPM  3 13 13.95
31 LPM  3  0 33.00
 0 MAG  1 13 10.60
 1 MAG  4 13 13.90
10 MAG  4 13 15.30
 8 MAG  3 13 18.30
31 MAG  4  0 19.00
 0 MLM  3 13 15.90
31 MLM  3  0 22.00
 1 SMC  3 13 24.10
31 SMC  3  0 30.00
 1 WTX  3 13 14.40
31 WTX  3  0 18.00


27 1985  4  7  0 28 45.00 1
 0 BAR  1 28 48.70
 1 BAR  4 28 52.00
31 BAR  3  0 52.00
 0 CAR  1 28 50.45
 1 CAR  3 28 55.00
31 CAR  3  0 50.00
 0 LAZ  2 28 50.20
 1 LAZ  3 28 54.20
31 LAZ  3  0 48.00
 0 LJY  0 28 47.25
31 LJY  4  0 51.00
 0 LPM  0 28 48.40
 1 LPM  4 28 51.00
```

```
31 LPM  3  0 37.00
 0 MAG  0 28 50.55
31 MAG  4  0 49.00
 0 SB   2 28 51.75
10 SB   2 28 56.00
 9 SB   2 28 53.70
 8 SB   4 28 60.30
31 SB   3  0 42.00
 0 SMC  1 28 53.75
10 SMC  3 28 57.80
 1 SMC  4 28 60.50
31 SMC  3  0 40.00
 0 WTX  1 28 48.00
31 WTX  3  0 50.00


31 1985  5  1 12 19 25.00 1
 0 BAR  2 19 30.80
 1 BAR  4 19 34.60
31 BAR  3  0 42.00
 0 CAR  0 19 29.75
 1 CAR  3 19 32.70
31 CAR  3  0 47.00
 0 LAZ  2 19 33.40
 1 LAZ  2 19 38.30
 9 LAZ  3 19 35.30
10 LAZ  4 19 37.60
 8 LAZ  4 19 42.10
31 LAZ  3  0 33.00
 0 LJY  3 19 31.50
 1 LJY  4 19 35.90
31 LJY  4  0 16.00
 0 LPM  2 19 32.25
 1 LPM  3 19 36.70
31 LPM  3  0 27.00
 0 MAG  1 19 31.35
 1 MAG  3 19 35.40
31 MAG  4  0 29.00
 0 SB   0 19 30.65
 1 SB   3 19 34.20
10 SB   4 19 36.05
 8 SB   3 19 39.30
31 SB   3  0 24.00
 0 SMC  0 19 31.95
 1 SMC  3 19 36.60
31 SMC  3  0 33.00
 0 WTX  1 19 26.60
31 WTX  3  0 37.00
```

```
25 1985  7  8  4 34 20.00 1
 0 BAR  3 34 24.40
10 BAR  3 34 28.90
31 BAR  0  0 32.00
 0 CAR  2 34 23.40
 1 CAR  3 34 26.90
31 CAR  3  0 35.00
 0 LAZ  2 34 25.25
 1 LAZ  3 34 29.70
 8 LAZ  3 34 33.25
31 LAZ  3  0 19.00
 0 LEM  3 34 20.15
10 LEM  3 34 26.70
 8 LEM  3 34 28.60
31 LEM  3  0 35.00
 0 LJY  3 34 24.20
10 LJY  3 34 28.60
31 LJY  1  0 20.00
 8 LPM  4 34 33.40
31 LPM  3  0 25.00
 1 MAG  4 34 25.80
 1 SB   3 34 26.10
31 SB   3  0 24.00
 1 SMC  4 34 29.40
 0 WTX  0 34 19.15
31 WTX  3  0 29.00


29 1985  8 17 18  4 27.20 1
 0 WTX  1  4 27.20
31 WTX  1  0 17.00
 0 LAZ  0  4 32.00
 1 LAZ  3  4 37.40
 8 LAZ  3  4 39.80
10 LAZ  3  4 35.20
31 LAZ  3  0 24.00
 0 BAR  0  4 28.30
 1 BAR  3  4 30.50
31 BAR  3  0 22.00
 0 LEM  1  4 27.30
 1 LEM  3  4 29.60
31 LEM  3  0 37.00
 0 LPM  3  4 29.40
31 LPM  3  0 30.00
 0 CAR  0  4 28.50
31 CAR  0  0 22.00
 8 SB   3  4 39.00
10 SB   3  4 35.00
 1 SMC  3  4 37.70
31 SMC  3  0 16.00
```

```
 0 LJY  1  4 29.50
31 LJY  1  0 22.00
 0 MAG  1  4 31.30
 1 MAG  3  4 36.00
 9 MAG  3  4 32.80
10 MAG  3  4 34.30
 8 MAG  3  4 39.00
31 MAG  3  0 19.00


25 1985  8 17 19 49 31.20 1
 0 MAG  0 49 31.20
 1 MAG  3 49 35.80
 8 MAG  3 49 38.80
 9 MAG  3 49 32.90
10 MAG  3 49 34.40
31 MAG  3  0 18.40
 0 SB   2 49 31.20
 1 SB   3 49 36.10
 0 LEM  0 49 27.50
31 LEM  0  0 35.00
 0 WTX  1 49 27.25
31 WTX  1  0 16.00
 0 LJY  2 49 29.50
31 LJY  2  0 17.00
 0 CAR  1 49 28.60
31 CAR  1  0 34.00
 0 LPM  1 49 29.35
31 LPM  1  0 25.00
 0 LAZ  1 49 31.90
 1 LAZ  3 49 36.90
 8 LAZ  3 49 39.50
10 LAZ  3 49 35.20
31 LAZ  3  0 19.00
 0 BAR  0 49 28.00
31 BAR  0  0 22.00


31 1985  8 19 22 23 51.00 1
 0 BAR  0 23 57.80
 1 BAR  3 23 63.20
10 BAR  3 23 62.20
31 BAR  3  0 31.00
 0 CAR  1 23 54.90
31 CAR  1  0 35.00
 0 LAZ  2 23 59.95
 1 LAZ  3 23 66.00
 9 LAZ  2 23 61.30
 8 LAZ  3 23 68.70
31 LAZ  3  0 35.00
```

```
 0 LEM  1 23 55.00
31 LEM  1  0 32.00
 0 LJY  3 23 59.10
 1 LJY  3 23 65.00
31 LJY  3  0 22.00
 0 LPM  2 23 59.45
 1 LPM  3 23 66.00
31 LPM  3  0 35.00
 0 MAG  1 23 56.30
 1 MAG  3 23 60.50
31 MAG  3  0 26.00
 0 SB   1 23 54.10
 1 SB   3 23 56.50
31 SB   3  0 24.00
 0 SMC  2 23 54.10
 1 SMC  3 23 56.50
31 SMC  3  0 25.00
 0 WTX  1 23 53.40
 1 WTX  3 23 55.40
31 WTX  3  0 20.00


25 1985 10 13 12 23 35.00 1
 0 BAR  1 23 42.25
 1 BAR  3 23 47.90
31 BAR  0  0 14.00
 1 CAR  2 23 50.85
 0 LAZ  0 23 36.25
 1 LAZ  3 23 37.45
31 LAZ  3  0 26.00
 0 LEM  0 23 38.50
 1 LEM  3 23 41.70
31 LEM  3  0 42.00
 0 LJY  1 23 37.60
31 LJY  1  0 20.00
 0 LPM  2 23 40.90
31 LPM  3  0 16.00
 0 MAG  1 23 39.30
 1 MAG  3 23 43.20
 8 MAG  4 23 45.75
31 MAG  4  0 19.00
 1 MLM  3 23 48.40
 0 WTX  2 23 40.20
 1 WTX  2 23 44.55
 9 WTX  3 23 41.70
 8 WTX  3 23 47.30
10 WTX  4 23 43.30
31 WTX  3  0 16.00
```

```
21 1985 10 14  4 21 26.00 1
 1 BAR  3 21 37.05
 0 CAR  2 21 32.50
 1 CAR  3 21 35.20
31 CAR  3  0 30.00
 1 LAZ  3 21 40.30
 0 LEM  1 21 30.20
 1 LEM  2 21 31.50
10 LEM  2 21 36.30
 8 LEM  3 21 38.60
31 LEM  3  0 22.00
 0 LPM  3 21 34.30
 1 LPM  3 21 38.80
 8 LPM  3 21 43.00
31 LPM  3  0 22.00
 0 MAG  2 21 33.40
10 MAG  3 21 38.10
 8 MAG  3 21 41.00
31 MAG  3  0 18.00
 0 WTX  1 21 28.90
 1 WTX  3 21 29.60
31 WTX  3  0 18.00

22 1985 10 18  6 16  0.00 1
 0 BAR  1 16 10.40
31 BAR  0  0 14.00
 1 CAR  4 16 17.90
 0 LAZ  3 16 10.30
 1 LAZ  3 16 14.15
31 LAZ  0  0 12.00
 0 LEM  0 16  8.95
 1 LEM  2 16 11.45
 8 LEM  3 16 16.50
10 LEM  4 16 13.80
31 LEM  0  0 19.00
 0 LJY  1 16  7.20
 1 LJY  4 16  8.70
 0 LPM  0 16  9.05
 1 LPM  3 16 12.10
10 LPM  2 16 14.10
 8 LPM  2 16 16.55
31 LPM  0  0 15.00
 0 MAG  2 16 12.20
10 MAG  2 16 16.00
 8 MAG  3 16 19.85
31 MAG  0  0 16.00

22 1985 11  3  2 40 20.00 1
 0 BAR  1 40 28.05
 1 BAR  4 40 30.65
31 BAR  3  0 30.00
 0 CAR  1 40 27.45
 1 CAR  3 40 30.00
31 CAR  3  0 36.00
10 LAZ  2 40 35.30
31 LAZ  3  0 24.00
 0 LPM  1 40 29.50
 1 LPM  2 40 33.15
 9 LPM  2 40 31.30
 8 LPM  4 40 36.80
31 LPM  3  0 23.00
 0 MAG  2 40 30.30
 1 MAG  3 40 34.60
 9 MAG  2 40 32.45
 8 MAG  4 40 37.65
31 MAG  4  0 24.00
 1 SMC  4 40 35.60
 0 WTX  0 40 25.80
 1 WTX  3 40 27.40
31 WTX  3  0 24.00

28 1986  2 19  7 32 51.00 1
 0 BAR  1 32 57.95
31 BAR  1  0 18.00
 0 CAR  1 32 55.65
 1 CAR  3 32 58.90
31 CAR  3  0 25.00
 1 LAZ  3 32 65.60
 0 LEM  1 32 55.00
 1 LEM  3 32 57.70
 8 LEM  4 32 61.10
31 LEM  4  0 25.00
 0 LPM  3 32 59.60
 1 LPM  3 32 65.10
31 LPM  3  0 14.00
 0 MAG  1 32 56.65
 1 MAG  3 32 60.55
 9 MAG  3 32 58.40
10 MAG  2 32 59.70
 8 MAG  4 32 63.70
31 MAG  3  0 17.00
 0 SB   3 32 55.25
 1 SB   3 32 57.80
31 SB   3  0 12.00
 0 SMC  2 32 55.80
 1 SMC  3 32 59.50
31 SMC  3  0 16.00
```

```
 0 WTX  0 32 53.70
 1 WTX  3 32 55.60
31 WTX  3  0 10.00


20 1986  2 20 14 44 40.00 1
 0 BAR  1 44 47.95
 1 BAR  3 44 52.50
31 BAR  3  0 21.00
 1 CAR  3 44 49.20
 1 LAZ  3 44 54.80
 8 LAZ  4 44 57.70
 0 LEM  2 44 44.70
 1 LEM  2 44 46.80
 8 LEM  2 44 51.30
 1 LPM  4 44 54.80
 8 LPM  5 44 57.40
 0 MAG  0 44 46.50
 1 MAG  3 44 50.10
 9 MAG  4 44 48.80
 8 MAG  3 44 54.50
31 MAG  3  0 21.00
 1 SMC  3 44 50.80
 0 WTX  0 44 43.45
 1 WTX  2 44 44.80
31 WTX  2  0 15.00


27 1986  2 22 11 58  8.00 1
 0 BAR  2 58 14.10
10 BAR  3 58 17.20
31 BAR  3  0 20.00
 0 CAR  0 58 12.45
 1 CAR  2 58 16.70
31 CAR  2  0 25.00
 0 LAZ  3 58 14.00
 1 LAZ  3 58 19.20
31 LAZ  3  0 20.00
 0 LEM  1 58 10.05
31 LEM  1  0 27.00
 0 LJY  1 58 13.70
 0 LPM  1 58 15.05
31 LPM  1  0 21.00
 0 MAG  0 58 10.60
 1 MAG  2 58 13.40
31 MAG  2  0 21.00
 1 SB   3 58 11.50
 0 SMC  0 58 11.95
 1 SMC  3 58 15.95
10 SMC  3 58 15.40
31 SMC  3  0 19.00
 0 WTX  0 58  9.25
 1 WTX  2 58 11.05
10 WTX  2 58 13.60
 8 WTX  3 58 16.25
31 WTX  3 58 14.00


24 1986  3 10  4 58 32.00 1
 0 BAR  2 58 36.15
 1 BAR  3 58 39.90
31 BAR  3  0 16.00
 0 LAZ  0 58 34.85
 1 LAZ  3 58 38.00
31 LAZ  3  0 15.00
 0 LEM  1 58 33.25
 1 LEM  3 58 35.20
31 LEM  3  0 12.00
 0 LJY  0 58 32.55
31 LJY  0  0 10.00
 0 LPM  0 58 35.10
 1 LPM  2 58 38.50
 8 LPM  2 58 42.20
 9 LPM  3 58 37.50
10 LPM  3 58 39.05
31 LPM  3  0 12.00
 0 MAG  1 58 36.20
 9 MAG  3 58 38.20
 8 MAG  3 58 43.20
31 MAG  3  0 17.00
 0 WTX  3 58 34.60
 1 WTX  3 58 37.75
31 WTX  3  0 10.00


26 1986  3 25  9  2 10.00 1
 0 BAR  3  2 17.00
 1 BAR  4  2 22.50
10 BAR  5  2 19.50
31 BAR  0  0 18.00
 1 CAR  3  2 19.10
 8 LAZ  5  2 24.60
 0 LEM  0  2 12.70
 1 LEM  3  2 15.20
10 LEM  3  2 16.40
 8 LEM  2  2 18.70
31 LEM  3  0 20.00
 1 LPM  3  2 24.40
31 LPM  0  0 16.00
 0 MAG  1  2 13.30
```

```
 1 MAG  3  2 16.20
10 MAG  4  2 17.30
31 MAG  4  0 16.00
 0 SB   0  2 12.50
 1 SB   3  2 14.70
31 SB   2  0 13.00
 0 SMC  4  2 14.80
 0 WTX  2  2 12.00
 1 WTX  3  2 13.80
10 WTX  2  2 16.35
 8 WTX  3  2 19.00
31 WTX  3  0 17.00

21 1986  4  5 14 52 20.00 1
 0 BAR  3 52 27.80
 1 BAR  3 52 32.90
31 BAR  2  0 15.00
 1 CAR  4 52 35.30
 0 LAZ  0 52 23.60
 1 LAZ  3 52 25.60
31 LAZ  3  0 25.00
 0 LEM  3 52 24.00
 1 LEM  3 52 26.40
10 LEM  3 52 28.70
 8 LEM  4 52 31.50
31 LEM  2  0 20.00
 0 LJY  0 52 23.40
31 LJY  3 52 26.00
 0 LPM  0 52 26.75
 8 LPM  3 52 34.30
31 LPM  3  0 30.00
 0 MAG  2 52 25.60
10 MAG  4 52 29.40
 8 MAG  3 52 32.60
31 MAG  3  0 25.00

29 1986  5 31  0 31  5.00 1
 0 BAR  1 31 15.40
 1 BAR  3 31 20.90
31 BAR  3  0 23.00
 0 CAR  1 31 13.55
 1 CAR  3 31 17.40
31 CAR  3  0 29.00
 0 LEM  1 31 11.45
 1 LEM  3 31 14.00
10 LEM  3 31 15.45
 8 LEM  3 31 18.50
31 LEM  3  0 22.00
 0 LPM  3 31 16.40
 1 LPM  3 31 22.80
31 LPM  3  0 19.00
 0 MAG  0 31 12.15
 1 MAG  3 31 15.20
 9 MAG  4 31 14.15
31 MAG  4  0 16.00
 0 SB   0 31 10.85
 1 SB   2 31 12.85
31 SB   2  0 15.00
 0 SMC  3 31 12.90
 1 SMC  3 31 16.60
31 SMC  3  0 18.00
 0 WTX  0 31 10.55
 1 WTX  2 31 12.40
 8 WTX  2 31 17.30
10 WTX  2 31 14.70
31 WTX  3  0 17.00

30 1986  8  8  7  8  0.00 1
 0 BAR  1  8  6.90
 1 BAR  2  8 11.70
31 BAR  3  0 19.00
 0 CAR  0  8  4.60
 1 CAR  2  8  7.90
31 CAR  3  0 38.00
 0 LAZ  0  8  8.50
 1 LAZ  3  8 14.20
10 LAZ  2  8 12.90
 9 LAZ  4  8 10.10
31 LAZ  3  0 19.00
 0 LEM  0  8  3.55
 1 LEM  3  8  6.10
31 LEM  3  0 34.00
 1 LPM  3  8 14.55
 8 LPM  4  8 17.20
31 LPM  3  0 24.00
 0 MAG  1  8  5.25
 1 MAG  1  8  9.00
 8 MAG  2  8 12.90
10 MAG  4  8  9.80
31 MAG  4  0 17.00
 0 SB   2  8  3.60
31 SB   2  0 15.00
 0 SMC  0  8  4.55
 1 SMC  3  8  8.05
31 SMC  3  0 27.00
 0 WTX  1  8  2.15
 1 WTX  2  8  3.50
```

```
31 WTX  3  0 20.00


29 1986  8 31  1  1 10.00 1
 0 BAR  0  1 15.15
 1 BAR  3  1 18.40
31 BAR  3  0 25.00
 0 CAR  3  1 16.25
 1 CAR  3  1 20.50
31 CAR  3  0 38.00
 1 LAZ  3  1 20.30
31 LAZ  3  0 23.00
 0 LJY  0  1 13.90
31 LJY  4  0 33.00
 0 LPM  0  1 15.10
 1 LPM  4  1 18.00
 9 LPM  3  1 17.00
31 LPM  3  0 35.00
 0 MAG  1  1 16.40
 1 MAG  3  1 20.40
 8 MAG  3  1 23.50
31 MAG  4  0 21.00
 0 SB   1  1 17.50
10 SB   2  1 21.00
31 SB   2  0 19.00
 0 SMC  1  1 19.50
 1 SMC  2  1 26.10
10 SMC  2  1 23.00
31 SMC  3  0 20.00
 0 WTX  1  1 13.75
 1 WTX  3  1 16.10
 8 WTX  3  1 20.70
31 WTX  3  0 26.00


32 1986 11  3 12 36 55.00 1
 9 BAR  3 36 64.85
 1 BAR  2 36 67.90
31 BAR  2  0 11.00
 0 CAR  1 36 61.20
 1 CAR  3 36 64.10
31 CAR  3  0 28.00
10 LAZ  3 36 67.80
31 LAZ  3  0 16.00
 1 LEM  3 36 63.00
 9 LEM  3 36 62.40
 8 LEM  2 36 66.80
31 LEM  2  0 16.00
 0 LJY  3 36 64.20
 0 LPM  3 36 65.00
 1 LPM  3 36 70.50
31 LPM  3  0 17.00
 0 MAG  0 36 62.45
 1 MAG  3 36 66.20
 9 MAG  2 36 64.20
10 MAG  3 36 65.40
 8 MAG  3 36 69.40
31 MAG  3  0 18.00
 0 SB   0 36 60.90
 1 SB   3 36 64.05
31 SB   3  0 23.00
 0 SMC  1 36 61.80
 1 SMC  3 36 65.50
10 SMC  3 36 64.60
31 SMC  3  0 25.00
 0 WTX  0 36 59.20
 1 WTX  3 36 60.80
31 WTX  3  0 17.00


28 1986 11  6 18 58  0.00 1
 0 BAR  1 58  6.20
 1 BAR  3 58 10.50
31 BAR  3  0 24.00
 0 CAR  1 58  4.10
 1 CAR  3 58  7.15
31 CAR  3  0 26.00
 0 LAZ  3 58  8.00
 1 LAZ  2 58 13.75
10 LAZ  2 58 10.80
 8 LAZ  2 58 16.00
31 LAZ  2  0 25.00
 0 LJY  3 58  7.20
 1 LJY  3 58 12.00
 0 LPM  3 58  7.80
 1 LPM  3 58 13.20
31 LPM  3  0 25.00
 0 MAG  0 58  5.15
31 MAG  0  0 28.00
 0 SB   0 58  3.80
 1 SB   2 58  6.80
31 SB   2  0 15.00
 0 SMC  0 58  4.55
 1 SMC  3 58  8.20
10 SMC  3 58  7.40
31 SMC  3  0 30.00
 0 WTX  0 58  2.00
 1 WTX  2 58  3.60
31 WTX  2  0 15.00
```

```
35 1987  8 22 10 49 44.00 1
 0 BAR  0 49 46.35
31 BAR  0  0 55.00
 0 CAR  0 49 48.25
 1 CAR  2 49 51.40
31 CAR  2  0 24.00
 0 LAZ  0 49 52.05
 1 LAZ  2 49 57.75
 9 LAZ  2 49 53.50
 8 LAZ  4 49 60.10
31 LAZ  4  0 41.00
 0 LEM  0 49 48.15
 0 LJY  1 49 49.05
 1 LJY  4 49 52.90
 9 LJY  3 49 51.55
10 LJY  4 49 53.00
31 LJY  4  0 20.00
 0 LPM  0 49 47.50
31 LPM  0  0 47.00
 0 MAG  0 49 52.00
 1 MAG  3 49 57.50
 9 MAG  2 49 53.25
31 MAG  2  0 32.00
 8 MLM  2 49 69.10
 0 SB   1 49 52.05
 1 SB   2 49 58.00
 9 SB   3 49 53.40
10 SB   4 49 55.70
 8 SB   4 49 61.00
31 SB   4  0 33.00
 0 SMC  1 49 52.70
 1 SMC  3 49 59.00
31 SMC  3  0 36.00
 0 WTX  1 49 48.00
 1 WTX  3 49 50.70
31 WTX  3  0 26.00

34 1987 11  3  2 11 15.00 1
 0 BAR  0 11 21.65
 1 BAR  3 11 26.55
31 BAR  0  0 30.00
 0 BMT  4 11 22.40
 1 BMT  1 11 27.60
10 BMT  2 11 25.30
 8 BMT  2 11 30.60
31 BMT  0  0 19.00
 0 CAR  0 11 19.45
 1 CAR  4 11 22.50
31 CAR  0  0 40.00
 0 LAZ  2 11 23.45
 1 LAZ  2 11 29.30
10 LAZ  3 11 26.50
 8 LAZ  4 11 31.80
31 LAZ  3  0 29.00
 0 LEM  0 11 18.75
 1 LEM  3 11 21.35
31 LEM  3  0 40.00
 0 LJY  0 11 22.55
 0 LPM  1 11 22.90
 1 LPM  2 11 28.90
31 LPM  0  0 31.00
10 MLM  4 11 33.90
 0 SB   0 11 18.80
 1 SB   3 11 21.50
31 SB   2  0 40.00
 0 SMC  0 11 19.55
 1 SMC  3 11 22.60
31 SMC  3  0 33.00
 0 WTX  1 11 17.30
 1 WTX  3 11 19.00
 8 WTX  5 11 24.50
31 WTX  3  0 28.00

32 1987 11 24  3 52  0.00 1
 0 BAR  0 52  8.40
 1 BAR  3 52 13.40
10 BAR  2 52 12.55
31 BAR  0  0 23.00
 0 BMT  3 52  9.10
 1 BMT  3 52 14.40
 9 BMT  2 52 11.40
10 BMT  2 52 13.00
 8 BMT  2 52 17.10
31 BMT  0  0 20.00
 0 CAR  0 52  5.85
 1 CAR  3 52  9.10
31 CAR  0  0 30.00
 0 LAZ  1 52 10.30
 1 LAZ  3 52 16.40
 9 LAZ  2 52 12.35
10 LAZ  2 52 14.25
31 LAZ  3  0 18.00
 0 LEM  0 52  5.45
 1 LEM  3 52  8.30
 0 LPM  1 52 10.10
 1 LPM  2 52 16.10
10 LPM  3 52 14.20
```

```
31 LPM  0  0 23.00
 0 SB   0 52  5.20
 1 SB   2 52  7.50
31 SB   2  0 18.00
 0 SMC  1 52  5.70
 1 SMC  3 52  8.80
31 SMC  3  0 25.00
 0 WTX  0 52  3.95
 1 WTX  2 52  5.55


30 1987 12 18  1 25 44.00 1
 0 BAR  2 25 49.50
 1 BAR  2 25 52.80
 9 BAR  3 25 52.20
31 BAR  3  0 23.00
 0 BMT  2 25 51.30
 1 BMT  3 25 55.50
 9 BMT  2 25 53.40
 8 BMT  4 25 58.90
31 BMT  4  0 22.00
 0 CAR  1 25 49.60
 1 CAR  3 25 53.00
31 CAR  3  0 26.00
 0 LAZ  1 25 51.25
 1 LAZ  2 25 55.50
 8 LAZ  4 25 59.00
31 LAZ  4  0 27.00
 0 LEM  0 25 46.30
31 LEM  0  0 28.00
 0 LJY  1 25 49.55
31 LJY  1  0 20.00
 0 LPM  1 25 50.30
 1 LPM  2 25 54.25
 9 LPM  4 25 52.90
31 LPM  4  0 24.00
 0 SMC  1 25 52.15
 1 SMC  3 25 57.40
31 SMC  3  0 26.00
 0 WTX  1 25 46.30
 1 WTX  3 25 47.50
31 WTX  3  0 22.00


29 1987 12 27 22 11 55.00 1
 0 BAR  0 11 63.90
 8 BAR  3 11 72.80
31 BAR  3  0 24.00
 0 BMT  0 11 59.90
31 BMT  0  0 41.00
 0 CAR  1 11 65.50
 1 CAR  3 11 72.70
 8 CAR  3 11 75.70
10 CAR  4 11 69.70
31 CAR  3  0 25.00
 0 LAZ  0 11 57.20
31 LAZ  0  0 51.00
 0 LEM  0 11 60.15
31 LEM  3  0 40.00
 0 LJY  1 11 59.00
31 LJY  1  0 40.00
 0 LPM  0 11 62.50
 1 LPM  3 11 67.40
31 LPM  3  0 43.00
10 MLM  3 11 68.30
 1 SB   3 11 70.40
 8 SB   3 11 73.40
 0 SMC  1 11 67.50
 1 SMC  3 11 76.25
31 SMC  3  0 42.00
 0 WTX  1 11 62.20
 1 WTX  2 11 66.50
 8 WTX  3 11 70.00
31 WTX  3  0 25.00


24 1988  1 21 15 19 26.00 1
 1 BAR  3 19 35.75
 0 BMT  0 19 33.15
 1 BMT  4 19 37.50
 8 BMT  4 19 40.70
 9 BMT  4 19 35.00
10 BMT  4 19 37.00
31 BMT  4  0 15.00
 1 CAR  3 19 39.50
 0 LAZ  1 19 31.50
 1 LAZ  2 19 34.80
 9 LAZ  4 19 34.30
10 LAZ  3 19 35.95
31 LAZ  3  0 15.00
 0 LEM  1 19 30.10
 1 LEM  2 19 32.40
 8 LEM  3 19 37.10
31 LEM  3  0 13.00
 0 LJY  1 19 28.40
 0 LPM  1 19 30.80
 1 LPM  3 19 33.80
 9 LPM  3 19 33.20
31 LPM  3  0 20.00
 0 WTX  1 19 31.60
```

```
 1 WTX  2 19 35.00


33 1988  1 25  3 18 50.00 1
 0 BAR  1 18 57.20
 1 BAR  3 18 63.10
 8 BAR  5 18 65.50
 9 BAR  4 18 59.30
 0 BMT  0 18 56.70
 1 BMT  2 18 61.85
10 BMT  3 18 61.00
 9 BMT  4 18 59.10
31 BMT  4  0 29.00
 0 CAR  0 18 54.65
 1 CAR  3 18 58.35
31 CAR  3  0 28.00
 1 LAZ  4 18 64.80
 0 LEM  1 18 53.80
 1 LEM  3 18 57.20
 8 LEM  3 18 61.00
31 LEM  3  0 19.00
 0 LJY  0 18 57.70
 1 LJY  3 18 64.20
 9 LJY  3 18 59.30
31 LJY  3  0 15.00
 1 LPM  3 18 65.50
 9 LPM  3 18 60.15
 8 LPM  5 18 67.65
 0 SB   1 18 52.20
 1 SB   3 18 54.20
31 SB   3  0 15.00
 0 SMC  0 18 53.15
 1 SMC  3 18 55.90
31 SMC  3  0 28.00
 0 WTX  0 18 52.50
 1 WTX  3 18 54.60
31 WTX  3  0 18.00


34 1988  1 27 13 59 25.00 1
 0 BAR  1 59 33.00
 1 BAR  3 59 38.00
31 BAR  3  0 16.00
 0 BMT  0 59 31.65
 1 BMT  2 59 35.80
 8 BMT  4 59 38.95
10 BMT  2 59 35.00
31 BMT  2  0 15.00
 0 CAR  0 59 31.50
 1 CAR  3 59 35.50
31 CAR  3  0 20.00
 1 LAZ  2 59 37.90
 8 LAZ  5 59 40.10
 0 LEM  1 59 28.85
 1 LEM  3 59 31.00
10 LEM  4 59 33.20
 8 LEM  4 59 35.20
31 LEM  4  0 17.00
 0 LPM  1 59 33.80
 1 LPM  3 59 39.60
 8 LPM  3 59 41.90
31 LPM  3  0 27.00
 0 LJY  0 59 32.55
31 LJY  0  0 12.00
 0 SB   0 59 29.00
 1 SB   3 59 31.60
31 SB   3  0 13.00
 1 SMC  3 59 35.50
10 SMC  4 59 34.50
 0 WTX  0 59 28.15
 1 WTX  3 59 29.50
10 WTX  2 59 32.50
 8 WTX  2 59 34.90
31 WTX  2  0 17.00


37 1988  1 28 17 49 55.00 1
 0 BAR  0 49 62.10
 1 BAR  2 49 67.60
10 BAR  5 49 65.20
31 BAR  5  0 43.00
 0 BMT  0 49 61.05
 1 BMT  4 49 65.70
 9 BMT  5 49 62.50
31 BMT  5  0 45.00
 0 CAR  2 49 60.25
 1 CAR  3 49 63.80
31 CAR  3  0 47.00
 0 LAZ  1 49 62.30
 8 LAZ  4 49 69.70
31 LAZ  4  0 49.00
 0 LEM  0 49 58.15
 1 LEM  3 49 60.60
 8 LEM  3 49 65.30
31 LEM  3  0 30.00
 0 LJY  0 49 61.90
 1 LJY  3 49 67.80
10 LJY  2 49 65.40
31 LJY  2  0 25.00
 0 LPM  0 49 63.25
```

```
 1 LPM  3 49 69.50
31 LPM  3  0 35.00
 0 SB   0 49 57.80
 1 SB   3 49 59.75
31 SB   3  0 40.00
 0 SMC  0 49 59.70
 1 SMC  4 49 63.30
 9 SMC  3 49 61.80
31 SMC  3  0 45.00
 0 WTX  0 49 57.25
 1 WTX  3 49 58.70
10 WTX  3 49 61.35
 8 WTX  3 49 63.75
31 WTX  3  0 40.00


27 1988  2  4 23 54 26.00 1
 0 BAR  0 54 31.25
31 BAR  3  0 36.00
 0 BMT  2 54 34.00
 1 BMT  3 54 39.35
 8 BMT  4 54 41.60
 9 BMT  2 54 35.20
10 BMT  3 54 36.90
31 BMT  3  0 15.00
 0 CAR  1 54 29.80
 1 CAR  3 54 32.20
31 CAR  3  0 22.00
 0 LAZ  3 54 34.50
 1 LAZ  3 54 40.00
31 LAZ  3  0 16.00
 0 LPM  3 54 33.10
10 LPM  2 54 36.00
 1 LPM  3 54 37.70
31 LPM  3  0 20.00
 0 SB   0 54 31.45
 1 SB   2 54 35.20
31 SB   2  0 14.00
 0 SMC  2 54 32.15
 1 SMC  4 54 36.30
31 SMC  4  0 18.00
 0 WTX  0 54 28.20
 1 WTX  3 54 29.50
31 WTX  3  0 14.00


32 1988  3  1  7 59 15.00 1
 0 BAR  0 59 23.10
 1 BAR  3 59 27.75
31 BAR  0  0 32.00
 0 BMT  2 59 23.20
 1 BMT  3 59 28.15
10 BMT  2 59 26.80
 8 BMT  5 59 31.20
31 BMT  0  0 21.00
 0 CAR  1 59 21.20
 1 CAR  3 59 24.60
 9 CAR  3 59 23.60
31 CAR  1  0 28.00
 1 LAZ  3 59 29.90
10 LAZ  2 59 27.45
 8 LAZ  4 59 31.90
 0 LPM  3 59 24.20
 1 LPM  3 59 29.90
 9 LPM  3 59 25.60
31 LPM  0  0 23.00
 0 SB   3 59 20.30
 1 SB   2 59 23.40
31 SB   2  0 15.00
 0 SMC  2 59 21.65
 1 SMC  3 59 25.60
31 SMC  1  0 22.00
 0 SNM  0 59 18.50
 1 SNM  3 59 19.90
31 SNM  1  0 15.00
 0 WTX  0 59 18.55
 1 WTX  4 59 19.80
 8 WTX  3 59 24.75
31 WTX  3  0 16.00


29 1988  3  6  4 19 17.00 1
 0 BAR  0 19 23.25
 1 BAR  3 19 27.80
31 BAR  3  0 33.00
 0 BMT  0 19 23.50
 1 BMT  3 19 28.40
 8 BMT  3 19 31.40
10 BMT  3 19 26.60
31 BMT  3  0 22.00
 0 CAR  0 19 21.40
 1 CAR  3 19 24.75
31 CAR  3  0 35.00
10 LAZ  2 19 27.60
 0 LJY  3 19 23.50
 9 LJY  4 19 25.00
 0 LPM  2 19 24.60
 1 LPM  3 19 29.90
 9 LPM  4 19 26.00
31 LPM  4  0 25.00
```

```
 0 SB   0 19 20.60
 1 SB   3 19 23.60
 8 SB   5 19 27.50
31 SB   5  0 16.00
 0 SMC  1 19 21.80
 1 SMC  3 19 26.00
31 SMC  3  0 25.00
 0 WTX  0 19 18.80
 1 WTX  3 19 20.30
 8 WTX  3 19 25.00
31 WTX  3  0 15.00


27 1988  3 17  8 15 56.00 1
 0 BAR  0 15 61.00
 1 BAR  3 15 66.60
10 BAR  4 15 64.50
31 BAR  4  0 35.00
 0 BMT  2 15 59.60
 0 CAR  2 15 59.80
 1 CAR  3 15 63.60
 0 LAZ  2 15 60.50
31 LAZ  4  0 28.00
 0 LJY  2 15 60.50
 1 LJY  3 15 65.20
31 LJY  3  0 20.00
 0 LPM  1 15 62.30
 1 LPM  3 15 68.50
10 LPM  3 15 65.60
31 LPM  3  0 29.00
 0 SB   0 15 56.80
 1 SB   2 15 58.70
 9 SB   4 15 59.40
31 SB   4  0 19.00
 0 SMC  3 15 59.30
 1 SMC  3 15 63.60
 0 WTX  0 15 56.25
 1 WTX  3 15 57.95
 8 WTX  3 15 63.35
10 WTX  3 15 60.90
31 WTX  3  0 24.00


28 1988  4 16 21 23 54.00 1
 0 BAR  0 23 58.45
 1 BAR  3 23 61.40
31 BAR  3  0 37.00
 0 BMT  0 23 63.25
 1 BMT  3 23 69.65
 8 BMT  3 23 71.70
10 BMT  2 23 67.10
31 BMT  2  0 20.00
 0 CAR  1 23 56.40
 1 CAR  3 23 58.00
31 CAR  3  0 36.00
 0 LAZ  3 23 63.60
 1 LAZ  3 23 70.20
10 LAZ  5 23 66.50
 8 LAZ  5 23 72.50
31 LAZ  3  0 20.00
 0 LPM  2 23 60.70
 1 LPM  3 23 65.30
31 LPM  3  0 25.00
 0 SMC  1 23 60.30
 1 SMC  3 23 64.30
31 SMC  3  0 30.00
 0 SNM  1 23 57.15
 1 SNM  3 23 59.20
31 SNM  3  0 25.00
 0 WTX  1 23 57.00
 1 WTX  3 23 59.10
31 WTX  3  0 22.00


36 1988  4 24  9 18 41.00 1
 0 BAR  0 18 46.80
 1 BAR  3 18 52.00
31 BAR  3  0 21.00
 0 BMT  0 18 45.90
 1 BMT  3 18 50.10
 9 BMT  3 18 47.50
10 BMT  4 18 48.80
31 BMT  4  0 29.00
 0 CAR  1 18 45.05
 1 CAR  4 18 48.60
 9 CAR  4 18 46.90
10 CAR  3 18 48.00
31 CAR  3  0 28.00
 0 LAZ  2 18 47.15
 1 LAZ  3 18 53.00
31 LAZ  3  0 26.00
 0 LJY  1 18 46.60
 1 LJY  3 18 51.90
31 LJY  3  0 17.00
 0 LPM  1 18 48.10
 1 LPM  3 18 54.15
31 LPM  3  0 27.00
 0 SB   2 18 43.00
 1 SB   3 18 45.15
31 SB   3  0 23.00
```

```
 0 SMC  1 18 44.80
 1 SMC  3 18 48.90
10 SMC  3 18 47.80
31 SMC  3  0 25.00
 0 SNM  0 18 42.15
31 SNM  0  0 35.00
 0 WTX  0 18 42.05
 1 WTX  3 18 43.70
10 WTX  2 18 46.15
 8 WTX  2 18 48.50
31 WTX  2  0 18.00


24 1988  4 28 16 13 18.00 1
 0 BAR  1 13 23.80
 1 BAR  3 13 27.90
 0 BMT  1 13 26.10
 1 BMT  2 13 32.00
 8 BMT  3 13 34.70
10 BMT  3 13 30.20
 9 BMT  3 13 27.70
31 BMT  3  0 27.00
 0 CAR  1 13 21.20
 1 CAR  3 13 23.60
 0 LAZ  0 13 26.85
 1 LAZ  3 13 33.30
 8 LAZ  5 13 36.10
31 LAZ  5  0 30.00
 0 LPM  1 13 25.60
 1 LPM  4 13 31.30
31 LPM  4  0 39.00
 0 SB   0 13 22.60
 1 SB   2 13 26.00
31 SB   2  0 20.00
 0 SMC  0 13 22.35
 1 SMC  3 13 25.70
31 SMC  3  0 37.00
 0 SNM  2 13 20.20


24 1988  5  3 21 34  4.00 1
 0 BAR  0 34  7.20
 1 BAR  3 34  9.75
31 BAR  3  0 28.00
 0 BMT  0 34 11.45
 1 BMT  2 34 16.85
 9 BMT  2 34 13.10
10 BMT  2 34 14.50
 8 BMT  3 34 19.40
31 BMT  3  0 18.00
 0 CAR  0 34  7.65
31 CAR  0  0 26.00
 0 LAZ  1 34 11.25
 1 LAZ  3 34 16.70
10 LAZ  3 34 14.30
 8 LAZ  3 34 19.15
31 LAZ  3  0 23.00
 0 LJY  1 34  8.70
 1 LJY  3 34 12.20
31 LJY  3  0 16.00
 0 LPM  2 34  8.50
 1 LPM  3 34 12.00
31 LPM  3  0 22.00
 0 SNM  3 34  6.30
 1 SNM  3 34  8.50


34 1988  5 16 15 21  7.00 1
 0 BAR  0 21 13.60
 1 BAR  3 21 18.75
31 BAR  3  0 27.00
 0 BMT  0 21 13.40
 1 BMT  3 21 17.75
 9 BMT  4 21 14.60
10 BMT  3 21 16.00
31 BMT  3  0 26.00
 0 LAZ  1 21 14.55
 1 LAZ  3 21 19.90
 9 LAZ  4 21 15.80
 8 LAZ  3 21 21.80
31 LAZ  3  0 30.00
 0 LPM  1 21 15.60
 1 LPM  3 21 21.50
 9 LPM  3 21 16.70
10 LPM  3 21 18.80
31 LPM  2  0 30.00
 0 SB   0 21 10.50
 1 SB   3 21 12.80
31 SB   3  0 18.00
 0 SMC  0 21 12.35
 1 SMC  3 21 16.50
10 SMC  4 21 15.50
31 SMC  4  0 32.00
 0 SNM  0 21  9.55
 1 SNM  3 21 11.05
 8 SNM  3 21 16.00
31 SNM  3  0 23.00
 0 WTX  0 21  9.45
 1 WTX  3 21 11.00
 8 WTX  3 21 16.00
```

```
10 WTX  4 21 13.45
31 WTX  3  0 19.00


28 1988  6 18 16 58 12.00 1
 0 BAR  1 58 18.60
 1 BAR  3 58 22.50
 9 BAR  3 58 20.60
31 BAR  3  0 32.00
 0 BMT  0 58 18.80
 1 BMT  4 58 22.90
31 BMT  4  0 27.00
 0 CAR  0 58 20.50
 1 CAR  3 58 26.20
10 CAR  5 58 24.50
 8 CAR  5 58 29.10
31 CAR  5  0 28.00
 0 LAZ  1 58 17.15
 1 LAZ  3 58 20.25
 9 LAZ  5 58 19.70
31 LAZ  5  0 24.00
 0 LJY  0 58 14.60
31 LJY  3  0 24.00
 0 LPM  1 58 17.55
 1 LPM  3 58 20.70
31 LPM  3  0 31.00
 0 SMC  3 58 23.35
 1 SMC  3 58 31.20
31 SMC  3  0 26.00
 0 WTX  1 58 17.70
 1 WTX  3 58 20.90
 8 WTX  5 58 24.70
31 WTX  4  0 15.00


18 1988  7 22  8 11  0.00 1
 0 BAR  0 11  3.25
31 BAR  2  0 37.00
 0 BMT  0 11  9.40
 1 BMT  3 11 16.10
10 BMT  2 11 12.55
31 BMT  2  0 37.00
 0 LAZ  1 11  7.50
 1 LAZ  3 11 12.80
31 LAZ  3  0 32.00
 0 LJY  0 11  4.30
31 LJY  3  0 18.00
 0 LPM  1 11  1.40
31 LPM  3  0 40.00
 0 MLM  3 11 12.30
 8 MLM  3 11 22.60
31 MLM  3  0 25.00
 1 SB   3 11 17.60
 8 SB   3 11 19.50


29 1988  8 18 16 23 20.00 1
 0 BAR  0 23 10.85
 1 BAR  3 23 16.10
31 BAR  0  0 43.00
 0 BMT  1 23 12.55
 1 BMT  3 23 19.00
10 BMT  3 23 16.95
 8 BMT  5 23 21.75
31 BMT  3  0 35.00
 0 CAR  0 23  7.75
31 CAR  3  0 45.00
 0 LAZ  0 23 13.65
 1 LAZ  3 23 20.65
 8 LAZ  3 23 23.70
31 LAZ  3  0 35.00
 0 LPM  2 23 12.70
 1 LPM  3 23 19.30
31 LPM  3  0 34.00
 0 MLM  4 23 21.10
 8 MLM  4 23 34.50
 0 SB   3 23  8.20
 1 SB   3 23 11.40
31 SB   3  0 30.00
 0 SMC  1 23  7.20
31 SMC  3  0 30.00
 0 SNM  0 23  7.20
 1 SNM  2 23  9.60
31 SNM  2  0 30.00
 0 WTX  0 23  7.10
 1 WTX  3 23  9.50


30 1988  9 30 14 28 25.00 1
 0 BAR  1 28 31.50
 1 BAR  3 28 34.90
31 BAR  3  0 32.00
 0 BMT  1 28 33.40
 1 BMT  4 28 38.40
 9 BMT  4 28 35.60
 8 BMT  5 28 41.60
31 BMT  5  0 28.00
 0 CAR  1 28 31.60
 1 CAR  3 28 35.20
31 CAR  3  0 32.00
```

```
 0 LAZ  1 28 33.30
 1 LAZ  3 28 38.00
 8 LAZ  4 28 41.70
31 LAZ  4  0 30.00
 0 LJY  2 28 31.60
 0 LPM  0 28 32.40
 1 LPM  3 28 36.30
 8 LPM  5 28 40.60
31 LPM  5  0 31.00
 0 SB   2 28 32.50
 1 SB   3 28 36.70
 8 SB   3 28 41.20
31 SB   3  0 22.00
 0 SMC  3 28 34.05
 0 SNM  1 28 28.50
 1 SNM  3 28 30.00
31 SNM  3  0 22.00
 0 WTX  0 28 28.50
31 WTX  0  0 26.00

21 1988 10  3  1  3 11.00 1
 0 BAR  0  3 17.10
 1 BAR  3  3 22.30
10 BAR  4  3 20.00
31 BAR  4  0 30.00
 0 BMT  1  3 15.60
 1 BMT  4  3 19.30
 9 BMT  4  3 18.00
31 BMT  4  0 33.00
 0 CAR  2  3 15.85
 1 CAR  3  3 20.20
 1 LAZ  4  3 21.40
 0 SB   1  3 14.10
31 SB   1  0 32.00
 0 SMC  1  3 16.40
 1 SMC  3  3 20.90
31 SMC  3  0 30.00
 0 SNM  3  3 12.50
 0 WTX  1  3 12.40
 1 WTX  3  3 13.80
10 WTX  5  3 17.10
 8 WTX  4  3 19.40

24 1988 10 27  4 26  0.00 1
 0 BAR  0 26 54.00
 1 BAR  3 26 57.80
 8 BAR  4 26 62.10
31 BAR  0  0 25.00
 0 BMT  1 26 55.60
 1 BMT  3 26 60.10
 8 BMT  4 26 63.80
 0 CAR  1 26 54.00
 1 CAR  3 26 57.40
10 CAR  3 26 59.00
31 CAR  3  0 29.00
 0 LPM  3 26 55.20
 1 LPM  3 26 59.30
31 LPM  0  0 16.00
 0 SB   3 26 54.40
10 SB   3 26 59.70
 8 SB   3 26 63.40
31 SB   3  0 20.00
 0 SMC  3 26 56.15
 1 SMC  3 26 61.50
31 SMC  3  0 17.00
 0 WTX  2 26 50.40
 1 WTX  3 26 51.30
31 WTX  3  0 20.00

23 1989  9 27 23 43  9.00 1
 0 BAR  0 43 15.30
 1 BAR  3 43 20.60
10 BAR  4 43 18.20
31 BAR  4  0 20.00
 0 BMT  2 43 14.80
 1 BMT  2 43 19.65
 8 BMT  2 43 21.70
31 BMT  4  0 20.00
 0 CAR  0 43 13.35
 1 CAR  3 43 17.20
31 CAR  3  0 32.00
 0 LPM  0 43 16.45
 1 LPM  3 43 22.70
 8 LPM  5 43 24.70
31 LPM  3  0 26.00
 0 SB   0 43 11.40
 1 SB   2 43 13.50
31 SB   2  0 27.00
 0 SMC  3 43 13.10
 1 SMC  3 43 16.80
31 SMC  3  0 33.00
 0 SNM  1 43 10.50
 1 SNM  3 43 12.50

26 1989 10 27  6 50 51.00 1
 0 BAR  0 50 57.50
```

```
 1 BAR  4 50 62.50
31 BAR  4  0 36.00
 0 BMT  1 50 58.30
 1 BMT  3 50 63.70
 8 BMT  2 50 66.35
10 BMT  3 50 61.00
31 BMT  3  0 24.00
 0 CAR  0 50 55.50
31 CAR  0  0 39.00
 0 LAZ  2 50 59.35
 1 LAZ  3 50 65.30
 8 LAZ  3 50 67.45
10 LAZ  2 50 62.10
31 LAZ  2  0 28.00
 0 LPM  1 50 58.80
 1 LPM  3 50 64.60
31 LPM  3  0 64.60
 0 SB   0 50 55.10
 1 SB   2 50 58.00
31 SB   2  0 30.00
 0 SMC  0 50 55.80
 1 SMC  3 50 59.50
10 SMC  4 50 58.80
 0 SNM  1 50 53.50
 1 SNM  3 50 55.20

24 1990  4 19 22 15 30.00 1
 0 BAR  0 15 33.80
31 BAR  0  0 90.00
 0 BDO  0 15 32.20
31 BDO  0  0 65.00
 0 BMT  0 15 36.35
31 BMT  0  0 85.00
 0 CAR  0 15 36.80
31 CAR  0  0 65.00
 0 LAZ  0 15 33.90
31 LAZ  0  1 50.00
 0 LPM  0 15 31.40
31 LPM  0  0 85.00
 0 SB   1 15 38.50
 1 SB   3 15 46.00
 8 SB   4 15 48.20
10 SB   3 15 42.40
 0 SMC  2 15 40.75
31 SMC  2  0 82.00
 0 WTX  2 15 35.00
 1 WTX  4 15 39.70
 8 WTX  4 15 42.80
 9 WTX  3 15 36.70
10 WTX  4 15 38.90
31 WTX  4  0 37.00

20 1990  5  5 20 55 56.00 1
 0 BAR  1 55 62.30
 1 BAR  3 55 67.80
31 BAR  3  0 33.00
 0 BDO  2 55 57.40
 0 BMT  0 55 62.40
 1 BMT  2 55 67.60
10 BMT  4 55 66.10
31 BMT  4  0 26.00
 0 CAR  1 55 65.10
 1 CAR  2 55 72.10
10 CAR  4 55 68.90
31 CAR  4  0 32.00
 0 LAZ  0 55 59.50
 1 LAZ  2 55 62.70
10 LAZ  3 55 64.45
 8 LAZ  5 55 67.65
31 LAZ  5  0 25.00
 0 LPM  0 55 60.00
 1 LPM  2 55 63.60
31 LPM  2  0 30.00

23 1990  5  6  7 12  0.00 1
 0 BAR  1 12  6.40
 1 BAR  3 12 11.40
 8 BAR  4 12 14.80
10 BAR  4 12 10.20
31 BAR  4  0 32.00
 0 BDO  0 12  1.50
 0 BMT  0 12  6.50
 1 BMT  2 12 11.60
10 BMT  5 12 10.20
 8 BMT  3 12 14.00
31 BMT  3  0 30.00
 0 CAR  1 12  9.15
 1 CAR  2 12 16.20
10 CAR  5 12 12.80
31 CAR  5  0 29.00
 0 LAZ  0 12  3.60
 1 LAZ  2 12  6.70
10 LAZ  3 12  8.50
 8 LAZ  5 12 11.70
31 LAZ  4  0 25.00
 0 LPM  0 12  3.95
 1 LPM  3 12  7.70
```

```
31 LPM  3  0 28.00


21 1990  6  3  0  8  8.00 1
 0 BAR  1  8 15.15
 1 BAR  2  8 20.30
 8 BAR  2  8 23.60
31 BAR  2  0 18.00
 0 BDO  0  8 10.25
 0 BMT  0  8 15.10
 1 BMT  2  8 20.40
 8 BMT  3  8 22.60
31 BMT  2  0 18.00
 0 CAR  1  8 17.80
 1 CAR  3  8 24.50
31 CAR  3  0 18.00
 0 LAZ  0  8 12.40
 1 LAZ  2  8 15.50
10 LAZ  2  8 17.30
 8 LAZ  2  8 20.15
31 LAZ  2  0 24.00
 0 LPM  0  8 12.70
 1 LPM  2  8 16.45
10 LPM  3  8 17.15
31 LPM  3  0 18.00


22 1990  6  3 11 14 14.00 1
 0 BAR  1 14 20.75
 1 BAR  3 14 26.40
 8 BAR  3 14 29.30
10 BAR  2 14 25.70
31 BAR  3  0 22.00
 0 BDO  0 14 15.90
 0 BMT  0 14 20.80
 1 BMT  2 14 26.05
 8 BMT  4 14 28.30
10 BMT  3 14 25.30
31 BMT  3  0 22.00
 0 CAR  1 14 23.40
 1 CAR  3 14 30.55
31 CAR  3  0 24.00
 0 LAZ  0 14 18.05
 1 LAZ  2 14 21.20
10 LAZ  1 14 22.90
 8 LAZ  3 14 25.90
31 LAZ  3  0 25.00
 0 LPM  0 14 18.65
 1 LPM  2 14 22.00
31 LPM  2  0 21.00


25 1990  6  4  7 29 41.00 1
 0 BAR  0 29 44.80
 1 BAR  3 29 47.05
31 BAR  3  0 38.00
 0 BMT  0 29 49.05
 1 BMT  3 29 54.60
10 BMT  3 29 52.30
31 BMT  3  0 30.00
 0 CAR  0 29 45.10
31 CAR  0  0 40.00
 0 LAZ  1 29 48.60
 1 LAZ  3 29 54.00
 8 LAZ  4 29 57.05
10 LAZ  3 29 51.90
31 LAZ  3  0 30.00
 0 LPM  2 29 46.00
 1 LPM  3 29 49.10
31 LPM  3  0 43.00
 0 SB   1 29 47.80
 1 SB   3 29 52.70
10 SB   3 29 51.35
 8 SB   3 29 55.70
31 SB   3  0 30.00
 0 SMC  1 29 48.60
 1 SMC  3 29 54.50
31 SMC  3  0 36.00


19 1990  6 13 12 36  7.00 1
 0 BAR  0 36 13.65
 1 BAR  2 36 18.90
10 BAR  5 36 17.70
31 BAR  5  0 35.00
 0 BDO  0 36  9.00
31 BDO  0  0 18.00
 0 BMT  0 36 14.00
 1 BMT  2 36 19.20
10 BMT  3 36 17.20
 8 BMT  4 36 22.00
31 BMT  4  0 22.00
 0 CAR  1 36 16.50
31 CAR  1  0 27.00
 0 LAZ  0 36 11.15
 1 LAZ  2 36 14.50
 9 LAZ  3 36 13.60
 8 LAZ  4 36 18.10
 0 LPM  0 36 11.50
31 LPM  0  0 33.00
```

```
23 1990  6 20  1 22 35.20 1
 0 BAR  0 22 33.90
31 BAR  0  0 43.00
 0 BDO  1 22 38.80
10 BDO  3 22 41.20
31 BDO  0  0 37.00
 0 BMT  0 22 37.70
 1 BMT  3 22 43.50
 9 BMT  4 22 38.75
31 BMT  0  0 50.00
 0 CAR  0 22 33.05
31 CAR  0  0 57.00
 0 LAZ  0 22 37.70
 1 LAZ  2 22 43.30
31 LAZ  0  1  1.00
 0 LPM  0 22 35.30
 1 LPM  3 22 39.40
31 LPM  0  1  0.00
 0 SB   0 22 35.60
 1 SB   2 22 40.00
10 SB   2 22 38.50
31 SB   0  0 40.00
 0 SMC  0 22 36.35
31 SMC  0  1 11.00

27 1990  6 21 15 54 46.00 1
 0 BAR  0 54 53.10
 1 BAR  2 54 58.60
10 BAR  2 54 57.00
31 BAR  2  0 45.00
 0 BDO  0 54 48.35
31 BDO  0  0 32.00
 0 BMT  0 54 53.40
 1 BMT  2 54 58.70
10 BMT  3 54 56.70
31 BMT  3  0 35.00
 0 CAR  1 54 55.80
 1 CAR  2 54 63.15
 8 CAR  4 54 65.20
31 CAR  0  0 30.00
 0 LAZ  0 54 50.60
 1 LAZ  2 54 54.00
 9 LAZ  3 54 52.85
 8 LAZ  4 54 58.00
31 LAZ  0  0 39.00
 0 LPM  0 54 51.00
 1 LPM  3 54 54.60
31 LPM  3  0 38.00
 0 SB   2 54 56.40
31 SB   0  0 27.00
 0 SMC  1 54 59.00
10 SMC  4 54 62.40
31 SMC  0  0 31.00

27 1990  9  1  8 41 25.00 1
 0 BAR  3 41 32.35
 1 BAR  3 41 38.20
 9 BAR  2 41 33.65
 8 BAR  4 41 40.45
31 BAR  0  0 31.00
 0 BDO  1 41 29.70
10 BDO  1 41 32.65
 0 BMT  0 41 26.80
 1 BMT  4 41 28.70
31 BMT  0  0 31.00
 0 CAR  2 41 33.20
 1 CAR  3 41 39.70
31 CAR  1  0 24.00
 0 LAZ  0 41 26.30
 1 LAZ  2 41 27.80
31 LAZ  0  0 30.00
 0 LPM  2 41 31.40
 1 LPM  3 41 36.60
31 LPM  0  0 29.00
 0 SMC  2 41 34.20
10 SMC  3 41 37.30
31 SMC  1  0 20.00
 0 WTX  2 41 29.25
 1 WTX  3 41 32.90
 8 WTX  3 41 36.00
10 WTX  3 41 32.20
31 WTX  1  0 21.00

27 1990  9  1 10 47 48.93 1
 0 BAR  0 47 41.20
 1 BAR  2 47 47.50
 9 BAR  4 47 42.70
31 BAR  0  0 46.00
 0 BDO  0 47 38.70
10 BDO  1 47 41.60
31 BDO  0  0 45.00
 0 BMT  0 47 35.80
31 BMT  0  0 45.00
 0 CAR  1 47 41.95
 1 CAR  4 47 48.60
```

```
31 CAR  1  0 46.00
 0 LAZ  0 47 35.30
31 LAZ  0  0 42.00
 0 LPM  0 47 40.40
 1 LPM  3 47 45.70
 8 LPM  5 47 48.50
31 LPM  0  0 44.00
 0 SMC  1 47 43.10
 1 SMC  3 47 51.05
10 SMC  4 47 46.30
31 SMC  1  0 54.00
 0 WPX  1 47 38.05
 1 WPX  2 47 41.90
 8 WPX  3 47 44.90
10 WPX  2 47 41.20
31 WPX  1  0 39.00
```

Arroyo del Coyote Data Set

```
25 1985  8 16  2 43  5.00 1
 0 BAR  1 43  9.70
31 BAR  1  0 27.00
 0 CAR  1 43 10.10
31 CAR  4  0 33.00
 0 LAZ  1 43 13.65
 1 LAZ  3 43 19.00
10 LAZ  3 43 17.00
 8 LAZ  3 43 21.40
31 LAZ  3  0 22.00
 0 LEM  1 43  9.20
31 LEM  1  0 23.00
 0 LJY  2 43 11.15
 0 LPM  2 43 11.35
 1 LPM  3 43 14.30
31 LPM  3  0 24.00
 0 MAG  1 43 13.00
 1 MAG  2 43 17.50
 9 MAG  2 43 14.55
10 MAG  2 43 16.05
 8 MAG  4 43 20.00
31 MAG  4  0 20.00
 0 WTX  0 43  8.80
 1 WTX  2 43 10.55
 9 WTX  2 43 11.30
31 WTX  2  0 17.00


14 1985  8 16 14 56 56.60 1
 0 ALQ  1 57  8.90
 0 BAR  1 56 56.20
 0 CAR  0 56 56.55
 0 LAZ  0 56 59.95
 0 LEM  0 56 55.45
 0 LJY  1 56 57.45
 0 LPM  1 56 57.40
 0 MAG  0 56 59.25
 0 MLM  0 57  6.35
 0 SB   1 56 59.10
31 SB   1  7 30.00
 0 SMC  0 56 60.20
 0 WTX  0 56 55.15
31 WTX  1  7 30.00


27 1985  8 16 15 31 60.50 1
 0 BAR  1 31 57.50
31 BAR  0  0 33.00
 0 CAR  1 31 57.90
31 CAR  1  0 38.00
 0 LAZ  0 31 61.20
 1 LAZ  3 31 66.20
 9 LAZ  3 31 62.80
10 LAZ  3 31 64.50
31 LAZ  3  0 32.00
 0 LJY  1 31 58.80
31 LJY  1  0 25.00
 0 LPM  0 31 58.50
31 LPM  0  0 40.00
 0 LEM  1 31 56.80
31 LEM  1  0 30.00
 0 MAG  0 31 60.60
 1 MAG  3 31 65.30
 9 MAG  4 31 62.30
10 MAG  4 31 64.00
31 MAG  4  0 22.00
 0 SB   1 31 60.50
 1 SB   3 31 65.50
 8 SB   3 31 68.25
31 SB   3  0 24.00
 0 WTX  0 31 56.60
 1 WTX  3 31 58.40
31 WTX  3  0 23.00


25 1985  8 16 15 35 38.80 1
 0 BAR  0 35 34.80
31 BAR  0  0 35.00
 0 CAR  0 35 35.25
31 CAR  0 35 45.00
 0 LAZ  0 35 38.80
 1 LAZ  3 35 44.20
10 LAZ  2 35 42.40
 8 LAZ  3 35 46.30
31 LAZ  3  0 30.00
 0 LEM  0 35 34.20
31 LEM  0  0 35.00
 0 LJY  1 35 36.30
31 LJY  1  0 23.00
 0 LPM  0 35 36.10
31 LPM  0  0 33.00
 0 MAG  0 35 38.00
 1 MAG  4 35 42.60
10 MAG  4 35 41.70
31 MAG  4  0 28.00
 0 SB   1 35 38.00
 1 SB   3 35 43.00
31 SB   3 35 21.00
 0 WTX  0 35 33.90
 1 WTX  3 35 35.80
```

```
31 WTX  3  0 29.00


29 1985  8 16 15 42 29.50 1
 0 BAR  0 42 26.25
31 BAR  0  0 30.00
 0 CAR  0 42 26.95
31 CAR  0  0 31.00
 0 LAZ  1 42 30.10
 1 LAZ  3 42 35.70
10 LAZ  3 42 33.90
31 LAZ  3  0 30.00
 0 LEM  0 42 25.80
31 LEM  0  0 30.00
 0 LJY  1 42 27.80
31 LJY  1  0 20.00
 0 LPM  0 42 27.55
31 LPM  0  0 35.00
 0 MAG  0 42 29.70
 1 MAG  3 42 34.50
31 MAG  3  0 30.00
 0 MLM  1 42 36.80
 0 SMC  0 42 30.50
 1 SMC  2 42 36.20
 9 SMC  3 42 32.10
31 SMC  3  0 24.00
 0 SB   0 42 29.50
 1 SB   3 42 34.50
10 SB   3 42 33.30
31 SB   3  0 23.00
 0 WTX  0 42 25.50
 1 WTX  3 42 27.50
31 WTX  3  0 26.00


32 1985  8 16 15 47 33.70 1
 0 BAR  1 47 30.10
31 BAR  1  0 40.00
 0 CAR  1 47 30.60
31 CAR  1  0 36.00
 0 LAZ  0 47 33.70
 1 LAZ  2 47 39.20
 9 LAZ  4 47 35.20
10 LAZ  4 47 37.30
 8 LAZ  3 47 41.30
31 LAZ  3  0 30.00
 0 LEM  1 47 29.50
31 LEM  1  0 30.00
 0 LJY  1 47 31.30
31 LJY  1  0 21.00
 0 LPM  0 47 31.10
31 LPM  0  0 39.00
 0 MAG  1 47 33.20
 1 MAG  4 47 37.80
 9 MAG  5 47 34.50
10 MAG  3 47 36.50
31 MAG  3  0 30.00
 0 SMC  0 47 34.00
 1 SMC  3 47 39.70
 8 SMC  3 47 41.50
31 SMC  3  0 26.00
 0 SB   0 47 33.20
 1 SB   3 47 38.00
10 SB   3 47 36.90
31 SB   3  0 21.00
 0 WTX  1 47 29.00
 1 WTX  3 47 31.00
31 WTX  3  0 26.00


30 1985  8 16 15 59 12.80 1
 0 BAR  1 59  9.10
31 BAR  1  0 33.00
 0 CAR  0 59  9.60
31 CAR  0  0 36.00
 0 LAZ  0 59 13.00
 1 LAZ  2 59 18.10
 9 LAZ  3 59 14.20
10 LAZ  3 59 16.20
 8 LAZ  4 59 20.60
31 LAZ  4  0 26.00
 0 LEM  0 59  8.40
31 LEM  0  0 30.00
 0 LJY  1 59 10.30
31 LJY  3  0 25.00
 0 LPM  0 59 10.00
31 LPM  0  0 37.00
 0 MAG  1 59 12.30
 1 MAG  4 59 16.90
31 MAG  4  0 24.00
 0 MLM  2 59 19.60
 0 SMC  1 59 13.00
 1 SMC  3 59 18.60
 9 SMC  5 59 14.75
31 SMC  5  0 25.00
 0 SB   1 59 12.00
 1 SB   3 59 17.00
31 SB   3  0 19.00
 0 WTX  0 59  8.10
 1 WTX  3 59 10.00
```

```
31 WTX  3  0 27.00


28 1985  8 16 16  0 30.30 1
 0 BAR  0  0 29.20
31 BAR  0  0 23.00
 0 CAR  0  0 29.70
31 CAR  0  0 35.00
 0 LAZ  0  0 33.00
 1 LAZ  3  0 38.20
 9 LAZ  3  0 34.20
10 LAZ  3  0 36.15
 8 LAZ  4  0 40.60
31 LAZ  4  0 27.00
 0 LEM  0  0 28.60
31 LEM  0  0 28.00
 0 LJY  1  0 30.30
31 LJY  1  0 20.00
 0 LPM  1  0 30.20
31 LPM  1  0 31.00
 0 MAG  1  0 32.30
 1 MAG  3  0 37.00
10 MAG  4  0 35.40
31 MAG  4  0 23.00
 0 SB   2  0 32.30
31 SB   2  0 20.30
 0 SMC  1  0 33.20
 1 SMC  3  0 38.90
31 SMC  3  0 22.00
 0 WTX  0  0 28.15
 1 WTX  3  0 30.20
31 WTX  0  0 30.00


31 1985  8 17  1 24 29.00 1
 0 BAR  0 24 25.75
31 BAR  4  0 25.00
 0 CAR  0 24 25.90
 1 CAR  4 24 29.00
31 CAR  0  0 30.00
 0 LAZ  0 24 29.40
 1 LAZ  2 24 34.80
10 LAZ  2 24 32.60
 8 LAZ  4 24 37.40
 9 LAZ  2 24 31.40
31 LAZ  3  0 20.00
 0 LEM  0 24 24.80
31 LEM  0  0 35.00
 0 LPM  0 24 26.75
 1 LPM  3 24 30.50
31 LPM  3  0 36.00
 0 MAG  2 24 28.80
 1 MAG  4 24 33.20
31 MAG  4  0 20.00
 0 SB   2 24 29.00
 1 SB   2 24 33.50
31 SB   2  0 20.00
 0 SMC  0 24 29.50
 1 SMC  3 24 35.30
31 SMC  2  0 26.00
 0 WTX  0 24 24.50
 1 WTX  3 24 26.40
 8 WTX  4 24 31.45
31 WTX  4  0 28.00
 0 FTS  0 24 24.10
 0 YRD  0 24 23.70


22 1985  8 17  5 14 50.50 1
 0 CAR  0 14 50.50
31 CAR  0  0 99.00
 0 LAZ  0 14 54.00
31 LAZ  0  1 42.00
 0 LEM  0 14 49.50
 0 LJY  2 14 51.50
31 LJY  2  0 70.00
 0 LPM  0 14 51.25
31 LPM  0  0 95.00
 0 MAG  0 14 53.25
31 MAG  0  0 55.00
 0 SB   0 14 53.00
 1 SB   4 14 58.00
 9 SB   4 14 54.50
10 SB   4 14 56.60
31 SB   3  0 48.00
 0 SMC  0 14 54.00
31 SMC  0  0 51.00
 0 WTX  0 14 49.00
31 WTX  0  0 65.00
 0 FTS  0 14 48.55
 0 YRD  0 14 48.25


31 1985  8 17 18  4 27.20 1
 0 BAR  0  4 28.30
 1 BAR  3  4 30.50
31 BAR  3  0 22.00
 0 CAR  0  4 28.50
31 CAR  0  0 22.00
 0 LAZ  0  4 32.00
```

```
 1 LAZ  3  4 37.40
 8 LAZ  3  4 39.80
10 LAZ  3  4 35.20
31 LAZ  3  0 24.00
 0 LEM  1  4 27.30
 1 LEM  3  4 29.60
31 LEM  3  0 37.00
 0 LJY  1  4 29.50
31 LJY  1  0 22.00
 0 LPM  3  4 29.40
31 LPM  3  0 30.00
 0 MAG  1  4 31.30
 1 MAG  3  4 36.00
 9 MAG  3  4 32.80
10 MAG  3  4 34.30
 8 MAG  3  4 39.00
31 MAG  3  0 19.00
 8 SB   3  4 39.00
10 SB   3  4 35.00
 1 SMC  3  4 37.70
31 SMC  3  0 16.00
 0 WTX  1  4 27.20
31 WTX  1  0 17.00
 0 FTS  0  4 26.60
 0 YRD  1  4 26.30


27 1985  8 17 19 49 31.20 1
 0 BAR  0 49 28.00
31 BAR  0  0 22.00
 0 CAR  1 49 28.60
31 CAR  1  0 34.00
 0 LAZ  1 49 31.90
 1 LAZ  3 49 36.90
 8 LAZ  3 49 39.50
10 LAZ  3 49 35.20
31 LAZ  3  0 19.00
 0 LEM  0 49 27.50
31 LEM  0  0 35.00
 0 LJY  2 49 29.50
31 LJY  2  0 17.00
 0 LPM  1 49 29.35
31 LPM  1  0 25.00
 0 MAG  0 49 31.20
 1 MAG  3 49 35.80
 8 MAG  3 49 38.80
 9 MAG  3 49 32.90
10 MAG  3 49 34.40
31 MAG  3  0 18.00
 0 SB   2 49 31.20
 1 SB   3 49 36.10
 0 WTX  1 49 27.25
31 WTX  1  0 16.00
 0 FTS  0 49 26.40
 0 YRD  1 49 26.20


31 1985  8 17 21 34 13.40 1
 0 BAR  0 34 14.30
31 BAR  0  0 40.00
 0 CAR  1 34 14.90
31 CAR  1  0 50.00
 0 LAZ  1 34 18.30
 1 LAZ  4 34 23.40
10 LAZ  4 34 21.50
 8 LAZ  4 34 26.40
31 LAZ  4  0 35.00
 0 LEM  0 34 13.55
31 LEM  0  0 47.00
 0 LJY  1 34 15.60
31 LJY  1  0 28.00
 0 LPM  1 34 15.50
31 LPM  1  0 50.00
 0 MAG  0 34 17.40
31 MAG  0  0 31.00
 0 SB   0 34 17.50
 1 SB   3 34 22.50
10 SB   3 34 21.30
 9 SB   4 34 19.80
31 SB   3  0 30.00
 0 SMC  0 34 18.40
 1 SMC  3 34 24.20
31 SMC  3  0 30.00
 0 WTX  0 34 13.30
 1 WTX  2 34 15.10
31 WTX  2  0 27.00
 0 FTS  0 34 12.60
 0 JHLS 0 34 12.20
 0 YRD  0 34 12.30


33 1985  8 18  0 28  8.50 1
 0 BAR  0 28  5.40
 1 BAR  3 28  7.70
31 BAR  3  0 19.00
 0 CAR  0 28  5.90
31 CAR  0  0 26.00
 0 LAZ  1 28  9.20
 1 LAZ  3 28 14.40
 9 LAZ  3 28 10.60
```

```
10 LAZ  3 28 12.60
31 LAZ  3  0 20.00
 0 LEM  0 28  4.80
31 LEM  3  0 29.00
 0 LJY  2 28  6.70
31 LJY  2  0 15.00
 0 LPM  1 28  6.40
 1 LPM  3 28  9.60
31 LPM  3  0 25.00
 0 MAG  1 28  8.50
 1 MAG  3 28 13.10
 8 MAG  4 28 15.50
10 MAG  3 28 11.70
31 MAG  3  0 23.00
 0 SB   3 28  8.60
 0 SMC  1 28  9.50
 1 SMC  2 28 15.20
31 SMC  2  0 16.00
 0 WTX  0 28  4.45
 1 WTX  4 28  6.50
31 WTX  4  0 13.00
 0 FTS  0 28  3.85
 0 JHLS 0 28  3.50
 0 SH   0 28  3.50
 0 YRD  0 28  3.45


29 1985  8 18  3 57 19.00 1
 0 BAR  1 57 15.00
31 BAR  3  0 21.00
 0 CAR  0 57 15.40
 1 CAR  3 57 18.00
31 CAR  3  0 20.00
 0 LAZ  0 57 18.90
 1 LAZ  3 57 23.90
10 LAZ  2 57 22.10
 8 LAZ  3 57 26.70
31 LAZ  3  0 21.00
 0 LEM  0 57 14.15
31 LEM  0  0 36.00
 0 LJY  1 57 16.25
31 LJY  1  0 14.00
 0 LPM  2 57 16.10
 1 LPM  3 57 19.00
31 LPM  3  0 25.00
 0 MAG  1 57 18.00
 1 MAG  3 57 22.60
 8 MAG  3 57 25.30
10 MAG  2 57 21.35
31 MAG  2  0 15.00
 0 WTX  0 57 14.00
 1 WTX  2 57 15.80
31 WTX  2  0 15.00
 0 FTS  0 57 13.30
 0 JHLS 0 57 13.00
 0 SH   0 57 13.00
 0 YRD  0 57 12.90


26 1985  8 18  6 24 36.20 1
 0 BAR  0 24 33.00
 1 BAR  3 24 35.70
31 BAR  3  0 15.00
 0 CAR  2 24 33.50
 1 LAZ  3 24 42.20
10 LAZ  4 24 40.00
 8 LAZ  4 24 44.60
31 LAZ  4  0 11.00
 0 LEM  0 24 32.40
 1 LEM  3 24 34.30
31 LEM  3  0 25.00
 1 LJY  3 24 37.60
 0 LPM  2 24 34.00
 1 LPM  3 24 37.60
31 LPM  3  0 18.00
 0 MAG  2 24 36.20
 1 MAG  3 24 41.00
10 MAG  3 24 39.40
31 MAG  3  0 11.00
 0 WTX  1 24 32.10
 1 WTX  3 24 34.00
31 WTX  3  0 10.00
 0 FTS  0 24 31.55
 0 JHLS 0 24 31.20
 0 SH   0 24 31.25
 0 YRD  0 24 31.20


36 1985  8 18 10 29 15.20 1
 0 BAR  0 29 12.00
 1 BAR  3 29 14.40
31 BAR  3  0 20.00
 0 CAR  0 29 12.40
31 CAR  0  0 24.00
 0 LAZ  0 29 16.00
 1 LAZ  3 29 21.20
 9 LAZ  3 29 17.40
10 LAZ  3 29 19.00
31 LAZ  3  0 20.00
 0 LEM  0 29 11.45
```

```
 1 LEM  3 29 13.40
31 LEM  3  0 29.00
 0 LJY  1 29 13.40
 1 LJY  3 29 17.25
31 LJY  3  0 17.00
 0 LPM  0 29 13.10
 1 LPM  3 29 16.40
31 LPM  3  0 29.00
 0 MAG  1 29 15.10
 1 MAG  2 29 19.90
 8 MAG  2 29 22.60
10 MAG  3 29 18.15
31 MAG  3  0 15.00
 0 SB   2 29 15.20
 1 SB   2 29 20.10
31 SB   2  0 11.00
 0 SMC  1 29 16.10
 1 SMC  3 29 21.70
31 SMC  3  0 17.00
 0 WTX  0 29 11.00
31 WTX  0  0 10.00
 0 FTS  0 29 10.40
 0 JHLS 2 29 10.20
 0 SH   0 29 10.20
 0 YRD  1 29 10.20

21 1985  8 18 13  3 45.10 1
 0 BAR  2  3 44.60
 1 BAR  3  3 47.00
31 BAR  3  0 13.00
 0 CAR  0  3 45.00
31 CAR  0  0 17.00
 0 LAZ  1  3 48.50
 1 LAZ  3  3 53.50
31 LAZ  3  0 12.00
 0 LEM  0  3 44.00
 1 LEM  3  3 46.00
31 LEM  3  0 20.00
 0 LJY  3  3 46.00
 0 LPM  1  3 45.80
 1 LPM  2  3 49.00
31 LPM  2  0 14.00
 1 MAG  2  3 52.20
 8 MAG  3  3 54.90
 0 FTS  0  3 43.10
 0 JHLS 0  3 42.80
 0 SH   2  3 42.85
 0 YRD  2  3 42.75

30 1985  8 18 14 47 45.10 1
 0 BAR  0 47  8.30
31 BAR  3  0 40.00
 0 CAR  1 47  8.80
31 CAR  1  0 57.00
 0 LAZ  0 47 12.25
 1 LAZ  3 47 17.20
31 LAZ  3  0 40.00
 0 LEM  0 47  7.90
31 LEM  3  0 60.00
 0 LJY  1 47  9.80
31 LJY  1  0 35.00
 0 LPM  0 47  9.50
31 LPM  2  0 50.00
 0 MAG  0 47 11.60
 1 MAG  3 47 16.00
31 MAG  0  0 32.00
 0 MLM  2 47 19.00
 0 SB   1 47 11.50
 1 SB   3 47 16.50
10 SB   4 47 15.40
 0 SMC  1 47 12.45
 1 SMC  3 47 18.00
31 SMC  4  0 45.00
 0 WTX  0 47  7.40
 1 WTX  3 47  9.30
31 WTX  3  0 30.00
 0 FTS  0 47  6.80
 0 JHLS 0 47  6.45
 0 SH   0 47  6.65
 0 YRD  0 47  6.55

27 1985  8 18 15 48 45.10 1
 0 AIQ  2 48 32.00
 0 BAR  0 48 19.20
31 BAR  3  0 87.00
 0 CAR  1 48 19.50
31 CAR  1  1 50.00
 0 LAZ  0 48 22.95
10 LAZ  3 48 25.90
31 LAZ  3  0 85.00
 0 LEM  2 48 18.30
 0 LJY  2 48 20.10
31 LJY  1  0 75.00
 0 LPM  2 48 20.00
31 LPM  2  0 75.00
 0 MAG  0 48 22.20
31 MAG  0  0 52.00
```

```
 0 MLM  0 48 29.35
31 MLM  0  0 65.00
 0 SB   1 48 22.20
 0 SMC  0 48 23.05
 1 SMC  2 48 28.90
31 SMC  4  0 90.00
 0 WTX  0 48 18.00
31 WTX  3  0 58.00
 0 FTS  0 48 17.45
 0 JHLS 0 48 17.10
 0 SH   0 48 17.15
 0 YRD  0 48 17.10


28 1985  8 18 16 54 45.10 1
 0 BAR  1 54 47.35
31 BAR  3  0 32.00
 0 CAR  1 54 48.00
31 CAR  1  1 35.00
 0 LAZ  0 54 51.20
 1 LAZ  2 54 56.50
10 LAZ  2 54 54.35
 8 LAZ  3 54 59.50
31 LAZ  3  0 24.00
 0 LJY  1 54 48.80
31 LJY  1  0 20.00
 0 LPM  1 54 48.60
31 LPM  2  0 34.00
 0 MAG  1 54 50.65
 1 MAG  3 54 55.10
 9 MAG  2 54 52.15
10 MAG  3 54 53.75
31 MAG  0  0 22.00
 0 SMC  1 54 51.60
 1 SMC  3 54 57.10
31 SMC  4  0 25.00
 0 WTX  0 54 46.40
 1 WTX  3 54 48.20
31 WTX  3  0 22.00
 0 FTS  0 54 45.70
 0 JHLS 0 54 45.50
 0 SH   0 54 45.50
 0 YRD  0 54 45.45


31 1985  8 18 22 14 45.10 1
 0 BAR  1 14 31.00
 1 BAR  3 14 33.30
31 BAR  3  0 21.00
 0 CAR  1 14 31.45
31 CAR  1  1 27.00
 0 LAZ  1 14 34.85
 1 LAZ  3 14 40.00
10 LAZ  2 14 38.10
 8 LAZ  3 14 42.60
31 LAZ  3  0 20.00
 0 LEM  1 14 30.25
 1 LEM  3 14 32.50
31 LEM  3  0 24.00
 0 LJY  2 14 32.40
 0 LPM  2 14 32.10
 1 LPM  3 14 35.10
31 LPM  2  0 30.00
 0 MAG  2 14 34.40
 1 MAG  3 14 38.60
 9 MAG  3 14 35.75
10 MAG  2 14 37.15
 8 MAG  4 14 41.30
31 MAG  0  0 15.00
 1 SMC  3 14 40.90
 0 WTX  1 14 30.10
 1 WTX  3 14 32.00
31 WTX  3  0 15.00
 0 FTS  0 14 29.40
 0 JHLS 0 14 29.05
 0 SH   0 14 29.05
 0 YRD  0 14 29.05


21 1985  8 19 19 35 41.15 1
 0 BAR  0 35 37.40
31 BAR  0  1 40.00
 0 CAR  0 35 37.90
31 CAR  0  1 40.00
 0 LAZ  0 35 41.15
31 LAZ  0  1 45.00
 0 LEM  0 35 36.70
31 LEM  0  0 77.00
 0 LJY  0 35 38.90
31 LJY  0  0 84.00
 0 LPM  0 35 38.50
31 LPM  0  1 57.00
 0 MAG  2 35 40.20
31 MAG  2  0 70.00
 0 MLM  2 35 47.80
 0 SB   1 35 40.35
31 SB   1  0 72.00
 0 SMC  0 35 41.40
31 SMC  0  1 56.00
 0 WTX  0 35 36.45
```

```
31 WTX  0  0 73.00


22 1985  8 20  2 26 45.10 1
 0 BAR  1 26  7.00
 1 BAR  3 26  9.80
31 BAR  3  0 22.00
 0 CAR  1 26  7.30
31 CAR  1  1 22.00
 0 LAZ  1 26 11.00
 1 LAZ  3 26 16.00
10 LAZ  2 26 14.00
 8 LAZ  3 26 18.50
31 LAZ  3  0 15.00
 0 LEM  0 26  6.30
31 LEM  0  0 20.00
 0 LPM  1 26  8.10
 1 LPM  2 26 11.65
31 LPM  2  0 22.00
 0 MAG  2 26 10.40
 1 MAG  3 26 14.60
10 MAG  2 26 13.10
 8 MAG  2 26 17.30
31 MAG  0  0 16.00
 0 WTX  1 26  5.90
 1 WTX  3 26  7.85


20 1985  8 20  7 36 45.10 1
 0 BAR  0 36 15.20
 1 BAR  3 36 17.60
31 BAR  3  0 24.00
 0 CAR  0 36 15.60
31 CAR  1  1 25.00
 0 LAZ  1 36 19.00
 1 LAZ  2 36 24.00
31 LAZ  3  0 15.00
 0 LEM  0 36 14.50
31 LEM  0  0 20.00
 0 LPM  2 36 16.40
 1 LPM  3 36 19.60
31 LPM  2  0 20.00
 0 MAG  1 36 18.20
 1 MAG  3 36 22.80
10 MAG  2 36 21.30
31 MAG  0  0 15.00
 0 WTX  1 36 14.10
 1 WTX  3 36 16.20
31 WTX  3  0 13.00
```

This dissertation is accepted on behalf of the faculty of the Institute by the following committee:

Allen R. Sanford

Adviser

Lawrence H. Jackson

John Knapp

Allan Gilbert

Marshall Cutler

July 22, 1991

Date